

1-1-2006

Strengthening full-scale damaged prestressed concrete bridge girders with CFRP sheets

David Cerullo
Ryerson University

Follow this and additional works at: <http://digitalcommons.ryerson.ca/dissertations>



Part of the [Civil Engineering Commons](#)

Recommended Citation

Cerullo, David, "Strengthening full-scale damaged prestressed concrete bridge girders with CFRP sheets" (2006). *Theses and dissertations*. Paper 471.

NOTE TO USERS

This reproduction is the best copy available.

UMI[®]

STRENGTHENING FULL-SCALE DAMAGED PRESTRESSED CONCRETE BRIDGE GIRDERS WITH CFRP SHEETS

TA
2.2
.044
0300

by

David Cerullo, B.Eng

Ryerson University, 2006

A Thesis

presented to Ryerson University

in partial fulfillment of the
requirements for the degree of
Master of Applied Science
in the Program of
Civil Engineering

Toronto, Ontario, Canada, 2006

© David Cerullo 2006

UMI Number: EC54171

INFORMATION TO USERS

The quality of this reproduction is dependent upon the quality of the copy submitted. Broken or indistinct print, colored or poor quality illustrations and photographs, print bleed-through, substandard margins, and improper alignment can adversely affect reproduction.

In the unlikely event that the author did not send a complete manuscript and there are missing pages, these will be noted. Also, if unauthorized copyright material had to be removed, a note will indicate the deletion.



UMI Microform EC54171
Copyright 2009 by ProQuest LLC
All rights reserved. This microform edition is protected against
unauthorized copying under Title 17, United States Code.

ProQuest LLC
789 East Eisenhower Parkway
P.O. Box 1346
Ann Arbor, MI 48106-1346

BORROWER'S PAGE

Ryerson University requires the signatures of all persons using or photocopying this thesis.

Please sign below, and give address and date.

This image shows a single sheet of white paper with horizontal blue or grey ruling lines. The lines are evenly spaced and run across the width of the page. There are no margins, text, or other markings on the paper.

ABSTRACT

Strengthening Full-Scale Damaged Prestressed Concrete Bridge Girders with CFRP Sheets

David Cerullo

MASc, 2006

Department of Civil Engineering, Ryerson University

A large percentage of bridges in Canada were constructed over thirty years ago and their condition steadily declining. A product of deterioration and corrosive environments, many structures have been rendered unfit as per design codes and structurally unsound. Constructing new structures and conventional repair methods are financially costly. A solution lies in fibre reinforced polymers (FRP).

This thesis summarizes experimental projects regarding FRP usage in field applications. An actual damaged bridge girder was removed and rehabilitated with the FRP system. It was loaded incrementally and statically, nearing failure, investigating the reliability of the rehabilitation technique proposed to revive strength capacity to an acceptable level. A finite element computer simulation was created, modeling the load-history of the rehabilitated girder, as well three full-scale damaged double-tee girders, recently rehabilitated and loaded to collapse. This full-scale testing program and computer replication shall provide engineers with confidence in using FRP technology in girder strengthening.

ACKNOWLEDGEMENTS

Grateful acknowledgement is due to Dr. Khaled Sennah, of Ryerson University, whose guidance, supervision and scholarly counsel has allowed this project to carry forward and fulfill expectations. A sincere thank you.

To the *MTO*, especially Clifford Lam and Howard Sahsuvar, whose assistance, hard work and enthusiasm, were essential pieces of this project, and have not gone unnoticed.

A great thank you goes out to the established companies who contributed to this undertaking: *The RJ Watson Group* of Buffalo and *Fyfe Co. The Fibrewrap Company* of San Diego, USA; *The Euclid Chemical Company* of Toronto, *Powell Contracting* of Gormley and *Premier Corrosion* of Oakville, Canada. Their cooperation and ongoing effort truly became the corner stone of this thesis.

The continuous support, commitment and dedication of Nidal Jaalouk was an integral part of all experimental work completed. Thank you very much.

To my family, my girl and especially my parents, who have always encouraged and supported my studies, and who have always been and remain my inspiration, I dedicate this to you!

TABLE OF CONTENTS

Author's Declaration.....	iii
Borrower's Page.....	v
Abstract.....	vii
Acknowledgements.....	ix
Table of Contents.....	xi
List of Tables.....	xv
List of Figures.....	xvii
Abbreviations.....	xxiii
Notation.....	xxv

CHAPTER I

INTRODUCTION

1.1	General	1
1.2	The Dilemma	3
1.3	Objectives	5
1.4	Scope of Research	6
1.5	Contents and Arrangement of Thesis	6

CHAPTER II

LITERATURE REVIEW

2.1	General	9
2.2	Evolution of Fibre Reinforced Polymers	11
2.3	Characteristics of Fibre Reinforced Polymers	13
2.3.1	Stress–Strain Relationship and Physical Properties	14
2.3.2	Fibres	15
2.3.3	Epoxy	16
2.3.4	Protective Coatings	17

2.3.5	Fire Resistance	17
2.3.6	Storage and Handling	19
2.4	Design with Fibre Reinforced Polymers	19
2.4.1	Creation Process	19
2.4.2	Anisotropic Nature	20
2.4.3	Material Properties	20
2.5	Installation of Fibre Reinforced Polymers	21
2.5.1	Surface Preparation	21
2.5.2	Primer and Putty Application	22
2.5.3	Fabric Preparation and Application	22
2.5.4	Quality Control Considerations	23
2.6	Review of Relevant Literature	23
2.6.1	Flexure Strengthening and Rehabilitation	23
2.6.2	Shear Strengthening and Rehabilitation	28
2.6.3	Strengthening and Rehabilitation for Combined Flexure and Shear	29
2.6.4	Finite Element Modeling Techniques	31
2.7	Review of Prior DT Girder Testing and Analysis	34
2.7.1	Geometry of the Tested Double-Tee Girders	35
2.7.2	DT Girder CFRP Layout	36
2.7.3	DT Girder Experimental Results	37

CHAPTER III

EXPERIMENTAL INVESTIGATION

3.1	General	39
3.2	Girder and Site Preparation	41
3.3	Preliminary Testing	42
3.3.1	Instrumentation	42
3.3.2	Preliminary Testing Results	43
3.4	Girder Experimental Preparation	45
3.4.1	Crack Mapping	46
3.4.2	Crack Injection and Repair	46

3.4.3	Concrete Girder Substrate Preparation	47
3.5	CFRP Arrangement	48
3.6	CFRP Application	50
3.6.1	Tyfo® S Epoxy	50
3.6.2	Tyfo® TC Epoxy	51
3.6.3	Tyfo® SCH-11UP High Strength Carbon Fabric	52
3.6.4	HDK Cabosil	52
3.6.5	The Application Process	53
3.7	Final Testing	54
3.7.1	Instrumentation	55
3.7.2	Additional Testing Equipment and Apparatus	57

CHAPTER IV

THEORETICAL FINITE ELEMENT ANALYSIS

4.1	General	61
4.2	The Finite Element Study	62
4.3	Synopsis of the ABAQUS Finite Element Program	66
4.4	Finite Element Verification Study	67
4.5	Finite Element Sensitivity Study	67
4.6	Finite Element Model	69
4.6.1	Element Nature and Application	70
4.6.2	Reinforced Concrete Modeling	71
4.6.3	Modeling of Prestressing Tendons	75
4.6.4	Modeling of CFRP	76
4.6.5	Nonlinear Model Attributes	77
4.7	Modeling of Concrete AASHTO Type III Girder	79
4.8	Modeling of Double-Tee Girders	81

CHAPTER V

EXPERIMENTAL AND FINITE ELEMENT FINDINGS

5.1	General	83
5.2	AASHTO Type III Girder Testing	83
5.3	Review of Testing Results	85
5.3.1	Instrumentation Results	86
5.3.2	Cross Sectional Strain Distribution	91
5.4	Comparison of Experimental and Finite Element Analysis Results	92

CHAPTER VI

CONCLUSIONS AND RECOMMENDATIONS FOR FUTURE RESEARCH

6.1	Summary of Study	99
6.2	Conclusions	100
6.3	Considerations for Future Research	102

REFERENCES	103
------------	-----

TABLES	109
--------	-----

FIGURES	125
---------	-----

APPENDICES

Appendix A	Input Files for ABAQUS Finite Element Models	A.1
	AASHTO Type III Girder ABAQUS Input File	A.3
	DT-41 Girder ABAQUS Input File	A.17
	DT-100 Girder ABAQUS Input File	A.35
	DT-102A Girder ABAQUS Input File	A.53
Appendix B	Manual Calculations	B.1
	AASHTO Type III Girder Calculations	B.3
	DT-41 Girder Calculations	B.25
	DT-102A Girder Calculations	B.31

LIST OF TABLES

	Page
Table 2.1 Double-tee girder dimensional properties.....	109
Table 2.2 Double-tee girder reinforcement properties.....	109
Table 2.3 Double-tee girder concrete properties.....	109
Table 2.4 Tyfo® SCH-41S carbon fibre sheet dry fibre properties.....	110
Table 2.5 Tyfo® Epoxy material properties.....	110
Table 2.6 Tyfo® SCH-41S Composite laminate properties.....	110
Table 3.1 AASHTO Type III concrete girder dimensional properties....	111
Table 3.2 AASHTO Type III concrete girder properties.....	111
Table 3.3 AASHTO Type III concrete girder cover.....	111
Table 3.4 Concrete slab properties.....	111
Table 3.5 Concrete slab cover.....	111
Table 3.6 Prestressing steel characteristics.....	111
Table 3.7 (a) Prestressing steel properties.....	112
Table 3.7 (b) Prestressing steel properties.....	112
Table 3.8 Reinforcing steel properties.....	112
Table 3.9 Reinforcing steel geometric properties.....	112
Table 3.10 Preliminary testing load application procedure	113
Table 3.11 Preliminary testing readings from LVDTs.....	114
Table 3.12 Preliminary testing readings from strain gages.....	115
Table 3.13 Concrete grout compression test results.....	115
Table 3.14 Concrete grout in-direct tension test results.....	115
Table 3.15 Tyfo® SCH-11UP carbon fibre sheet dry fibre properties.....	116
Table 3.16 Tyfo® S Epoxy material properties.....	116
Table 3.17 Tyfo® SCH-11UP Composite laminate properties.....	117
Table 3.18 Final testing load application procedure and corresponding moment.....	118
Table 4.1 Finite element modeling calibration values.....	123

LIST OF FIGURES

	Page
Figure 2.1	Stress vs. strain comparison for various reinforcing materials... 125
Figure 2.2	DT-41 girder reinforcement details..... 125
Figure 2.3	DT-100 girder reinforcement details..... 126
Figure 2.4	DT-102A girder reinforcement details..... 126
Figure 2.5	DT-41 girder CFRP layout..... 127
Figure 2.6	DT-100 girder CFRP layout..... 127
Figure 2.7	DT-102A girder CFRP layout..... 128
Figure 2.8	DT-41 girder barrier load application..... 129
Figure 2.9	DT-100 girder barrier load application..... 130
Figure 2.10	DT-102A girder barrier load application..... 131
Figure 2.11	Condition of DT-41 girder after loading completion..... 132
Figure 2.12	Crack pattern of DT-41 girder after load removal..... 132
Figure 2.13	Condition of DT-102A girder during loading..... 133
Figure 2.14	Crack pattern of DT-102A girder near the support location..... 133
Figure 2.15	DT-100 girder after ultimate failure loading..... 134
Figure 2.16	Close up of severed prestressing tendons of the DT-100 girder. 134
Figure 3.1	AASHTO Type III girder cross sectional dimensions..... 135
Figure 3.2	A typical stress-strain curve for the 34.5 MPa Type III girder concrete..... 135
Figure 3.3	AASHTO Type III girder reinforcement details..... 136
Figure 3.4	AASHTO Type III girder slab reinforcement details..... 136
Figure 3.5	A typical stress-strain curve for the 400 MPa reinforcing steel.. 137
Figure 3.6	AASHTO Type III girder prestressing steel details..... 137
Figure 3.7	AASHTO Type III girder longitudinal section details for stirrups and tendons..... 138
Figure 3.8	A typical stress-strain curve for 1860 MPa prestressing steel.... 139
Figure 3.9	Existing cracks as delivered to test site (mapped by MTO)..... 140
Figure 3.10	Existing cracks due to accident impact..... 141

Figure 3.11	CFRP orientation for longitudinal and cross section.....	142
Figure 3.12	Cross section view of CFRP orientation.....	143
Figure 3.13	Formwork for the east and west foundations and support walls.	143
Figure 3.14	Close up of west foundation and support walls.....	144
Figure 3.15	West foundation and support walls after removal of formwork.	144
Figure 3.16	Arrival of AASHTO Type III prestressed concrete girder.....	145
Figure 3.17	View of the girder over the steel pedestal.....	145
Figure 3.18	View of steel bracing to guard against lateral movement.....	146
Figure 3.19	Location of preliminary testing instrumentation	146
Figure 3.20	Loading during preliminary testing.....	147
Figure 3.21	Comparison of preliminary testing results in the elastic range...	147
Figure 3.22	Moment vs. deflection with camber for the Type III girder.....	148
Figure 3.23	Moment vs. deflection, without camber, for the Type III girder.	148
Figure 3.24	Comparison of pre and post grouting for the north face.....	149
Figure 3.25	Comparison of pre and post grouting for the south face.....	149
Figure 3.26	Comparison of pre and post grouting for bottom flange underside.....	150
Figure 3.27	Core testing of the Concrete Top Supreme grout.....	150
Figure 3.28	Core testing of the Verticoat Supreme grout.....	151
Figure 3.29	Full view of girder upon completion of sandblasting.....	151
Figure 3.30	View of two girder sections after sandblasting procedures.....	152
Figure 3.31	Component A and B resin mix for Tyfo® S Epoxy.....	152
Figure 3.32	Component A and B resin mix for Tyfo® TC Epoxy.....	153
Figure 3.33	Comparison at midspan: First application of Saturant Epoxy....	153
Figure 3.34	Comparison at midspan: First application of Tack Coat Epoxy.	154
Figure 3.35	Comparison at midspan: First layer of CFRP U-wrap.....	154
Figure 3.36	Comparison at midspan: Longitudinal anchor strips and second CFRP U-wrap layer.....	155
Figure 3.37	Comparison at midspan: Completion of CFRP system.....	155
Figure 3.38	First layer of CFRP U-wraps on one half the girder.....	156
Figure 3.39	First application of Saturant Epoxy.....	156

Figure 3.40	First application of Tack Coat Epoxy.....	157
Figure 3.41	Saturant and Tack Coat Epoxy application on a girder section..	157
Figure 3.42	Completion of first CFRP U-wrap layer on entire girder.....	158
Figure 3.43	First and second CFRP U-wrap layers with longitudinal anchor strips.....	158
Figure 3.44	Completion of one full layer of the CFRP system for entire girder length.....	159
Figure 3.45	Completion of entire CFRP system.....	159
Figure 3.46	Bottom and top chamfers after CFRP strengthening.....	160
Figure 3.47	Bottom flange underside after CFRP strengthening.....	160
Figure 3.48	CFRP anchoring to lateral support locations.....	161
Figure 3.49	Fully completed CFRP strengthened girder.....	161
Figure 3.50	Full view of fully completed, CFRP strengthened girder.....	162
Figure 3.51	Data acquisition system test control software SYSTEM 6000...	162
Figure 3.52	Final testing instrumentation location for LVDTs and PI gages.	163
Figure 3.53	Strain gages and LVDTs on top slab.....	163
Figure 3.54	Strain gage placement on south and north girder faces.....	164
Figure 3.55	Strain gages on the underside of the bottom flange.....	164
Figure 3.56	LVDTs setup for lateral deflection.....	165
Figure 3.57	PI gages setup on the top slab and underside of bottom flange..	165
Figure 3.58	Final testing instrumentation location for strain gages.....	166
Figure 3.59	Mechanical dial gages, at supports, for bearing pad and foundation settlement.....	166
Figure 3.60	Torsion supports near midspan, and at support.....	167
Figure 3.61	One ton block dimensions.....	167
Figure 3.62	Jersey barrier dimensions.....	168
Figure 3.63	Barrier deposit.....	169
Figure 3.64	One ton block deposit.....	169
Figure 3.65	Barriers and one ton blocks at girder test site.....	170
Figure 3.66	First row of loading: one ton blocks.....	170
Figure 3.67	Nearing completion for the first row of loading.....	171
Figure 3.68	Second row of loading, and positioning.....	171

Figure 3.69	Nearing completion of the second row of loading.....	172
Figure 3.70	Completion of first two rows of one ton block loading.....	172
Figure 3.71	Third and fourth rows of loading: one ton blocks.....	173
Figure 3.72	Nearing completion of third and fourth rows of loading.....	173
Figure 3.73	Installation and layout of wooden posts for barrier stability.....	174
Figure 3.74	Completion of all loading concerning the one ton blocks.....	174
Figure 3.75	Placement of first Jersey barrier.....	175
Figure 3.76	Jersey barrier loading on one half the girder span.....	175
Figure 3.77	Midspan view of final loading configuration.....	176
Figure 3.78	Final loading.....	176
Figure 3.79	Elevation view of final loading configuration.....	177
Figure 3.80	Cracks at midspan portion on south and north faces.....	177
Figure 3.81	Web section near midspan, south face.....	178
Figure 3.82	Web section near midspan on south face, and bottom flange at midspan on north face.....	178
Figure 3.83	Crack propagation through epoxy on south face.....	179
Figure 3.84	South face cracks on bottom flange.....	179
Figure 4.1	Newton's method for tangent stiffness determination.....	180
Figure 4.2	Moment-deflection curves for the Type III girder for various tension stiffening values.....	180
Figure 4.3	Enlarged view of Figure 4.2 in the nonlinear range for clarity..	181
Figure 4.4	Finite element mesh for the DT-41 girder.....	181
Figure 4.5	Finite element mesh for the DT-100 girder.....	182
Figure 4.6	Finite element mesh for the DT-102A girder.....	182
Figure 4.7	Finite element mesh for the Type III girder.....	183
Figure 4.8	Typical stress vs. strain curve for concrete.....	183
Figure 4.9	Stress-strain relationship for plain concrete.....	184
Figure 4.10	Plane stress failure surfaces for concrete.....	184
Figure 4.11	Shear retention model for reinforced concrete.....	185
Figure 4.12	Tension stiffening model; reinforced concrete.....	185
Figure 4.13	Typical stress vs. strain curve for steel.....	186

Figure 4.14	Idealized stress-strain relation for steel.....	186
Figure 4.15	Typical stress vs. strain curve for prestressing steel.....	187
Figure 4.16	Riks method application.....	187
Figure 5.1	Crack mapping due to final test loading.....	188
Figure 5.2	Moment vs. vertical deflection for Type III girder.....	189
Figure 5.3	Moment vs. lateral deflection for Type III girder.....	190
Figure 5.4	Moment vs. slab strain for Type III girder.....	191
Figure 5.5	Moment vs. top flange strain for Type III girder	192
Figure 5.6	Moment vs. top chamfer strain for Type III girder	193
Figure 5.7	Moment vs. top web strain for Type III girder	194
Figure 5.8	Moment vs. mid web strain for Type III girder	195
Figure 5.9	Moment vs. bottom web strain for Type III girder	196
Figure 5.10	Moment vs. bottom chamfer strain for Type III girder	197
Figure 5.11	Moment vs. bottom flange underside strain for Type III girder..	198
Figure 5.12	Moment vs. PI gage strain for Type III girder	199
Figure 5.13	Moment vs. settlement for Type III girder	200
Figure 5.14	Cross sectional Type III girder strain at 500 kN·m.....	201
Figure 5.15	Cross sectional Type III girder strain at 1000 kN·m.....	201
Figure 5.16	Cross sectional Type III girder strain at 1500 kN·m.....	202
Figure 5.17	Cross sectional Type III girder strain at 2000 kN·m.....	202
Figure 5.18	Cross sectional Type III girder strain at 2500 kN·m.....	203
Figure 5.19	Cross sectional Type III girder strain at 3000 kN·m.....	203
Figure 5.20	Cross sectional girder strain, at midspan, for various values of moment.....	204
Figure 5.21	Cross sectional girder strain, on CFRP, for various values of moment.....	205
Figure 5.22	DT-41 girder verification of modeling results in the linear-elastic range.....	206
Figure 5.23	DT-100 girder verification of modeling results in the linear-elastic range.....	207
Figure 5.24	DT-102A girder verification of modeling results in the linear-elastic range.....	208

Figure 5.25	Type III girder verification of modeling results in the linear-elastic range.....	209
Figure 5.26	DT-41 moment-deflection relation for different CFRP element types.....	210
Figure 5.27	DT-41 moment-strain relation between experimental and finite element findings.....	211
Figure 5.28	DT-100 moment-strain relation between experimental and finite element findings.....	212
Figure 5.29	DT-102A moment-strain relation between experimental and finite element findings.....	213
Figure 5.30	Type III girder moment-deflection relation for finite element models exhibiting constant and varying prestress.....	214
Figure 5.31	Type III girder moment-strain relation for finite element models exhibiting constant and varying prestress.....	215

ABBREVIATIONS

AASHTO	American Association of State Highway and Transportation Officials
ACI	American Concrete Institute
ACIC	American Concrete Institute Committee
CFRP	Carbon Fibre Reinforced Polymer
CHBDC	Canadian Highway Bridge Design Code
CPCI	Canadian Prestressed Concrete Institute
DOF	Degree of Freedom
DT	Double-Tee
FEM	Finite Element Method
FRP	Fibre Reinforced Polymer
GTT	Glass Transition Temperature
ISIS	Intelligent Sensing for Innovative Structures
LVDT	Linear Variable Displacement Transducer
MTO	Ministry of Transportation Ontario
RC	Reinforced Concrete
S Epoxy	Saturant Epoxy
SG	Strain Gage
TC Epoxy	Tack Coat Epoxy
TCS	Test Control Software
WWF	Welded Wire Fabric

NOTATION

β	Angle between inclined FRP stirrups and longitudinal axis of member
β	Target reliability index
β_1	Stress block factor
ε	Strain, L/L
ε_{ci}	Initial concrete strain, L/L
ε_{cu}	Ultimate strain for concrete, L/L
ε_{cp}	Ultimate strain for epoxy resin, L/L
$\varepsilon_{frp,bot}$	Strain at the bottom chamfer FRP location, L/L
ε_{frpe}	Effective strain of FRP reinforcement, L/L
$\varepsilon_{frp,top}$	Strain at the top chamfer FRP location, L/L
ε_{frpu}	Ultimate strain of FRP reinforcement, L/L
ε_{pi}	Initial prestressing steel strain, L/L
ε_{pu}	Ultimate prestressing steel strain, L/L
ε_{si}	Initial tensile steel strain, L/L
ε_u	Rupture strain, L/L
$\varepsilon_{u,comp}$	Ultimate strain for fibre reinforced polymer composite system, L/L
$\varepsilon_{u,frp}$	Ultimate strain for fibre reinforced polymer, L/L
ε_y	Yield strain, L/L
α	Reduction coefficient for the effective strain
α_D	Dead load resistance factor
α_L	Live load resistance factor
α_1	Stress block factor
λ	Load proportionality factor
λ_1	Coefficient for the effective strain expression
λ_2	Coefficient for the effective strain expression
$\Delta\lambda_{in}$	Preliminary load proportionality factor
ρ	Ratio of non-prestressed reinforcement, (A_s / bd)

ρ'	Ratio of compression reinforcement, (A'_s / bd)
ρ_{frp}	Ratio of FRP reinforcement
ρ_p	Ratio of prestressed reinforcement, (A_p / bd_p)
σ	Stress, F/L^2
ϕ	Load resistance factor
μ	Shear retention factor
μ_{close}	Shear retention factor for a reduced shear modulus as a crack closes
γ_c	Mass density of concrete, M/L^3
γ_{frp}	Mass density of fibre reinforced polymer, M/L^3
γ_p	Factor accounting for shape of stress-strain relationship of prestressing steel
A	Area, L^2
A_{frp}	Cross sectional area of FRP material, L^2
$A_{frp,bot}$	Cross sectional area of FRP material located on the bottom chamfer, L^2
$A_{frp,top}$	Cross sectional area of FRP material located on the top chamfer, L^2
A_p	Cross sectional area of prestressing steel, L^2
A_s	Cross sectional area of tensile steel, L^2
A_v	Cross sectional area of stirrup legs, L^2
a	Depth of equivalent rectangular compression stress block, L
b	Width of extreme top fibre member, L
b_w	Width of web, L
C_c	Internal force due to compression in concrete, F
C_f	Correction factor
c	Distance from extreme compression face to neutral axis, L
D	Nominal unfactored dead load presence in consideration
d	Distance from extreme compression fibre to centroid of non-prestressed reinforcement, L
d_{frp}	Distance from extreme compression fibre to centroid of FRP, L
$d_{frp,bot}$	Distance of extreme compression fibre to centroid of bottom chamfer FRP, L
$d_{frp,top}$	Distance of extreme compression fibre to centroid of top chamfer FRP, L

d_p	Distance from extreme compression fibre to centroid of prestressed reinforcement, L
E_c	Modulus of elasticity of concrete, F/L^2
E_{comp}	Modulus of elasticity of fibre reinforced polymer composite system, F/L^2
E_{ep}	Modulus of elasticity of epoxy resin, F/L^2
E_{fip}	Modulus of elasticity of fibre reinforced polymer, F/L^2
E_{girder}	Modulus of elasticity of the Type III girder concrete, F/L^2
E_p	Modulus of elasticity of prestressing steel, F/L^2
E_s	Modulus of elasticity of reinforcing steel, F/L^2
E_{slab}	Modulus of elasticity of the Type III girder overlying concrete slab, F/L^2
e_c	Eccentricity of prestressing steel at midspan, L
e_c	Eccentricity of prestressing steel at support, L
F	Live load capacity factor
F	Width dimension for load distribution, L
F_m	Amplification factor
F_{pe}	Effective working force in prestressing strand after all losses, F
F_{pi}	Initial strand force, F
F_{pu}	Minimum ultimate tensile strength of prestressing steel, F
F_u	Ultimate tensile strength of reinforcing steel, F/L^2
F_y	Yield strength of reinforcing steel, F/L^2
f'_c	Compressive 28-day strength of concrete, F/L^2
f_{pe}	Effective stress in prestressing strand after all losses, F/L^2
f_{pi}	Initial strand stress, F/L^2
f_p	Prestressing steel stress, F/L^2
f_{pu}	Ultimate tensile strength of prestressing steel, F/L^2
f_{py}	Yield strength of prestressing steel, F/L^2
f_u	Ultimate tensile strength of reinforcing steel, F/L^2
$f_{u,comp}$	Ultimate tensile strength of fibre reinforced polymer composite system, F/L^2
$f_{u,ep}$	Ultimate tensile strength of epoxy resin, F/L^2
$f_{u,fip}$	Ultimate tensile strength of fibre reinforced polymer, F/L^2
f_y	Yield strength of reinforcing steel, F/L^2

G	Shear modulus, F/L^2
h	Total of height of a cross section, L
I	Moment of inertia, L^4
jd	Flexural lever arm, L
k	Stiffness, F/L
k_1	Parameter accounting for relative concrete shear strength
k_2	Parameter accounting for FRP ply configuration
L	Nominal unfactored live load presence in consideration
L	Length of girder, L
L_c	Effective anchorage length for FRP shear reinforcement, L
l	Dynamic load allowance factor
l_{period}	Total arc length scale factor
Δl_{in}	Initial increment in arc length
M_{beam}	Moment obtained via simple beam analysis, FL
M_{cr}	Moment value at which the onset of cracking occurs, FL
M_{exp}	Moment achieved experimentally, FL
M_g	Longitudinal moment per girder, FL
$M_{g \text{ avg}}$	Average longitudinal moment per girder, FL
M_n	Nominal flexural strength, FL
M_T	Maximum longitudinal moment per design lane, FL
M_u	Ultimate flexural strength, FL
N	Number of longitudinal girders or beams in a bridge deck width
n	Modular ratio
n	Number of design lanes
n_c	Number of free ends of an FRP stirrup on one side of a member
P_o	Existing load magnitude at beginning of a Riks step, F
P_{ref}	Load magnitude of the reference loading in a Riks step, F
P_{total}	Current load magnitude in a Riks step, F
p	Pressure stress, F/L^2
q	Deviatoric stress, F/L^2
R	Ratio of FRP effective strain to ultimate tensile strain

R	Nominal unfactored resistance
R_L	Modification factor for multi-lane loading
S	Center-to-center girder spacing, L
s	Spacing, L
s_{frp}	Spacing of FRP shear reinforcement along longitudinal axis of member, L
T_{frp}	Internal tensile force in carbon fibre reinforcement, F
$T_{frp,bot}$	Internal tensile force in carbon fibre reinforcement at bottom chamfer, F
$T_{frp,top}$	Internal tensile force in carbon fibre reinforcement at top chamfer, F
T_p	Internal force due to tension in prestressing steel reinforcement, F
T_s	Internal force due to tension in steel reinforcement, F
t	Thickness, L
t_{comp}	Thickness of fibre reinforced polymer composite system laminate, L
t_{frp}	Total thickness of FRP reinforcement, L
U	Resistance adjustment factor
u	Displacement, L
V_c	Nominal shear strength provided by concrete, F
V_{frp}	Nominal shear strength provided by FRP, F
V_n	Nominal shear resistance of a section, F
V_p	Nominal shear strength provided by the longitudinal prestressing tendons, F
V_s	Nominal shear strength provided by stirrup / web reinforcement, F
ν	Poisson's ratio
W_c	Width of design lane, L
w	$\rho (f_y / f'_c)$
w'	$\rho' (f_y / f'_c)$
w_{frp}	Width of FRP shear reinforcement, perpendicular to fibres, L
y_b	Centroid of a material from the extreme tensile face, L
$y_{b,frp,bot}$	Centroid of bottom chamfer FRP material from the extreme tensile face, L
$y_{b,frp,top}$	Centroid of top chamfer FRP material from the extreme tensile face, L
[B]	Strain displacement matrix
[E]	Elasticity matrix

$[F]$	Force vector
$[K]$	Stiffness matrix
$[K_i]$	Stiffness matrix for i^{th} cycle
$[K_o]$	Initial tangent stiffness matrix
$[K]_i$	Stiffness matrix for an individual element i
$[K_{i-1}]$	Tangent stiffness matrix after previous step
$[P]$	Load matrix
$[P_i]$	Load matrix for i^{th} cycle
$[P_{i-1}]$	Load equilibrium matrix after previous step
$[P_o]$	Initial load matrix
$[U]$	Displacement or degrees of freedom matrix
$[U_i]$	Displacement matrix for i^{th} cycle
$[U_{i-1}]$	Displacement matrix after previous step
$[U_o]$	Initial displacement matrix

1.0 INTRODUCTION

1.1 GENERAL

Currently in Canada, more than 40% of bridges in use were constructed over 30 years ago (Canadian Network of Centres of Excellence on Intelligent Sensing for Innovative Structures, 2001). As is expected in Canada's harsh and diverse climate, a large significant number of these bridges are in dire need of some sort of rehabilitation all across the country. The main culprit, being deterioration or corrosion due to de-icing salts and freeze-thaw cycles from season to season, as well as overweight truck loads, is evident throughout Canada, exemplified in parking garages and concrete and steel bridges. To make matters worse, an increase in loads over the life of a structure as well as constantly altered design codes, are rendering many structures outdated, inadequate based on current standards, and obsolete.

In all of North America, most bridges are subjected to biannual inspections. In the United States alone, more than one third of highway bridges are deemed substandard in one mode or another (Tavakkolizadeh and Saadatmanesh, 2003). According to the National Bridge Inventory, there are approximately 81,000 in service obsolete bridges. In essence, a major infrastructure problem is on the rise.

So what is to be done? Rebuilding any structure takes a large amount of time, human resources, planning and money, not to mention the inconvenience and possible hazards

to public life. But are they, or is it, worth rebuilding? The answer is yes, if financial funds are endless. However, when funding for structure replacement is not available, a probable solution lies in the use of FRPs, known as Fibre Reinforced Polymers.

Fibre reinforced polymers contain high-resistance fibres embedded in a polymer resin, and are produced as sheets, plates and laminates. They are of high strength and are extremely light weight, about one fifth the weight of steel, and are versatile in many applications. They offer resistance to corrosion, are durable, and relatively easy to apply. The initial higher expenditure of the FRP system and materials are soon offset by their low installation, and maintenance costs.

Conventionally, any structure which needed any form of rehabilitation was to undergo a series of activities in order to be deemed appropriate. To do so, a section or the entire bridge, for example, was cordoned off and work begun. This partial or full closure, may cause drastic traffic delays and inconvenience to the tax-paying public. Afterwards, any damaged concrete was chipped away or cut out, cleaned of debris and patching commenced. This proved to be quite costly, inconvenient, and possible of offering only partial assistance. The rate of continued deterioration, in years to come, still remained high.

The use of carbon fibre reinforced polymers is not only more cost effective and efficient, but it also provides a considerable value of protection and rehabilitation for a relatively low cost. It is an adaptive solution, where its method is not solely specific to

only one application. CFRP rehabilitation may be applied to concrete and steel bridges, columns and beams, applied as laminates or sheets, and in many diverse configurations.

The research presented in this thesis dictates a preliminary, yet stable, unwavering and proven solution to depreciating infrastructure all over the world, where a balance between economics and construction, and safety and national development are at the foreground.

1.2 THE DILEMMA

The continuing severe weather that structures of all sorts are subjected to in Canada, is becoming a threat to infrastructure well being and longevity. De-icing chemicals, such as road salts, accelerate and inflame the detriments to corrosive environments. Corrosion cases began appearing in Canada in the early 1960s, primarily in steel reinforced concrete in highway bridges (American Concrete Institute Committee, ACIC, 1996). It is due to this corrosive atmosphere that expansion is caused allowing foreign harmful substances to interact with reinforcing steel and structural concrete, deteriorating the structure and leading to a lower level of structural stability.

The first methods of treatment included a galvanized coating to reinforcing steel bars. This quickly became non-preferable because of the electrolytic reaction between the steel and zinc coating, leading to further corrosion. Other techniques used were design-based, for example: lowering concrete permeability and the use of mix additives.

Epoxy coated rebars were also first introduced as a remedy to this problem in the early 1970s (ACIC, 1996).

The method of choice that is rapidly becoming more main stream is the use of fibre reinforced polymers, throughout the world, in many applications. A few decades ago, the FRP technology was still in its infant state, while today in age they offer an alternative to certain aspects in almost every type of project, and keeping up to date with publications is becoming near impossible (Teng et al., 2002).

Strengthening, rehabilitating and retrofitting are all possible to a high degree of confidence via the FRP system. The need for maintaining and upgrading aging infrastructure, becoming ever so popular, is made effortless because of the reduction in cost, enhanced durability, and high strength offered by FRPs.

All the research conducted on the use of FRP technology in bridge girder strengthening involved laboratory scale models. This research has resulted in few FRP codes and specifications in North America. However, many bridge authorities, contractors and consulting engineers are still not satisfied and do not have enough confidence in this material, as of yet. What is presented in this thesis provides a new shift from laboratory testing to actual-size field projects, where it can be established just how practical and useful these revolutionary FRP materials can be to full-scale damaged structures. In this thesis, the computer modeling of the load-history of a damaged girder, before and after rehabilitation, will provide engineers with a reliable and economical tool to

examine similar cases of damaged structures, without going into repeated cycles of costly experiments.

1.3 OBJECTIVES

The main intentions of this research are:

- (1) Detailing the structural rehabilitation, using FRP technology, of an AASHTO Type III precast pretensioned concrete bridge girder, recently damaged when struck by a truck.
- (2) Testing the rehabilitated girder under increasing gravity loading to assess the efficiency of the proposed rehabilitation scheme in regaining any lost structural capacity.
- (3) Conducting a verification study computer simulation, using the nonlinear finite element technique, of three full-scale damaged double-tee precast pretensioned concrete girders, recently rehabilitated and tested to collapse. This would help establish a finite element model capable of predicting the load-history of an FRP strengthened girder of similar characteristics, which will assist in creating the Type III girder finite element model.
- (4) Performing a computer simulation, using the nonlinear finite element technique, for the Type III girder, before and after rehabilitation, and calibrating the model with the experimental findings so that a reliable computer model can be established for similar future rehabilitation proposals.

1.4 SCOPE OF RESEARCH

The scope of this thesis revolves around a damaged concrete prestressed girder. The girder was the exterior girder of a two lane, slab-on-girder underpass for Mitchell Road. The bridge allowed north and southbound traffic to cross over Highway 401 in Kingston, Ontario, just north of Toronto. The girder was struck and impaired by a dump truck which had its hydraulic box lift up unexpectedly and involuntarily, while travelling on Highway 401 westbound. The girder was removed and taken to a test site in Toronto, strengthened with FRPs, tested, and its response evaluated.

The FRP configuration used was appropriate for a gain in shear and flexure capacity, being placed as U-wraps and longitudinal strips for the full length of the AASHTO Type III I-girder. Uni-directional Tyfo® SCH-11UP composite was used, along with Tyfo® S Epoxy.

The finite element models developed in this thesis are for the sole purpose of verifying and simulating results of this specific test and others from past demonstration projects. Results and methods presented, are explicit to the circumstances at hand, and may be used with vigilance, as guides to future research and rehabilitation projects.

1.5 CONTENTS AND ARRANGEMENT OF THESIS

In order of appearance, the literature review of the study, offering an insight to the FRP system, as well as previous work compiled and related to this topic, is situated in Chapter II. The following, Chapter III, sheds light on the experimental portion of the

project, both preliminary examination as well as the final loading test. It also includes the carbon fibre fabric installation procedure. The finite element model, calibration, verification and comparison are discussed in Chapter IV. Also explored is the finite element program ABAQUS, the nonlinear modeling technique and idealization and discretization of elements. Chapter V presents the final testing results and comments on the degree of comparison to the finite element model. Chapter VI summarizes the findings of this research, outlines conclusions reached, and sets recommendations for further future research.

After the body of the report, all relevant tables and figures have been placed, followed by an Appendices. They represent structural drawings, material properties and tables, experimental graphs and charts, the finite element analysis input files, and conclude with the final appendix containing manual calculations.

2.0 LITERATURE REVIEW

2.1 GENERAL

The recent advent of the use of fibre reinforced polymers (FRP), although successful already in its early stages, has yielded a limited amount of research material dedicated to its purpose. As versatile as FRPs have been, used in projects ranging from retrofitting, rehabilitation, strengthening and for durability concerns, there seems to be a lack of experimental studies conducted on full-scale structural members. The main objective of this literature review is to obtain a general understanding for the behaviour of FRPs in a wide range of applications. This information will aid in the creation of a finite element model, discussed in the proceeding chapters, and assist to better comprehend possible experimental and analytical outcomes with minimal difficulty. To assist in the classification of project application types in regards to the use of FRPs, the following definitions are provided (Chen, 2000):

- *Maintenance* - The technical aspect of the upkeep of a structure or structural element; it is preventative in nature. Maintenance is the work required to keep a structure in its present condition and to control potential future deterioration.
- *Rehabilitation* - The process of restoring a structure to its original service level.
- *Repair* - The technical aspect of rehabilitation; action taken to correct damage or deterioration on a structure or element to restore it to its original condition.
- *Retrofitting* - The process of upgrading an older, existing structural system or member in accordance with present day standards.

- *Stiffening* - Any technique that improves the in-service performance of an existing structure and thereby eliminates inadequacies in serviceability (such as excessive deflections, excessive cracking, or unacceptable vibrations).
- *Strengthening* - The increase of the load carrying capacity of an existing structure by providing the structure with a service level higher than the structure originally had.

Before a bridge, or any other structure for that matter, is to be replaced, an impact study must be compiled to discover whether repair or retrofitting is an option. Rehabilitation, repair cost and time are far less than those of replacement methods.

Many rehabilitation techniques exist. Among the most common are: (1) member strengthening, (2) addition of members, (3) composite action development, (4) producing continuity at support locations, and (5) post-tensioning (Tavakkolizadeh and Saadatmanesh, 2003). All the above mentioned techniques work well, yet require heavy machinery, possible closure of the structure, and are significantly costly. The exceptional mechanical and physical properties of fibre reinforced fabrics allow them to be a far superior candidate for the strengthening, retrofitting and rehabilitation of almost any structure or structural component.

2.2 EVOLUTION OF FIBRE REINFORCED POLYMERS

In Canada, as past infrastructure continues to age, a significant number of these structures are developing an urgent need for strengthening or rehabilitation. The reason for the existence of this situation is due to the fact that, although being constructed mainly in the economic boom of the 1960s and 1970s, many structures are slowly deteriorating. Ranging from bridges to parking structures, the main cause of this ongoing structural decline is the range of extreme climate and use of de-icing salts. Also contributing, are the increasing service loads on structures, and the more inflexible building and design codes, continually updated and revised. This, in some instances, renders existing structures obsolete and unfit for today's society.

The introduction of FRPs to the engineering world has helped shed new light and meaning on the rehabilitation and strengthening of structures. In turn, this is helping save valuable economic funds, increase productivity, prolong structure life and ultimately maintaining an elevated level of safety and comfort.

Although fairly new to masses of the engineering realm, the use of fibre reinforcement can be primitively traced back to 3000 B.C., where ancient Egyptians used straw to reinforce bricks made from mud. It was in the early 1950s that the first application of FRPs was implemented in aerospace engineering, where light weight and high strength materials are an imperative. The first civil engineering function of FRPs occurred in 1968, in Benghazi, Libya, incorporated on a dome type structure (Mair, 1999).

Fibre reinforced polymers belong to a category of materials referred to as *composite* materials. They consist of two or more materials that, when combined, retain their respective chemical and physical characteristics and work in unison, allowing the properties of each material to be utilized to their greatest effect (Mair, 1999).

Fibre reinforced polymers are made up of high resistance fibres which are embedded in a polymer resin. They are produced as sheets, laminates and plates. Their advantage in becoming the material of choice in strengthening and rehabilitation applications, is due to being light weight, high strength, and resistant to corrosion. Aside, they are immensely durable and relatively easy to apply, and exhibit a linear-elastic response to axial loading (Chung, 2002). These special and unique properties are making FRPs an attractive solution to projects all over the globe, being put into practice in a wide spectrum of practical applications.

The methodology behind the use of FRPs, is to orient the fibres in highly stressed regions in a particular position, direction, and volume. This allows for the obtainment of maximum efficiency from the reinforcement within the member.

FRPs have been used in the aid of column and beam strengthening, seismic retrofitting, corrosion damaged structural elements, bridge decks, piles, roof structures, and prestressed water tanks, to name a few. Adding to the above, FRPs can be and have been used in many regions of varying environmental conditions (Canadian Network of Centres of Excellence on Intelligent Sensing for Innovative Structures, 2001).

As is the case with all structural materials, FRPs too, have their disadvantages. Among such, is the fact that they have been correlated with uncertainty in the civil engineering and construction industry as a direct result of their infrequent use in past years. Research regarding FRPs and their applications are not nearly as frequent or widespread as other common materials, such as concrete and steel. Furthermore, FRPs are associated with brittle behaviour, are susceptible to deformation under long-term loading, may suffer from ultra-violet (UV) and photo degradation by excessive exposure to light, and display poor fire resistance qualities (Chung, 2002).

If FRPs are to become main stream in engineering design, strength and rehabilitation circumstances, and design codes must be made readily available (Canadian Network of Centres of Excellence on Intelligent Sensing for Innovative Structures, 2001). Most recently, there have been a series of guidelines, relative equations and design principles proposed by researchers and industry personnel. Preliminary design manuals have also been composed and recent steel and concrete design codes updated, with more expected to materialize in the near future (Canadian Network of Centres of Excellence on Intelligent Sensing for Innovative Structures, 2001).

2.3 CHARACTERISTICS OF FIBRE REINFORCED POLYMERS

Essentially, the composition of fibre reinforced polymers is a system or conglomeration of materials. The system is comprised of strategically oriented fibre reinforcement, which may be of carbon or glass nature, matched together with epoxy resin, aramid strengthening fibres and a protective coating. The strength of this composite material is

a function of the reinforcing fibres, the matrix and the bond between the two. Each is discussed in further detail in the sections that follow.

2.3.1 Stress–Strain Relationship and Physical Properties

Advantages to the FRP composites are endless, yet the few disadvantages that exist, may be detrimental to their widespread use in all types of industries. Most FRP composites become impaired in a frail, brittle fashion. Like most materials, they too can be subjected to stress concentrations if applied to areas where the adhering structure has holes, notches or cuts attributed with it. Though this may be a deterrent to their use, they do offer many signs when approaching ultimate failure. Among these are: acoustic emissions, cracking, snapping of fibres, resin cracking, a whitening of the surface feature and delamination (Chung, 2002).

Fatigue of FRP occurs gradually, employing failure characteristics as discussed previously. The fatigue strength of an FRP composite is greatly dependent on the properties of the epoxy resin, fibres and laminate quality. Steel generally develops fatigue cracks in tension only, while FRP laminates may experience fatigue fractures in compression and tension. FRP composites may not eliminate crack occurrences, but have been shown to reduce the crack growth rates (Nozaka et al., 2005). The stress-strain relationships for several reinforcing materials are compared in Fig. 2.1.

2.3.2 Fibres

The high tensile strength apparent in FRPs comes primarily from its fibres. They are an integral part of the composite matrix material, amounting to anywhere between 30 to 70% of the material, by volume. Fibres may be oriented in many manners, such as, uni-directional, chopped strand mat, continuous or woven and apply the use of amorphous or crystalline fibre material. The most commonly used fibre types in today's industry are glass and carbon fibres; the latter being of specific importance in this thesis, and thus will be discussed to further detail. In woven composites, aramid fibres are interwoven with the tensile fibres, providing increased strength and stability to the matrix.

Carbon fibres, in comparison to being among the strongest in regards to tensile strength, tend to be brittle and may be conducive to failure at low strain levels. Usually of little importance to construction projects, carbon fibre polymers are electrically conductive. This would be of great implication to note if applied to a structure near power lines, for instance. A great advantage of carbon is that it is not corrosive, but since it is a catalyst for electrolysis behaviour, it may corrode other metals, such as aluminium.

Aramid fibres help to stabilize the composite matrix and increase its strength. Usually of a Kevlar base, they enhance tensile resistance, and fail at higher than normal elongations. Due to their characteristics, they are extensively used primarily for resistance to impact. They exhibit a relatively low density, thus making them attractive for light weight projects.

There are five categories in which carbon fibres may be broken down into, relative to physical properties: general purpose, high strength, ultra high strength, high modulus and ultra high modulus. Besides offering a high value of tensile strength, carbon fibres demonstrate the highest percentage of compressive strength gain than any other fibre type. Studies have proven that carbon fibres have distinct strength advantages over other fibres. Carbon fibres also have a higher modulus of elasticity, broadening their application possibilities (Toutanji, 1998). They are preferred in constant wet-dry environments over any other fibre type, because of their proven ability to withstand such conditions appropriately without compromise to ductility or strength (Toutanji, 1998). Freeze-thaw surroundings, however, have confirmed detrimental damage and deterioration to any fibre type (Toutanji and Balaguru, 1998).

2.3.3 Epoxy

Epoxy for FRP application come in two major forms. The first, thermoplastics, are produced as a common epoxy and then developed into various products afterwards, depending on specifications. Polyolefins, polyamides, vinylic polymer, polyacetals, polysulphones, polycarbonates, polyphenylenes, and polyimides are among the most commonly used thermoplastic epoxies. Their characteristics include being very malleable, and even more so when heated. A cooling process is applied once the desired configuration is achieved, whereby they retain their moulded shape and features. The main advantage of these epoxies is that they can be cast and formed many times with a proper heat-cool cycle, therefore reducing waste and lowering costs.

The second form of epoxy used in conjunction with FRPs is thermoset epoxy. As the name implies, these polymers set or retain their shape upon heating and are not as malleable and formable as the preceding thermoplastic polymers. Polyesters and epoxides are the favourable types of thermoset polymers.

All epoxy composites are mixed on site, at proper temperature and ambient conditions and in the correct ratio. Small quantities are mixed to ensure that no left over epoxy remains and to allow for ample placing time. Any resin that exceeds placing time should not be used, since its viscosity may elevate and adversely affect penetration or fibre saturation (Canadian Network of Centres of Excellence on Intelligent Sensing for Innovative Structures, 2001).

2.3.4 Protective Coatings

Once the surface of the FRP has dried, a protection system may be implemented. This protective coating is of an inert nature to the FRP and may be a paint like coating. It is allowed to dry for a period of at least 24 hours under favourable conditions. This gives the FRP system added protection against the elements.

2.3.5 Fire Resistance

Generally, in the past and present, application of the FRP system has been concentrated in areas where resistance to fires was of minimal importance. Currently, the only proven resistance of FRPs to fire is via the use of a fire retardant coating applied after curing is complete, to the surface of the FRP. Most epoxies used, for example, have

combustible properties activated at high temperatures, and if a fire begins, the toxins released are highly carcinogenic and potentially fatal. Furthermore, fibres begin to lose strength and degrade at the onset of a fire. The fibre orientation slowly becomes disoriented, and adherence to the structure surface questionable. The following are of main concern in such situations:

- the reduction of strength and stiffness due to matrix softening,
- loss of bond with underlying structure surface,
- increase in heat generation, leading to material yielding, and
- spalling potential due to the entrapment of water inside the impermeable wrap.

Manufacturer specifications require that any fibre-epoxy composite matrix shall cease to reach temperatures above 70°C for glass fibre systems. This is known as the glass transition temperature (GTT). Surpassing this temperature renders the matrix redundant. Carbon fibres, on the other hand, can withstand temperatures up to 1000°C successfully. Despite this, upon failure of the epoxy at high temperatures, the stress redistribution amongst fibres drastically reduces the tensile strength of the FRP system. It is at temperatures in the region of 200°C that the epoxy's strength is reduced to the point where its chief intention, to ensure composite action between the application surface and the fibre matrix, is greatly compromised. Literature suggests, that the increase in strength to a structure or element due to FRPs, may be unrecoverable in as little as 15 to 30 minutes upon commencement of a fire (Canadian Network of Centres of Excellence on Intelligent Sensing for Innovative Structures, 2001).

2.3.6 Storage and Handling

In order to ensure the integrity of the material, a clean, dry and sun free area must be chosen for storage of FRPs and epoxy. The area must be adequately ventilated and temperature controlled if need be. Any catalysts, initiators or flammable materials or substances are to be kept in safe distance with the material. The approximate shelf life for FRPs and epoxy is ten years (temperatures $< 38^{\circ}\text{C}$), and two years (4°C to 32°C), respectively.

Special care is to be exercised when handling the epoxy materials especially. All necessary equipment is to be worn (gloves, safety glasses, respiratory protection, etc.) and necessary precautions taken.

2.4 DESIGN WITH FIBRE REINFORCED POLYMERS

Unlike many commonly used materials in engineering practice, fibre reinforced polymer composites are not isotropic; that is, they do not have the same properties in all directions. A perfect example of a non-isotropic, or anisotropic, material is wood, being much stronger along the grain, than against it. Among other differences is that composite materials lack a definitive yield, and have a low value of shear modulus.

2.4.1 Creation Process

Composites are not created as metals are, for example, from an initial manufacturing stage. They are created as components and assembled to form a material. Different shapes, sizes and configurations may be developed, as well as quantity and

performance. Composites used may be an 'off the shelf' type, as standard structural steel shapes are, or custom made to fit a specific requirement.

2.4.2 Anisotropic Nature

Anisotropic materials, as defined earlier, have differing properties in all directions. If a fibre composite, composed of uni-directional fibres slightly off axis, is loaded in tension, the composite would deform in the direction of the force and in shear, across the fibres. This may introduce premature failure, or a rotation out of plane. In order to ward off such an occurrence, some composites imply the use of directional reinforcements, such as aramid, as a woven fabric. These reinforcements are isotropic in nature.

2.4.3 Material Properties

Composite materials fail to display a distinct yield region on their stress-strain curve. For instance, if the sheet metal of a vehicle fender were impacted hard enough, a permanent deformation would be anticipated. If the same dimension sheet, made of FRP, were impacted one could expect it to regain its shape due to its elasticity. If hit hard enough, the FRP section would illustrate local damage, star crazing and or delamination, and may once more return to its usual form (Chung, 2002).

Local yielding in composites is not clearly defined; opposite is the case of the design of steel elements, where any stress concentrations are relieved in the steel as it yields. In

the case of FRPs, any stress build up would not dissipate, and ultimately lead to failure (Chung, 2002).

The elastic modulus and shear stiffness is less for some composites, as in glass fibres, as opposed to other materials. In design, deflection and buckling requirements are of great importance.

2.5 INSTALLATION OF FIBRE REINFORCED POLYMERS

Installation may differ slightly from contractor to contractor and engineering specifics for different FRP applications and projects. The following guidelines of the procedure are general, yet vital and commonplace to all circumstances. Even though the rehabilitation of a concrete girder is the focus of this thesis, the subsequent information may be applied to any circumstance with the use of engineering judgement.

2.5.1 Surface Preparation

A material substrate is composed of the original material, or materials used in previous repairs, or both (Canadian Network of Centres of Excellence on Intelligent Sensing for Innovative Structures, 2001). The surface preparation of the structure on which the FRP is to be applied is of utmost importance. If the surface is cracked or deteriorated in any way, concrete removal and replacement, or crack injection, may be necessary. This ensures a better bonding surface. An optimal rough surface, for bonding reasons, is obtained via sandblasting, if required. Sharp corners are to be rounded off to prevent

stress concentrations in the FRP sheets and possible tearing sections. Afterwards, a thorough cleaning of the surface, removing dust and loose material, is performed.

2.5.2 Primer and Putty Application

Where compulsory, primer is applied to the surface where FRPs are to be placed in order to promote bonding and discourage resin permeation into the substrate. The primer shall be of low viscosity and applied at the rate of coverage.

Putty is to be used only to fill voids and to smooth minor surface irregularities. This material is to be a high quality, high viscosity putty. Both primer and putty should be allowed to dry sufficiently before applying other materials.

2.5.3 Fabric Preparation and Application

The FRP may be cut on site, at a clean location near the structure of application, or off site if exact measurements are known. Saturation of the fabric should be uniform, and may be done manually or mechanically. The saturating resin is to have sufficiently low viscosity in order to saturate the fibre thoroughly, but a high enough viscosity to avoid dripping. No air is to be entrapped between composite layers.

When applying FRP sheets, they are carefully placed and air pockets removed. Smoothing is carried out parallel to the fibre direction, from one end to the other. No deviation whatsoever is acceptable upon placement. A difference of only 5 degrees may negotiate the final strength. Any kinks or folds are to be prohibited.

2.5.4 Quality Control Considerations

The curing time shall not be less than 24 hours. Temperature is to be maintained to a desirable degree and condensation strictly prevented. The fabric is to be checked periodically to ensure proper adherence, no sagging or movement occurs and that air bubbles are non existent.

When the cure cycle concludes, a protective coating may be applied, and serves as two functions. This last layer of epoxy acts as a protectant against harmful UV rays and as a sealant layer.

2.6 REVIEW OF RELEVANT LITERATURE

Due to the lack of a vast selection of research material based on FRPs, the following section lists information obtained regarding FRPs, and is used to great value during this thesis. The articles summarized below, not only offer an insight into better understanding FRP behaviour and such, but also provide a stable and effective means to the finite element modeling conducted in this thesis.

2.6.1 Flexure Strengthening and Rehabilitation

The literature written by Bonacci and Maalej in 2001, offers a preliminary yet concise representation and characteristics of the behaviour of reinforced concrete beams strengthened with externally bonded FRPs. The beams were tested primarily for flexure resistance, involving 127 specimens, with data based on failure modes, strength increase and ductility.

The prevalent failure mode proved to be via debonding of the FRP sheets from the surface of the test specimens. A third of the tests showed that strengthening techniques could increase flexure capacity by 50%; this value being greater in some.

The studied specimens were not subjected to prior loading, and hence were in sound structural condition, and thus not fully representative of a realistic situation. The study concluded by mentioning that a more realistic scenario must be implemented for existing field conditions, but did provide useful insight.

Bonacci and Maalej (2000) studied the effect of externally bonded fibre reinforced polymers used in the rehabilitation of corrosion damaged concrete beams. An experimental program, providing evaluation and possible outcome of using FRPs to repair and strengthen reinforced concrete (RC) flexural members, was implemented. Seven short RC beams, measuring 270×400 mm in cross section, and 4350 mm in length, took part in the study. Of the seven, four were reinforced externally with one or two layers of CFRP composite sheets, while the remaining were left without.

The focal point of the study was to determine the state of damage of each beam by introducing damaged induced beams. Although the study was built around corrosion prevention, it stresses the precautions needed to be taken due to the effects of corrosion and superimposed loading on the flexure capacity of beams when a composite FRP is to be used. Aside, the possibility of achieving rehabilitation and resistance to corrosion with externally bonded CFRP remains quite feasible and practical.

A more comparative testing procedure was examined by Fanning and Kelly (2001). Concrete beams, pre-loaded from 30 to 70% capacity, were strengthened and tested for ultimate response. FRP plates and sheets were used, with emphasis on the former. The initial loading subjected the beams to cracking stresses, lower than the yield point of the reinforcing steel, in order to accurately represent a beam in field conditions for some period of time.

Tests signified a shift from widely spread large cracks to narrow and more closely dispersed crack propagations in beams strengthened with FRPs, than in those without. Closer investigation showed that as the FRP layer thickness increased, so did the amount of strengthening. This also led to an increase in peeling or delamination stresses because of the tensile force resultant moving progressively farther away from the concrete surface, as thickness was increased. They concluded that, only adequate, not excessive amounts of FRP, shall be used in all circumstances and with vigilance.

Strength and ductility of reinforced concrete beams repaired with bonded carbon fibre reinforced polymers was studied by Spadea et al. (2001). Three diverse tests were realized, with the use of eleven beam samples, recording ultimate load capacity. Variables considered were longitudinal steel ratio, stirrups and the location and configuration of external anchorages. Results illustrated that with the employment of strengthening with CFRPs, deflection was significantly reduced, and the use of external anchorages allowed any lost ductility to be regained considerably.

Keeping with the flexure aspect in FRP strengthening, De Lorenzis et al. (2001) took this concept one step further. Reinforced concrete beams were reinforced with FRP and tested in flexure. In addition to flexural resistance, laminate bond length, concrete strength, laminate plies and width, as well as substrate and surface preparation, were held as variables. Strain distribution at varying load levels were found to be predicted by use of a linear bond stress-slip relationship, and verified using a simple shear finite element model.

Brena et al. (2003) experimented with different FRP laminate configurations and their effect on increasing flexural capacity of reinforced concrete beams. They aimed at providing a general idea of how to strategically place FRP composite sheets and obtain their advantages to the utmost degree, with minimal compromise to delamination failure. Results indicated that relying solely on the contact area, comprised of the concrete and composite surface, is not ample to eliminate the possibility of debonding. In order to do so, the implementation of transverse sheets or strips was introduced, resulting in a decrease in debonding failures.

The investigation towards the significance of debonding failure at midspan in fibre reinforced polymer-plated concrete beams, was examined by Sebastian (2001). Reinforced concrete beams enhanced in flexure using fibre reinforced polymer plates are susceptible to a brittle form of failure. This failure is characteristic of delamination of the cover concrete layer in direct contact with the bonding adhesive. This debonding was the culprit that allowed the plates to debond away from the beam.

The author stresses that, while previous research persisted that one debonding mode reigned, where concrete delamination progresses from the ends of the plates inwards, there is also an additional potential debonding style. This manner of delamination initiates near flexural cracks, dominant to the midspan regions, and lengthens out towards the ends of the FRP plates.

Full-scale testing of several typical example specimens, established the fact that the debonding action, specific to the latter mode of failure, was prompted by high shear stresses transmitted from the plates through the epoxy adhesive to the substrate concrete. The high values of stress exhibited initially, arised from tension stiffening in the cracked concrete and corrosion of the embedded reinforcing steel. Strain gages placed accordingly for the bonded and exposed surfaces of the plates quantified these results.

Incorporating the strengthening of a prestressed concrete girder with FRPs is the article written by Harraq et al. (2002). Due to the very nature of prestressed concrete, such members may be under adverse stresses even before service loading takes place. Loss of prestress, damage to structural components and increased loading all contribute to the instability of a structure or beam.

Seven half-scale standard CPCI 900 pretensioned bridge girders were tested; five of which had FRP sheets applied to their exterior, and two remained without. The addition

of the composite sheets was shown to be able to provide an offsetting effect of the losses incurred due to prestress.

2.6.2 Shear Strengthening and Rehabilitation

As a prelude to shear strengthening, Antonopoulos and Triantafillou (2003) presented a basic contribution to the understanding of this setting. The fundamentals of the behaviour of shear-critical exterior reinforced concrete joints strengthened with FRPs, under simulated seismic load, were offered. Likely exceeding the scope of this thesis, the key to the study does not. The main parallel which may be beneficially extracted is the importance of anchorage in high shear regions.

Deniaud and Cheng (2001) explored many different methods of shear design throughout literature. Common shear design methods included are as follows: effective FRP strain, bond mechanism and shear friction approach. Tests were arranged for T-section beams, totalling 16 full-scale specimens. Given credibility by experimental data collected, it became apparent that the mechanical model of the strip method with shear friction approach, gave better approximation of the shear capacity contribution of the FRP system.

The configuration importance of FRP sheets, specific to uni-directional fibres, was presented by Taljsten (2003). The author examined various placement schemes and verified their efficiency, in regards to the consideration of principal directions of shear cracks. Shear failure traditionally begins with combined flexure and shear, followed by

the advent of shear cracks. When CFRP fibres were placed perpendicular to cracks, a large increase in stiffness and strength was observed, as well as brittle failures due to concrete rupture; a direct product of the build up of stress near the ends of the CFRP sheets. When composite sheets were placed obliquely, (slanted or sloped; in a fan like manner), to cracks, an increase in the formerly mentioned parameters was recorded, although considerably less. Failure with off-axis placing was of a more ductile nature and preceded failure warnings, such as snapping of fibres or visible signs of delamination.

In design, it is assumed that the composite fibres only withstand forces along their direction, shear cracks form at 45° angles to the horizontal, and that FRP does not have a definite yield limit, remaining elastic until failure. At times, placing FRP fibres perpendicular to shear cracks may over strengthen a member in shear, and thus is avoided by placing fibres vertical, as is the case with steel reinforcing stirrups.

2.6.3 Strengthening and Rehabilitation for Combined Flexure and Shear

Retrofitting techniques for existing concrete structures are explored by Sheikh et al. (2002). Damaged test specimens engaged the use of carbon and glass FRPs, and then were subjected to ultimate loading. With the use of control testing, or specimens without FRPs, a comparative study was undertaken to assess the degree of retrofitting to each rehabilitated concrete beam. The performed experiment explored the strengthening of beams in both flexure and shear. Observantly so, tests showed that

over reinforcing a beam, say for flexure, would result in an alteration in failure mode, to primarily being due to shear.

Similar to the case at hand, Chaallal et al. (2002) investigated various retrofitting techniques for reinforced concrete bridges. Damage sustained to T-section concrete bridge girders was principally a result of environmental aspects, such as de-icing salts in winter climates. The girders had CFRP sheets adhered to their exterior in shear dominant areas under static loading. It was witnessed that deflection, moment and shear capacity were notably improved in contrast to the control tests.

A full-scale, field testing experiment was described by Labossiere et al. (2000) to assess the structural performance of an existing bridge. The subject bridge was the Sainte-Emelie Bridge in Quebec, which is a single span bridge type, supported by T-section girders. Upon evaluation of the bridge, it was clear that an increase in bending and shear strength was needed to satisfy current loading conditions in the area.

CFRP composite sheets were applied to the underside of the beam for flexure strengthening. Composite fibres were strategically placed parallel to the span. Shear capacity was increased using U-shape wraps, acting similar to steel reinforcing stirrups, the anchoring band or wrap being wide enough to transfer shear stresses to the concrete girders. A series of 1:3 scale tests of T-section beams took place and were compared to reference specimens; without FRP reinforcing. Test showed strength gains upwards of 60% in some cases. The experimental data proved the already known common failure

modes: (1) concrete crushing, (2) steel yielding, followed by concrete crushing, (3) steel yielding, followed by FRP rupture, and (4) debonding of FRP.

In a case similar to that being presented in this thesis, the Blue Heron Bridge, located in Florida, had to be strengthened, after a truck, violating height restrictions, caused severe damage. An article by Shahawy and Okeil (2004) introduced the fundamentals in the use of composite laminate strengthening of damaged concrete girders, using manual calculations for load rating. However, no field testing or finite element modeling were conducted.

Testing variables included number of FRP wraps, size of laminates and configuration. Confirmed was the fact that an increase in CFRP contribution tends to lead to a brittle failure. The use of more laminate layers led to adherence quality issues, rendering, as in the previous case, portions of the CFRP system redundant. Optimization of CFRP arrangement yielded the least amount of material used, in the most beneficial manner, and ultimately higher load capacities.

2.6.4 Finite Element Modeling Techniques

The works compiled by Hu et al. (2004) offered a preliminary and verified design proposal concerning finite element modeling of reinforced concrete beams and FRP. A numerical analysis was carried out, using ABAQUS, to predict the ultimate loading capacity of rectangular reinforced concrete beams strengthened by FRPs.

Nonlinear behaviour of the steel reinforcement was modeled using an equivalent smeared uni-axial material through elements containing reinforcement. The bond-slip effect between the steel-concrete interfaces was neglected. The CONCRETE option, offered in ABAQUS, allowed for concrete representation after the elastic range was surpassed.

Upon cracking of the nonlinear concrete material, the element's ability to continue to carry reduced tensile stresses normal to cracks was approximated using the TENSION STIFFENING option. The post-cracking stage, where shear forces were transferred via aggregate interlock and friction, was replicated by the SHEAR RETENTION option.

FRP lamina layers were considered orthotropic in a plane stress condition and modeled using 4 node shell elements (6 DOF per node). Again, perfect FRP-concrete bonding interaction was assumed. Transverse loading was neglected, and only longitudinal or axial stresses were taken into account.

The sensitivity analysis by Kwasniewski et al. (2000) in regards to slab-on-girder bridges also proved beneficial to this study. A finite element program was carried out to test and validate many significant design altering variables.

The concrete portions were modeled using solid elements, allowing for detailed analysis of local stresses and distributions. Steel sections were modeled using shell elements, with elastic-plastic stress-strain relationships, without hardening for steel, and with

isotropic hardening for concrete in compression and a crack detection surface for tension.

Reinforcement was once again modeled by an equivalent smeared layer within the respective elements. Springs placed at either end of the bridge replicated any elastic constraint for longitudinal displacements and rotations, due to wear of bearings.

Using the finite element modeling technique, Abdalla and Kennedy (1993) ran trials on prestressed concrete beams with openings subjected to static and dynamic loading, for single and continuous span T and I-beam sections. Openings were placed at differing locations and spans, for both section types.

Plane stress elements were employed for the beams. Concrete nonlinearity was reproduced with the ABAQUS software, using the corresponding option, and the TENSION STIFFENING option, made operational to take into account stresses transferred at cracking via the steel reinforcement. Reinforcement, both longitudinal and stirrups, was defined as an element property. They were also modeled as reinforcing rods and governed by the one dimensional strain theory (axial behaviour).

Prestressing strands used solid continuum element sets. The INITIAL CONDITIONS option, along with PRESTRESS HOLD parameters, made possible the application of an initial prestress in the strands due to post-tensioning. The prestress elements were applicable for results in one dimensional loading only.

Making a worthy statement in regards to the application of this thesis, is the article by Ebead and Marzouk (2004). They discuss the benefit, in relation to flexure, of strengthening concrete two-way slabs with carbon fibre reinforced polymer sheets. The strengthened specimens were tested and compared to a reference, non-strengthened slab, to verify any increase in load capacity. Afterwards, a finite element model was created and calibrated using the experimental samples.

Modeling of the CFRP was done so by defining the composite material as a uni-directional, smeared external reinforcement layer. It was then located at the tension surface of the concrete slab. Once again, perfect bonding was assumed to exist between the concrete slab substrate, and the FRP fabric layers.

The article also explored the degree of interference or accordance that tension stiffening plays in the finite element modeling analysis. It defined the tension stiffening effect on concrete by considering two distinct parameters dealing with the post-peak zone only: maximum tensile stress, and tensile strain in the concrete. The report concluded that increasing the tensile strain in the model will decrease the slope of the curve after cracking, thus increasing the stiffness of the concrete in the post-cracking stage.

2.7 REVIEW OF PRIOR DT GIRDER TESTING AND ANALYSIS

In a similar undertaking, three actual-size double-tee (DT) girders were tested (Cofini, 2005 and Sennah et al., 2006). The project dealt with the full-scale testing of these partially damaged, precast pretensioned girders, strengthened in shear and flexure, and

loaded until collapse. Nonlinear finite element models of all three DT girders were created, and experimental results obtained from the above mentioned full-scale testing were used to calibrate the FE analysis.

The following subsections summarize the DT girder geometry, rehabilitation layout and test procedure and results, as obtained in Cofini's M.Eng project (2005).

2.7.1 Geometry of the Tested Double-Tee Girders

There were three different DT girders used, being the standard shapes DT-41, DT-100 and DT-102A, with material properties listed in Table 2.1 to 2.3. The DT-41 girder was of 16,900 mm length, and 3190 mm width, with a slab thickness of 100 mm, and total depth of 810 mm. Welded wire fabric (WWF) mesh was used as reinforcement, for all girders, along with seven, 7 wire strand, 12.7 mm diameter prestressing centric strands per web. The concrete compressive strength was 35 MPa. Consult Fig. 2.2.

The DT-100 and DT-102A girders had lengths of 19,150 mm, and widths of 2415 mm and 3400 mm, respectively. Their slabs measured 100 mm in thickness, their depth 660 mm, and they exhibited five, 7 wire strand, 15.8 mm diameter prestressing centric tendons, per web. The concrete strength specified was 45 MPa. Figure 2.3 and 2.4 exhibit relevant structural information regarding girders DT-100 and DT-102A, respectively.

2.7.2 DT Girder CFRP Layout

All three DT girders had suffered diverse damage. The DT-41 girder had cracks at support locations and midspan. The DT-102A girder had similar defects, only with more cracks apparent at supports and with additional concrete spalling at one support, revealing the reinforcement. Only shear cracks at support locations characterised the level of damage to the DT-100 girder.

CFRP strengthening differed for all three girders. The DT-41 girder was strengthened for shear and flexure, with CFRP configuration on display in Fig. 2.5. Each web was strengthened using U-wrap CFRP uni-directional sheets, covering the midspan portion from the girder quarter points, 400 mm from the bottom side of the webs. Dapped ends, directly over supports, used FRP sheets with fibres arranged vertically and horizontally away from supports, covering the entire depth of the webs. The shear strengthening scheme extended 1550 mm from the exterior support points. CFRP sheets were applied as a one ply system.

The DT-100 girder was strengthened for shear only at support locations, as seen in Fig. 2.6, for a length of 1550 mm extending towards the midspan. CFRP sheets were adhered with fibres oriented vertically for one ply, and then horizontally for the second ply. Each ply covered the entire web depth.

Similar CFRP arrangement was apparent for the DT-102A girder, with layout as described in Fig. 2.7, in comparison to the DT-41 girder. Again, it was strengthened in shear and

flexure. The only dissimilar attribute, was the added ply of composite fibre sheets at the shear strengthened area, with fibres adjusted vertically.

All material properties for the CFRP sheets and adhesives used in the DT girder experimental analysis can be found by citing Table 2.4 to 2.6.

2.7.3 DT Girder Experimental Results

Each girder was loaded incrementally using Jersey barriers, weighing 2200 kg each. The DT-41 girder used a total of 13 barriers, shown in Fig. 2.8. It exhibited major shear-flexure cracks at quarter points (at the ends of the CFRP sheets), significantly beginning with the application of the tenth barrier load. Diagonal cracks were primarily present between these cracks and the midspan, with irregular spacings of 150 to 450 mm. Delamination of the CFRP sheets, as well as minor concrete spalling, occurred at the ends of the composite sheets, concentrated in the maximum moment region.

A loading sequence closely resembling a uniformly distributed load was used to fail the DT-100 girder, strengthened in shear only at the supports. Twelve Jersey barriers were needed to induce failure, while their placement was as shown in Fig. 2.9. Major cracks due to flexure were observed after applying barrier number eight, at the midspan. As the applied load was increased, the cracks propagated towards the supports, and the girder failed due to pure flexure consequences.

The loading scheme specific to the DT-102A girder was of a uniformly distributed nature, as referred to in Fig. 2.10. An astonishing twenty four barriers were needed to cause the girder to fail in a most ductile manner. Cracks formed relatively homogeneously from midspan to supports, as crack slopes decreased along this direction as an effect of shear and flexure interaction. In comparison to the comparably strengthened DT-41 girder, major flexure-shear cracks and delamination were non-existent at CFRP sheet ends; perhaps due to the presence of uniform loading. Figure 2.11 through 2.16 show the tested double-tee girders and crack patterns associated with failure.

3.0 EXPERIMENTAL INVESTIGATION

3.1 GENERAL

This chapter presents the test program proposed for the damaged AASHTO Type III girder, from start to finish. Preparations for girder placement are also discussed.

Upon removal of the girder from its original setting in Kingston, Ontario, it was transported to its final resting point, an MTO testing site in Downsview, Ontario. The testing program, apparatus, instrumentation and layout are outlined in the subsequent sections of this chapter.

The following descriptions are of the original state of the girder, as delivered to the MTO site and verified on the structural drawings.

The girder, an AASHTO Type III concrete prestressed girder, is of a 21,895 mm length. It has a 1143 mm depth, and a composite acting overlying slab of 190 mm depth and 1600 mm width. Cross section details are shown in Fig. 3.1 and Table 3.1.

Concrete strengths were 27.6 MPa and 34.5 MPa for the slab and girder, respectively, as the structural drawings indicated. Further concrete property information is listed in Table 3.2 to 3.5. A stress-strain curve for the girder concrete is displayed in Fig. 3.2.

Deformed reinforcing steel bars, referenced in Fig. 3.3 for the precast girder and Fig. 3.4 for the concrete slab, are of a yield strength of 400 MPa. A typical stress-strain curve for the reinforcing steel is posed in Fig. 3.5. Prestressing tendons have a tensile strength of 1860 MPa, and are of straight and harped alignments, as show in Fig: 3.6 and 3.7. A typical stress-strain relationship for this specific prestressing steel is visualized in Fig. 3.8. Reinforcement properties are also listed in Table 3.6 through 3.9.

The girder was struck by a large construction vehicle which did not heed height restrictions. As such, it suffered irreparable damage and was deemed inappropriate for the structural bridge system it was part of, and consequently, is now the focal point in this study. The collision forced a lateral movement response upon the girder, as the face which was struck suffered torsion-shear cracks between the girder quarter points. Concrete pop out was prevalent on the tensile face of the girder. The effect of torsion is also noticeable, as the bottom flange has undergone cracking, diagonal in direction, and considerable concrete pop out customary. Despite the apparent damage, notably the reinforcing steel now exposed minimally at certain points of the bottom flange, the girder seemed to have suffered no significant structural ruin whatsoever.

Figure 3.9 verifies crack mapping of the girder as recorded by the MTO Eastern Region at the original bridge site. Figure 3.10 shows the crack mapping of each face of the girder in the state of condition after reaching the test site. Figure 3.11 and 3.12 portray the CFRP application arrangement which will be discussed in the following subsections.

3.2 GIRDER AND SITE PREPARATION

The asphalt wearing surface at the top of the concrete slab was removed prior to test site delivery. Since the girder was an exterior girder, the integral barrier was also separated from the girder top slab before being transported to the test site.

Prior to delivery of the girder, two concrete foundations were constructed over ground at the test site, which would be the east and west sides of the girder, using 25 MPa concrete. Each concrete foundation was 4 m in length, 1.5 m wide and 0.5 m in height, and were reinforced with 10M bars in both directions. To stabilize the precast girder laterally at the supports, concrete walls were erected on top of the foundations, on both sides of the girder. The walls, two per foundation, measured 800 mm wide by 200 mm thick and 1.5 m high, enabling the entire foundation to reach 2 m in height. They were also reinforced, using a cage-like configuration of 10M bars. Figure 3.13 through 3.15 views the foundations and concrete walls before and after removal of the formwork. A gap of 800 mm between the walls accommodated a steel pedestal to support the girder over the foundation. A 406 × 254 × 25 mm thick neoprene bearing pad was placed between the girder and the steel pedestal. The support location, underneath the girder, was levelled, to ensure proper girder alignment.

Once the girder was delivered and placed between its supports, steel bracing was introduced to further reduce any occurrence of lateral movement or rotation at support locations. W-shaped, rolled steel beams were cut to required lengths, and then attached mechanically to the concrete walls using stainless steel threaded rods and bolts. The

steel beams were oriented diagonally and normal to the girder web and were in firm contact with the girder at its top and bottom flanges, and the web. Pieces of timber were wedged between the W-shape steel beam sections and concrete girder, ensuring a well-fitting and secure interface. Figure 3.16 shows a view of the girder during placement over the supports using a mobile crane. In Fig. 3.17 and 3.18 the support system at the girder ends can be visualized.

3.3 PRELIMINARY TESTING

Initial testing was deemed necessary in order to assess the structural state of the girder and to decipher which type and degree of rehabilitation would be needed. This would provide a ‘meter stick’ approach to measure gained structural capacity after completing the final ultimate loading test.

3.3.1 Instrumentation

Strain gages measuring strain variance, and linear variable displacement transducers (LVDTs) recording deflection were used. Figure 3.19 shows the locations of the strain gages and LVDTs at the midspan region of the girder. A data acquisition system scanned, monitored and recorded all strains and displacements at regular intervals, during the static testing experiment.

Four strain gages, strategically placed, were used. The concrete adhering surface was first cleaned with a degreaser, removing dust particles and preparing the surface for a conditioner type solvent application. Once dry, a cementitious adhesive was applied

which would bond the strain gage to the concrete. Strain gages were positioned as follows to measure longitudinal strains only:

- (i) underside of bottom flange, 1 m off center towards the west,
- (ii) south side of the girder, centered on the web,
- (iii) underside of bottom flange, centered, and
- (iv) top of concrete slab, centered.

LVDTs used were four in total. They were placed in such a manner, as to yield vertical and horizontal displacement values. The locations of all the LVDTs used during the experiment are listed below:

- (i) underside of bottom flange, 2 m off center towards the west; measuring vertical displacement,
- (ii) underside of bottom flange, centered; measuring vertical displacement,
- (iii) underside of bottom flange, 2 m off center towards the east; measuring vertical displacement, and
- (iv) perpendicular to concrete slab edge, south side; measuring horizontal or lateral displacement.

3.3.2 Preliminary Testing Results

Preliminary testing initiated the use of one ton concrete blocks placed at the central portion of the girder, assessing the state of the girder in the elastic range. Blocks were placed, one at a time, with a total of twenty four blocks. This loading procedure is illustrated in Table 3.10. After full load was reached, blocks were removed one by one,

as experimental recording was continued. Figure 3.20 shows a view of the girder during preliminary testing. From the obtained results, a moment-deflection curve was obtained and compared with various theoretical results, shown in Fig. 3.21. Preliminary testing results may be viewed in Table 3.11 and 3.12.

As it is explained later in this thesis in detail, the RESPONSE 2000 software (Bentz, 1999) was utilized to provide the moment-deflection history of the girder in its original state, without cracking, as a theoretical approach. This moment-deflection relationship is shown in Fig. 3.22, with corresponding results, using manual calculations, for both cracked and uncracked sections. Moment-deflection values in Fig. 3.21 were graphed, using various means, in the elastic stage, considering no flexural or shear cracks in the girder. The straight line portion seen in Fig. 3.23, was used in Fig. 3.21 after eliminating the initial camber due to prestressing, as well as the nonlinear portion prior to failure. Also, in Fig. 3.21, results from the finite element modeling, using the ABAQUS software (Hibbitt et al., 2006), were considered in this comparison. Further details regarding the finite element modeling are presented in the following chapter.

The last source of data in Fig. 3.21 illustrates the manual calculations for deflection values corresponding to the applied bending moment. Additional information about these calculations, including the differences in moment of inertia of a strengthened section opposed to an original, non-strengthened section, is referenced in Appendix B.

It can be observed from Fig. 3.21 that all results follow a linear trend, yet differ slightly. This may be attributed to the sequence of loading, FE modeling approach and material properties. For example, RESPONSE 2000 does not model harped tendons and considers a case of uniform load on the entire girder span. Also, ABAQUS modeling takes into account straight tendons for the entire girder length. It is also noteworthy to state that both the ABAQUS and RESPONSE 2000 generated curves were in close agreement, as was required.

Since the results from testing and manual calculations were very close, it was established that the girder had not suffered substantial damage to its flexural capacity, and so concluding that strengthening for flexure basis was not primarily warranted. Furthermore, strengthening the girder for flexure, given its relatively sound state, would possibly lead to induced shear failure due to over strengthening. It was therefore conceded that the girder be strengthened foremost in shear only.

Shear failure is known to be activated by combined flexure and shear, producing shear cracks. For this reason, as well as to provide the minimum reinforcement, as is the case for steel stirrups, the girder was strengthened for shear throughout its entire length.

3.4 GIRDER EXPERIMENTAL PREPARATION

Many steps are imperative to transpire before CFRP application begins. The required measures are listed in order of implementation below.

3.4.1 Crack Mapping

A mapping or graphical representation of cracks was collected, as made evident in Fig. 3.10, whereby crack location, length, width and depth (where applicable) were noted. The north and south faces of the web and the bottom flange were divided into 500 mm long sections and the cracks were recorded. Afterwards, each section was transposed and scaled accordingly in AutoCAD. Crack lengths ranged from approximately 50 mm of hairline cracks, to 350 mm worth of cracks between 20 to 25 mm thick. Any concrete spalling was also documented, logging position, depth and length. A total spalled concrete area of approximately 2 m² was found to be existent on the concrete girder.

Crack mapping allowed for fairly accurate estimates for patching material, and provided a better overall assessment of what may have occurred due to the force the girder was subjected to during vehicle impact. Documenting concrete faults and spalling categorized the more structural troublesome areas along the girder.

3.4.2 Crack Injection and Repair

The filling and patching of the girder imperfections due to the suffered damaged was completed using two distinctly diverse materials. One type of patching material was used for overhead and vertical surfaces and another for those horizontal and for smaller cracks, namely Verticoat Supreme and Concrete Top Supreme, respectively, whose properties can be found in Table 3.13 and 3.14.

Verticoat Supreme is a one component, micro silica and latex modified, non-sagging mortar used for repairs. It works best for overhead surfaces, such as the bottom side of the bottom flange, where gravity works against application. Concrete Top Supreme is a latex and micro silica modified cementitious mortar, well suited for vertical application on the web area. Both materials offer strong bonding characteristics, exhibit high resistance to wear with low permeability, and are uncomplicated to apply.

Cracks and spalling areas were cleaned free of dust, loose material and any deleterious substances that would mitigate adherence problems. The areas were grouted and let cure. In Fig. 3.24 through 3.26, the pre and post grouting of the girder faces are compared.

Testing of concrete cores of the Verticoat Supreme grout material yielded an average 28 day compressive strength of 39.3 MPa and 12.4 MPa for in-direct tensile strength. The Concrete Top Supreme grout material gave respective values of 50.8 MPa and 14.3 MPa. Figure 3.27 and 3.28 show views of the tested concrete core samples for each grout type used. All testing was carried out at the Ryerson University concrete laboratory.

3.4.3 Concrete Girder Substrate Preparation

Before CFRP application could proceed, the concrete substrate must be made porous enough for the epoxy to adhere to the concrete and composite surfaces, as well as any

sharp edges dulled, removing possible stress concentration areas and avoiding tearing of the fabric. In order to do so, sandblasting operations were undertaken.

The material used during sandblasting was called *black beauty*. It is sometimes referred to as boiler slag or coal slag. It is an amorphous mixture of iron, aluminium and calcium silicates. It offers many advantages over other blasting materials such as, a low moisture content, high degree of etching, inert qualities, fast cutting action due to sharp angular edges, high hardness, and produces minimum residue and waste.

Approximately 1500 lbs, or 680 kg, of this material was used during the sandblasting of the girder. Both faces, including webs and chamfers, and the underside of the beam were sandblasted accordingly. Afterwards, any imperfections and minor pop outs were noted and scheduled to be filled and repaired with epoxy during the CFRP application stage. Figure 3.29 illustrates the full view of the girder upon completion of sandblasting, while Fig. 3.30 views a close up of certain portions of the girder after sandblasting operations as well.

3.5 CFRP ARRANGEMENT

The CFRP sheets were strategically arranged based on the preliminary testing results, which concluded that the girder's flexure state had not been compromised and accordingly, shear strengthening only would be undertaken.

CFRP sheets were arranged as U-wraps, or stirrups. A longitudinal view of the girder with CFRP applied is shown in Fig. 3.11. The U-wraps began at the top chamfer of one side, continued down the web, onto the bottom chamfer, along the underside, and back up the opposite face of the beam, ending at the top chamfer. They were placed 600 mm wide at similar intervals along the beam. The mid section of the Type III girder was vacant of U-wraps, since shear is non existent at midspan. The two most central U-wraps began at 300 mm from the middle of the beam, leaving a 600 mm portion free of CFRP U-wrap sheets at this location.

In order to provide an anchor for these and subsequent layers of U-wraps, longitudinal strips of CFRP sheets ran along the top and bottom chamfers, with respective width. The strengthening scheme was comprised of four layers: two U-wraps, and two longitudinal strips. The first 18 U-wraps were placed, followed by four longitudinal strips; two on each girder face, one per chamfer. This was repeated once more. A cross sectional view of the girder is represented in Fig. 3.12 to further reinforce the formerly cited. In total, 36 U-wraps and 8 longitudinal strips were placed as a strengthening composite CFRP material system, on the previously damaged AASHTO Type III prestressed concrete girder (Fig. 3.11).

3.6 CFRP APPLICATION

To apply the CFRP sheets, preliminary steps must be taken prior to the commencement of the application process. Materials incorporated in this procedure are:

- 1) Tyfo® S Epoxy,
- 2) Tyfo® TC Epoxy,
- 3) Tyfo® SCH-11UP High Strength Carbon Fabric, and
- 4) HDK Cabosil

Additional information regarding material properties for the above listed, are referenced in Table 3.15 to 3.17.

The materials used and their manner and means of employment are reviewed below.

3.6.1 Tyfo® S Epoxy

This particular epoxy acts as a saturating primer, encouraging bonding between the substrate surface and the FRP sheets. It may also be thickened and used as a primer or finish coat. It is a two-component epoxy matrix material, mixed thoroughly as 42% component B into 100% component A, by volume, for about five minutes. Both components are considered irritants with prolonged exposure. Component B is most severe, labelled as a corrosive material. Thus, safety goggles, respirators, chemical resistant gloves and Tyvex® coverall suits must be worn at all times. The epoxy can be applied using a brush or roller, as well as a Tyfo® Saturator for larger applications.

Its advantages include the offering of a long working time, good high and low temperature properties, high elongation and a high tensile modulus and strength. It cures well at ambient temperatures and preferably not below 4°C, for nominal results. Both components A and B are supplied in 22L pails, as depicted in Fig. 3.31.

3.6.2 Tyfo® TC Epoxy

Once the Tyfo® S primer is applied and allowed to come to a tacky consistency, the Tyfo® TC Epoxy may be applied. This epoxy resembles a tack coat, enhancing the system's adherence properties, especially for vertical and overhead surfaces. Like the primer epoxy, the tack coat is also a two-component material, mixed as 30% component B into 100% component A. Mixing procedure and safety precautions are similar to that of Tyfo® S Epoxy, with extreme caution to be used with the corrosive component B material. Once applied, the CFRP sheets may be adhered immediately. It may be applied using a roller or trowel.

As is the case with the Tyfo® S Epoxy, advantages for the Tyfo® TC Epoxy include a long working time, good high and low temperature properties, and a high tensile modulus and strength. It too cures at ambient temperatures and is not recommended for use at temperatures below 4°C. It exhibits excellent adhesive characteristics with high elongation and multiple uses. Once again, components A and B are supplied in 22L pails, and are shown in Fig. 3.32.

It should be noted that both epoxy types (S and TC) may contain harmful and explosive vapours, even when containers are empty, and thus, shall be disposed of carefully.

3.6.3 Tyfo® SCH-11UP High Strength Carbon Fabric

The Tyfo® SCH-11UP High Strength Carbon Fabric is a custom, uni-directional carbon fabric, applied using the Tyfo® system. It is manufactured in 2 ft, or 60 cm, wide rolls, and may be cut to size on site. Once placed strategically, as an integral part of the composite system, the carbon fabric provides an increase in strength to its adhering surface.

The fabric is incredibly flexible, and as a result may be manipulated in most any application, whereby its usefulness becomes widespread. It is non-corrosive and will not cause further damage to deteriorating surfaces.

3.6.4 HDK Cabosil

This product is essentially fumed silica. It is a synthetic amorphous, hydrophilic (having an affinity for water, readily absorbing or dissolving in water) material, used as a thickening agent for the Tyfo® TC Epoxy, and increases adherence properties. When mixing, respiratory masks, gloves and suits are to be worn to protect from accidental inhalation or spills. Friction, induced by mixing, may cause a build up of static electric charge, and so proper grounding precautions should be taken and all flammable materials removed from surroundings.

3.6.5 The Application Process

The application process of the CFRP system is a step by step procedure and is outlined in the proceedings. The method is exclusive of substrate preparation for brevity.

Step (1): Primer Application.

Once mixed, the Tyfo® S Epoxy was applied using a paint roller. It coated only the locations, previously mapped, that were needed for the application of the CFRP. This means that only 600 mm wide strips, beginning and ending at the top chamfers and wrapping completely around the girder faces and bottom flange, at 600 mm intervals, were saturated. Also saturated with the primer epoxy were the top and bottom chamfers, spanning the length of the beam.

Only the first 18 sections of stirrups, or U-wraps, were primed at one time. Once this coat was let set until it became of a tacky-like nature, the next step began.

Step (2): Tack Coat Application.

The tack coat, or Tyfo® TC Epoxy, was mixed accordingly and spread on the previously primed sections. It was of a thick, sticky, taffy-like adhesive layer. This was to be spread as evenly as possible.

Step (3): CFRP Application.

Each pre-cut segment of CFRP sheet was laid out on a saturation tray, lined with thin plastic sheeting. It was then saturated using the Tyfo® S Epoxy primer and placed on

its designated rehabilitating area of the concrete beam. The first layer of stirrups were allowed to cure and set well enough before another layer was applied overtop.

Steps 1 through 3 were repeated for the top and bottom chamfers. This completed the first layer of CFRP strengthening. The second and final layer was prepared and applied as the first and succeeded by step 4.

Step (4): *Final Protective Primer Coat.*

Tyfo® S Epoxy was mixed with Cabosil to create a thicker, almost opaque liquid. This was applied over the CFRP sheets as was the primer in step 1. This is a protective coating against moisture entry, UV rays, de-icing chemicals, and helps seal the CFRP layers. It dries as a clear, candy-like coating, needing little or no maintenance throughout its lifetime. Figure 3.33 through 3.50 show steps of the CFRP application process and the final orientation.

3.7 FINAL TESTING

The final testing stage for the FRP strengthened girder was primarily conducted to verify strength gain, if any, in shear and moment capacities. The experimental results obtained over a full day of testing, are later compared to the analytical results, achieved through a finite element model.

3.7.1 Instrumentation

As was the case with the preliminary assessment testing procedure, strain gages and linear variable displacement transducers (LVDTs), were used in the final testing program. The only difference was the introduction of PI gages, or π -shape displacement transducers, to measure deformation strains on the extreme tensile and compressive faces of the girder bottom flange and concrete slab, respectively. Also exclusive to the final testing was the use of mechanical dial gages at the supports to measure rotation and settlement. Data was acquired via the data acquisition system test control software (TCS) SYSTEM 6000, seen in Fig. 3.51, which scanned and recorded experimental data every one second.

A sum of six LVDTs were used, all placed at midspan. Their locations are outlined below (see Fig. 3.52 for visual):

- (i) four LVDTs, transversely, on the top of the slab,
- (ii) horizontal to the ground at mid height of the top slab, and
- (iii) horizontal to the ground, at mid height of the bottom flange.

The latter two LVDTs were instrumented in order to monitor any lateral deflection and the possibility of a torsional response from the girder.

PI gages were placed at girder midspan, on the top slab and bottom flange in order to measure any deformation on extreme faces in the longitudinal direction, as shown in Fig. 3.52. A gage length of 210 mm was used for both PI gages (Fig. 3.52).

Figure 3.53 to 3.56 show views of the LVDTs on the girder before testing, while Fig. 3.57 shows the PI gages at the top and bottom portions of the girder.

A total of 38 strain gages were used during testing and their positioning revealed in Fig. 3.58. Thirty strain gages were of the 50 mm length variety, with a 350 ohm resistance quality. The remaining eight strain gages, which are placed on the top and bottom chamfers, measure 30 mm in length and exhibit a 120 ohm resistance. Again, the concrete surface to which the strain gage would be adhered was cleaned with a degreaser, an epoxy resin was applied over top and then the strain gage positioned appropriately.

Strain gages were placed at midspan and 600 mm off center, in the middle of a CFRP U-wrap layer. Nineteen gages were adhered at midspan and 19 upon the CFRP layer. Strain gage positioning was as follows (all gages placed longitudinal to the girder direction):

- (i) four gages, transversely, on the top slab (midspan and 600 mm offset),
- (ii) mid point of the top flanges (midspan and 600 mm offset, both faces),
- (iii) mid point of the top and bottom chamfers (midspan and 600 mm offset, both faces),
- (iv) maximum height of web (midspan and 600 mm offset, both faces),
- (v) mid height of web (midspan and 600 mm offset, both faces),
- (vi) minimum height of web (midspan and 600 mm offset, both faces), and

- (vii) three gages, transversely, on the underside of the bottom flange (midspan and 600 mm offset).

Figure 3.53, 3.54 and 3.55 show the top slab, elevation, and bottom flange underside views of the girder with appropriate strain gage placement.

Two mechanical dial gages were placed at the east support and are seen in Fig. 3.59. One was used to measure the deflection of the neoprene bearing pad directly under the girder during loading. A second dial gage was placed on the interior of the girder span, evaluating support settlement. Due to the mechanical nature of the gages, readings were taken for each load increment.

3.7.2 Additional Testing Equipment and Apparatus

Careful consideration and anticipation to what may occur during testing led to the discovery that a torsional moment, about the longitudinal axis of the girder, may be excited due to eccentric loading and the slope of the test site. Although the support area, where the steel 500 mm high pedestals rest, for the girder was levelled and the girder was restrained laterally at both supports via steel I-beam members, there was some cause for concern.

To alleviate this possibility, supports were placed at 3 m from the midspan, directly underneath the top slab. Four supports were built, comprised of three one ton blocks placed one on top of the other. A timber reinforced box was build to cover the protruding hooks and acted as a foundation for additional timber pieces that would be

slowly and carefully removed as the concrete girder would deflect. A clear distance of approximately 100 mm was kept at all times between the tops of these torsion supports and the underside of the top slab. The reasoning behind this type of support was that any torsion or excessive and sudden deflection would be eliminated by 'bottoming out' above the supports. The supports, essentially, would break and impede the involuntary collapse of the girder.

Also, similar supports were built at the support locations. Steel pedestals were placed over each other in a comparable manner as noted above with the exact function as the torsion supports. All supports were continuously monitored during each load increment. Figure 3.60 shows various views of the safety precautions mentioned above.

A mobile crane was used for load placement during testing. The crane, having a lift capacity of 30 tons, was comprised of a flat bed truck with a boom lift.

Uniform load application was completed via two loading specimens: Jersey barriers and one ton blocks. Originally, only the barriers were to be used, but due to the fact that their 4 m length would well surpass the 1.6 m wide concrete slab atop the girder, an undesirable cantilever moment would be applied to the slab. This moment would ultimately fail the slab and halt testing prematurely.

It was decided to use one ton MTO test blocks in addition to the 2.4 ton Jersey barriers for load application (see Fig. 3.61 and 3.62, respectively). Deposit of the one ton blocks and barriers at the test site, before testing, are evident in Fig. 3.63, 3.64 and 3.65.

Loading commenced, as depicted in Table 3.18, with the symmetrical placement of blocks on either side of the central portion of the girder. Figure 3.66 to 3.84 denote the testing procedure further. A 300 mm gap, 150 mm each direction from midspan, was left free and unloaded for instrumentation purposes. A total of 68 blocks were placed transverse to the girder direction, two rows one on top of each other. In the middle of the girder, atop the first four blocks on each side, immediate from the midspan, another two rows of blocks were placed. Thus far, 84 blocks had been applied to the girder's concrete slab.

The blocks consisted of protruding hooks for transport purposes on their top face, causing a non-flush surface to exist. This was corrected by using 4" × 4" (100 mm × 100 mm) wooden posts, 12 ft (3.65 m) long, placed longitudinally, allowing for the barriers to be placed as even and stable as possible. Jersey barriers were then placed on both sides of the girder midspan, for an entirety of 22 barriers. The total load applied to the girder amounted to 136.8 tons, (136,800 kg or 1368 kN).

A line was drawn directly down the center of the top slab, acting as a guide during loading, to eliminate or at least decrease the risk of eccentric loading.

After each load increment, readings were taken and evaluated. The LVDTs on the top slab, especially the two most exterior, were observed to be very similar during testing as well as LVDT 5 and 6, placed horizontally at mid thickness of the top slab and the bottom flange, respectively. These were compared to ensure no torsion existed. Support settlement readings were also recorded, along with the observation of support walls, had cracks begun to appear.

In the later stages of testing, micro cracks in the girder were constantly monitored and noted, especially in the overlying and weaker epoxy coating. These cracks were noted to begin appearing at an applied load equating to approximately a moment value between 2500 kN·m to 3000 kN·m. FRP layers were inspected and an ear was lent to any possible snapping and popping sounds expressed by the carbon fibre.

4.0 THEORETICAL FINITE ELEMENT ANALYSIS

4.1 GENERAL

The theoretical aspect of this research was prepared using the finite element approach. The finite element technique is a numerical method used for deciphering problems relating to engineering, mathematics and physics. Ranging from structural analysis, heat transfer and fluid flow, it offers an incredibly wide spectrum of application. The finite element formulation of a particular problem constructs a system of algebraic equations. These are solved simultaneously, as opposed to gathering a solution of differential equations, which are not always easy to conjure due to geometry, loading and complications.

Solutions are developed by dividing the problem at hand into smaller bodies, being finite elements, connected at nodal points and assigning boundary conditions to the body. This procedure is known as *discretization* of the model. Each finite element has its equations formulated and combined with other elements to establish a solution for the entire body. In relation to structural type problems, displacements at each node are determined, followed by stresses within each element under whatever the loading condition may be.

A great advantage offered by the finite element method is its capability to model bodies in the most realistic manner and exceptionally quicker than previous methods. It provides a

full description of structural response for either static or dynamic loading to arbitrarily arranged elements, material properties and boundary conditions (Logan, 2002). It is therefore apparent that the finite element method, namely the commercially available ABAQUS (Hibbitt et al., 2006) program, will suffice for the theoretical study regarding the strengthening of concrete girders using fibre reinforced composite materials.

This chapter presents a brief overview of the ABAQUS program, and the techniques undertaken to model different aspects of the reinforced concrete prestressed girder, and the FRP applied externally. Any assumption made due to ease of replication or lack of proper program function is discussed.

4.2 THE FINITE ELEMENT STUDY

In the formulation of a structural based problem, many steps exist which lead ultimately to a finite element solution. The general steps are listed below.

Step (1): Discretization and selection of an element type.

The body to be studied is divided into an equivalent arrangement of finite elements. Each element type is classified and connected through nodes. Essentially, elements shall be made small enough to yield accurate results and sufficiently large to reduce computation time. In addition, element types must represent realistic conditions.

Step (2): *Selecting a displacement function and relationship.*

Nodal values are utilized to calculate initial values using linear, quadratic, or cubic functions, to name a few, depending on the element characteristics. Strain-displacement and stress-strain relationships are vital in defining material behaviour, which may be linear or nonlinear.

Step (3): *Assembling the stiffness matrix and equations.*

With the use of displacement attributes, the stiffness matrix for elements and the entire structural system (the global stiffness matrix) may be arranged. This relates nodal forces to nodal displacements. Several methods may be used such as, direct stiffness or work energy; the former will be focused on.

Step (4): *Obtaining element equations and solving for unknowns.*

The stiffness matrices, in conjunction with initial and boundary conditions, can be solved to produce the system displacement, force, stress and strain values. The relation of nodal displacement and force is written in the matrix form:

$$[F] = [K][U] \quad (4.1)$$

where, $[F]$ = nodal force vector,

$[K]$ = stiffness matrix, and

$[U]$ = nodal displacement or degrees of freedom vector.

If Eq. (4.1) is desired for global or local formulation, then all vectors and matrices are of respective values.

The structure stiffness matrix $[K]$, is the collection of individual element stiffness matrices, $[K]_i$, given by:

$$[K] = \sum [K]_i \quad (4.2)$$

and,

$$[K]_i = \int_{vol} [B]^T [E] [B] dv \quad (4.3)$$

where,

$$[B] = \{\epsilon\} \{u\}^{-1} \quad (4.4)$$

$$[E] = \{\sigma\} \{\epsilon\}^{-1} \quad (4.5)$$

Above, $[B]$ = strain displacement matrix, and
 $[E]$ = elasticity matrix.

In a linear type analysis, the loading response applied to a body is obtained directly. Finite element problems of nonlinearity are solved by a series of iterative linear steps. ABAQUS uses a numerical technique, the Newton-Raphson method, to solve nonlinear equilibrium equations. Loads are applied gradually, divided into load increments, and the approximate equilibrium at the end of each increment is found. The sum of all the incremental responses is the approximated solution for the nonlinear analysis. Figure 4.1 serves for graphical representation.

Assume $[P_o]$ is the initial load, $[U_o]$ the initial displacement, and $[K_o]$ is the tangent stiffness at point $[P_o], [U_o]$. For the i^{th} cycle of the iteration process, the applicable load is given by,

$$[P_i] = [P] - [P_{i-1}] \quad (4.6)$$

where,

$[P]$ = total load to be applied, and

$[P_{i-1}]$ = load equilibrated after the previous step.

Each increment to the displacement, during the i^{th} step, is defined as,

$$[K_i][\Delta U_i] = [P_i] \quad (4.7)$$

while the total displacement after the i^{th} iteration is,

$$[U] = [U_o] + \sum_{j=1}^i [\Delta U_j] \quad (4.8)$$

This procedure is repeated until the increments of displacement, or the unbalanced forces become minute according to predetermined tolerance values.

The value of $[K_i]$ is the tangent stiffness matrix at the end of the previous step,

$$[K_i] = [K_{i-1}] \quad (4.9)$$

or, simply the slope of the $[P]$ - $[U]$ curve at the point $[P_{i-1}], [U_{i-1}]$.

Another approach, rather than calculating stiffness for each iteration, is the modified iterative technique. This method applies only the initial stiffness $[K_o]$.

Step (5): Interpretation of results.

Proper analysis of the results is key to achieve accurate models. For example, a simple check of known high stress areas or large displacements is a necessity.

4.3 SYNOPSIS OF THE ABAQUS FINITE ELEMENT PROGRAM

As aforementioned, the versatile ABAQUS program allows for both linear and nonlinear analysis. The program contains an extensive library of elements, options and parameters, enforcing its broad simulation potential.

The evaluative routine, expressed by ABAQUS is that of a batch-running program, which reads from a data deck, depicting the problem, and performs the necessary calculations to produce desired results. The data deck is what contains model data and history data for the program to interpret. The model data defines the finite element model. The variables being: nodes, element type and property, orientation, material and their assignment, constraints, boundary conditions and any other data specific to the model. History data explains the events associated with the model, such as loading. This data is read and input in a chain of commands, each identifying a different time frame and response, as is the case for a static or dynamic loading circumstance, and is referred to as a step. In order to correctly define a step analysis, certain factors are to be taken into account, similar to the following: step type, control parameters; to assist in time integration for nonlinear solutions, loading type and value, and output request.

Data definitions are accomplished using option blocks. These are sets of model-describing information organized in a fashion that is readily interpreted by the program. The user introduces built in options through keywords, followed by input data, if need be.

4.4 FINITE ELEMENT VERIFICATION STUDY

The process of accurately depicting actual conditions, structural behaviour and response with a finite element program is a lengthy and daunting task. The slightest error or approximation may have the tendency to grossly distort results, often realized after quite some time. To avoid such error, and to increase the overall reliability of the study, a verification process was created and followed through.

Preliminary testing and final results from ABAQUS were compared to assorted, already credible sources and graphed in Fig. 3.21. The program, RESPONSE 2000, a nonlinear sectional analysis program, was used to contrast these results. These findings were also compared with hand calculations from simple beam analysis, seen in Table 4.1, as well as engineering common sense and experience. It is obvious that the linear range for all girders tested was replicated, and of utmost importance at first. Once this was registered as a comparative representation, the finite element model was encouraged to enter the inelastic range assertively and confidently, followed by the models strengthened with CFRP.

4.5 FINITE ELEMENT SENSITIVITY STUDY

It was decided that in order to make valid comparisons and theoretical models of full-scale structural members, strengthened and non-strengthened, that a sensitivity-type exploration had to be carried out.

To replicate the CFRP, two distinct elements were used; shell and membrane. These were used for each of the three double-tee girders. The element which yielded the closest results to the experimental data would be the element used exclusively for the Type III I-girder modeling.

Once the above mentioned calibration-type analysis was complete, an equivalent inspection was organized to determine the effect, if any, that tension stiffening may exhibit in the modeling. For the Type III girder modeled without CFRP, various runs were made using ABAQUS with varying values for the TENSION STIFFENING option, ranging from 0.003 to 0.015, as documented in Fig. 4.2. These values represent the difference between the absolute value of tensile strain minus the cracking strain, or the tensile strain after cracking occurs. They are also known as values of tensile strain after maximum stress has been reached. The greater this value, the more tensile stresses are distributed to the concrete bonded to the reinforcement, thus increasing overall strength. This of course is a function of concrete strength, as a stronger concrete will be able to transfer more tensile stresses.

Diverse values for the TENSION STIFFENING option were used for the Type III girder. They were compared against experimental findings, resulting in the choosing of the best fitting tension stiffening parameters possible. Figure 4.3, signifies that the higher the value used for tension stiffening modeling, the stiffer, stronger and more resilient the analysis outcome would be. As a product of this assessment, a value of

0.002 was used in all finite element modeling cases to exemplify tensile strain after concrete cracking, common with previously visited literature.

4.6 FINITE ELEMENT MODEL

The finite element model was partitioned into smaller elements, potentially varying in dimension and classification, in what is known as the mesh of the model. The mesh layout is refined through trial runs and modeling experience. It is a trade off between accuracy, and run time. Element meshes, for all DT girders and the Type III girder, are cited in Fig. 4.4 through 4.7.

All models implemented by means of ABAQUS, applied the strategic use of their geometric symmetry for ease of input, reduced running time and brevity. Symmetry is defined as corresponding in size, shape, and position of loads, material properties, and boundary conditions that are on opposite sides of a dividing line or plane (the plane of symmetry) (Logan, 2002). Symmetry models customarily employ symmetry operations through reflection in a plane, rotation about an axis or inversion through a center (McGuire, 2000). Three important aspects to consider when applying the use of symmetry are outlined as follows: (1) recognition and definition of the type of symmetry, (2) manipulation of loads and forces and their distribution throughout the model, and (3) proper boundary conditions (McGuire, 2000).

The use of symmetry in a finite element model allows for consideration of a reduced problem, stiffness matrix, and equations, without compromising results. This may

permit the use of a finer element mesh and other aspects since the problem size is decreased.

While using symmetry is advantageous, it must be applied correctly. A general and essential rule, for example, is that at a plane of symmetry, displacement in the direction perpendicular to the plane must equal zero. This circumstance is usually effectively modeled using rollers at reference nodes. Also, no rotations about two orthogonal (at right angles) axes in the plane of symmetry shall be allowed. Another instance is exemplified using a single span beam, where at the midspan point of maximum deflection, slope is equal to zero. If this beam were modeled as half by using symmetry properties, the slope at the exterior point (formerly the midspan), must be set to zero.

4.6.1 Element Nature and Application

Elements were selected based on experience and through extensive research of previous similar studies.

The 3D, four node shell element, S4R, was chosen to model all concrete portions, being the deck slab and concrete girder. It is a doubly curved general purpose shell, meaning it may consist of straight or curved boundaries, depending on node definition. This element has six degrees of freedom, three for displacement (U_1 , U_2 , U_3), and three rotations (ϕ_1 , ϕ_2 , ϕ_3). Finite membrane strains are easily handled with this element and it allows for alteration in thickness as a result of deformation. It employs reduced (lower order) integration to form the element stiffness. It helps to increase solution

accuracy, granted no distorted elements exist, and lessens model run time. The element also employs hourglass control, used for first order (linear) elements, but is not always required. The S4R element is suitable for large membrane strain analysis, without large rotations, and is excellent for modeling materials exhibiting Poisson's ratio.

Prestressing tendons are modeled using a two dimensional, two node linear displacement truss element. The T2D2 element chosen, has two degrees of freedom, (U_1 , U_2). Truss elements are long, slender structural members that only transmit axial forces. A 2D truss element uses linear interpolation for position and displacement and has a constant stress.

4.6.2 Reinforced Concrete Modeling

When concrete is loaded in compression, it initially exhibits elastic response. As stresses increase, irrecoverable strains or inelastic behaviour, occur and the material slowly softens. As the material's ultimate strength is reached, strain continues to increase while stresses can no longer be withstood. When loaded in tension, the concrete response is elastic until a stress between 7 to 10% of the ultimate compressive strength is reached. Once surpassed, cracks begin to form, and at such a high rate that the exact behaviour is difficult to observe. A typical stress-strain curve for concrete is shown and explained in detail in Fig. 4.8. ABAQUS permits the cracks to affect the model by reducing stiffness accordingly, modeling the cracks as strain-softening, dependent on the size of the elements in the cracked region. The stress-strain relationship for plain concrete is characterized in Fig. 4.9.

The modeling of the reinforced concrete slab and prestressed girder is to include nonlinear behaviour. ABAQUS provides the CONCRETE option to take the inelastic range and response of elements into account, for various modeling applications of concrete members, structures, etc. The option characterizes the stress-strain curve response of concrete at the elastic stage of loading. The curve may also be implemented beyond the ultimate stress region, as strain-softening becomes more present.

In ABAQUS, cracking in the concrete model is assumed to occur when stresses reach a failure surface, called the *crack detection surface*. This surface consists of a linear relationship between the equivalent pressure stress, p , and the Mises equivalent deviatoric stress, q . The Mises yield surface is used to define isotropic yielding by specifying the yield stress of a material. This is exemplified further in Fig. 4.10. The figure displays the different modes of failure for concrete. The crack detection surface represents the occurrence of both tensile and compressive stresses, as the concrete fails at lower stresses than if it were stressed uni-axially. In this zone and in the bi-axial tension zone, concrete fails by cracking. The compression surface and the uni-axial compression zones, represent concrete failure due to crushing.

The cracking model is of a smeared crack, and does not track individual macro cracks. At each integration point, calculations are performed independently, and cracks are taken into consideration based on their affect on stress and material stiffness, at the integration point.

All cracks are irrecoverable, and may widen or contract, and as the concrete continues to crack, its shear strength reduces. The SHEAR RETENTION option defines this event by specifying the shear modulus reduction as a function of the opening or closing strain present across the crack. The new or reduced shear modulus will continue to alter as the analysis carries on. The shear retention model, Fig. 4.11, uses the assumption that shear stiffness of open cracks reduces linearly to zero as the crack width increases:

$$\mu = (1 - \varepsilon / \varepsilon_{\max}) \quad \text{for} \quad \varepsilon < \varepsilon_{\max} \quad (4.10)$$

$$\mu = 0 \quad \text{for} \quad \varepsilon \geq \varepsilon_{\max} \quad (4.11)$$

Above, μ is the shear retention parameter, ε is the strain across the crack, and ε_{\max} is entered on the data line as a maximum strain value for the analysis. This value is very large in order to imply full shear retention.

The program specifies the value of $\mu = \mu_{\text{close}} = 1.0$, when $\varepsilon < 0$. This represents the reduced shear modulus as the crack closes. If values of $\mu = 1$, and ε_{\max} are used, full shear retention is applied. This is a reasonable model, since for most cases, the overall response is not greatly affected by the amount of shear retention present.

Concrete behaviour is independent of that of the reinforcing steel in ABAQUS. The effects due to the concrete-rebar interface are modeled using different options available in ABAQUS. Loads on a reinforced concrete member are carried by the reinforcement and concrete prior to cracking. Once cracking occurs, a small length of the reinforcing bar becomes debonded, and over this entire length the load is beared solely by the bar. The friction against the bar and the tensile strength existing in the pieces lying between

the cracks, allow the cracked concrete to, in some degree, aid in reducing the stretch of the bar. The modeling of the interaction between the steel reinforcement and concrete, such as bond slip and dowel action, is represented with the TENSION STIFFENING option and represented in Fig. 4.12. This essentially simulates load transfer across cracks through the reinforcement. The user may define any strain-softening behaviour here.

As concrete is loaded slowly with compressive forces, it initially demonstrates a linear elastic response to loading. As this load is increased, some strains in the concrete become inelastic strains. This irrecoverable deformation induces the softening behaviour of the material. The ultimate stress is then reached, where after no more loads can be withstood. If all applied loads are removed a permanent deformation exists, and thus, elasticity of the material impaired. The ABAQUS concrete model fails to replicate this phenomenon, but introduces other possible reproduction techniques. ABAQUS assumes that cracks pose a damaged state on the model by decreasing the elastic stiffness, and are modeled as such, with no permanent strain imminent. This allows cracks to open and close depending on the magnitude of the stress across their width. The option, FAILURE RATIOS, is introduced to imitate the failure surface for the concrete model.

The modeling of rebar may be of two forms, and neither contributes any mass to the model. The REBAR option defines discrete or individual rebar as an element property, one dimensional strain theory element. In some elements, rebar may be defined

singularly, or as layers using the option REBAR LAYER. This option is preferred for defining uniformly spaced layers of reinforcement in membrane, shell, surface or solid elements. The reinforcing layer or layers, are modeled as a smeared layer of thickness, t , within an element. The rebar area, A , is divided by the rebar spacing, s , in order to calculate the thickness of the equivalent smeared layer of reinforcement.

A typical stress-strain curve for steel is documented and detailed in Fig. 4.13. The stress-strain relation, as accepted by ABAQUS, is set in Fig. 4.14.

4.6.3 Modeling of Prestressing Tendons

As formerly mentioned, prestressing strands are modeled using the two dimensional, two node linear displacement T2D2 truss element. ABAQUS provides the INITIAL CONDITIONS option, installing a prestress force in the tendons, and may be valid for pretensioning and post-tensioning practices; the former being the case of the concrete girder being studied. In the occasion of post-tensioning, the PRESTRESS HOLD option, keeps stresses in the tendons constant during initial equilibrium solutions. This is compulsory since the structure must be brought to an equilibrium state before it is loaded, as if the tendons are sliding through the concrete. Figure 4.15 shows a typical stress-strain curve for prestressing steel. A fully-plastic stress-strain curve, shown in Fig. 4.14, was employed in the finite element analysis.

The subject Type III girder includes harped tendons. In ABAQUS, the modeling technique for this girder was two fold. One model included continuous straight

tendons, as is in actuality near the midspan portion of the beam, but extended fully to the supports. Another model included similar prestressing tendon profiles, with the inclusion of an appropriate and applicable decrease in prestress, per element, where harped tendons would lie. This truthfully reflects the reduction of prestress along a straight path, extending from the straight portion of the strands, at the bottom of the girder, as is the case in a harped tendon member.

4.6.4 Modeling of CFRP

The CFRP was modeled using both shell and membrane elements as part of a sensitivity study as to which element configuration would yield the most reasonable and accurate results. The shell element chosen is the 3D, four node S4R element. It is identical to that used to model the concrete portions of the model. It consists of three degrees of freedom each for displacement (U_1 , U_2 , U_3) and rotations (ϕ_1 , ϕ_2 , ϕ_3), respectively. The element responds to gradients in thickness and deformation.

The membrane element employed in the study is a 3D quadrilateral, general membrane element, known as M3D4R. It contains four nodes, as the shell element, with three degrees of freedom (U_1 , U_2 , U_3). A membrane element is a surface type element which only transmits in-plane forces, thus no bending moment may be withstood, since it has no bending stiffness. ABAQUS describes membrane elements as ideal for modeling thin surfaces, such as FRPs, in three dimensional models where deformation can develop in 3D.

The properties of these elements used in the CFRP modeling were provided using the ELASTIC option, with the TYPE parameter set to LAMINA. This defines the elastic material properties for the CFRP material, as orthotropic behaviour in plane stress. In this condition, normal and shear stresses perpendicular to the element plane are zero. This is true to CFRP, as it is not nearly as strong in one direction as it is in the opposite. On the data lines in the input file, the modulus of elasticity was input for both directions of fibre orientation.

4.6.5 Nonlinear Model Attributes

The necessity to examine the finite element program at nonlinear stages requires ABAQUS to undergo a series of iterative steps using proven mathematical numerical formulae. The Newton-Raphson method is of choice for ABAQUS.

Each increment produces a step to verify equilibrium. If not obtained, the process continues until equilibrium is exactly or closely achieved, depending on tolerances. Increments are kept small to increase the possibility of convergence, but shall also be kept of appropriate size to assist in computation efficiency, since larger increments surrender to greater running times. Equilibrium tolerances should be of tight proportion to guarantee reputable convergence and model reliability. Maximum and minimum increment values may be input by the user, as well as maximum load or deflection, where if surpassed, the analysis is discontinued.

For nonlinear problems, ABAQUS lends use of the RIKS parameter. This parameter was utilized in circumstances concerning an unstable structure, or the geometrically nonlinear collapse of a structure. The Riks method may also provide accurate solutions to even the most complex and unstable responses, such as that represented in Fig. 4.16.

The RIKS parameter depends on choosing increment values based on controlling the path length, or arc length, along the load-displacement response curve. The load magnitude was considered as an additional unknown, while the program solves for values of displacement and load, simultaneously. Loading for each increment is always proportional to the previous increment. The current load magnitude, P_{total} , is defined as

$$P_{total} = P_o + \lambda(P_{ref} - P_o) \quad 0 < \lambda < 1 \quad (4.12)$$

where, P_o = existing load magnitude at beginning of the step (dead load),
 P_{ref} = load magnitude of the reference load, defined in the Riks step, and
 λ = load proportionality factor.

All prescribed loads are ramped from the initial (dead load) value, up to the reference values specified.

As mentioned earlier, Newton's method was applied to decipher nonlinear problems, in this case, along with the Riks method. A 1% extrapolation of the strain increment is incorporated in the method. An initial increment in arc length, Δl_{in} , along the load-

displacement curve, is identified by the user in the step. The preliminary load proportionality factor, $\Delta\lambda_{in}$, is then given by,

$$\Delta\lambda_{in} = \Delta l_{in} / l_{period} \quad (4.13)$$

Above, l_{period} , is a user input total arc length scale factor, which is normally set to 1. For the next set of iterations, until completion, the value of the load proportionality factor is computer generated. This causes the user to have absolutely no control in regards to the load magnitude. Figure 4.1 shows the methodology of Newton's approach for tangent stiffness determination.

For both linear and nonlinear analysis, ABAQUS offers the use of the NLGEOM parameter in conjunction with the STEP option. This helps account for geometric nonlinearities in a stress analysis, adding to the credibility of the model and results.

4.7 MODELING OF CONCRETE AASHTO TYPE III GIRDER

The concrete girder is an AASHTO Type III prestressed girder. It was originally part of structural bridge system, damaged due to a construction vehicle impact, removed and transported to the test site. Its total length was 21,895 mm. For further, instructive information, consult Tables 3.6 to 3.17, and Fig. 3.1 to 3.7. Half of the girder was modeled effectively using symmetry, with a length of 11,000 mm, and a 190 mm overlying deck slab, measuring 1600 mm in width. Average thicknesses were used for each element set longitudinally to take into account varying girder thickness, such as the sloped top and bottom chamfers. Element sizing was decreased for the chamfers since a

reduction in cross section is apparent at their location. The number of elements used to model the deck slab in the transverse direction is 16, as well as 25 elements along the girder depth, and 55 elements in the longitudinal direction. A total of 2255 elements were used to model the entire concrete Type III girder, alone. Figure 4.7 shows the finite element mesh for the Type III girder.

Reinforcement bars were present and modeled in three forms; vertical stirrups, longitudinal and transverse rebar. There were a total of 26 prestressed, 7 wire strand, 13 mm nominal diameter tendons embedded in the girder. With these, three groups, of corresponding prestressing steel area are modeled; six, eight and twelve tendons, equivalency. Tendons and rebar were grouped specific to similar spacing, and portray properties in proportion, for brevity purposes. A sum of 165 elements were used to model the prestressing strands.

CRFP sheets were used to strengthen the girder and were modeled appropriately. As a refresher, FRP sheets enclose the girder along its cross sectional perimeter, as U-wraps, at 600 mm intervals. Longitudinal FRP sheets were placed along the top and bottom chamfers, acting as a restraint-type system for the U-wraps. Overall, 540 elements were used to model the CFRP U-wraps, and 330 elements used to represent the CFRP longitudinal strips.

4.8 MODELING OF DOUBLE-TEE GIRDERS

Three, previously damaged, double-tee girders were modeled, with standard designations, DT-41, DT-100, and DT-102A (Cofini, 2005). Their lengths were 16,900 mm for the former and 19,150 mm for the latter two. Reference can be made to Table 2.1 to 2.6, and for explanatory diagrams see Fig. 2.2 to 2.10. Again, symmetry was used during modeling, by considering half the girder length, yielding 8400 mm and 9600 mm lengths, respectively. The width of the concrete slab, respectively for each girder, was 3190 mm, 2415 mm and 3400 mm. All three DT girders consisted of a 100 mm thick top slab portion, straight prestressing tendons, and depths ranging from 760 to 810 mm. Wire welded fabric (WWF) was used for both slab and web reinforcement, and modeled as an equivalent layer of rebar.

Elements used in modeling, for the respective DT girders, are: 31, 23 and 25 elements for the slab in the transverse direction; 15, 14 and 14 elements along the depth of the girder; and 42, 48 and 48 elements longitudinally. A total of 2562 elements were used to model the concrete DT-41 girder, 2448 elements for DT-100 and 2544 elements for DT-102A. For the prestressing tendons, 588 elements helped model the strands for the DT-41 girder, and 672 elements replicated the prestressing strands for each of the DT-100 and DT-102A girders.

CFRP strengthening differs for all three girders. The DT-41 girder was strengthened for shear and flexure, DT-100 for shear only, and DT-102A as the first girder. The CFRP was modeled suitably. For the DT-41 girder, 598 elements were used in modeling the

CFRP, and the same number of elements were employed by the DT-102A girder. The DT-100 girder incorporated only 246 elements as CFRP elements, since it was only strengthened for shear capacity gain at support locations. Figure 4.4 to 4.6 show the finite element meshes for all the double-tee girders, respectively.

5.0 EXPERIMENTAL AND FINITE ELEMENT FINDINGS

5.1 GENERAL

The rehabilitation of structures is becoming vastly more commonplace in many application types. For reasons ranging from corrosive environments to out of date, superseded structures, the use of carbon fibre technology is increasing in engineering related works.

For the above cited reasons, among others, it was decided to rehabilitate an accidentally damaged, full-scale AASHTO Type III girder and compare the experimental findings with those obtained from a calibrated and verified computer, finite element analysis generation.

5.2 AASHTO TYPE III GIRDER TESTING

As previously stated, the test subject is a 21.895 m long, prestressed concrete, AASHTO Type III bridge girder. It was accidentally damaged during service by an elevated steel dump-truck box. The girder was then separated from its structure, and delivered to a test site in Downsview, Ontario. After a preliminary examination of the structural state of the girder, it was collectively decided to strengthen it with carbon fibre reinforced polymer sheets, primarily for shear, and secondary for flexure.

After successful grouting and patching of pop out sections and cracks, the FRP application process was conducted. U-wraps, adhered to the perimeter of the girder cross section, were applied at 600 mm intervals. Longitudinal strips, acting as anchor type reinforcement, cover the girder's top and bottom chamfers. Each CFRP system contained 2 plies of both configurations.

The girder was loaded using one ton MTO test blocks in combination with 2.4 ton Jersey barriers. Each load increment was made up of two blocks or two barriers. One load, block or barrier, was placed on one side of the midspan and the other placed symmetrically on the other side. This helped ensure centric loading and behaviour. A total of 84 blocks and 22 barriers were used, calculated as being 136.8 tons (approximately 1368 kN) applied to the girder uniformly.

Upon completion of each load increment, test readings were examined, a walk around the girder and foundations was performed, an eye for the initiation of or propagating cracks was kept, and deflection and torsion, if any, assessed. Dependent on the findings of this investigation was the verdict of whether or not to proceed with testing. Figure 3.66 to 3.79, show views of the loading procedure during experimental testing.

The load achieved experimentally, was approximately twice the design live load capacity for the Type III girder. The design live load capacity considered is equal to an Ontario truck loading of 625 kN, multiplied by two and then divided by four, for a two lane, 4 girder bridge, multiplied by a 1.75 live load factor and the 1.25 dynamic load

allowance. This equates to the girder having a design live load capacity of 684 kN. The live load capacity factor, calculated in accordance with the CHBDC, was founded as being 1.53 for the Type III girder in its original bridge system, as compared to a conservative value of 1.49 achieved experimentally. It must be noted that although the girder during experimental testing did not reach ultimate conditions, it was evident that the ultimate state was being approached since deflection and strain readings were seen to be increasing with constant load. The calculations determined above can be viewed in Appendix B.

5.3 REVIEW OF TESTING RESULTS

Once testing was complete, all cracks along the girder were mapped and photographed. Some cracks commenced in the run-off, excess epoxy, the weaker of the materials, and did not propagate further. Other cracks wrapped around the cross section of the girder, being more prevalent near the midspan as flexure cracks. Shear cracks did begin to appear, although very seldom, as the supports were approached. All crack details can be documented visually in Fig. 5.1. For further viewing consult Fig. 3.80 to 3.84.

All flexural cracks at the midspan region, started from the bottom flange and propagated towards the top of the girder. No concrete crushing was observed at the top deck slab, since the test was discontinued after reaching twice the value of the design live load capacity. Once again, ultimate conditions were imminent as deflection and strain readings intensified with constant load.

Rupture of the CFRP sheets was nonexistent. However, whitening of the epoxy top coating was perceived, signifying visual cracks, due to tension in the epoxy and CFRP materials.

The testing procedure returned incremental readings for individual testing apparatus, which included LVDTs, strain gages, PI gages and settlement values at the supports and bearing pad. These were graphed appropriately and assessed.

5.3.1 Instrumentation Results

The six LVDTs setup to measure downward deflection on the top slab and lateral deflection of the slab and bottom flange, all produced similar values, especially in the linear elastic range. LVDT 2 and 3 are most distinct due to their upward movement just before reaching 3500 kN·m. They are the two inner most LVDTs and may have experienced some interference since the top slab had previously consisted of an asphalt wearing surface, concrete barrier and sidewalk during service. Removal of these common components has rendered the top slab as rough, uneven and jagged. Another possible incidence is due to the fact that since LVDT 2 and 3 experience a vertical rise in their graphs, where strain is constant while load increases, their spring loaded mechanism may have been maxed out. This would imply that instrumentation readings would remain constant once the LVDT extension limit had been reached.

LVDT 1 and 4 were of utmost importance during testing. They were constantly monitored since any large deviation between the two would signify the occurrence of

torsion. As seen on the graph of Fig. 5.2, they are quite similar and thus, torsion averted.

The lateral displacement readings, given by LVDT 5 and 6, are also somewhat similar in the elastic range, referring to Fig. 5.3. Subsequently, they become more dispersed, as seen by LVDT 6. The reason being, that as the girder deflected downwards, so too did the LVDT needle, causing it to extend and bend and not remain horizontal. Physical adjustments were made throughout the test to correct this visual discrepancy.

The strain gage results, for longitudinal strain readings, consist of eight graphs, amalgamating both the strain gages placed on the concrete substrate surface and the CFRP, for relation intent. These graphs are: slab, top flange, top chamfer, top web, mid web, bottom web, bottom chamfer and bottom flange underside.

The *slab* graph plots (Fig. 5.4) all the strain gages placed on the top slab; four at midspan, and four at a 600 mm offset from the midspan. As can be deciphered, all eight gages generated parallel results, all signifying compressive values as expected, and following a general trend.

The *top flange* graph (Fig. 5.5) shows relative results as well, shifting from negative to positive, or compressive to tensile strains, as load is increased. The alteration from compressive to tensile strain occurs at the cracking moment of 2500 kN·m. It is noteworthy to mention that the strain gages, respective to each face of the girder, are

almost identical, signifying that loading is centric to the longitudinal axis of the girder and that torsion is averted.

Review of the *top chamfer* graph (Fig. 5.6) introduces the conclusive fact of similarity in reference to all four strain gages at this location, since all gages here are placed on the CFRP. Again, the elastic range is quite linear and much alike for all gages. Strain gage 22, begins to deviate at 3500 kN·m, quite possibly due to a crack interception. As is the case with the *top flange* graph, strain gages on common faces of the girder are most akin, and a change in strain polarity is observed at approximately 2500 kN·m.

All plots for the *top web* portion graph (Fig. 5.7) are comparable. Strain gages 17 and 29 experience a sudden vertical rise at a moment of just above 3000 kN·m, once cracks have begun to appear. This sudden onset of an increase in load and a constant strain may be a sighting of the phenomenon known as *relaxation* of the concrete. Further probable cases to explain this shift may be a defective or severed strain gage, as well as varying crack propagation. One should note that this increase in load with constant strain is recorded by the strain gages placed on the concrete and is not common for the CFRP strain gages, which continue to withstand strain forces as load is continually applied to the girder.

The *mid web* and *bottom web* graphs (Fig. 5.8 and 5.9, respectively) yield very similar results to the formerly mentioned plot. The only difference being that the two graphs mentioned above reflect purely tensile strains, since the neutral axis is well above the

location of these strain gages, while the *top web* graph reflects both compressive and tensile strains. Again, it is clearly noticeable that the vertical portion of the graphs, where strain is relatively constant as load intensifies, is much more apparent in the gages placed on the concrete as compared to the gages placed on the CFRP. Both the concrete and CFRP experience a slight *relaxation*, but the CFRP does so at a higher moment and at a much higher strain than the concrete strain values. Once more, eccentric or rare crack extension or a faulty strain gage may perhaps hold culpability.

As is the case with the *top chamfer* graph, similar observations can be made for the *bottom chamfer* diagram (Fig. 5.10). Yet again, all strain gages are placed on the CFRP, thus reinforcing the fact that all four graphs should be somewhat equivalent. This is proven by the above mentioned graph which shows corresponding relationship particularly in the elastic range as expected. After the elastic range is surpassed and the nonlinear portion of behaviour is entered, values continue with some gradient property, due to the formation of tensile cracks, as expected at a cracking moment between 2500 kN·m and 3000 kN·m.

The final strain graph (Fig. 5.11), for the *bottom flange underside*, renders allied curves for all strain gages at this location in the elastic range. Theoretically, the strain on a CFRP portion at 600 mm off midspan, should be less than that of a concrete portion at midspan for the same load or moment application. This is evidently regarded on this graph, as CFRP strain gages 33, 34 and 35 possess up to eight times less the strain endured by strain gages 36, 37 and 38, situated on the concrete substrate.

PI gages were placed longitudinally at midspan, on the top slab and underside of the bottom flange to measure compressive and tensile strains, respectively. This is confirmed on the graph shown as Fig. 5.12. PI gage 2, on the top slab, was compared to the strain gage reading for the top slab to verify results. By observation, it is apparent that all values are in the range of $600 \mu\epsilon$. PI gage 1 yields tensile strains upwards of $4000 \mu\epsilon$ at a moment of $4000 \text{ kN}\cdot\text{m}$. These values correspond well to similar values from strain gages also placed on the bottom flange underside.

Settlement recordings from mechanical dial gages at the bearing pad and foundation support were plotted versus moment during loading. Figure 5.13 presents rather alike curves, and as expected, the neoprene bearing pad gave higher settlement values than the support foundation. The maximum value for the bearing pad and support deflection from their original position, being 5.10 mm and 1.96 mm respectively, are so small that they are negligible in regards to the entire structure's deflection.

In general, all the graphs indicated some sort of parallel, especially notable in the elastic range, up until the cracking moment, M_{cr} , was reached. Beyond this range and into the nonlinear range, values become more distributed, yet those for the CFRP continue to illustrate matching trends. Values gained by instrumentation placed on the girder concrete at midspan also tend to have comparable results. Any disagreement encountered may be the result of a propagating crack, some inconsistency on the substrate surface or the specific instrumentation device.

5.3.2 Cross Sectional Strain Distribution

During testing, the onset of visual cracks began within the moment range bounded by 2500 kN·m to 3000 kN·m. Strain values for all positions along the cross section of the girder were gathered for moment values below the cracking moment, in the elastic region, and plotted against the girder height. The objective was to create a cross sectional strain diagram for stages during loading, in order to establish that strain was linear across the cross section, when the cracking moment occurred, the initial onset of cracking and the entrance into the inelastic region of behaviour.

Plots were generated from experimental data, and it was confirmed that the strain was indeed linear up to a moment value of 2500 kN·m, where after nonlinearity was observed. Longitudinal strains at midspan on the concrete surface and the strain at a 600 mm offset on the CFRP, are plotted in Fig. 5.14 to 5.21. The plots, which range from Fig. 5.14 to 5.19 and cover moment values from 500 kN·m to 3000 kN·m, show that as the moment increased, the neutral axis was raised. To further reinforce this extracted fact, strain values for different moment values are plotted on the same graph. Figure 5.20 assembles all strain and moment values beared by the girder at midspan. Similar values, taken on the first U-wrap layer, 600 mm from midspan, are documented in Fig. 5.21. Note, the lesser value of strain at similar points of moment for the CFRP. Also, it is evidently clear that the section depth of the neutral axis decreases with an increase in applied loading.

5.4 COMPARISON OF EXPERIMENTAL AND FINITE ELEMENT ANALYSIS RESULTS

The prior experimental data of three double-tee girders was used to compare their finite element models. All three DT girders had similar attributes to the integral Type III bridge girder. All double-tee girders had prior damage, some more so than others. Each full-scale girder was strengthened using CFRP and tested. This verification-type study went one step further by achieving a sensitivity study, which used both shell and membrane elements to represent the CFRP in the models. The results, based on their degree of agreement, were used to model the Type III I-girder, specific to this study.

ABAQUS analysis of both the DT girders and the Type III I-girder without CFRP strengthening, were compared with that from RESPONSE 2000 in the elastic range. Figure 5.22 to 5.24, for each DT girder correspondingly, show that all three double-tee girders behave similarly in the linear range to their comparison partner. Analogous validation of the ABAQUS modeling is shown in Fig. 5.25 for the AASHTO Type III girder. The reason for this vital yet necessary correlation is to ensure that all dimensions and material properties have been modeled correctly and accurately in consideration to the linear-elastic range of each specimen, respectively. It should be made note of, that RESPONSE 2000 is based on sectional analysis and was verified before using experimental data of the prestressed beams (Bentz, 1999).

After certifying the FE model for accuracy, the CFRP simulation was added to the model. Nonlinear material modeling was then conducted using the appropriate

ABAQUS built-in capabilities. The following paragraphs summarize experimental and theoretical findings for each girder.

The moment-deflection history was documented for the finite element modeling of the DT-41 girder, with and without CFRP application. The former was simulated twice; considering membrane and shell elements, respectively, for CFRP laminates. It can be observed from Fig. 5.26, that considering a two-dimensional element in the analysis did not alter the response. It can also be observed that the structural response of the girders, with CFRP and without CFRP application, is aligned with the experimental findings in the elastic range. The graphs prove that the inclusion of CFRP sheets in rehabilitation did not enhance the flexural stiffness of the girder. However, CFRP strengthening improved the ultimate load carrying capacity of the girder. For example, the maximum moment that was carried theoretically by the girder, in its original state, was $750 \text{ kN}\cdot\text{m}$, while $900 \text{ kN}\cdot\text{m}$ was achieved with the presence of CFRP strengthening; an increase in load capacity of 20%. It is fascinating to mention that the failure moment obtained using the finite element modeling of the rehabilitated girder, at $900 \text{ kN}\cdot\text{m}$, is almost that obtained experimentally. Another observation of interest is that the nonlinearity (the end of the straight line of the elastic range) started at an earlier load increment experimentally, at a moment of $400 \text{ kN}\cdot\text{m}$, compared to the ABAQUS obtained results. This may be attributed to the presence of cracks that accelerated the reduction in the girder flexural stiffness.

The moment-strain relationships for girders DT-41, DT-100 and DT-102A are depicted in Figs 5.27, 5.28 and 5.29, respectively. Fine agreement was generally observed between the experimental findings and the finite element modeling. In the finite element analysis simulations, the elastic response was quite similar with the experimental data. As the response slowly approached the nonlinear range, the slope of the curve changed proportionally for the experimental findings and finite element results.

As a common trend, it can be observed that the nonlinear portion of the response always lags behind the experimental one. This may indicate that the ABAQUS modeling produces a stiffer structure than in reality. With respect to the failure moment, obtained experimentally and using ABAQUS modeling, it can be observed that these moment values are 900 kN·m, and 880 kN·m, respectively for the DT-41 girder, 900 kN·m and 780 kN·m, respectively for the DT-100 girder, and lastly, 1500 kN·m and 1000 kN·m, correspondingly for the DT-102A girder. The discrepancy observed in the last girder may be attributed to the fact that the DT-102A girder modeled with ABAQUS, considered increasing uniform loading over the loading area, while the girder was actually loaded incrementally with barriers from the midspan towards the support. This may have forced the girder to fail, theoretically, at an earlier stage. So, it may be recommended to revisit the finite element modeling analysis and apply the loading increments at exact locations to replicate the testing procedure. It should be noted that this discrepancy was not observed in the first two DT girders, since the applied load was over a short length between the girder quarter points.

Any additional measure of variance in the data may be attributed to many naturally encountered factors. The CFRP was modeled directly over top of the concrete elements, sharing nodal points amongst them. The most apparent fact, was that the finite element model was stiffer than the actual corresponding girder, under nominal conditions. The workmanship of the FRP systems, during the application process, may have been compromised and was not apparent in the FE model, which assumed perfect bonding and no delamination, which occurred in double-tee girders DT-41 and DT-102A. The FE model also did not take into account the existing damage to the girders, which inevitably results in a lower capacity than expected.

Since the verification study, which used previously tested DT girders as the reference specimen, was successful in giving rise to finite element models which duplicated experimental data, it was decided to apply this knowledge to the modeling of the Type III girder. The sensitivity study to yield the most effective manner of replicating CFRP material concluded that no large difference exists between the usage of membrane and shell type elements. Thus for brevity, a similar membrane element was applied to the Type III girder, in a similar manner.

The Type III I-girder finite element model was created using a comparable approach to the modeling technique behind the double-tee girders. Results using the two models discussed earlier; being constant and varying prestress applied to straight tendons, is deliberated. Again, moment-strain and moment-deflection curves were generated and compared to the experimental outcome. The latter set of data is discussed foremost.

The moment-deflection curves for both models put forth relating results, being evident in Fig. 5.30. The elastic range was realistically exemplified and the beginning of the nonlinear portion, even more so. As deduced, the varying prestress model illustrated higher deflection values than the constant prestress model, and both curves stand below that of the experimental product, as should be.

The moment-strain curves, as was the case with the DT girders, also yielded superior results for the I-girder. It is apparent, in Fig. 5.31, that the linear-elastic range has been reproduced extremely well, in addition to the nonlinear range. The constant and varying prestress models are in closer agreement with each other and complement the experimental results rightfully.

For all models, possibilities for any inconsistency are the loss of prestress over time in the prestressing tendons, over the service life of the girders. For pretensioned members these losses include elastic shortening, relaxation of tendons, as well as the creep and shrinkage of the concrete. The FE model, not accounting for any prestress loss, would then have replicated the girder strength as it would have been directly after construction and erection, and hence the higher strength capacity exhibited by all the finite element models.

Specific to the Type III girder, discrepancy in results may lie in the modeling of the prestressing strands. The strands in the physical specimen are harped, and lie straight in a 6096 mm portion at midspan, as seen in Fig. 3.7. This causes an arch-like response to

combat shear at locations near the supports, with the added vertical component from prestressing, and deflection at midspan. A girder with similar strands positioned longitudinally only, would exhibit higher values of deflection, as was the case with the Type III girder finite element model. The harped tendon profile was chosen accordingly, ultimately making the eccentricity at zero moment locations equal to zero. This eccentricity, multiplied by the force in the strand at a certain location, opposes the moment at that specific location. The prestressed member has then only to resist the axial compression exhibited by the strands and the live load applied throughout its structural life.

The ultimate strength of the Type III girder was not reached while testing, thus nominal values in the range exceeding that achieved experimentally will not be discussed in detail.

Figure 5.30 shows the moment-deflection curves for experimental data and that achieved with ABAQUS analysis. The experimentally obtained data yielded a moment of 4057.69 kN·m at a deflection of -113 mm, compared to the constant prestress finite element model, which reached a 3553.4 kN·m moment and a deflection of -111.87 mm. This leads to a 14% difference in moment values obtained for relatively the same deflection. Comparing the analytical results from ABAQUS, being without CFRP (2959 kN·m) and with CFRP, with constant prestress in the tendons (3553.4 kN·m), dictates a 20% gain in flexure capacity.

Evaluating the two ABAQUS Type III girder models concluded that the varying prestress model was approximately 4.3% less stiff than the constant prestress model, as presumed.

Analysis of the moment-strain relationships in Fig. 5.31 reveal the ABAQUS obtained curves in between a series of experimental ones. Relating the maximum experimental value, from strain gage 4, with the constant prestress modeling curve indicated a 5.8% discrepancy in the model. To illustrate further, respective values for moment and strain were 3759.16 kN·m and -437 $\mu\epsilon$ experimentally, in addition to 3553.4 kN·m at a reached strain of -448.36 $\mu\epsilon$.

For all graphs, it can be easily deciphered that the linear-elastic range is very similar in all cases. As cracks formed and the nonlinear range commenced, the proportionality limit was surpassed. The moment at which this occurs, in the region bordered by moment values of 2500 kN·m to 3000 kN·m, is paralleled by all graphs, both experimental and from finite element analysis, adding to the credibility and efficacy of this study. The assumption concerning the occurrence of the cracking moment is further substantiated by the cross sectional strain diagrams originating from the experimental data (Fig. 5.14 to 5.21).

6.0 CONCLUSIONS AND RECOMMENDATIONS FOR FUTURE RESEARCH

6.1 SUMMARY OF STUDY

As structures age, deteriorate and become ever more possible of being replaced by newly constructed and improved ones, a more cost effective method becomes increasingly more attractive. The use of carbon fibre technology is at the forefront of such a vision.

The subject of study, a 21.895 m long AASHTO Type III prestressed I-girder, suffered structural damage when impacted by a heavy construction-type vehicle. It was rendered unfit for service, removed from an integral bridge system, and transported to a test site. The Type III girder then underwent a preliminary loading test which concluded that the girder was well within its sound elastic limit. It was then decided to strengthen the girder with carbon fibre reinforced polymer sheets and evaluate its response to further loading.

Upon completion of strengthening procedures, the girder was fitted for instrumentation and loaded up to 136.8 tons, or 1368 kN. Also of note, is the fact that the Type III girder was loaded experimentally to double the value of its design live load capacity.

A finite element application was established for the girder by modeling formerly tested, and CFRP strengthened, double-tee girders using the ABAQUS program. Once the

values from the finite element modeling were in agreement with the experimental results, a similar modeling technique and procedure was used to predict the structural response of the Type III girder and CFRP material. The finite element results serve to correlate experimental results, and accurately model CFRP strengthened structures.

6.2 CONCLUSIONS

It was confirmed through preliminary testing that the Type III girder, investigated in this study, had not suffered severe damage due to the accident which left it in need of some sort of repair. Based on these test results, it was made clear that this full-scale experimental and analytical venture would incorporate a strengthening procedure, first and foremost.

The creation of finite element models for the DT girders, and their resemblance to experimental results, help to establish a credible basis for the evaluation of the Type III girder and bridges of similar variety. The developed finite element models most accurately predicted and replicated the response of CFRP strengthened structural members, of double-tee and standard I-girder cross section, in the linear-elastic and nonlinear ranges equally. Results concluded that the CFRP strengthening technique applied, efficiently rehabilitated the girder back to its original structural state and enhanced its flexure capacity, as was echoed by the experimental results. The elastic limit was proven as similar in all readings, and then made factual with the cross sectional strain analysis of the girder.

The Type III girder, was essentially rehabilitated back to its original structural capacity, as experimental, and reliable finite element analysis products mutually recorded moment-deflection and moment-strain relations akin to the girder's nominal response. A 20% increase in flexure capacity was realized, via ABAQUS finite element simulation, in contrast to a 13.5% gain formerly predicted to occur at ultimate conditions. As was consistent with all obtained data, the finite element analysis yielded stiffer models in the nonlinear range.

The finite element modeling proved to be conservative in comparison to the experimental data. The same trend was observed when comparing the live load capacity factors for the Type III girder in its original bridge system, as well as the tested condition. This fact is also apparent in design codes where the strength of a member or element is always underestimated, imposing a factor of safety to a certain structure.

Any reduction in strength, due to the damage and deterioration suffered, has at the very least been restored to the previously existing structural state. This shows that the proposed rehabilitation schemes were effective in raising the girder's rating to acceptable and operable levels.

The adopted rehabilitation system for the AASHTO Type III girder was proved very efficient, since only three full days were needed to apply the CFRP system and strengthen the girder, imposing minimal road closures during application execution, had the girder been rehabilitated in-situ.

6.3 CONSIDERATIONS FOR FUTURE RESEARCH

Since values obtained comment on the flexural state of the girder predominantly, an almost necessary future endeavour seems to be the reproduction of this study to evaluate shear capacity. The configuration of the CFRP composite system dictates that the girder has been mainly strengthened for shear capacity gain purposes.

Diverse CFRP configurations are also of interest. Literature suggests that the application of CFRP fibres be perpendicular to cracks, or diagonally placed, in the case of the Type III girder. It would be anticipated that this application layout would add to the shear strength of a member.

The effect of creep, CFRP resistance to weathering, and the overall resilience of the Type III girder can all be assessed in a few years time, by reloading the girder, similarly, once more. This would allow for constructive comment on the ability of the CFRP system to withstand freeze-thaw cycles on a full-scale, outdoor specimen, in an extensively harsh climate.

Another possible future undertaking is the extension of the finite element study to incorporate certain important attributes of the DT and Type III girders more accurately. The study would look to include the effects of prestress loss specific to pretensioned elements, sustained structural damage and the differences in the modeling of epoxy adhesives and fibre reinforced polymers as two separate entities.

REFERENCES

- Abdalla, H. and Kennedy, J.B. 1993. *Analysis of Prestressed Girders with Openings*. Computers & Structures, Vol. 47, No. 3, pp. 505-510.
- Abdalla, H. and Kennedy, J.B. 1995. *Dynamic Analysis of Prestressed Concrete Beams with Openings*. Journal of Structural Engineering, Vol. 121, No. 7, pp. 1058-1068.
- American Association of State Highway Officials. 1969. *Standard Specifications for Highway Bridges, 10th ed.* Washington, DC: Association General Officers.
- American Concrete Institute Committee 440. 1996. *State-of-the-Art Report on Fiber Reinforced Plastic Reinforcement for Concrete Structures*. USA: ACI.
- Antonopoulos, C.P., and Triantafillou, T.C. 2003. *Experimental Investigation of FRP Strengthened RC Beam Column Joints*. Journal of Composites for Construction, Vol. 7, No. 4, pp. 39-49.
- Bakht, B. 1998. *Observed Behavior of a New Medium Span Slab-On-Girder Bridge*. Toronto: The Research and Development Branch, MTO.
- Bakht, B., Al-Bazi, G., Banthia, N., et al. 2000. *Canadian Bridge Design Code Provisions for Fiber-Reinforced Structures*. Journal of Composites for Construction, Vol. 4, No. 1, pp. 3-15.
- Bentz, E. 1999. *RESPONSE 2000, version 1.1, Nonlinear Sectional Analysis Program*. Toronto, Canada.
- Bettingole, N. and Robison, R. 1997. *Bridge Decks*. New York: American Society of Civil Engineers.
- Bonacci, J.F. and Maalej, M. 2000. *Externally Bonded Fiber Reinforced Polymers for Rehabilitation of Corrosion Damaged Concrete Beams*. ACI Structural Journal, Vol. 97, No. 5, pp. 703-711.
- Bonacci, J.F. and Maalej, M. 2001. *Behavior Trends of RC Beams Strengthened with Externally Bonded FRP*. ASCE Journal of Composites for Construction, Vol. 5, No. 2, pp. 102-113.
- Brena, S.F., Bramblett, R.M., Wood, S.L. and Kreger, M.E. 2003. *Increased Flexural Capacity of Reinforced Concrete Beams Using Carbon Fiber Reinforced Polymer Composites*. ACI Structural Journal, Vol. 100, No. 1, pp. 36-46.

- CAN/CSA-S6-00, 2000. *Canadian Highway Bridge Design Code*. Ontario: Canadian Standards Association.
- Canadian Network of Centres of Excellence on Intelligent Sensing for Innovative Structures. 2001. *Strengthening Reinforced Concrete Structures with Externally-Bonded Fibre Reinforced Polymers*. Canada: ISIS Canada.
- Chaallal, O., Nollet, M. and Perraton, D. 2002. *Strengthening of Reinforced Concrete Beams with Externally Bonded Fiber-Reinforced-Plastic Plates: Design Guidelines for Shear and Flexure*. Canadian Journal of Civil Engineering, Vol. 25, No. 4, pp. 692-704.
- Chansawat, K., Yim, Soloman C.S. and Miller, Thomas H. 2006. *Nonlinear Finite Element Analysis of a FRP-Strengthened Reinforced Concrete Bridge*. Journal of Bridge Engineering, Vol. 11, No. 1, pp. 21-32.
- Chen, W.F. 1999. *Structural Engineering Handbook*. USA: CRC Press LLC.
- Chen, W.F. and Duan, Lian. 2000. *Bridge Engineering Handbook*. USA: CRC Press LLC.
- Chen, W.F. and Liew, J.Y. Richard. 2003. *The Civil Engineering Handbook, 2nd ed.* USA: CRC Press LLC.
- Chung, Natalie Y.L. 2002. *Fibre Reinforced Polymer Composites* [online]. Available from World Wide Web: (www.gnatching.tripod.com/FRP/).
- Cofini, A. 2005. *Strengthening Full-Scale Damaged Precast / Prestressed Concrete Double-Tee Girders Using CFRP Sheets*. M.Eng Thesis, Civil Engineering Department, Ryerson University, Toronto, Ontario, Canada.
- Collins, M.P., and Mitchell, D. 1997. *Prestressed Concrete Structures, 2nd ed.* Canada: Copywell Response Publications.
- Colombi, P. and Poggi, C. 2006. *An Experimental, Analytical and Numerical Study of the Behavior of Steel Beams Reinforced by Pultruded CFRP Strips*. Elsevier Composites, Vol. 37, pp. 64-73.
- De Lorenzis, L., Miller, B. and Nanni, A. 2001. *Bond of Fiber Reinforced Polymer Laminates to Concrete*. ACI Materials Journal, Vol. 98, No. 3, pp. 256-264.
- Deniaud, B. and Cheng, O. 2001. *Review of Shear Design Methods for Reinforced Concrete Beams Strengthened with Reinforced Polymer Sheets*. Canadian Journal of Civil Engineering, Vol. 28, pp. 271-281.

- Ebead, U. and Marzouk, H. 2004. *Fiber-Reinforced Polymer Strengthening of Two-Way Slabs*. ACI Structural Journal, Vol. 101, No. 5, pp. 650-659.
- Fanning, P.J. and Kelly, O. 2001. *Ultimate Response of RC Beams Strengthened with CFRP Plates*. ASCE Journal of Composites for Construction, Vol. 4, No. 2, pp. 122-127.
- Fisher, J.W. 1984. *Fatigue and Fracture in Steel Bridges*. New York: John Wiley & Sons.
- Gopinath, A. and Mullen, C. *Computational Modeling of CFRP Retrofitted Design for Seismic Upgrade of CMU Walls*.
- Gottemoeller, F. 1988. *Bridgescape: The Art of Designing Bridges*. New York: John Wiley & Sons.
- Harraq, A., Neale, K.W., Paultre, P. 2002. *Investigation of Prestressed Concrete Girders Strengthened with Externally Bonded Carbon Fiber Sheets*. 4th Structural Specialty Conference of the Canadian Society for Civil Engineering, Montreal, Quebec, Canada Society for Civil Engineering, pp. 1-10.
- Heins, C.P., and Firmage, D.A. 1979. *Design of Modern Steel Highway Bridges*. New York: John Wiley & Sons, Inc.
- Hibbitt, H.D., Karlson, B.I. and Sorenson, E.P. 2006. *ABAQUS, version 6.5, Finite Element Program*. Providence, R.I., USA: Hibbitt, Karlson & Sorenson, Inc.
- Hollaway, L.C. and Leeming, M.B. 1999. *Strengthening of Reinforced Concrete Structures Using Externally-Bonded FRP Composites in Structural and Civil Engineering*. England: Woodhead Publishing Limited.
- Hu, H.T., Lin, F.M. and Jan, Y.Y. 2004. *Nonlinear Finite Element Analysis of Reinforced Concrete Beams Strengthened by Fiber-Reinforced Plastics*. Elsevier Composite Structures, Vol. 63, pp. 271-281.
- Kwasniewski, L., Szerszen, M.M. and Nowak, A.S. 2000. *Sensitivity Analysis for Slab-on-Girder Bridges*. 8th ASCE Specialty Conference on Probabilistic Mechanics and Structural Reliability, pp. 1-6.
- Labossiere, P., Neale, K.W., Rochette, P., Demers, M., Lamothe, P., Lapierre, P. and Desgagne, G. 2000. *Fibre Reinforced Polymer Strengthening of the Sainte-Emelie-de-L'Energie Bridge: Design, Instrumentation, and Field Testing*. Canadian Journal of Civil Engineering, Vol. 27, pp. 916-927.
- Logan, Daryl L. 2002. *A First Course in the Finite Element Method*, 3rd ed. USA: Wadsworth Group, Brooks / Cole.

- Mair, Robert Ian. 1999. *Fibre Reinforcement Polymers: From Aerospace to Infrastructure*. ATSE Focus Journal, No. 107.
- McGuire, W., Gallagher, R.H. and Ziemian, R.D. *Matrix Structural Analysis*, 2nd ed. USA: John Wiley & Sons, Inc.
- Mertol, H.C., Kim, S.J., Mirmiran, A., Rizkalla, S. and Zia, P. *Behavior and Design of HSC Members Subjected to Axial Compression and Flexure*. Proceedings of the Seventh International Symposium on Utilization of High-Strength/High Performance Concrete, Washington, D.C., June 20-24, 2005.
- Nawy, Edward G. 2003. *Prestressed Concrete: A Fundamental Approach*. USA: Prentice Hall.
- Nozaka, K., Shield, Carol K. and Hajjar, Jerome F. 2005. *Effective Bond Length of Carbon-Fiber-Reinforced Polymer Strips Bonded to Fatigued Steel Bridge I-Girders*. Journal of Bridge Engineering, Vol. 10, No. 2, pp. 195-205.
- Ontario Highway Bridge Design Code, 2nd ed. 1983. Toronto: The Highway Engineering Division.
- Pritchard, B. edition 1994. *Continuous and Integral Bridges*. Great Britain: E & FN Spon.
- Sebastian, W.M. 2001. *Significance of Midspan Debonding Failure in FRP-Plated Concrete Beams*. ASCE, Journal of Structural Engineering, Vol. 127, No. 7, pp. 792-798.
- Sennah, K., Cofini, A., Emam, A., Okeil, A., and Attalla, M. 2006. *Strengthening Full-Scale Damaged Precast / Pretensioned Concrete Double-Tee Girders using CFRP Sheets*. 7th International Conference on Short and Medium Span Bridges, CSCE, Montreal, Quebec, 2006, pp. 1-10.
- Shahawy, M. and Okeil, A.M. 2004. *Hybrid Bridge Strengthening: The Structural Rehabilitation of Blue Heron Bridge*. TRB 2004 Annual Meeting CD-ROM, pp. 1-23.
- Sheikh S.A., DeRose, D. and Mardukhi, J. 2002. *Retrofitting of Concrete Structures for Shear and Flexure with Fiber Reinforced Polymers*. ACI Structural Journal, Vol. 99, No. 4, pp. 451-459.
- Spadea, G., Swamy, R.N. and Bencardino, F. 2001. *Strength and Ductility of RC Beams Repaired with Bonded CFRP Laminates*. Journal of Bridge Engineering, Vol. 6, No. 5, pp. 349-355.

- Taljsten, B. 2003. *Strengthening Concrete Beams for Shear with CFRP Sheets*. Elsevier Construction and Building Materials, Vol. 17, pp. 15-26.
- Taly, N. 1998. *Design of Modern Highways Bridges*. New York: McGraw Hill Companies Inc.
- Tavakkolizadeh, M. and Saadatmanesh, H. 2003. *Strengthening of Steel-Concrete Composite Girders Using Carbon Fiber Reinforced Polymer Sheets*. Journal of Structural Engineering, Vol. 129, No. 1, pp. 30-40.
- Teng, J.G., Chen, J.F., Smith, S.T. and Lam, L. 2002. *FRP Strengthened RC Structures*. England: John Wiley & Sons, Inc.
- Toutanji, H. and Balaguru, P. 1998. *Durability and Characteristics of Concrete Columns Wrapped with FRP Tow Sheets*. Journal of Materials in Civil Engineering, Vol. 10, No. 1, pp. 52-57.

Table 2.1 – Double-tee girder dimensional properties

Dimensional Characteristic (mm)	Girder Designation		
	DT-41	DT-100	DT-102A
Length	16,900	19,150	19,150
Width	3190	2415	3400
Depth	810	760	760
Slab Thickness	100	100	100
Dapped End Depth	445	500	500
Dapped End Length	200	200	200
Bottom Web Width	100	100	100
Top Web Width	170	170	170
Distance between Webs	1500	1500	1500

Table 2.2 – Double-tee girder reinforcement properties

Reinforcement Characteristic	Girder Designation		
	DT-41	DT-100	DT-102A
Longitudinal	12.7 mm 7 wire strand tendon (70% prestress)	15.8 mm 7 wire strand tendon (72% prestress)	15.8 mm 7 wire strand tendon (72% prestress)
Shear	102 × 102- MW25.8 × MW25.8	152 × 152- MW18.7 × MW18.7	152 × 152- MW18.7 × MW18.7
Flange	300 × 102- MW18.7 × MW25.8	300 × 102- MW13.3 × MW25.8	300 × 102- MW13.3 × MW25.8
Flange Connectors	10 @ 125 mm o/c	varied	varied

Table 2.3 – Double-tee girder concrete properties

f'_c (MPa)		
DT-41	DT-100	DT-102A
35	45	45

Table 2.4 – Tyfo® SCH-41S carbon fibre sheet dry fibre properties

Typical Dry Fibre Properties		
Notation	Property	Value
$f_{u,frp}$	Tensile Strength	3790 MPa
E_{frp}	Tensile Modulus	230,000 MPa
$\epsilon_{u,frp}$	Ultimate Elongation	0.017
γ_{frp}	Mass Density	1740 kg/m ³
	Weight per Square Meter	0.664 kg/m ²

Table 2.5 – Tyfo® Epoxy material properties

Epoxy Material Properties		
Notation	Property	Value
$f_{u,ep}$	Tensile Strength	50.7 MPa
E_{ep}	Tensile Modulus	2230 MPa
ϵ_{ep}	Elongation	0.035
	Temperature Gradient Post Cure	82°C
	Flexural Strength	86.4 MPa
	Flexural Modulus	2180 MPa

Table 2.6 – Tyfo® SCH-41S Composite laminate properties

Composite Gross Laminate Properties			
Notation	Property	Test Value	Design Value
$f_{u,comp}$	Ultimate Tensile Strength (primary fibre direction)	876 MPa	745 MPa
$\epsilon_{u,comp}$	Elongation at Break	0.012	0.01
E_{comp}	Tensile Modulus	72,400 MPa	61,500 MPa
$f_{u,comp}$	Ultimate Tensile Strength (90° to primary fibre direction)	40.6 MPa	34.5 MPa
t_{comp}	Laminate Thickness	1.0 mm	1.0 mm

Table 3.1 – AASHTO Type III concrete girder dimensional properties

A (mm ²)	y _b (mm)	I (mm ⁴)	Weight	
			(kg/m)	(kN/m)
361,290	514.86	5.22×10^{10}	869	8.52

Table 3.2 – AASHTO Type III concrete girder properties

f _c (MPa)	E _c (MPa)	ε _y (mm/mm)	ε _{cu} (mm/mm)	γ _c (kg/m ³)	ν
34.5	26,400	0.002	0.0035	2400	0.20

Table 3.3 – AASHTO Type III concrete girder cover

Minimum Concrete Cover (mm)	
Top	Bottom
40	25

Table 3.4 – Concrete slab properties

f _c (MPa)	E _c (MPa)	ε _y (mm/mm)	ε _{cu} (mm/mm)	γ _c (kg/m ³)	ν
27.6	23,600	0.002	0.0035	2400	0.20

Table 3.5 – Concrete slab cover

Minimum Concrete Cover (mm)	
Top	Bottom
50	40

Table 3.6 – Prestressing steel characteristics

Tendon Type	Grade f _{pu} (MPa)	Size Designation	Nominal Dimension		Mass (kg/m)
			Diameter (mm)	Area (mm ²)	
Seven wire strand	1860	13	12.70	99	0.775

Table 3.7 (a) – Prestressing steel properties

f_{py} (MPa)	f_{pi} (MPa)	f_{pc} (MPa)	E_p (MPa)
1690	1298	1058	200,000

Table 3.7 (b) – Prestressing steel properties

F_{pu} (kN)	F_{pi} (kN)	F_{pc} (kN)	ϵ_y (mm/mm)	ϵ_u (mm/mm)
183.7	128.5	104.75	0.0086	0.043

Table 3.8 – Reinforcing steel properties

f_y (MPa)	f_u (MPa)	E_s (MPa)	ϵ_y (mm/mm)	F_u (MPa)	F_y (MPa)	G (MPa)	ν
400	600	200,000	0.0021	520 - 690	400	77,000	0.30

Table 3.9 – Reinforcing steel geometric properties

Bar No.	Nominal Dimension		Mass (kg/m)
	Diameter (mm)	Area (mm ²)	
10M	11.3	100	0.785
15M	16.0	200	1.570
20M	19.5	300	2.355
25M	25.2	500	3.925

Table 3.10 – Preliminary testing load application procedure

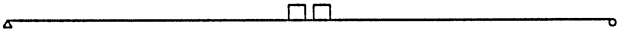
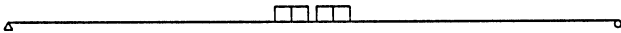
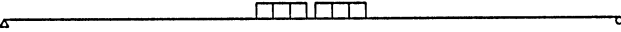
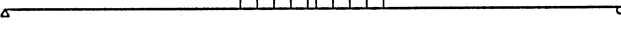
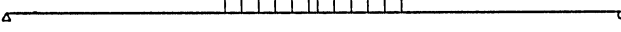
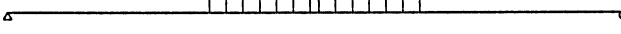
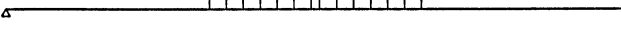
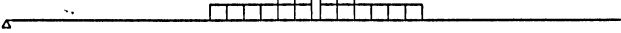
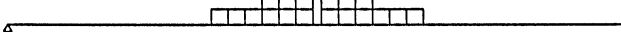
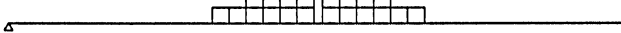
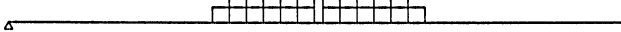
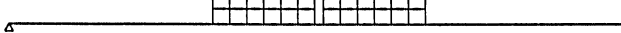
Tons	kN	Load Increment (Two Layers of Blocks)
2	19.6	
4	39.2	
6	58.9	
8	78.5	
10	98.1	
12	117.7	
14	137.3	
16	157	
18	176.6	
20	215.8	
22	235.44	
24	255.1	

Table 3.11 – Preliminary testing readings from LVDTs

Load		Moment (kN·m)	Deflection (mm) from LVDTs			
Tons	kN		1	2	3	4
2	19.6	104.66	-0.32	-0.48	-0.42	-0.05
4	39.2	203.43	-1.01	-1.16	-1.17	-0.25
6	58.9	296.30	-1.75	-1.95	-1.94	0.08
8	78.5	383.26	-2.49	-2.69	-2.73	0.49
10	98.1	464.34	-3.16	-3.36	-3.4	0.41
12	117.7	539.51	-3.99	-4.14	-4.22	0.1
14	137.3	644.17	-4.86	-5.03	-5.14	0.02
16	157	742.94	-5.71	-5.91	-6.04	0.39
18	176.6	835.80	-6.63	-6.83	-6.97	0.2
20	215.8	922.77	-7.28	-7.53	-7.62	0.1
22	235.44	1003.84	-8.36	-8.61	-8.72	0.76
24	255.1	1079.02	-9.06	-9.37	-9.43	1

Table 3.12 – Preliminary testing readings from strain gages

Load		Moment (kN·m)	Strain values ($\mu\epsilon$) from strain gages			
Tons	kN		1	2	3	4
2	19.6	104.66	22.49	4.31	15.29	1.92
4	39.2	203.43	57.89	8.15	28.19	17.24
6	58.9	296.30	66.03	11.98	43.95	18.2
8	78.5	383.26	70.33	16.29	56.85	13.89
10	98.1	464.34	83.25	20.13	64.02	8.14
12	117.7	539.51	90.43	24.44	74.53	0.48
14	137.3	644.17	101.91	26.36	91.73	-7.66
16	157	742.94	119.62	30.19	108.45	-11.5
18	176.6	835.80	140.68	34.02	120.87	-16.76
20	215.8	922.77	158.38	37.38	131.39	-22.03
22	235.44	1003.84	178.48	44.57	150.5	-29.7
24	255.1	1079.02	196.19	48.4	159.58	-32.09

Table 3.13 – Concrete grout compression test results

Material	Core Value (MPa)			Compressive Strength (MPa)
	1	2	3	Test Average
Concrete Top Supreme	51.82	50.42	50.16	50.8
Verticoat Supreme	39.05	42.05	36.78	39.3

Table 3.14 – Concrete grout in-direct tension test results

Material	Core Value (MPa)			Tensile Strength (MPa)
	1	2	3	Test Average
Concrete Top Supreme	14.18	13.46	15.14	14.3
Verticoat Supreme	11.15	13.70	12.35	12.4

Table 3.15 – Tyfo® SCH-11UP carbon fibre sheet dry fibre properties

Typical Dry Fibre Properties		
Notation	Property	Value
$f_{u,frp}$	Tensile Strength	3790 MPa
E_{frp}	Tensile Modulus	230,000 MPa
$\epsilon_{u,frp}$	Ultimate Elongation	0.017
γ_{frp}	Mass Density	1740 kg/m ³
t_{frp}	Fibre Thickness	0.127 mm
	Weight per Square Meter	0.298 kg/m ²

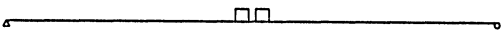
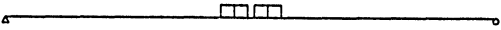

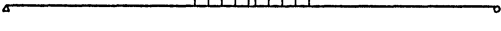
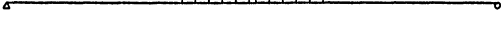








Table 3.16 – Tyfo® S Epoxy material properties

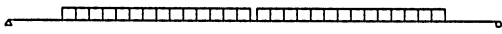
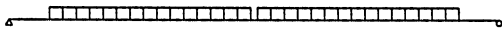
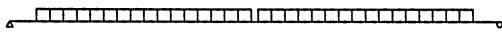
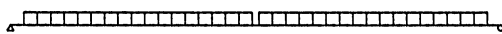
Epoxy Material Properties		
Notation	Property	Value
$f_{u,ep}$	Tensile Strength	72.4 MPa
E_{ep}	Tensile Modulus	3180 MPa
ϵ_{ep}	Elongation	0.05
	Temperature Gradient Post Cure	82°C
	Flexural Strength	123.4 MPa
	Flexural Modulus	3120 MPa

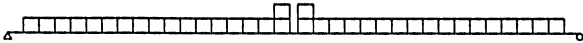
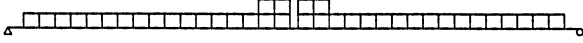
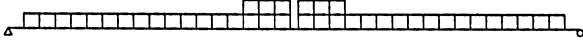
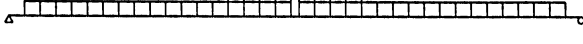
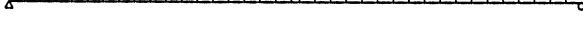

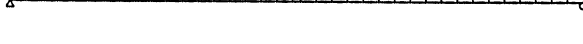

Table 3.17 – Tyfo® SCH-11UP Composite laminate properties

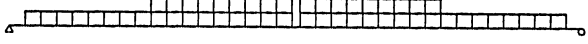
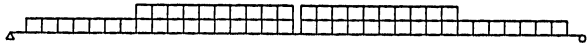
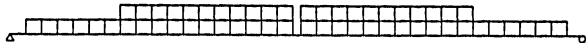
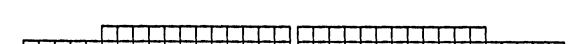
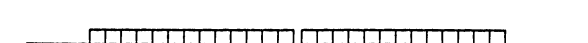
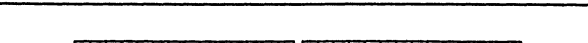
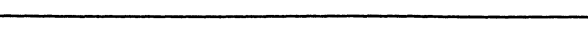
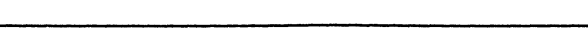
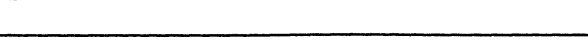
Composite Gross Laminate Properties			
Notation	Property	Test Value	Design Value
$f_{u,comp}$	Ultimate Tensile Strength (primary fibre direction)	1062 MPa	903 MPa
$\epsilon_{u,comp}$	Elongation at Break	0.0105	0.0105
E_{comp}	Tensile Modulus	102,000 MPa	86,900 MPa
$f_{u,comp}$	Ultimate Tensile Strength (90° to primary fibre direction)	0	0
t_{comp}	Laminate Thickness	0.25 mm	0.25 mm



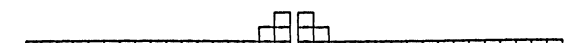
Table 3.18 – Final testing load application procedure and corresponding moment

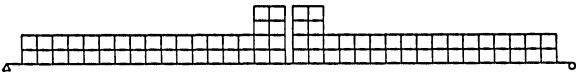
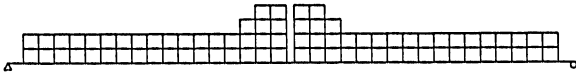
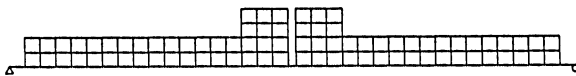
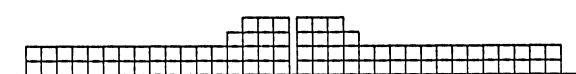
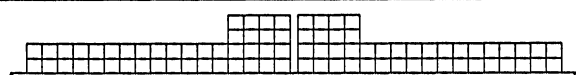
Tons	kN	Load Increment (First Layer of Blocks)	Moment (kN·m)
2	19.6		104.66
4	39.2		203.43
6	58.9		296.30
8	78.5		383.26
10	98.1		464.34
12	117.7		539.51
14	137.3		608.78
16	157		672.16
18	176.6		729.64
20	196.2		781.22
22	215.8		826.91
24	235.44		866.69
26	255.1		900.58

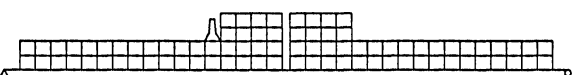
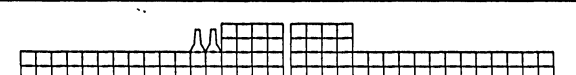
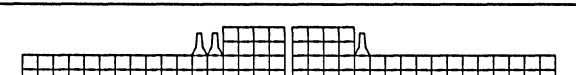
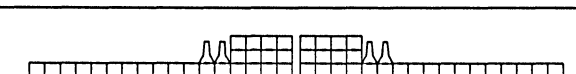
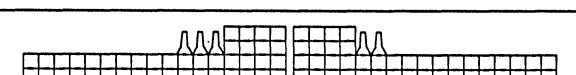
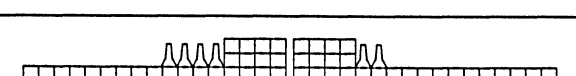
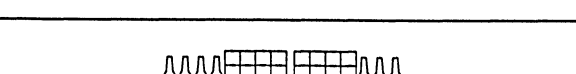
Tons	kN	Load Increment (First Layer of Blocks)	Moment (kN·m)
28	274.7		928.57
30	294.3		950.67
32	313.9		966.86
34	333.5		977.16

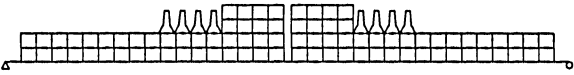
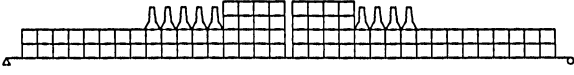

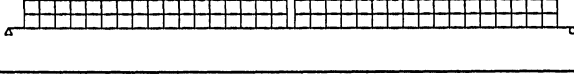
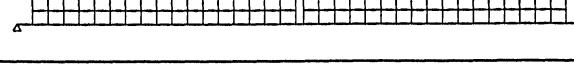
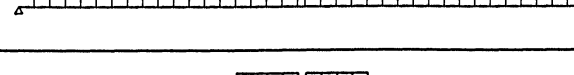
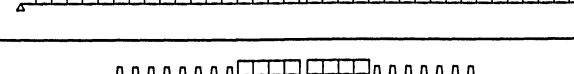
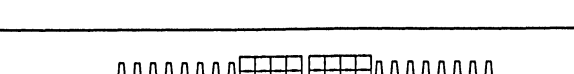
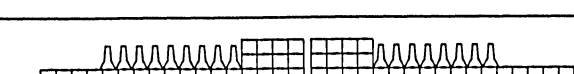
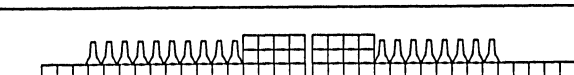
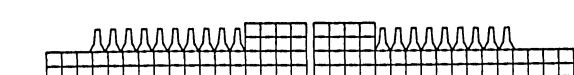
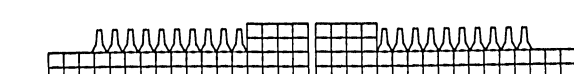

Tons	kN	Load Increment (Second Layer of Blocks)	Moment (kN·m)
36	353.2		1081.82
38	372.8		1180.58
40	392.4		1273.45
42	412		1360.42
44	431.6		1441.49
46	451.3		1516.66
48	470.9		1585.94
50	490.5		1649.32

Tons	kN	Load Increment (Second Layer of Blocks)	Moment (kN·m)
52	510.1		1706.80
54	529.7		1758.38
56	549.4		1804.06
58	569		1843.85
60	588.6		1877.74
62	608.2		1905.73
64	627.8		1927.82
66	647.5		1944.02
68	667.1		1954.31

Tons	kN	Load Increment (Third and Fourth Layer of Blocks)	Moment (kN·m)
70	686.7		2058.97
72	706.3		2163.64
74	725.9		2262.40

Tons	kN	Load Increment (Third and Fourth Layer of Blocks)	Moment (kN·m)
76	745.6		2361.17
78	765.2		2454.03
80	784.8		2546.90
82	804.4		2633.87
84	824		2720.84

Tons	kN	Load Increment (Jersey Barrier Layer)	Moment (kN·m)
86.4	847.6		2816.35
88.8	871.1		2904.90
91.2	894.7		3000.41
93.6	918.2		3088.97
96	941.8		3170.58
98.4	965.3		3245.24
100.8	988.8		3326.85

Tons	kN	Load Increment (Jersey Barrier Layer)	Moment (kN·m)
103.2	1012.4		3401.51
105.6	1036		3469.23
108	1059.5		3529.99
110.4	1083		3597.71
112.8	1106.6		3658.47
115.2	1130.1		3712.29
117.6	1153.7		3759.16
120	1177.2		3812.98
122.4	1200.7		3859.85
124.8	1224.3		3899.77
127.2	1247.8		3932.74
129.6	1271.4		3972.67
132	1294.9		4005.64

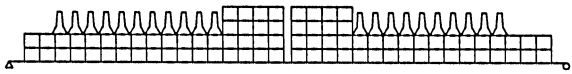
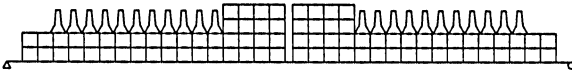
Tons	kN	Load Increment (Jersey Barrier Layer)	Moment (kN·m)
134.4	1318.5		4031.67
136.8	1342		4057.69

Table 4.1 – Finite element modeling calibration values

Maximum Stress at Midspan (MPa)			
Girder	ABAQUS	Bending Formula	% Difference
DT-41	9.567	10.054	4.84
DT-100	12.21	12.646	3.45
DT-102A	14.43	14.241	1.31
Type III	5.428	5.030	7.33

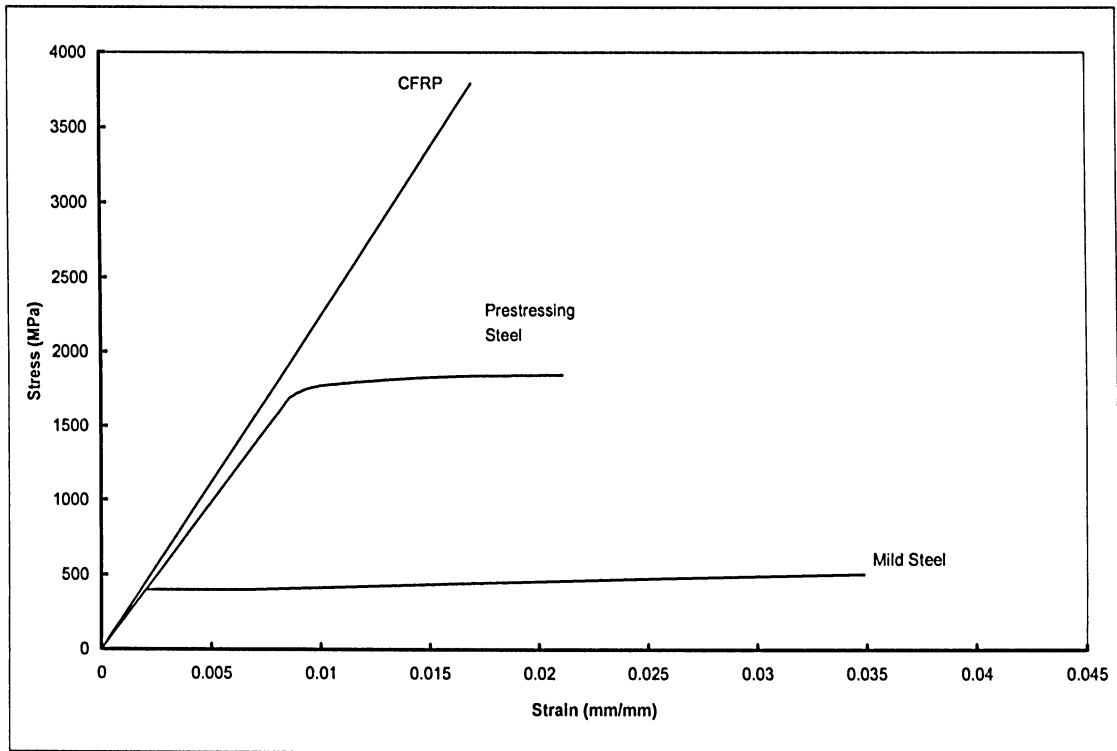


Figure 2.1 – Stress vs. strain comparison for various reinforcing materials

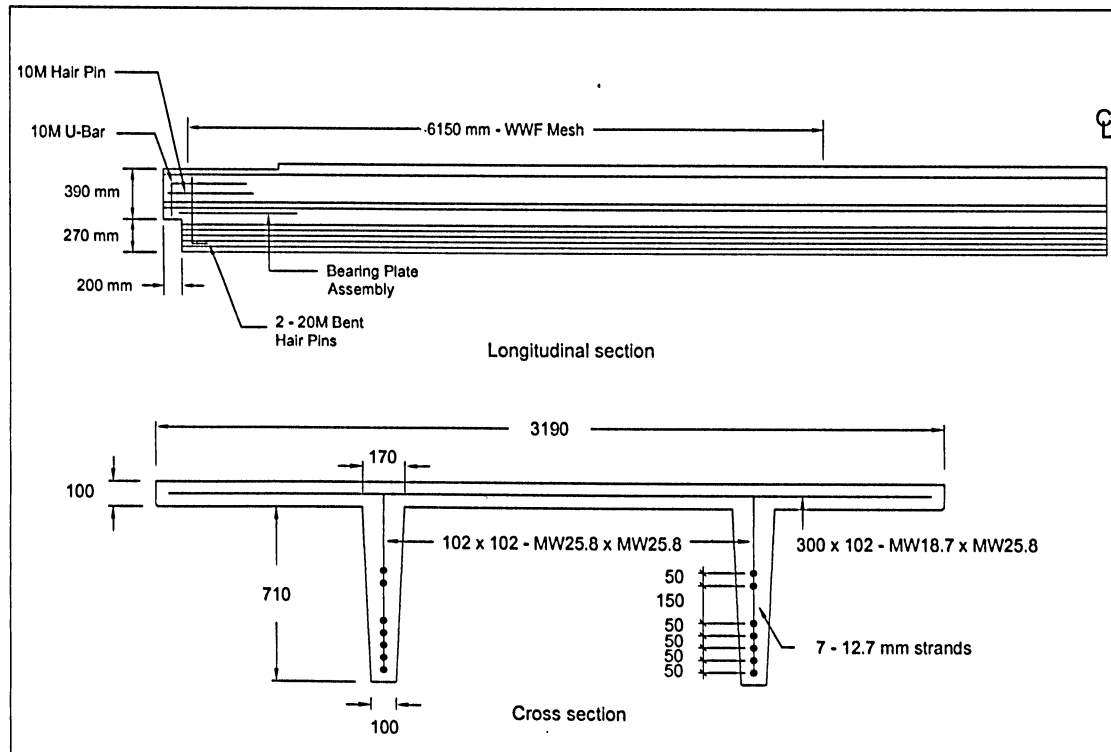


Figure 2.2 – DT-41 girder reinforcement details (Cofini, 2005)

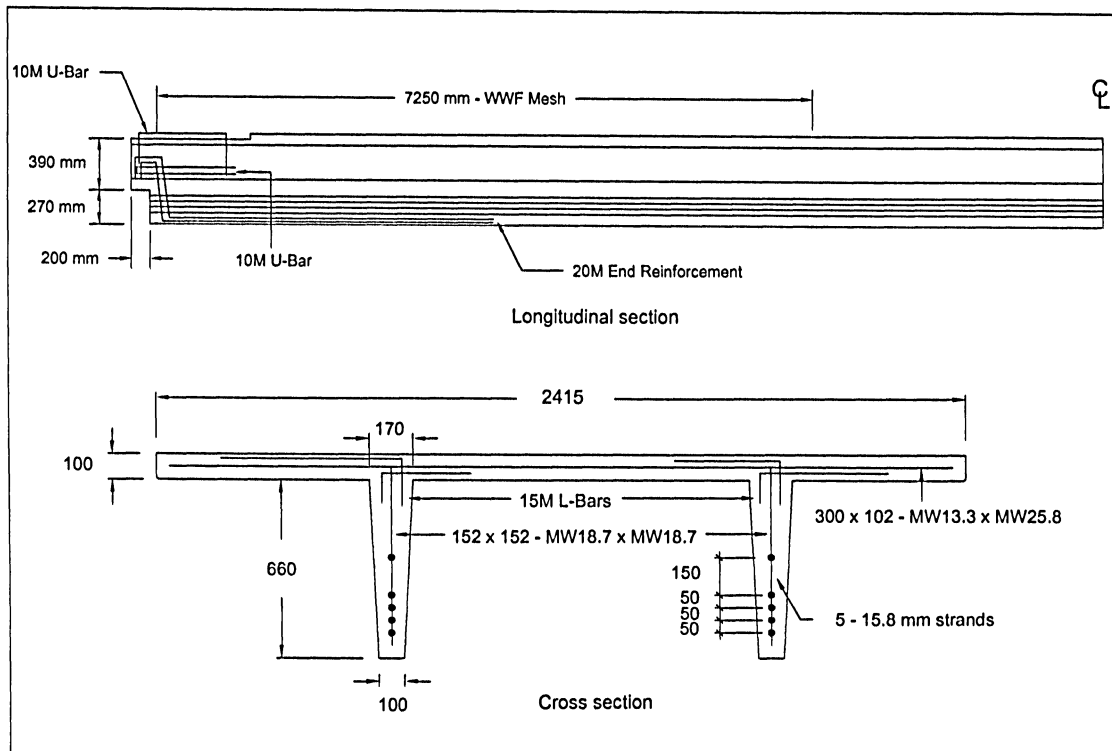


Figure 2.3 – DT-100 girder reinforcement details (Cofini, 2005)

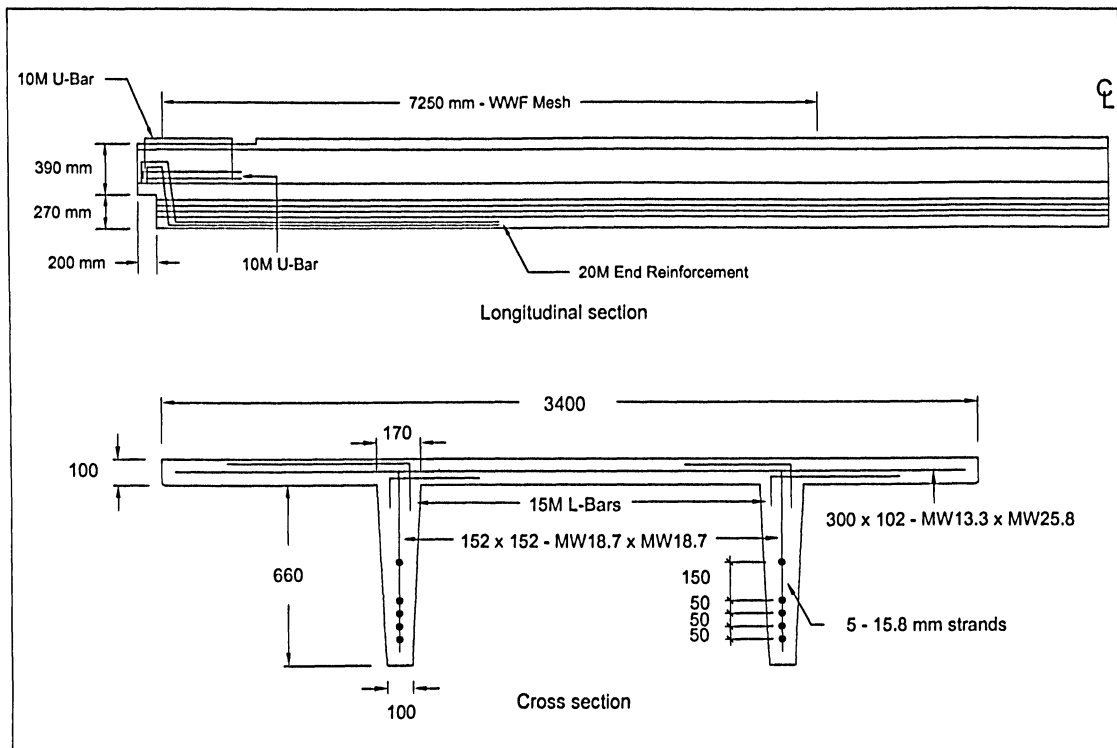


Figure 2.4 – DT-102A girder reinforcement details (Cofini, 2005)

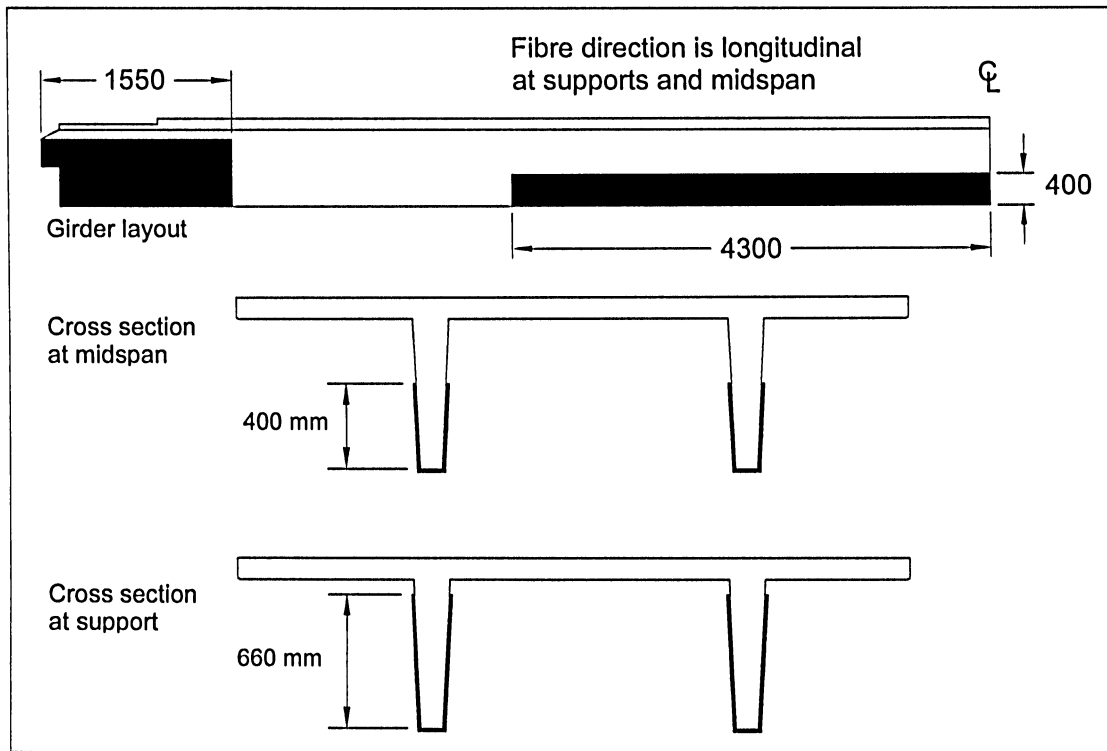


Figure 2.5 – DT-41 girder CFRP layout (Cofini, 2005)

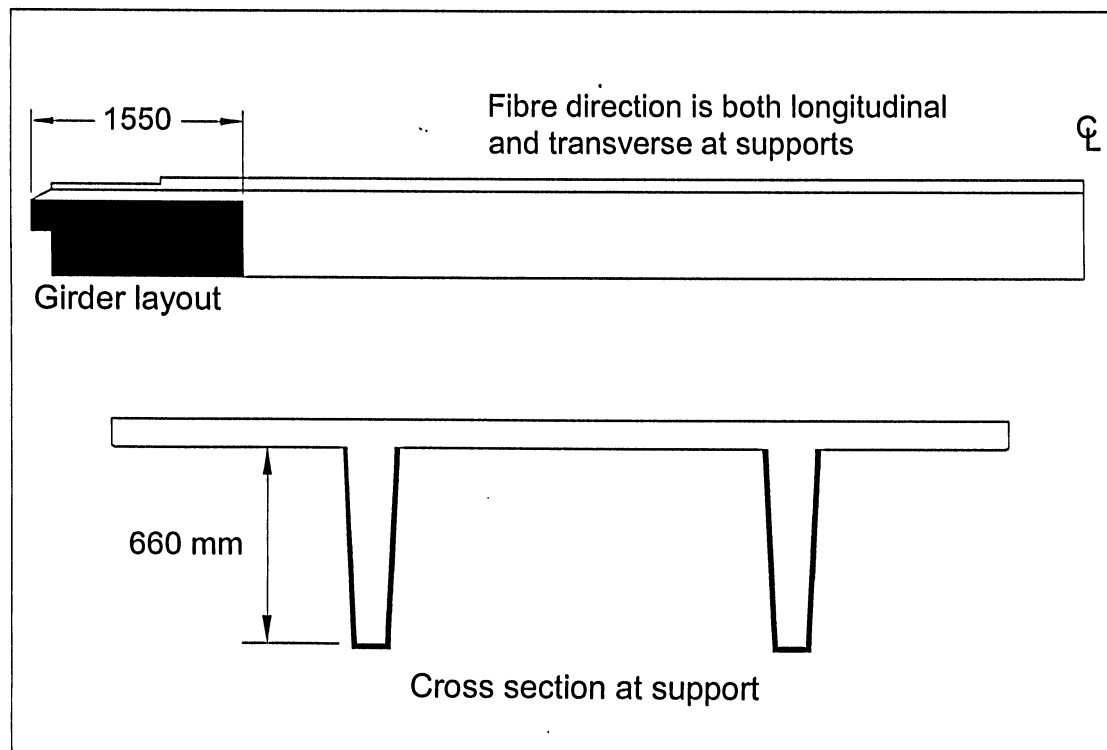


Figure 2.6 – DT-100 girder CFRP layout (Cofini 2005)

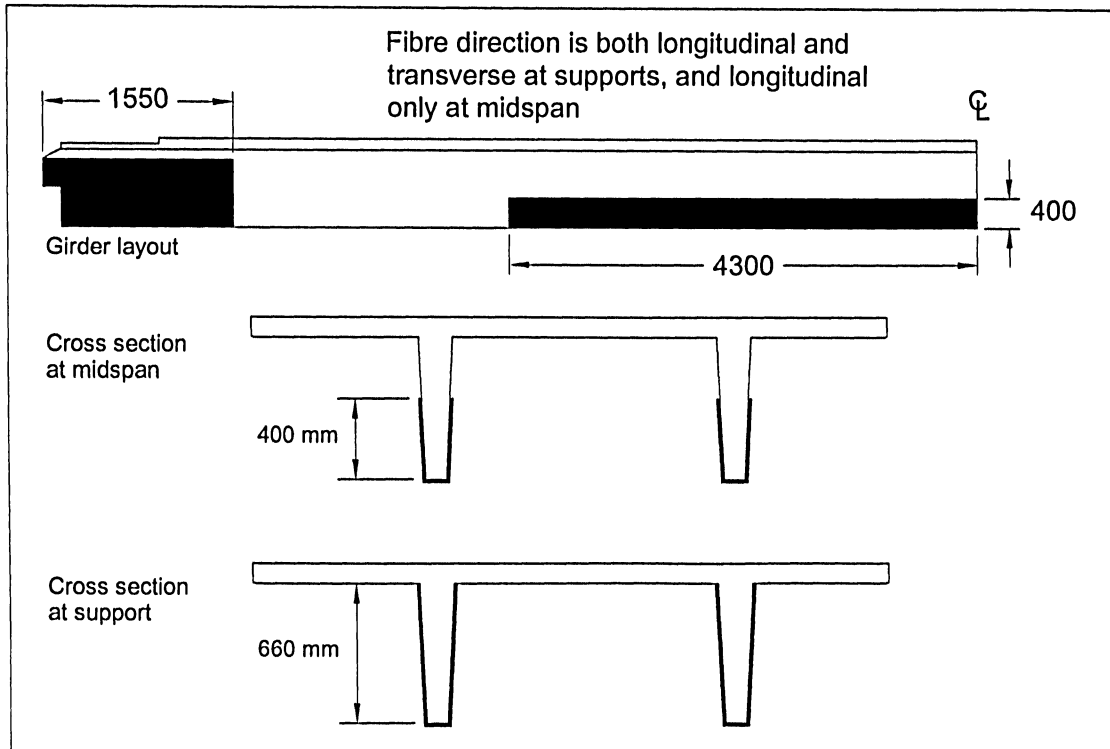


Figure 2.7 – DT-102A girder CFRP layout (Cofini, 2005)

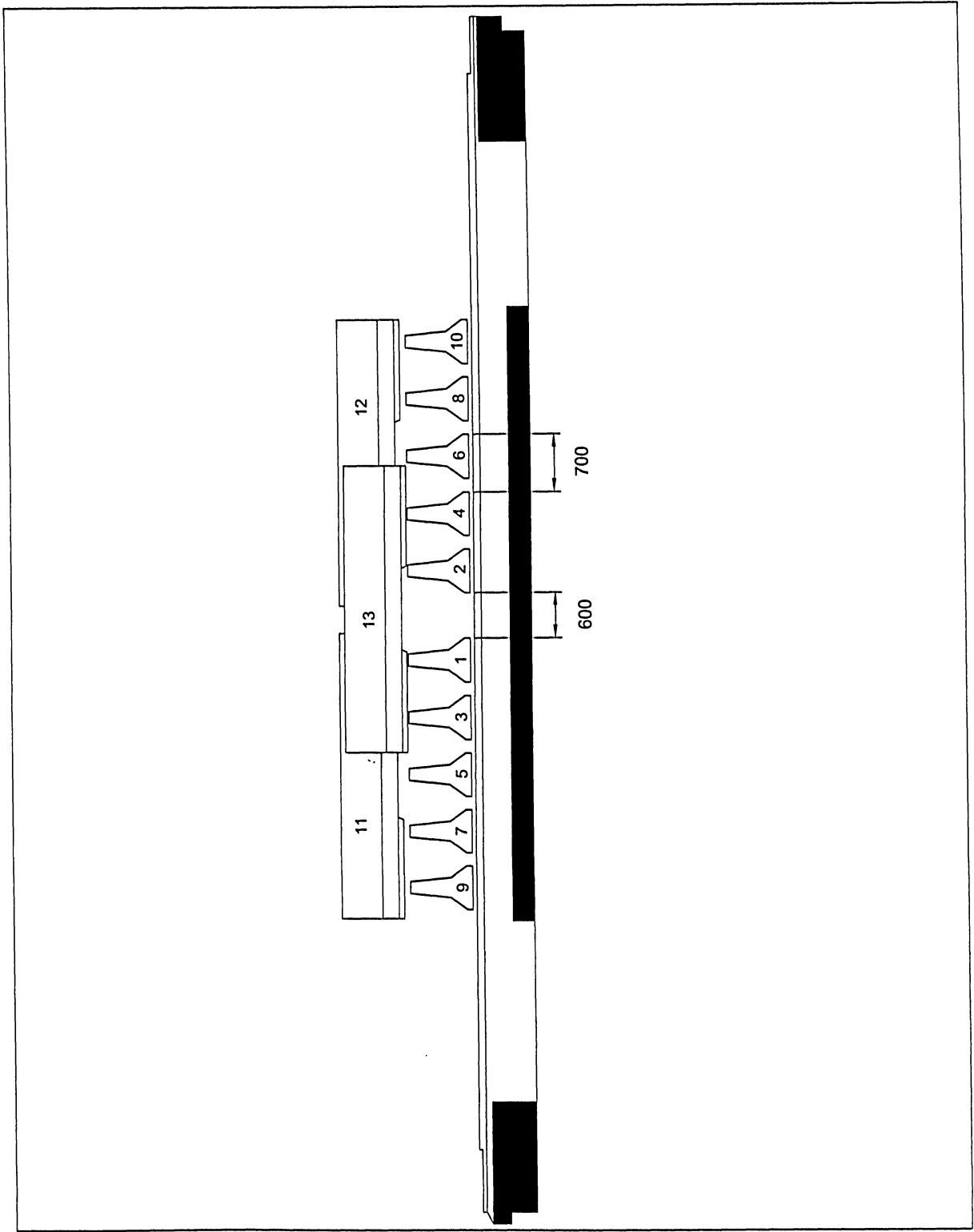


Figure 2.8 – DT-41 girder barrier load application (Cofini, 2005)

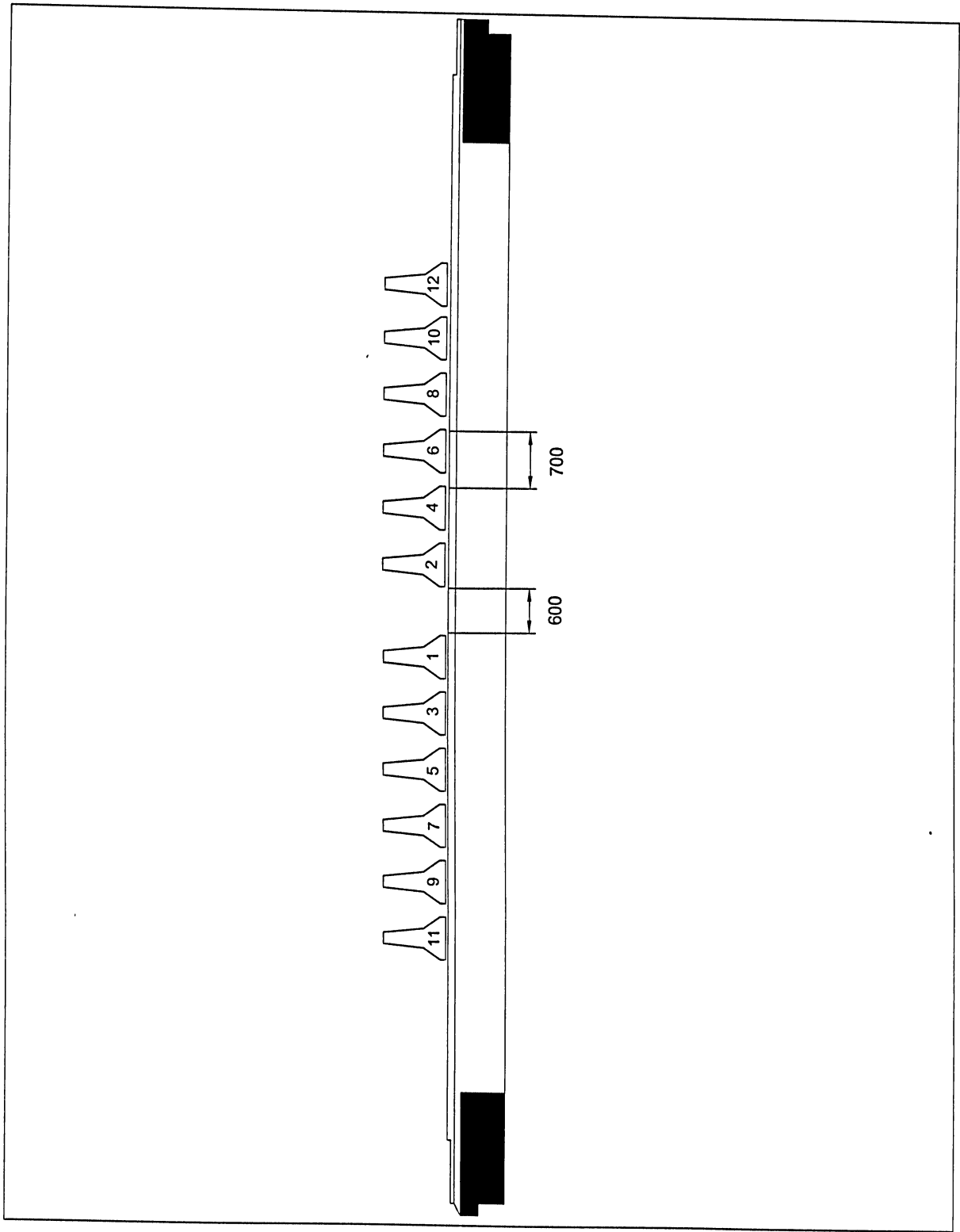


Figure 2.9 – DT-100 girder barrier load application (Cofini, 2005)

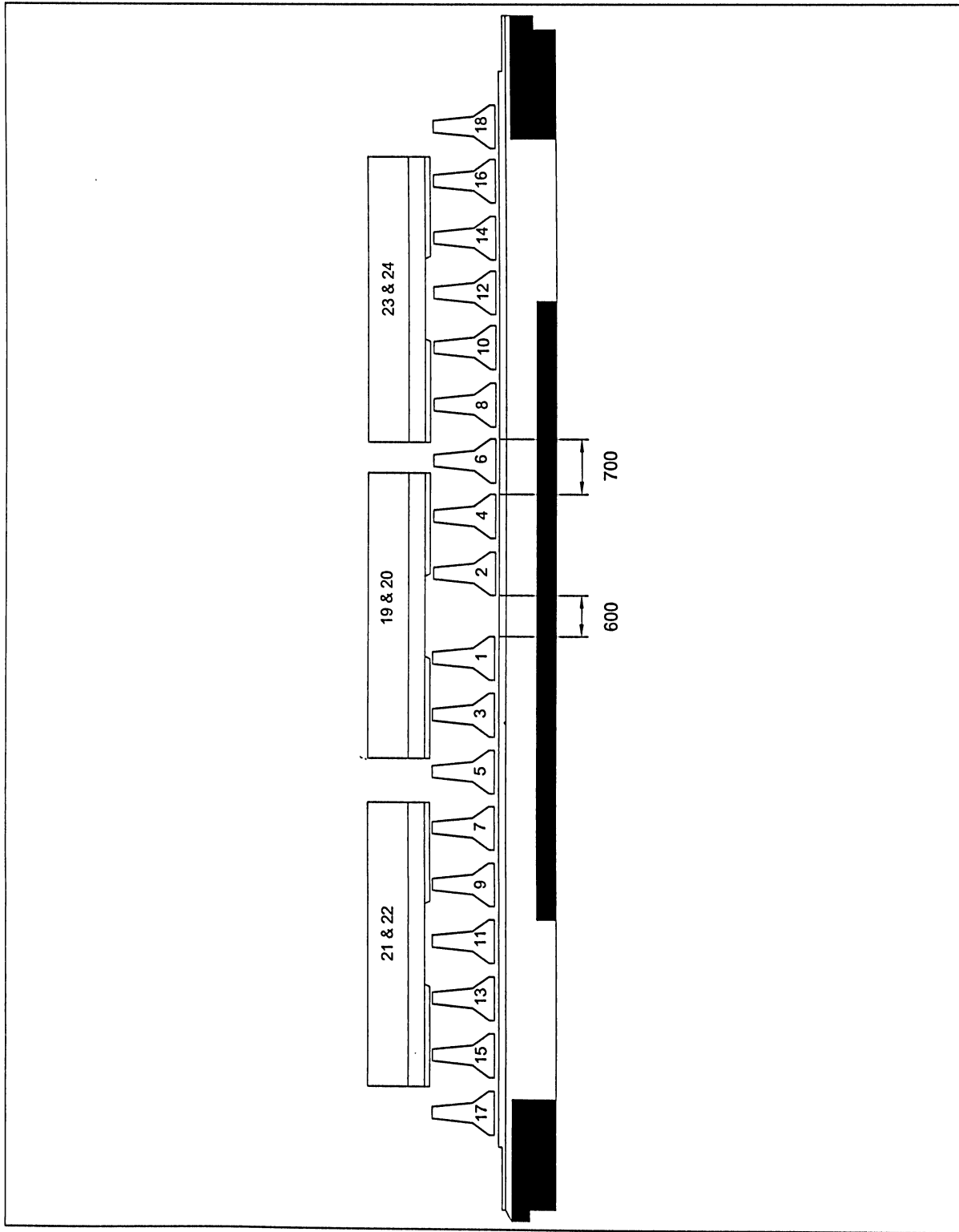


Figure 2.10 – DT-102A girder barrier load application (Cofini, 2005)

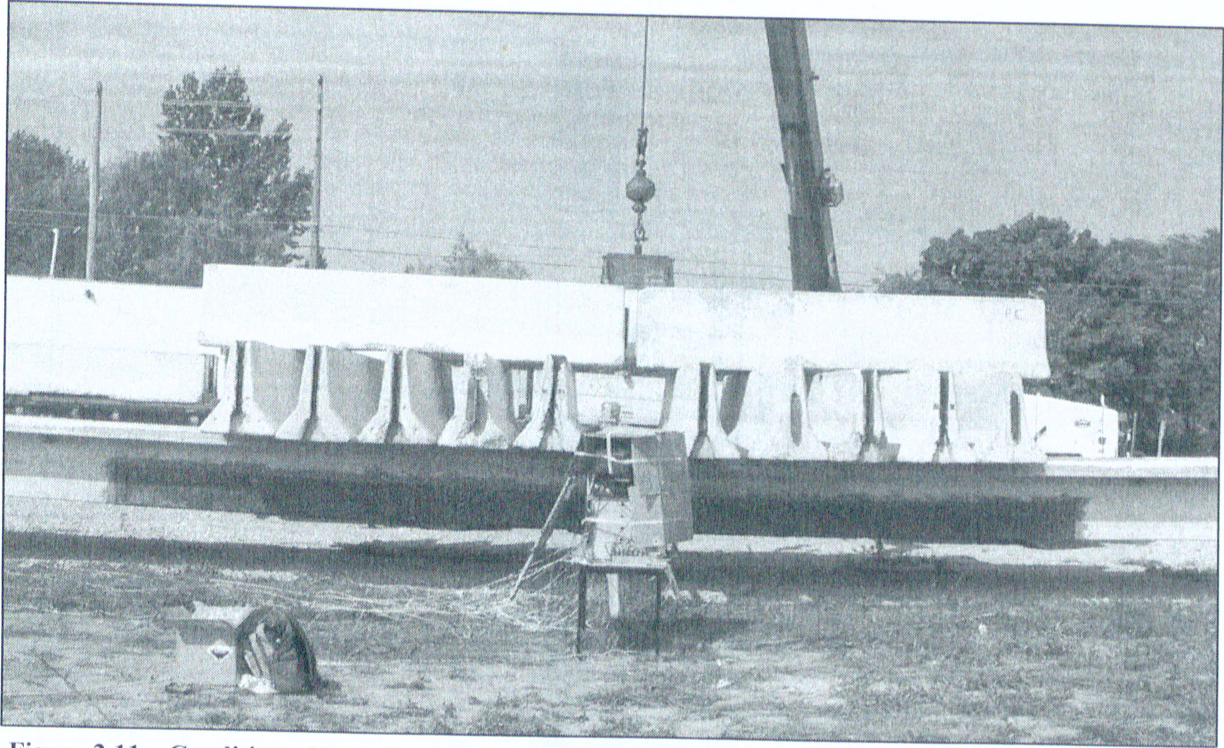


Figure 2.11 – Condition of DT-41 girder after loading completion (Cofini, 2005)

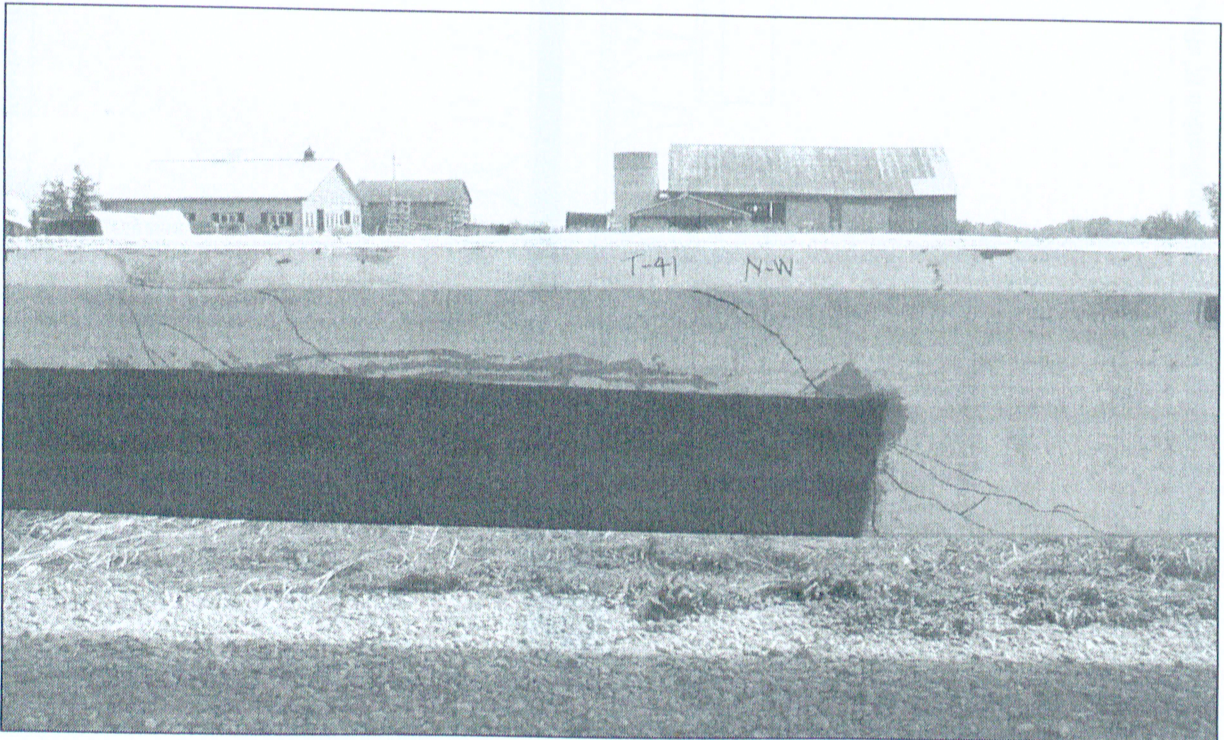


Figure 2.12 – Crack pattern of DT-41 girder after load removal (Cofini, 2005)

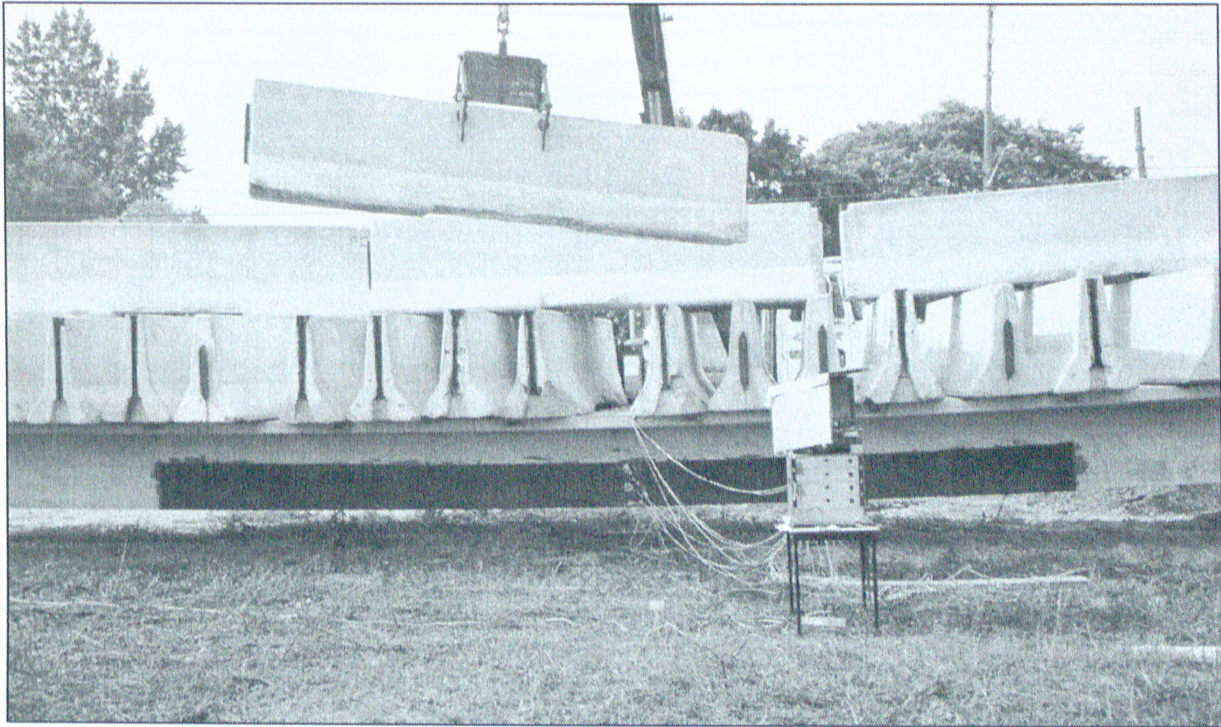


Figure 2.13 – Condition of DT-102A girder during loading (Cofini, 2005)

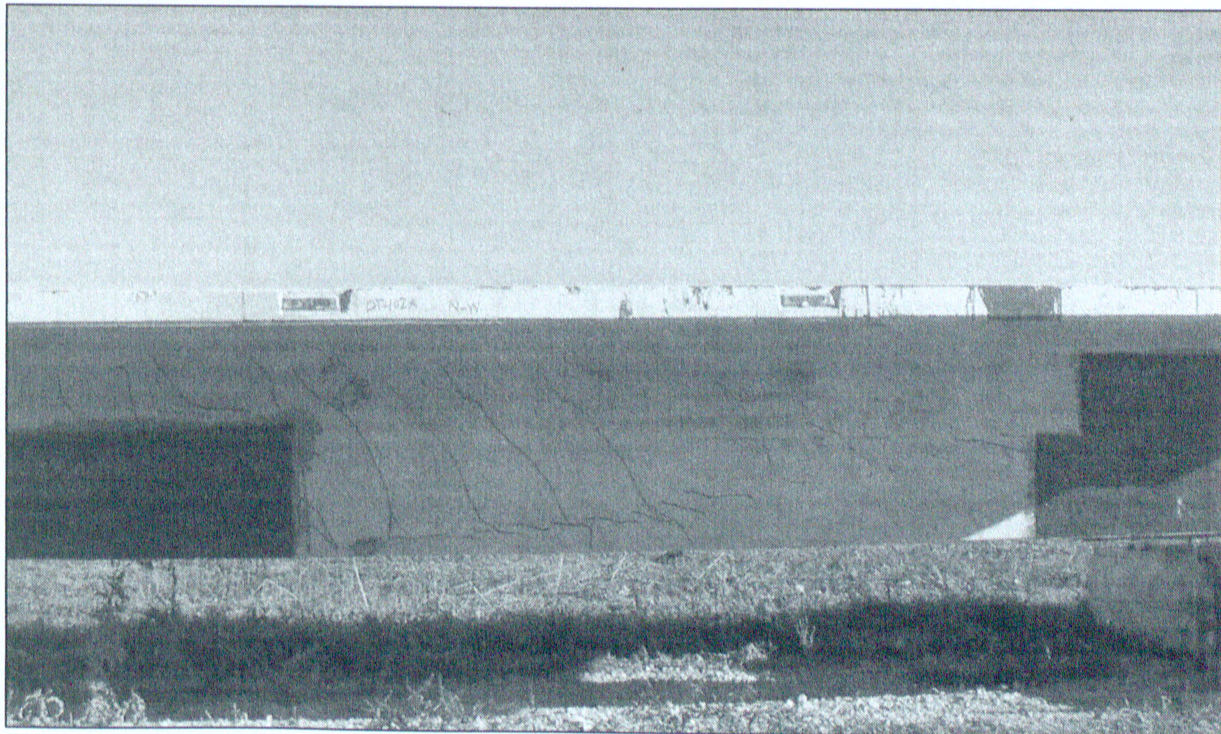


Figure 2.14 – Crack pattern of DT-102A girder near the support location (Cofini, 2005)



Figure 2.15 – DT-100 girder after ultimate failure loading (Cofini, 2005)

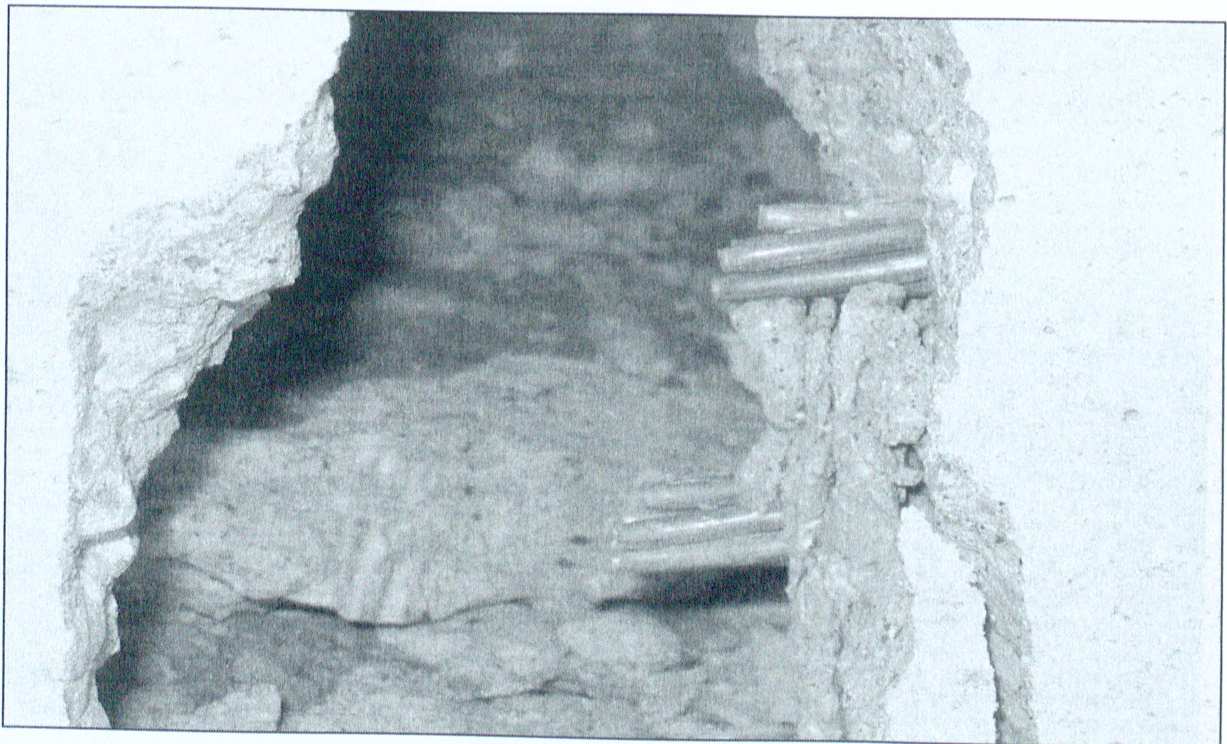


Figure 2.16 – Close up of severed prestressing tendons of the DT-100 girder (Cofini, 2005)

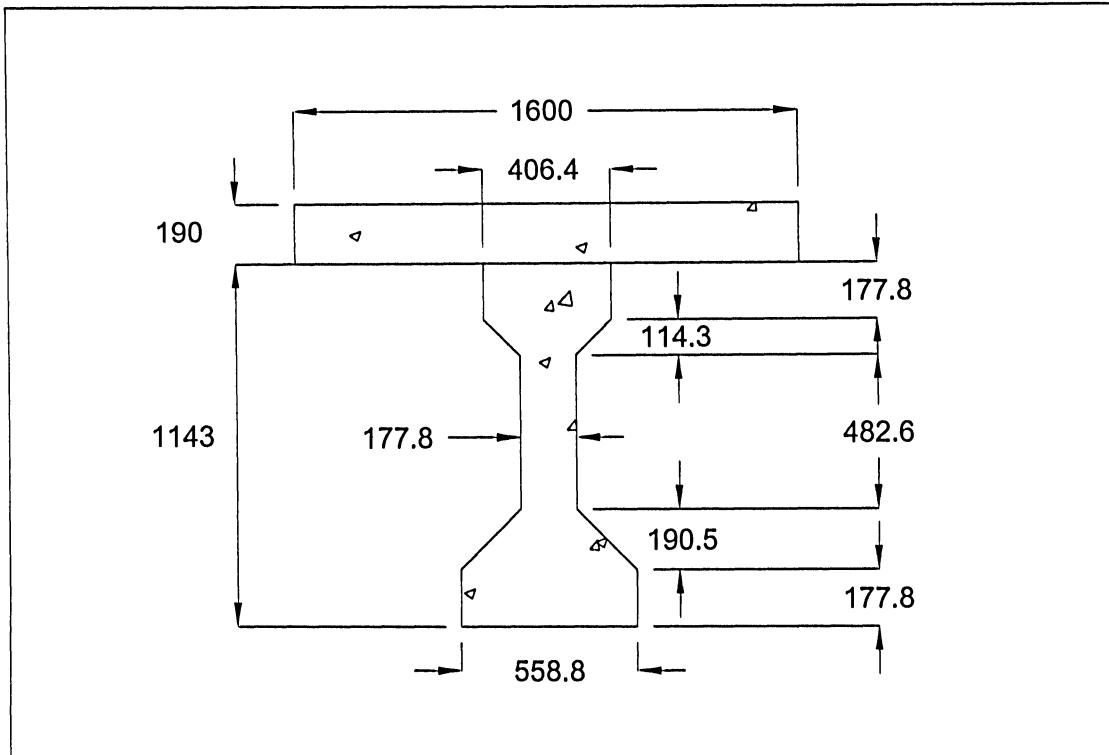


Figure 3.1 – AASHTO Type III girder cross sectional dimensions

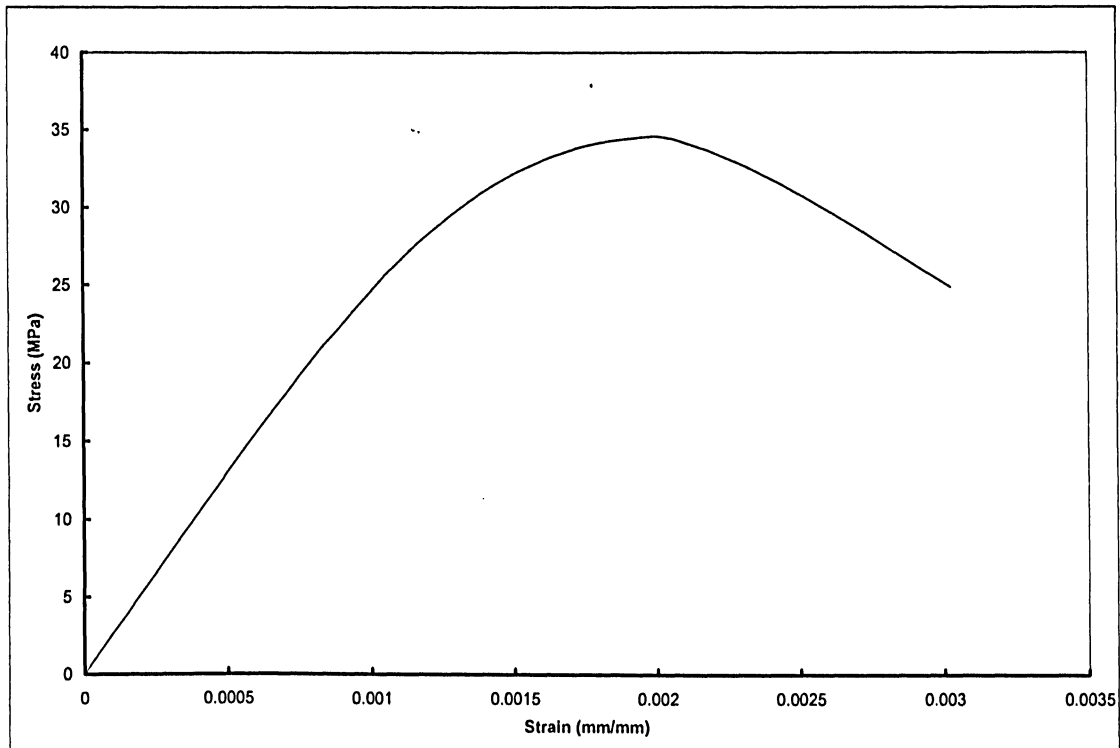


Figure 3.2 – A typical stress-strain curve for the 34.5 MPa Type III girder concrete

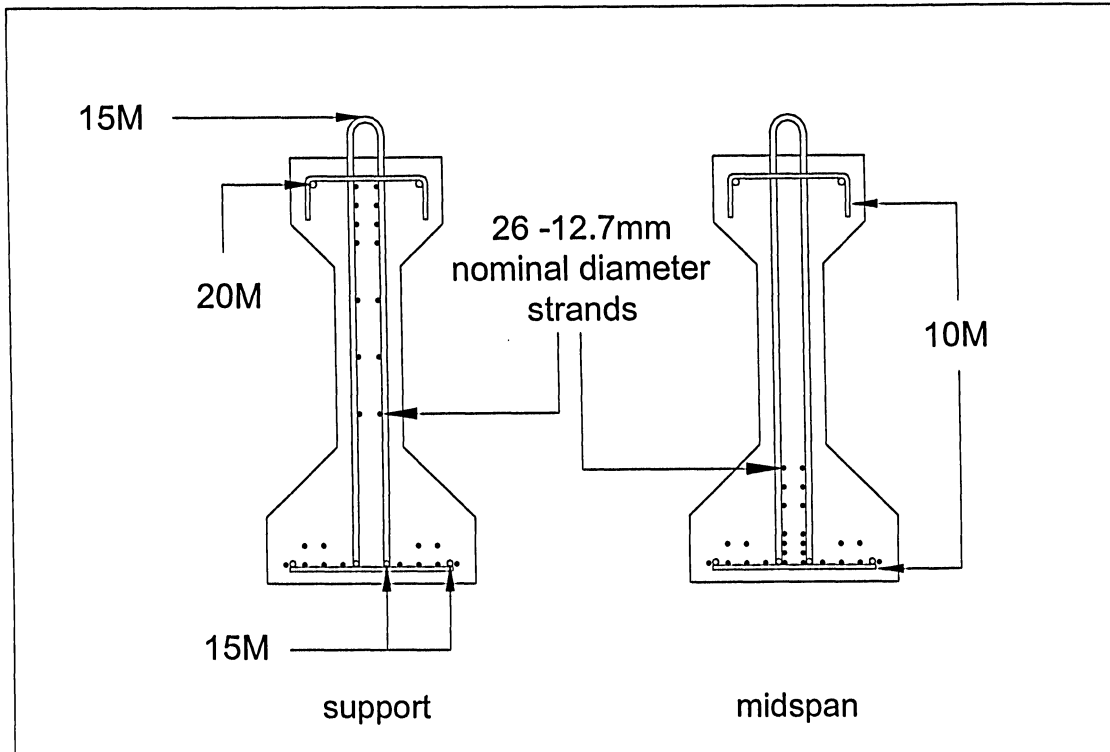


Figure 3.3 – AASHTO Type III girder reinforcement details

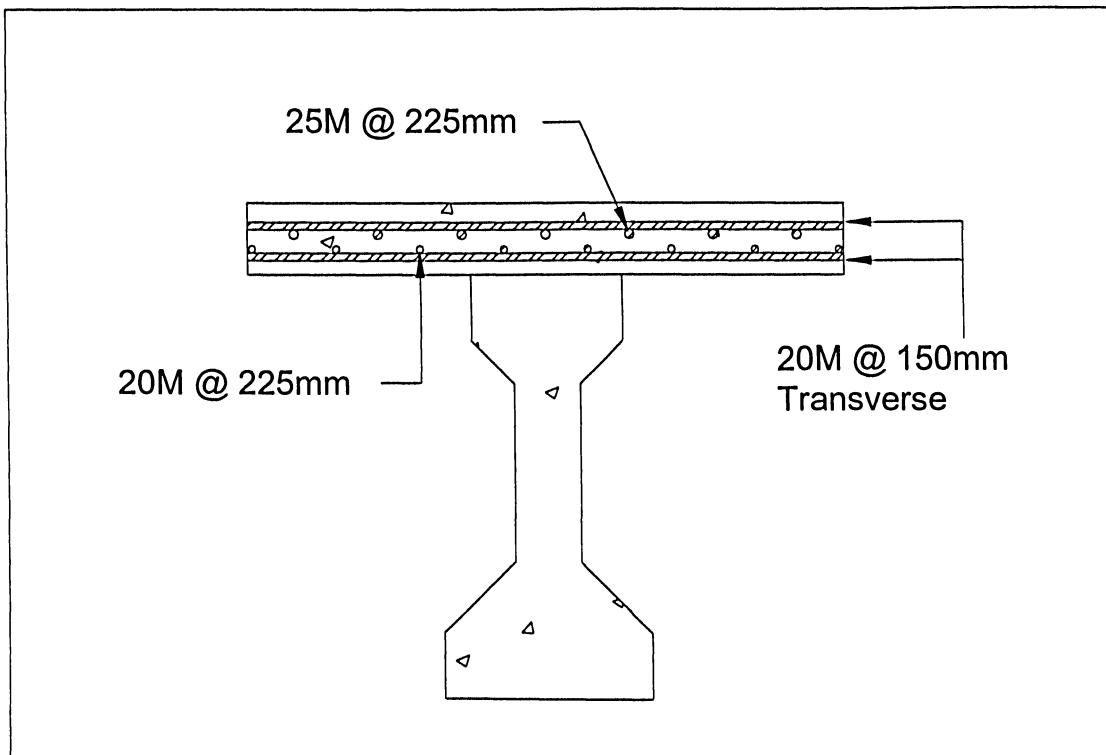


Figure 3.4 – AASHTO Type III girder slab reinforcement details

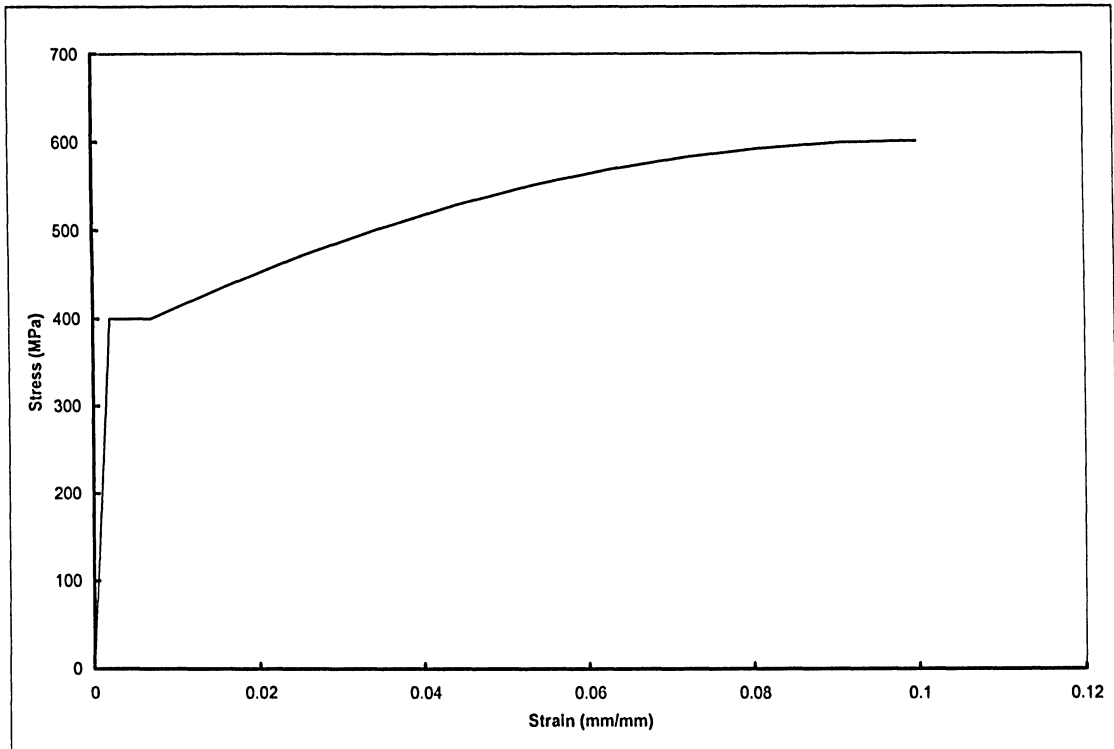


Figure 3.5 – A typical stress-strain curve for the 400 MPa reinforcing steel

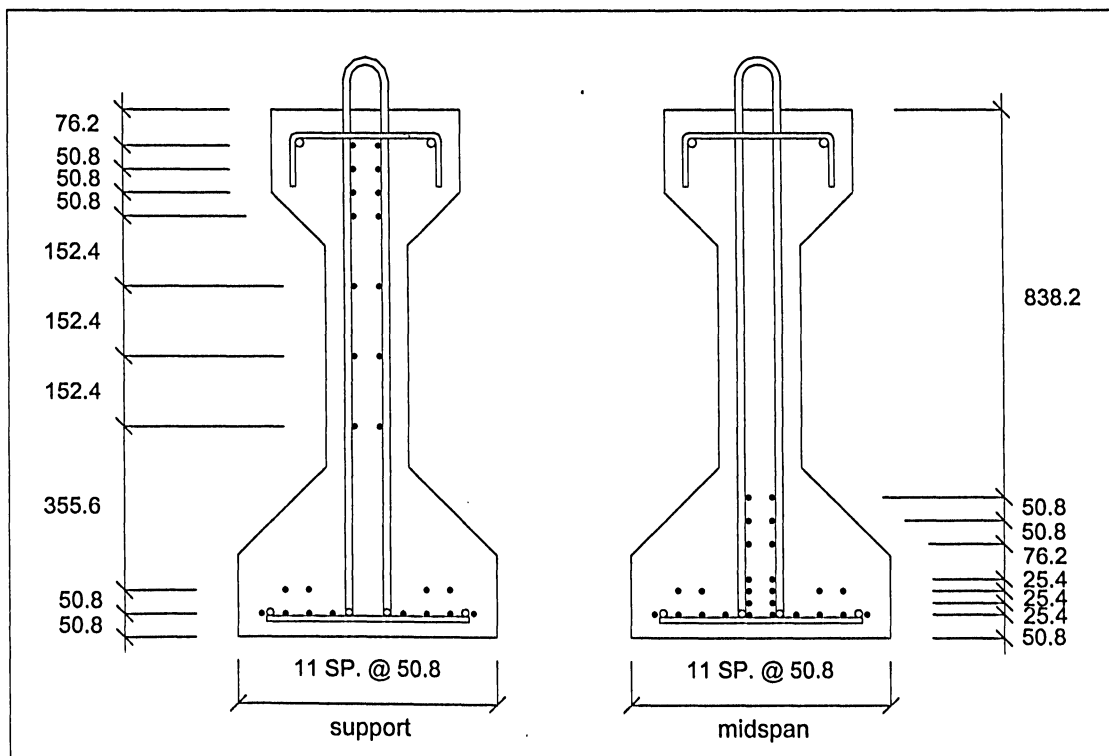


Figure 3.6 – AASHTO Type III girder prestressing steel details

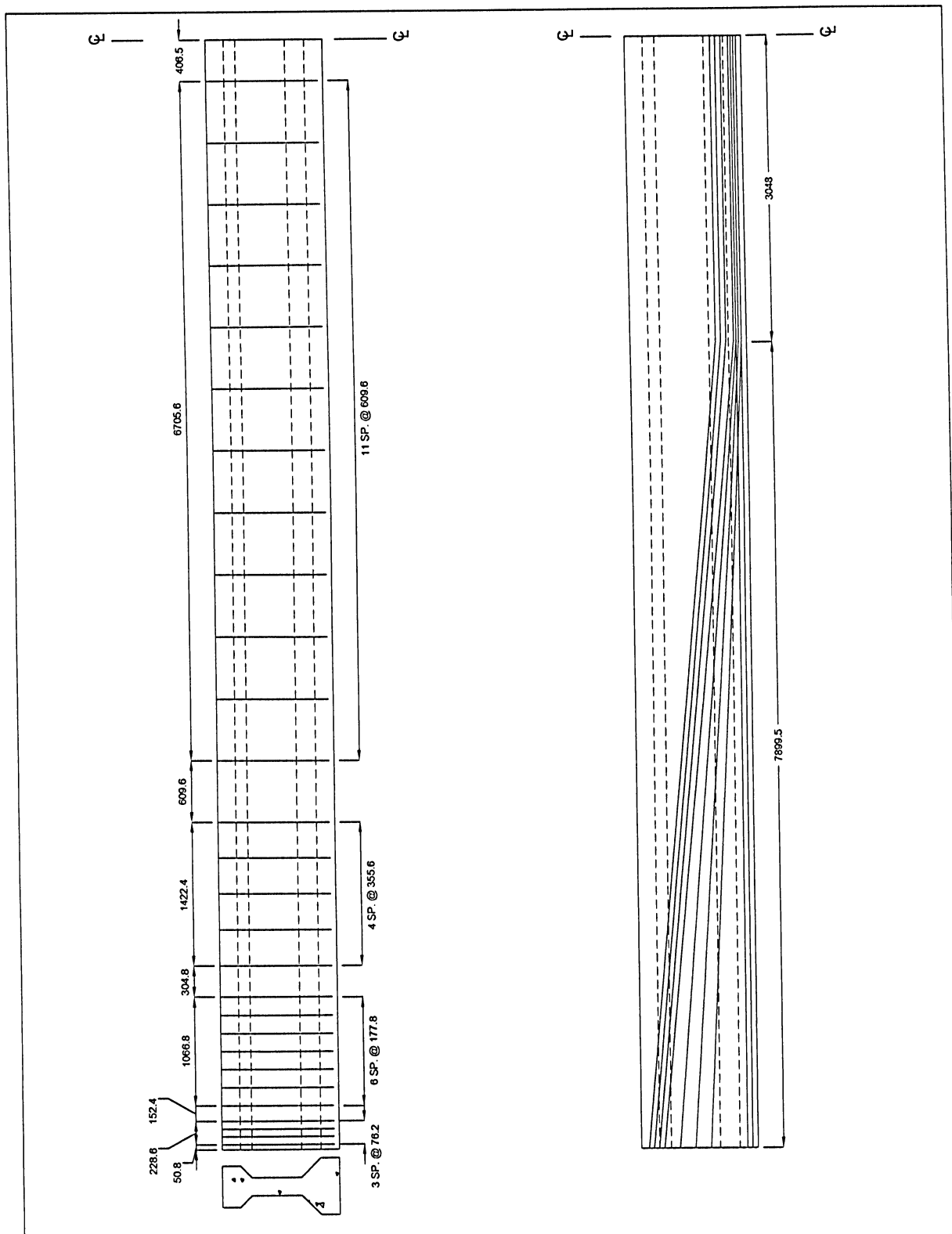


Figure 3.7 – AASHTO Type III girder longitudinal section details for stirrups (top), and tendons (bottom)

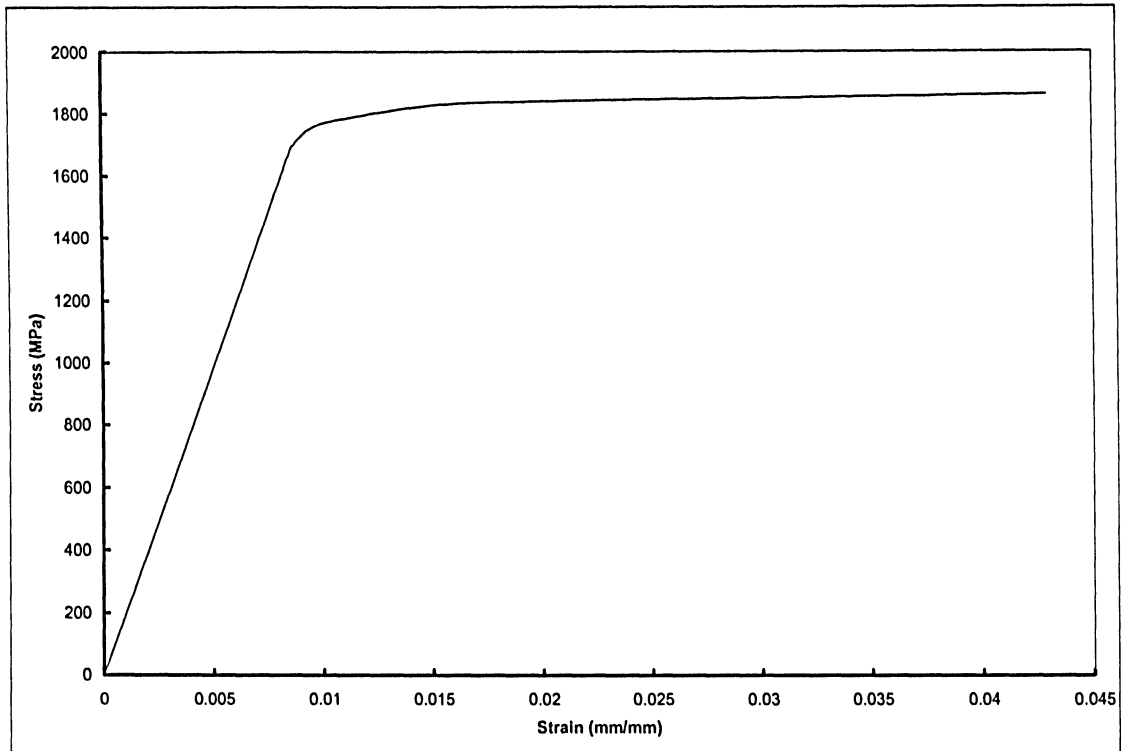
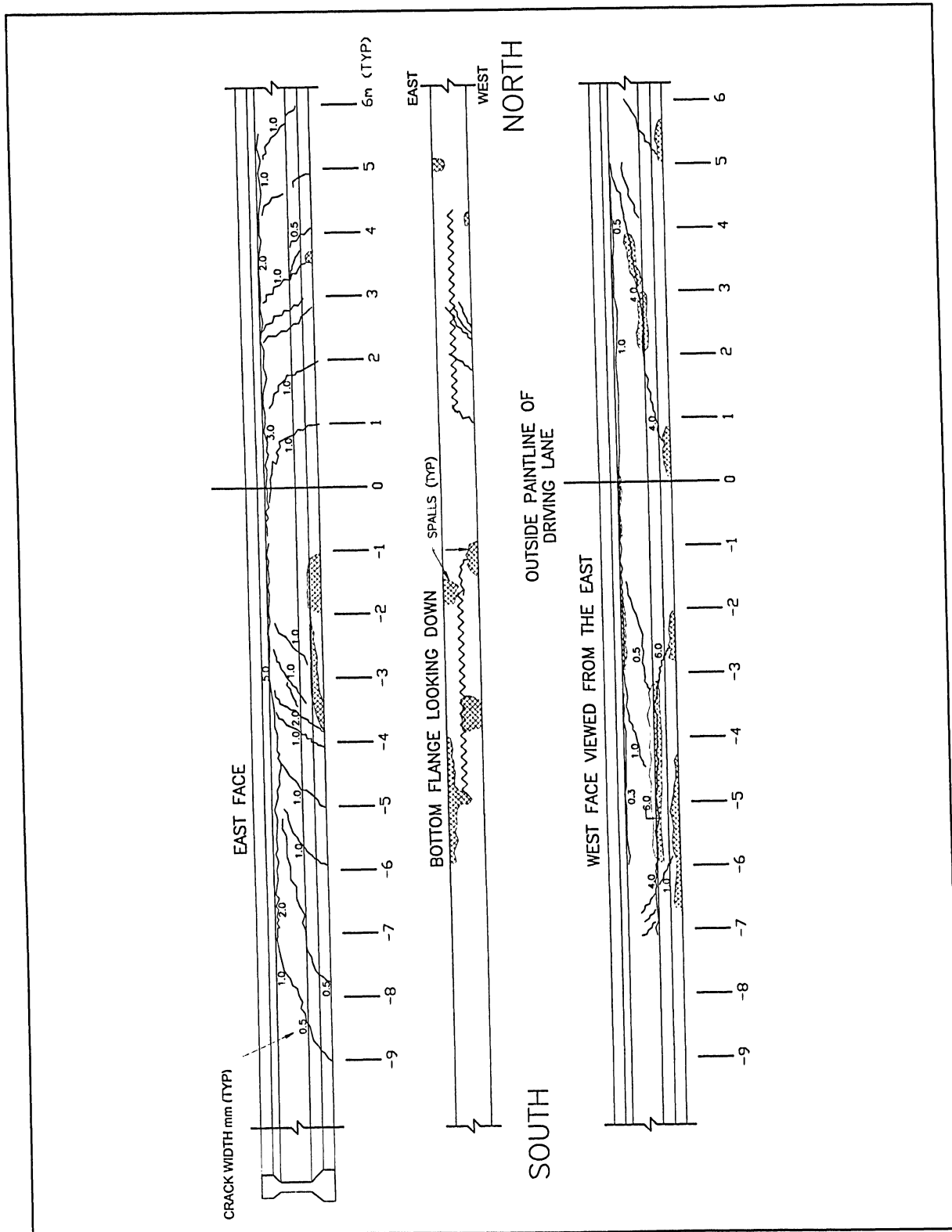


Figure 3.8 – A typical stress-strain curve for the 1860 MPa prestressing steel



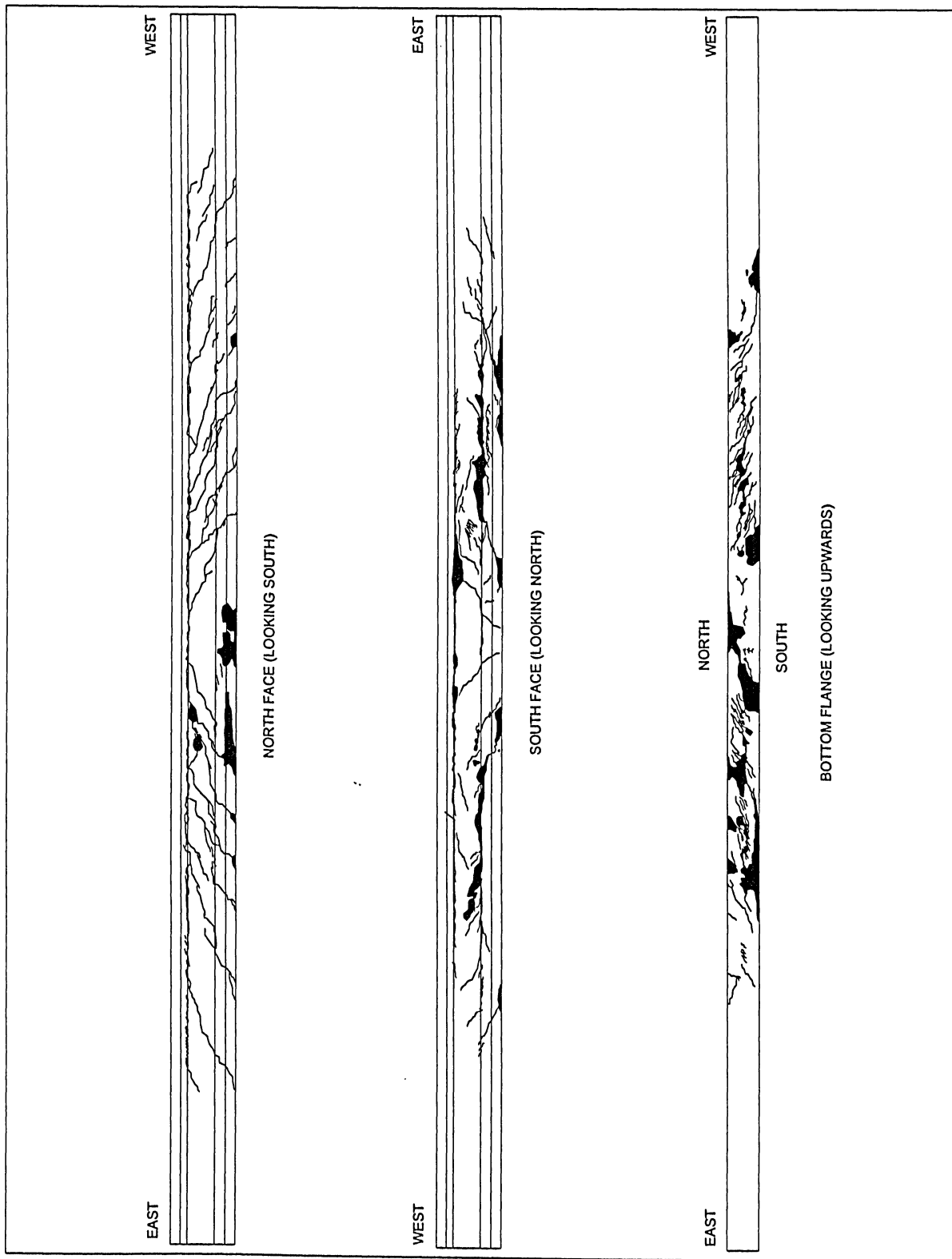


Figure 3.10 – Existing cracks due to accident impact

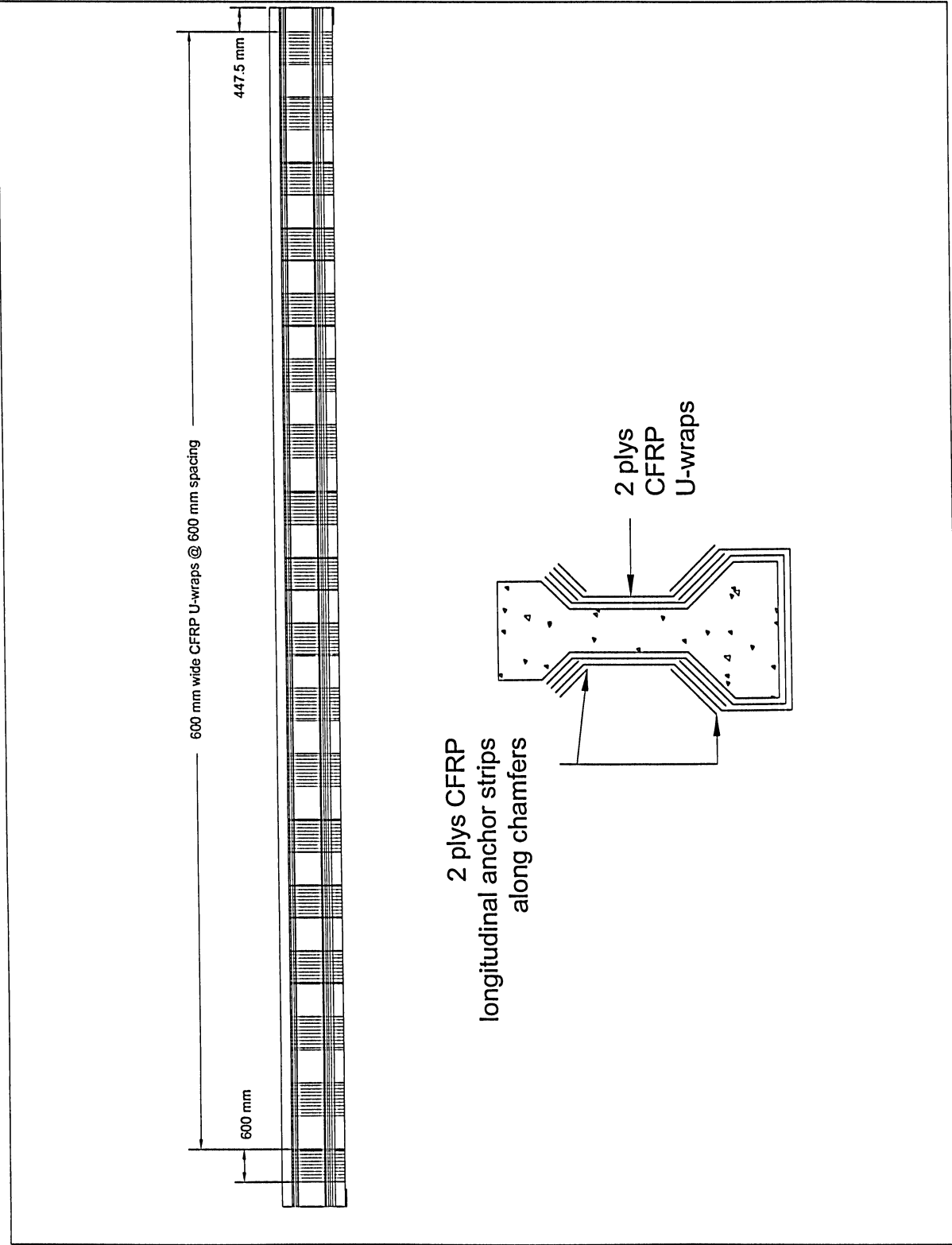


Figure 3.11 – CFRP orientation for longitudinal (top), and cross section (bottom)

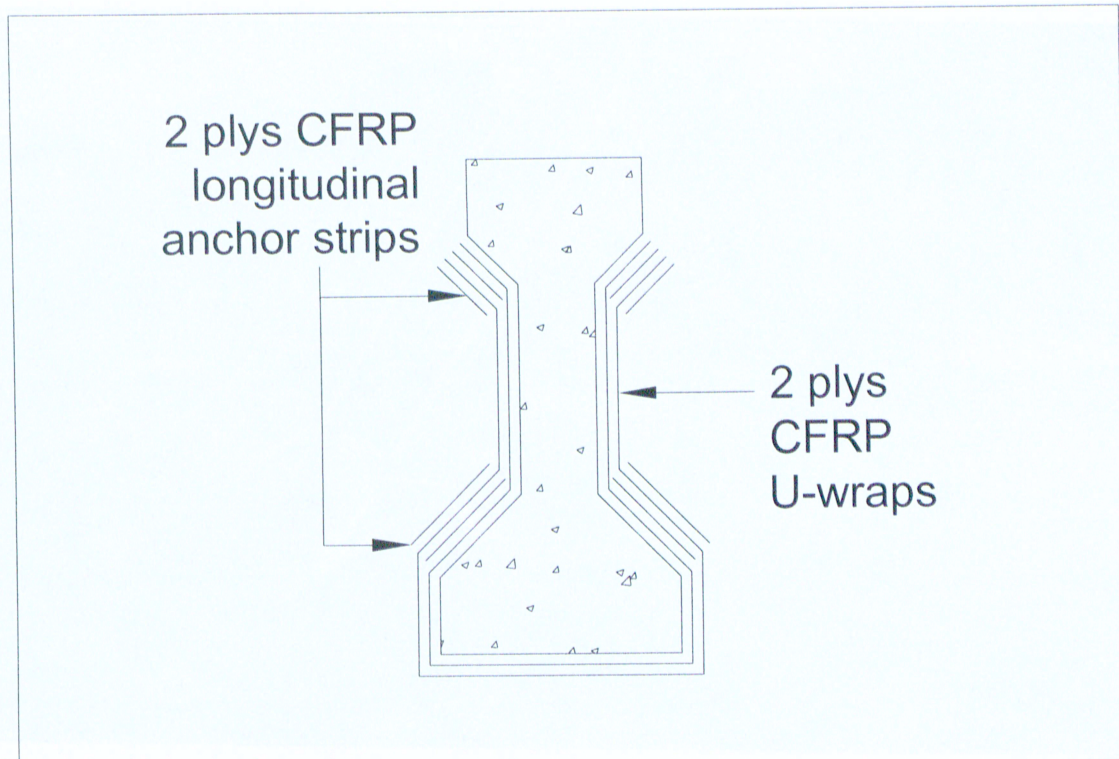


Figure 3.12 – Cross section view of CFRP orientation

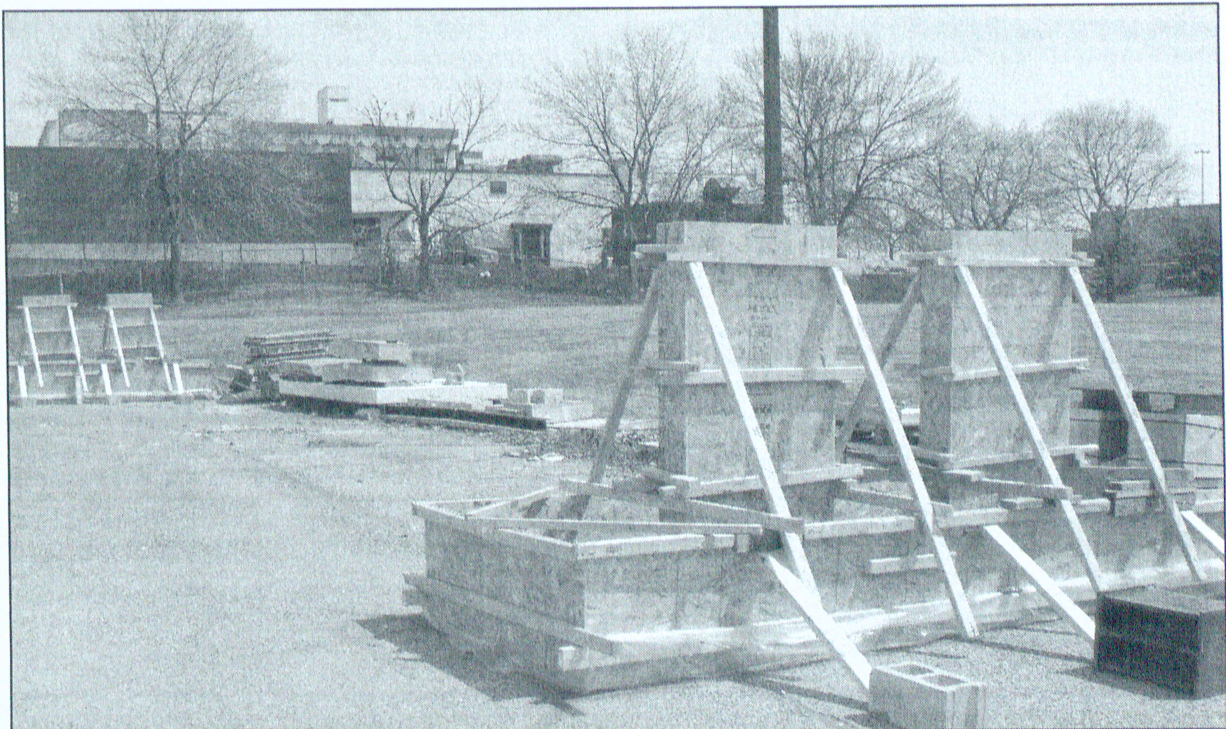


Figure 3.13 – Formwork for the east (background) and west (foreground) foundations and support walls

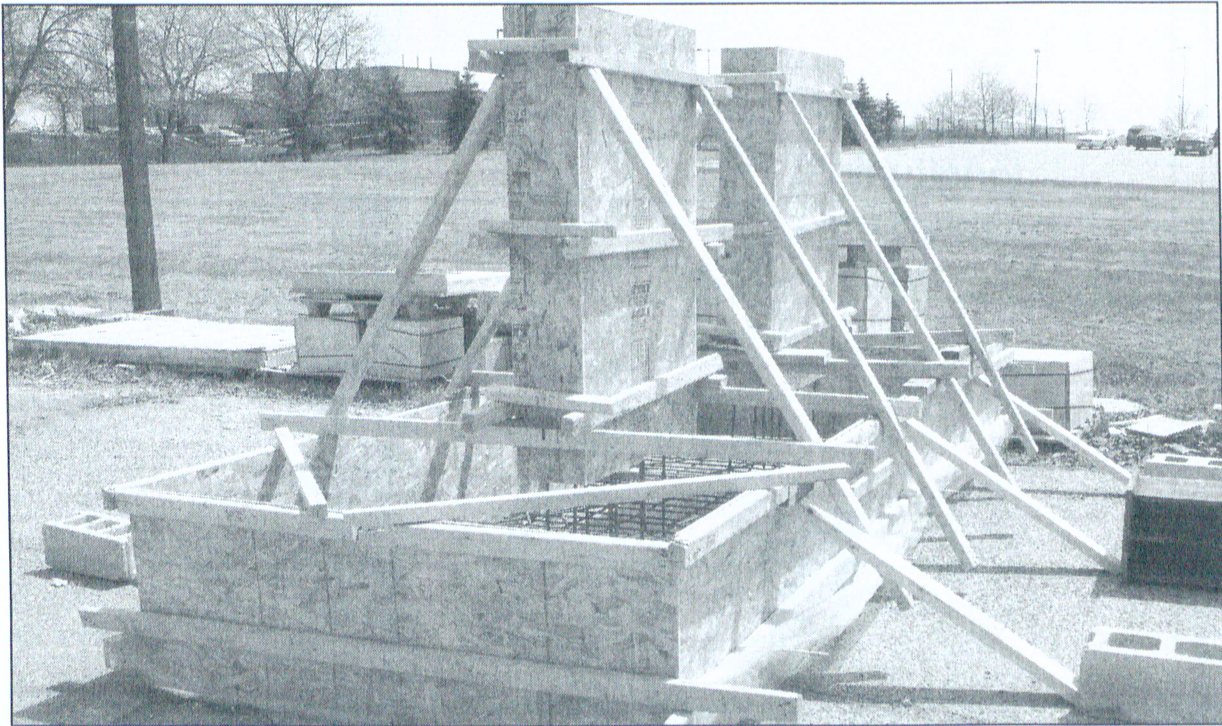


Figure 3.14 – Close up of west foundation and support walls

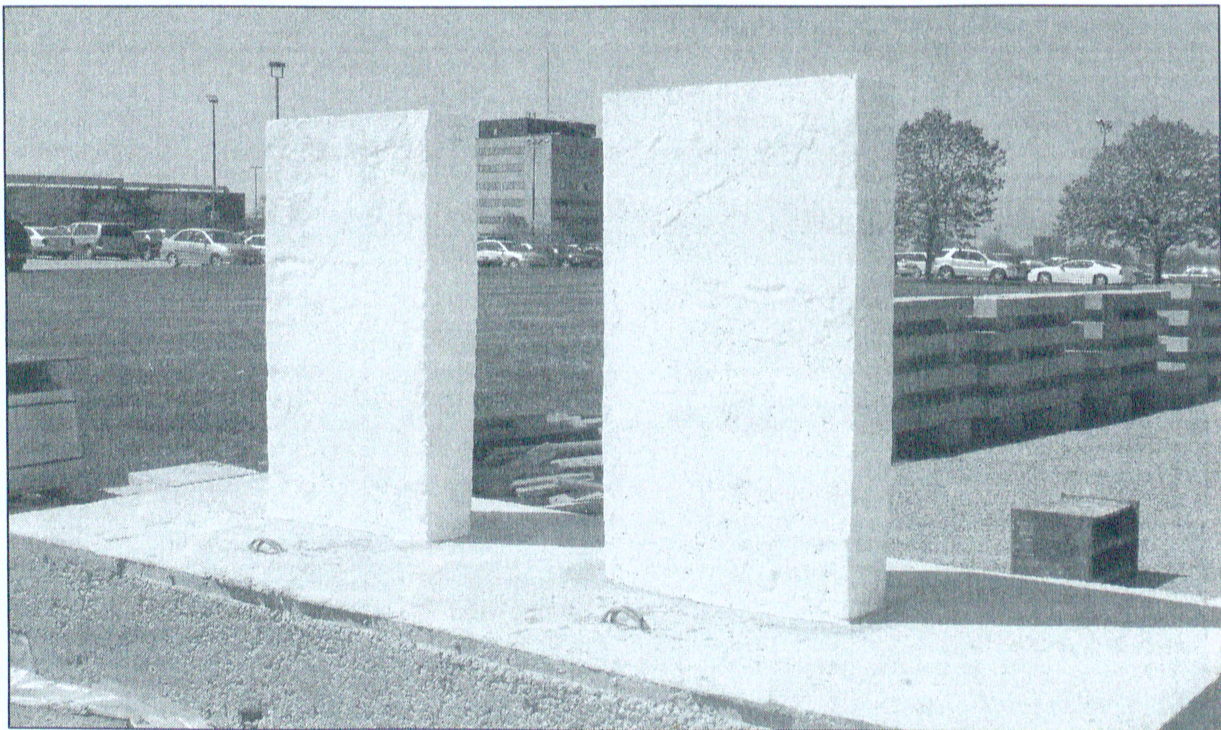


Figure 3.15 – West foundation and support walls after removal of formwork



Figure 3.16 – Arrival of AASHTO Type III prestressed concrete girder

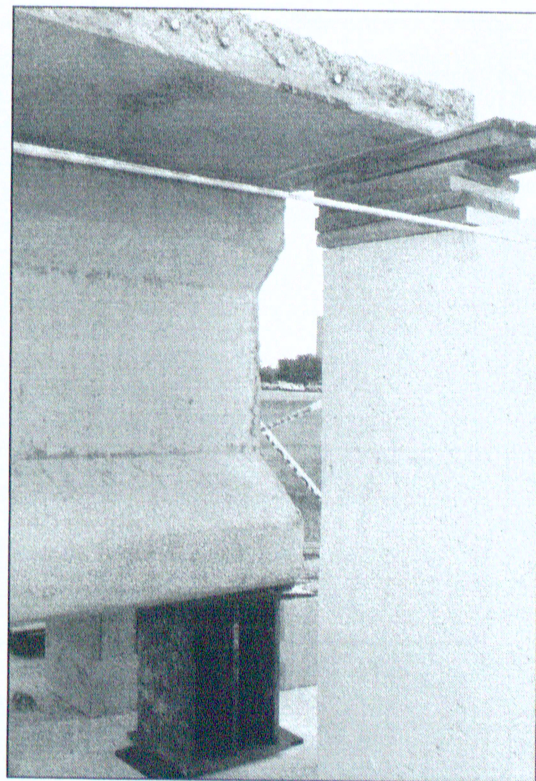


Figure 3.17 – View of the girder over the steel pedestal

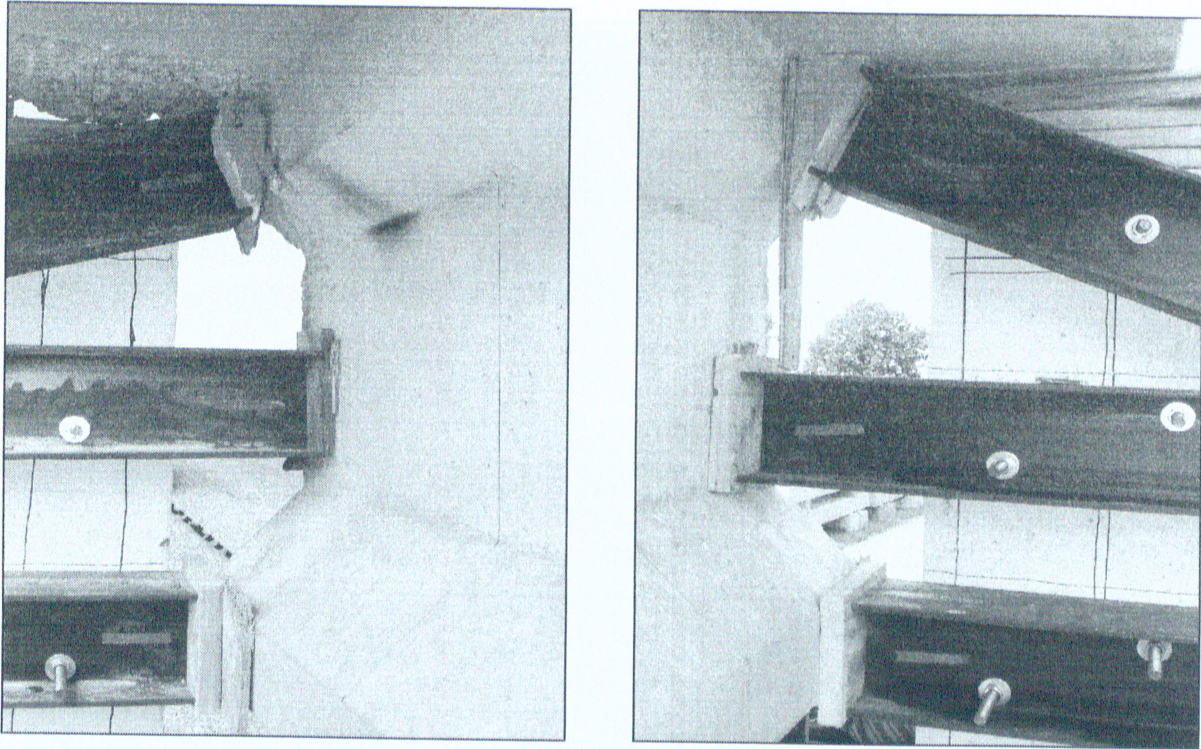


Figure 3.18 – View of steel bracing to guard against lateral movement

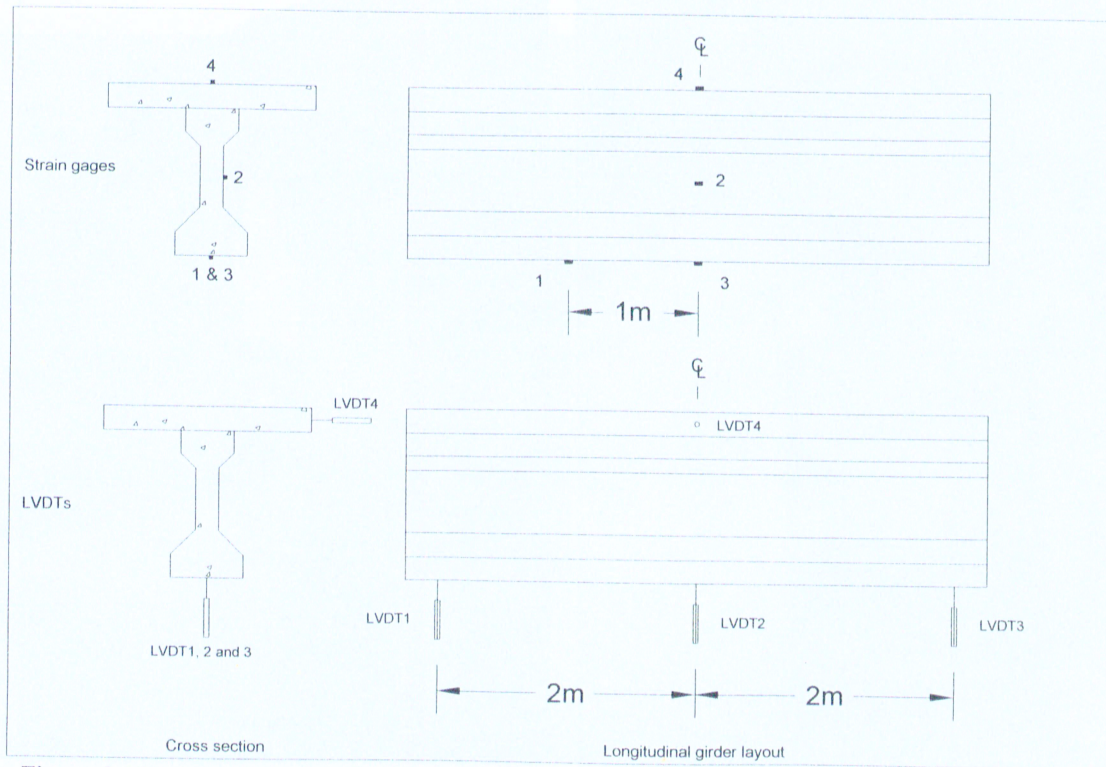


Figure 3.19 – Location of preliminary testing instrumentation

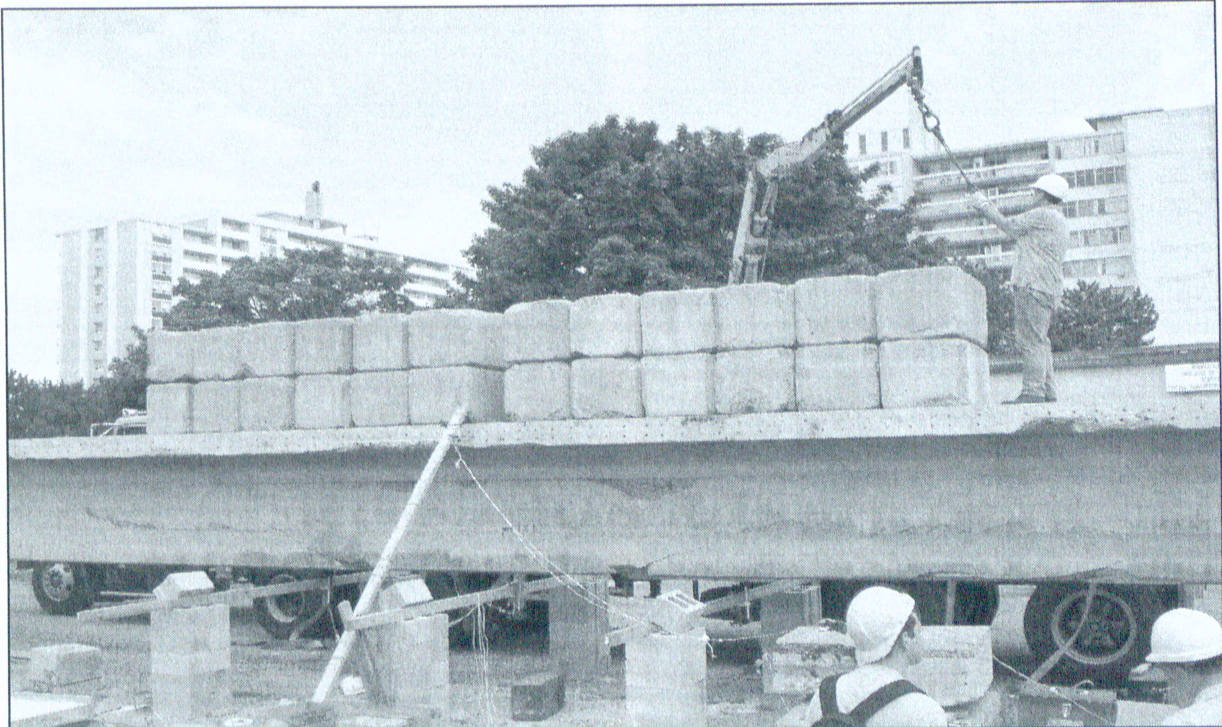


Figure 3.20 – Loading during preliminary testing

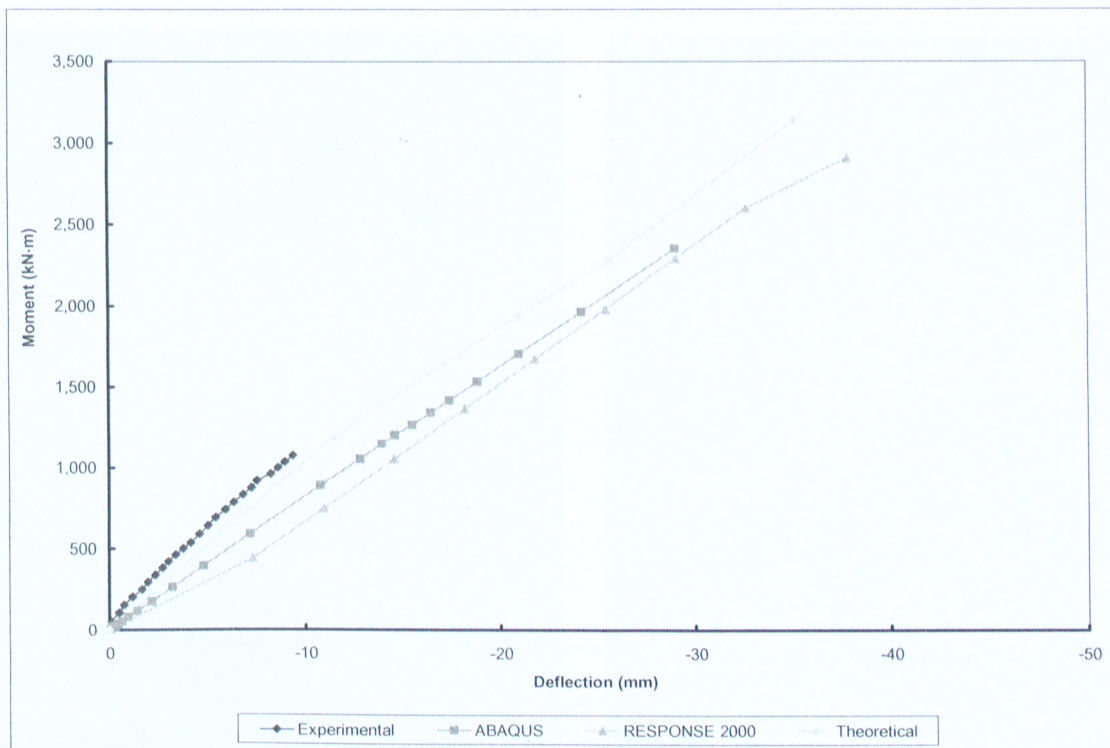


Figure 3.21 – Comparison of preliminary testing results in the elastic range

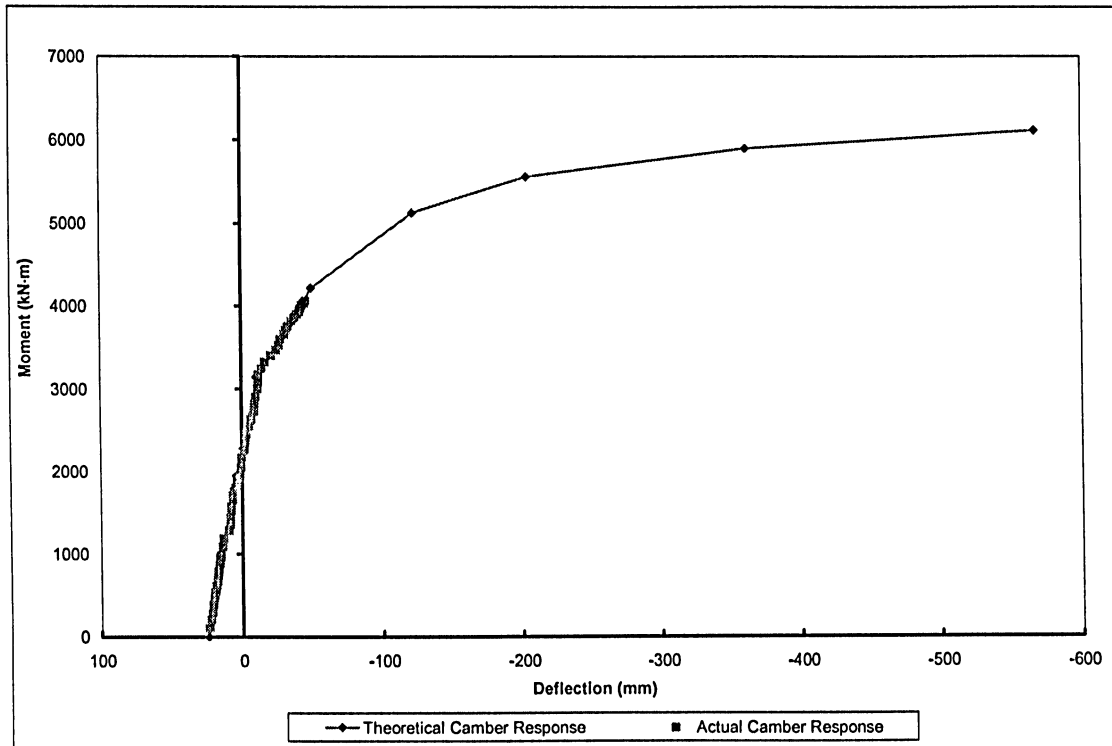


Figure 3.22 – Moment vs. deflection with camber for the Type III girder

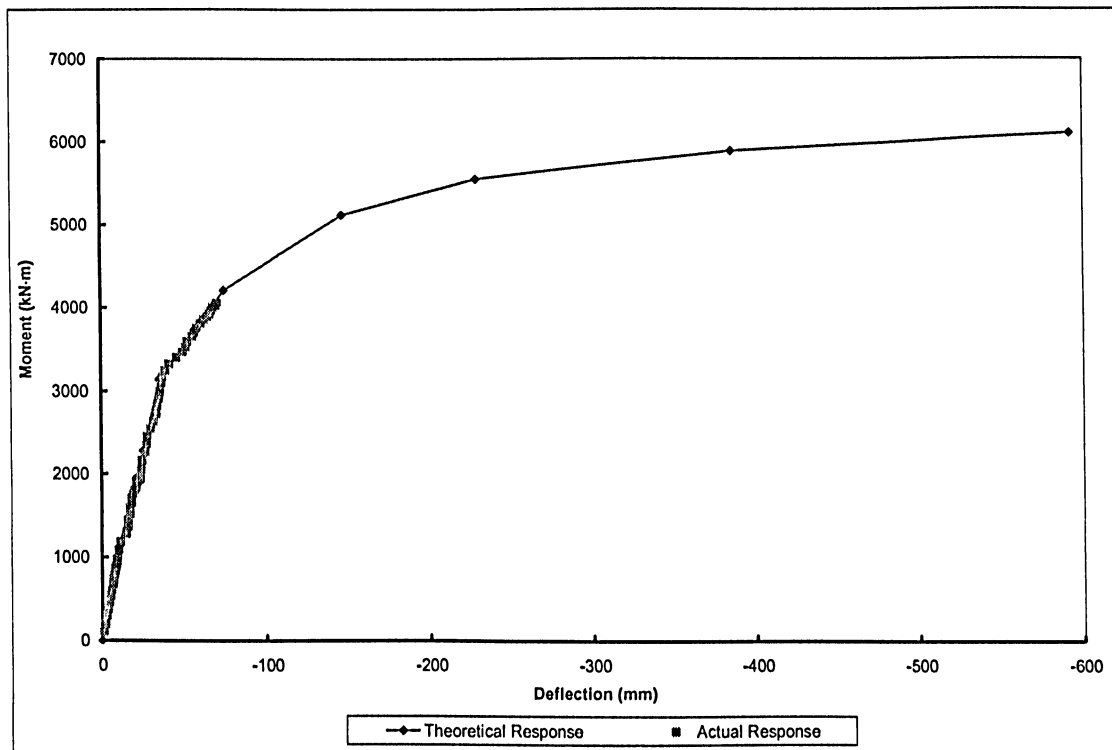


Figure 3.23 – Moment vs. deflection, without camber, for the Type III girder

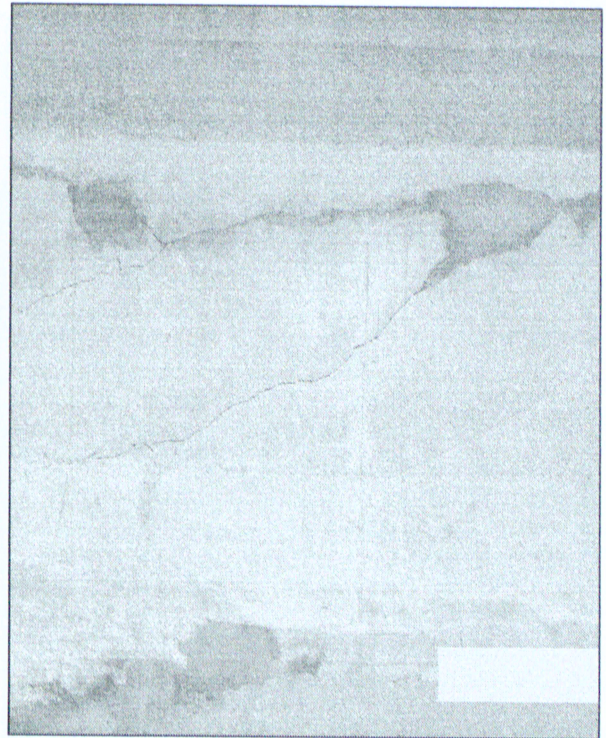
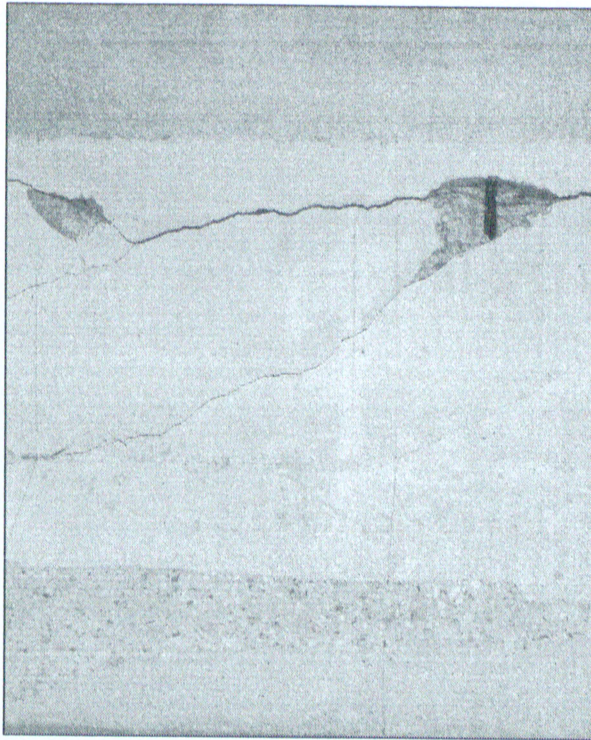


Figure 3.24 – Comparison of pre and post grouting for the north face

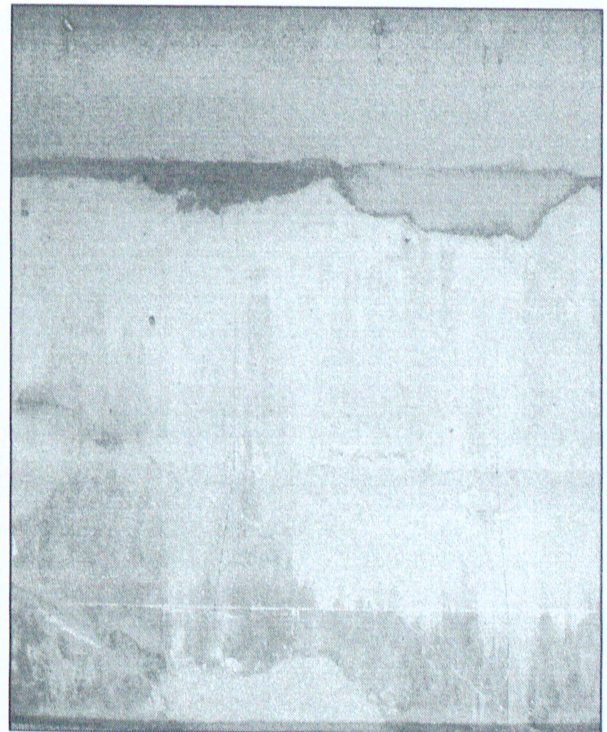


Figure 3.25 – Comparison of pre and post grouting for the south face

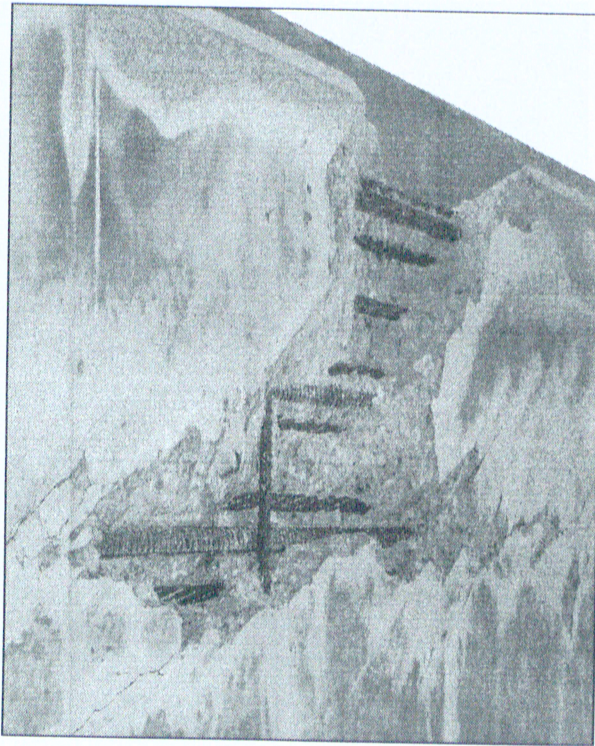


Figure 3.26 – Comparison of pre and post grouting for bottom flange underside

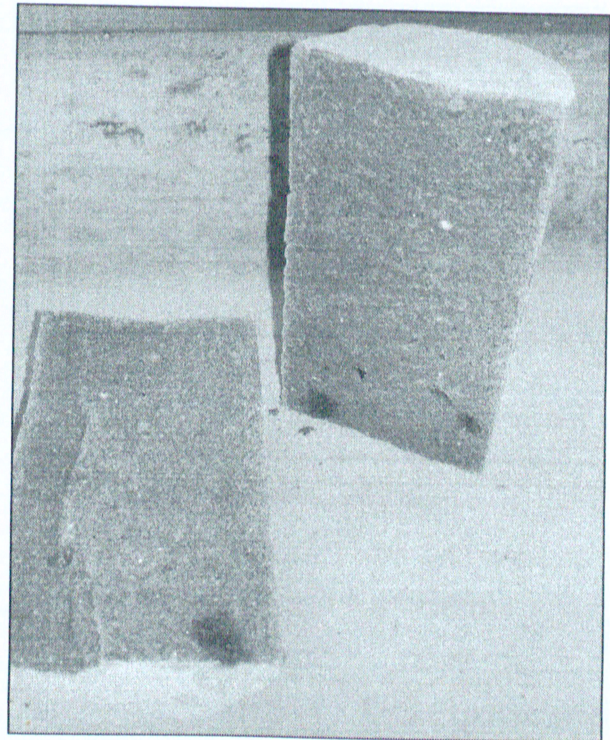


Figure 3.27 – Core testing of the Concrete Top Supreme grout (compression and in-direct tension tests)

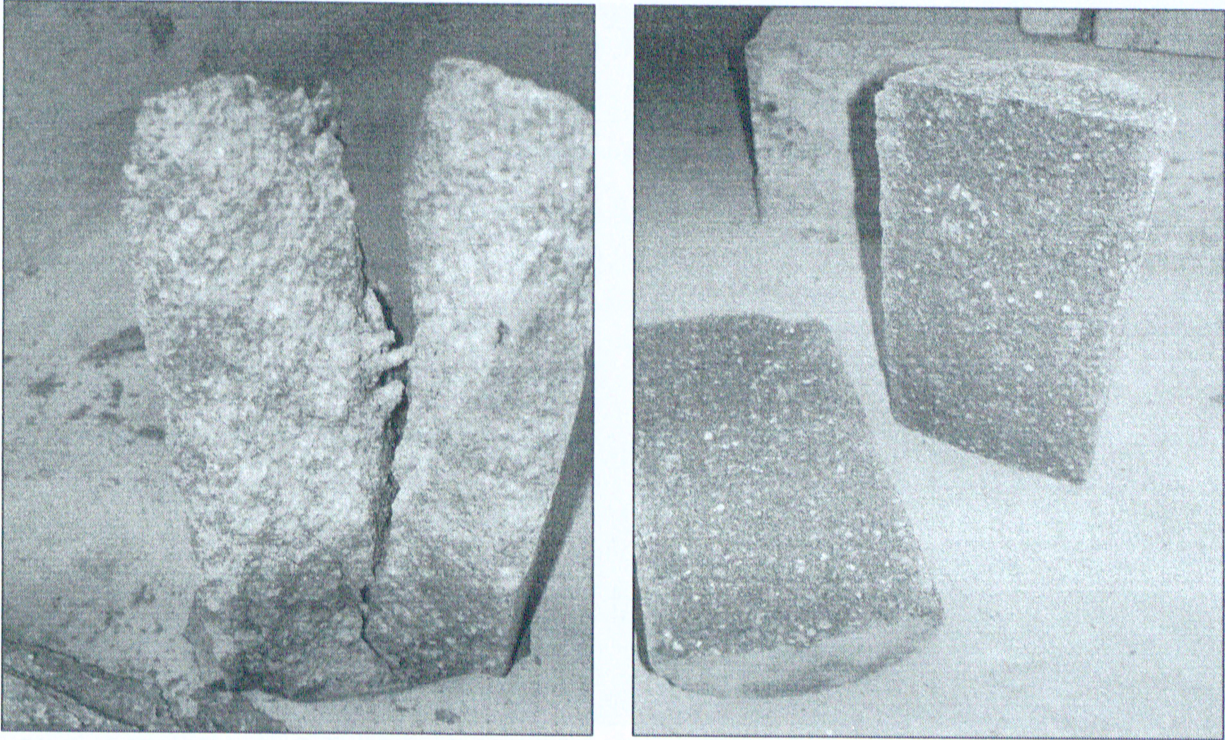


Figure 3.28 – Core testing of the Verticoat Supreme grout (compression and in-direct tension tests)

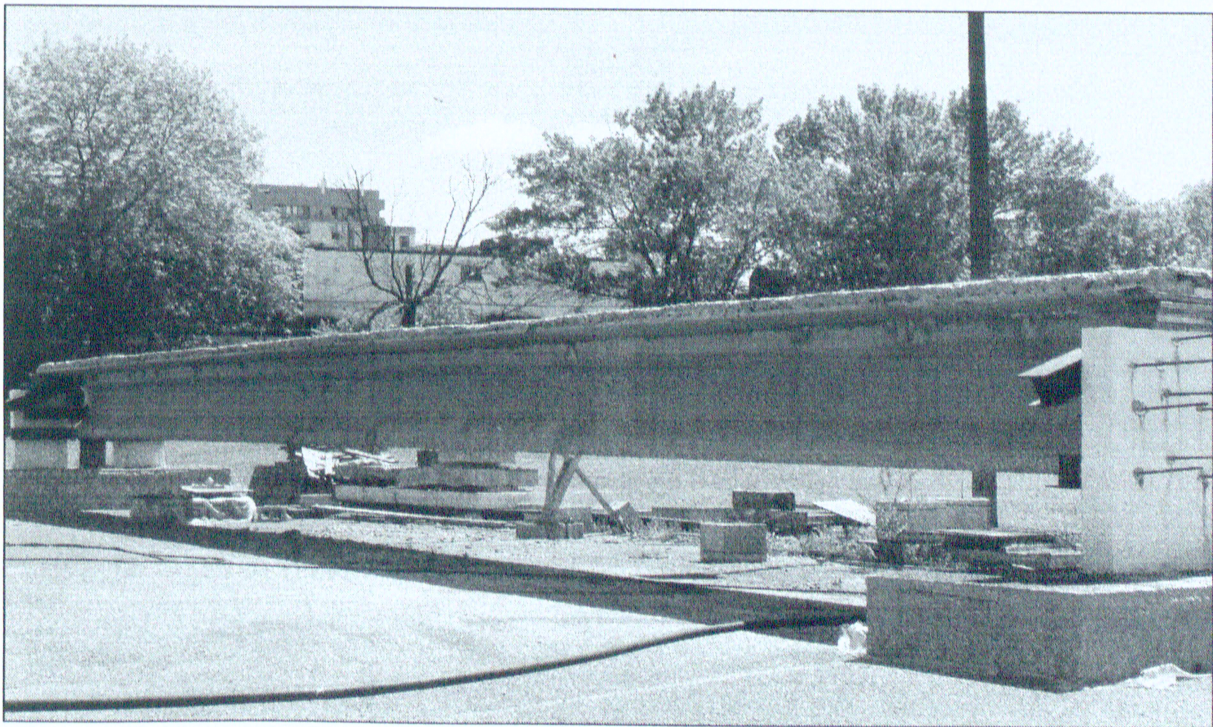


Figure 3.29 – Full view of girder upon completion of sandblasting

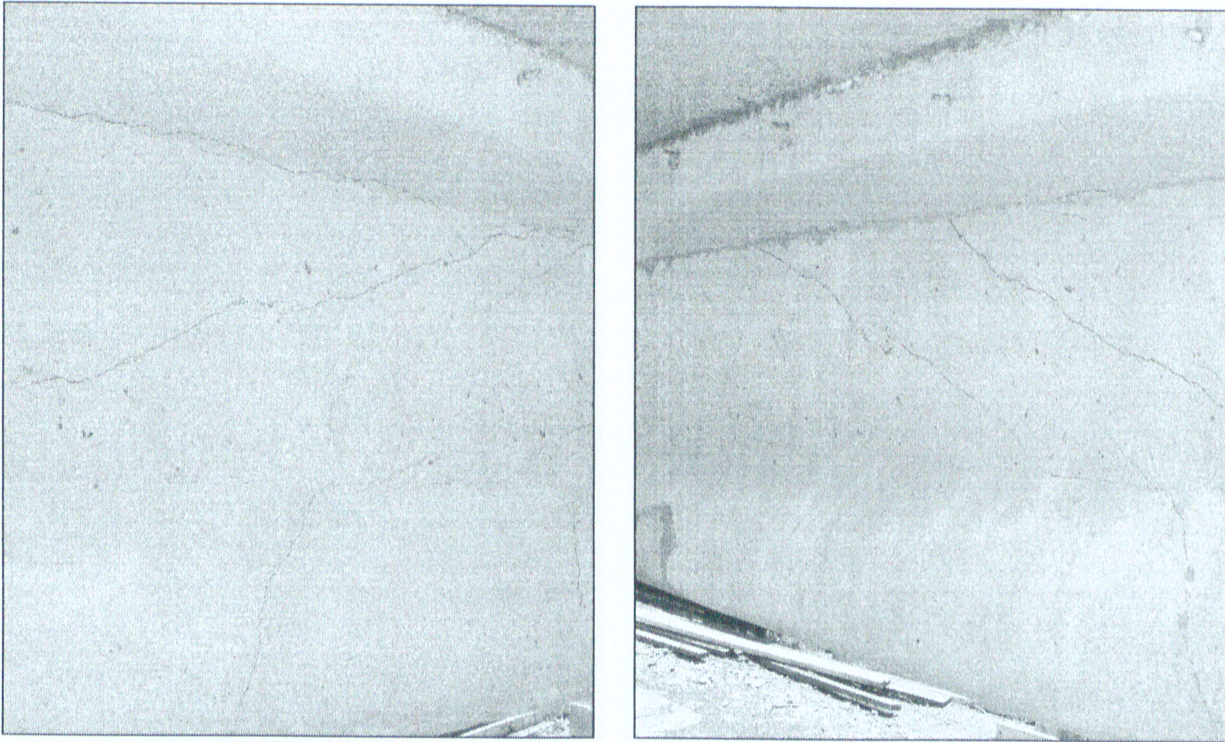


Figure 3.30 – View of two girder sections after sandblasting procedures (north face)

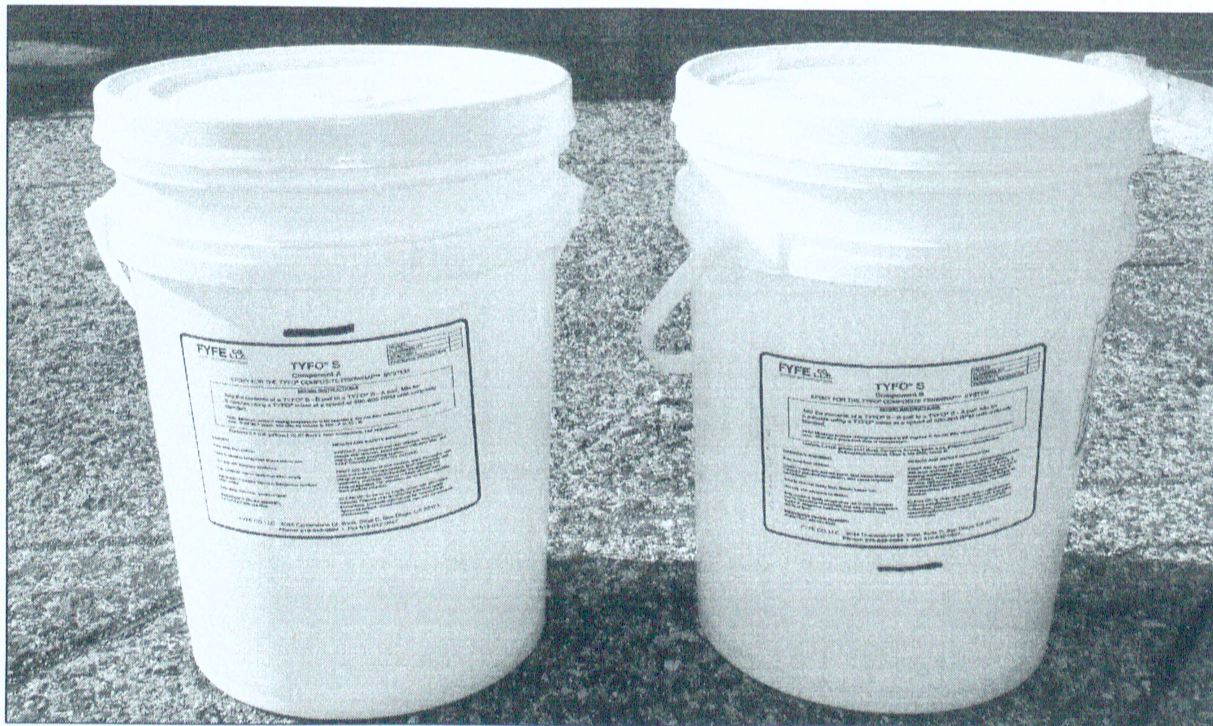


Figure 3.31 – Component A and B resin mix for Tyfo® S - Saturant Epoxy



Figure 3.32 – Component A and B resin mix for Tyfo® TC - Tack Coat Epoxy

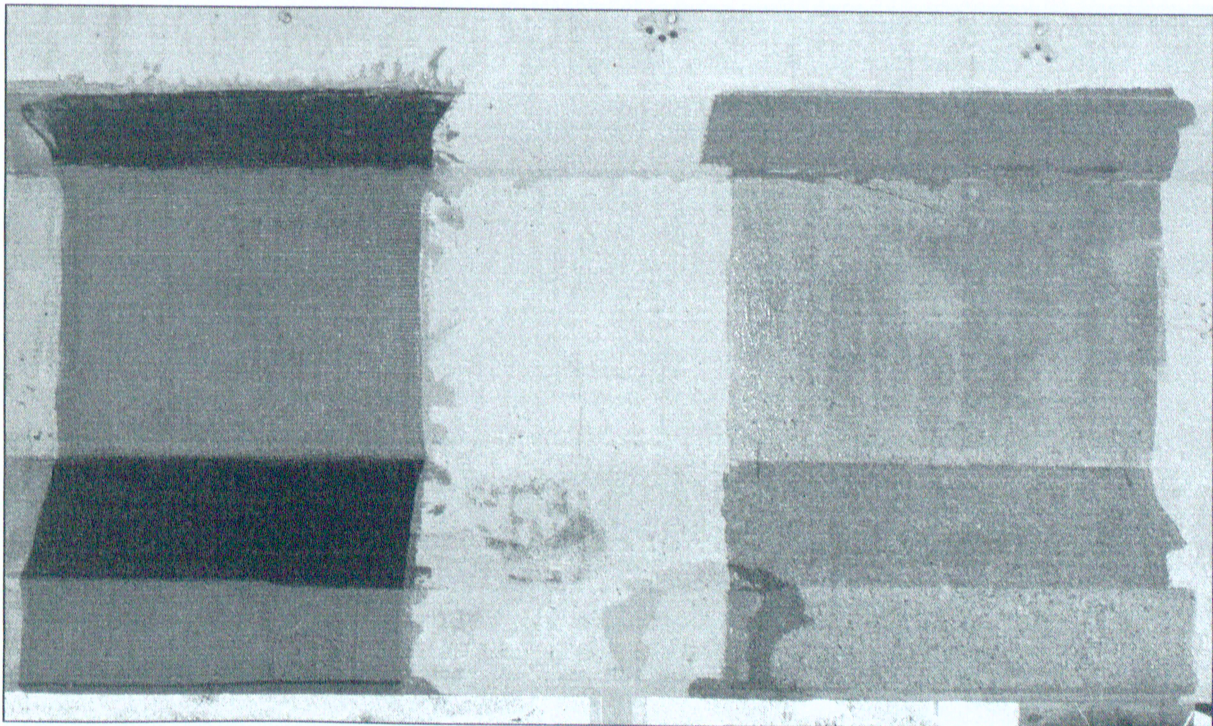


Figure 3.33 – Comparison at midspan: First application of Saturant Epoxy

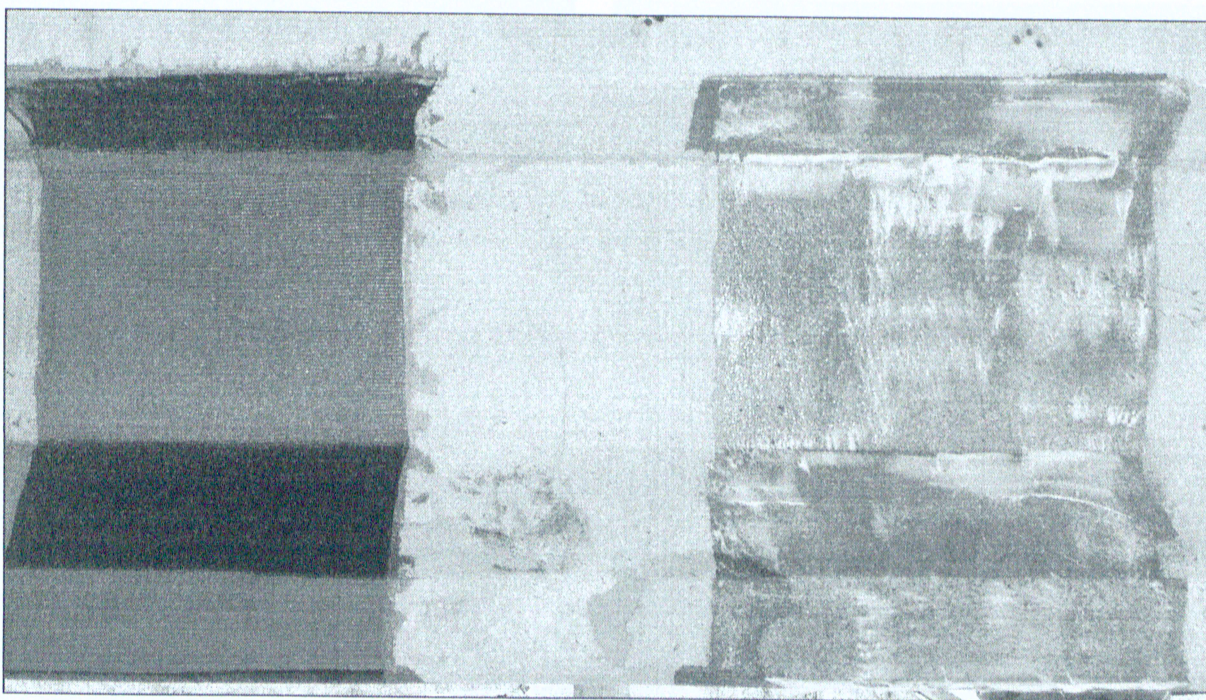


Figure 3.34 – Comparison at midspan: First application of Tack Coat Epoxy

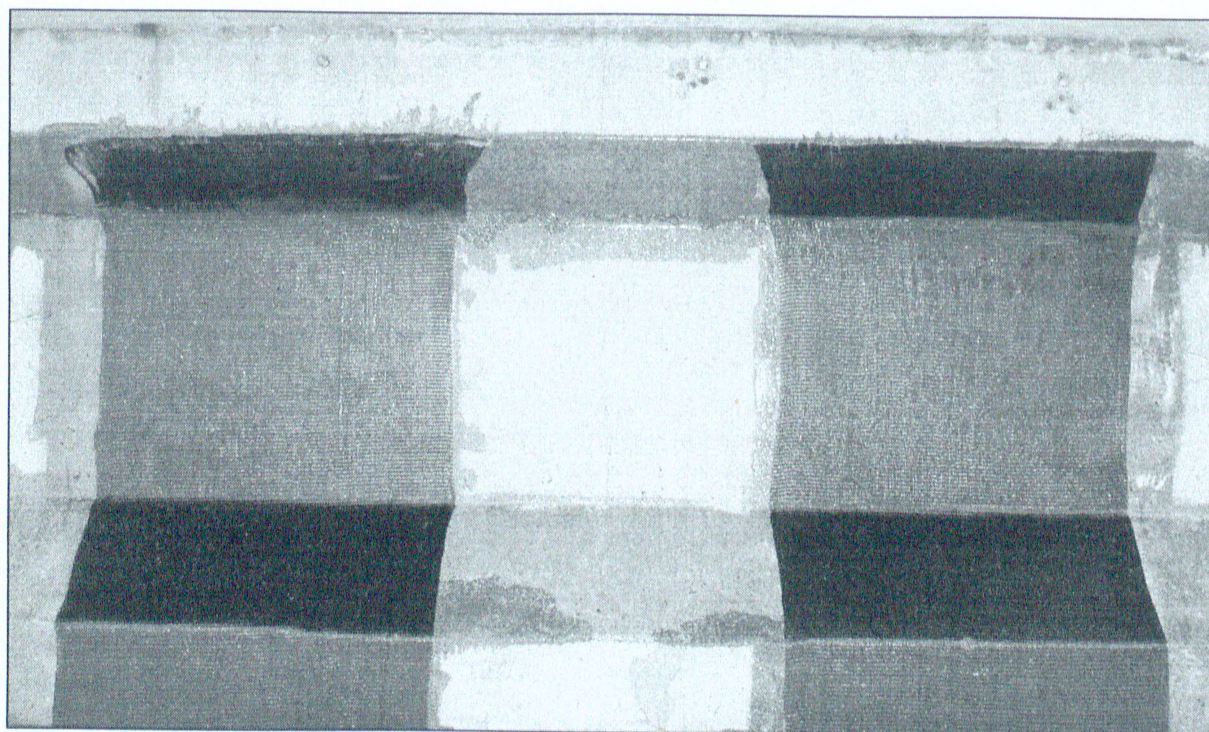


Figure 3.35 – Comparison at midspan: First layer of CFRP U-wrap

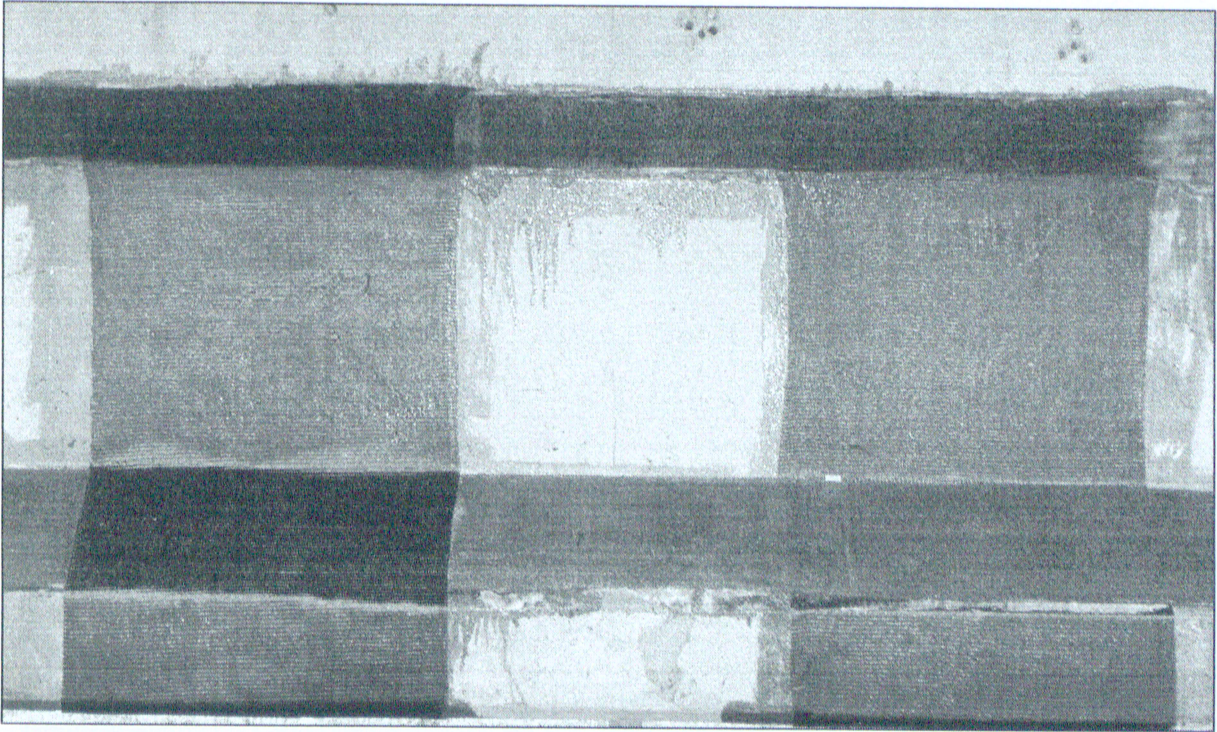


Figure 3.36 – Comparison at midspan: Longitudinal anchor strips and second CFRP U-wrap layer

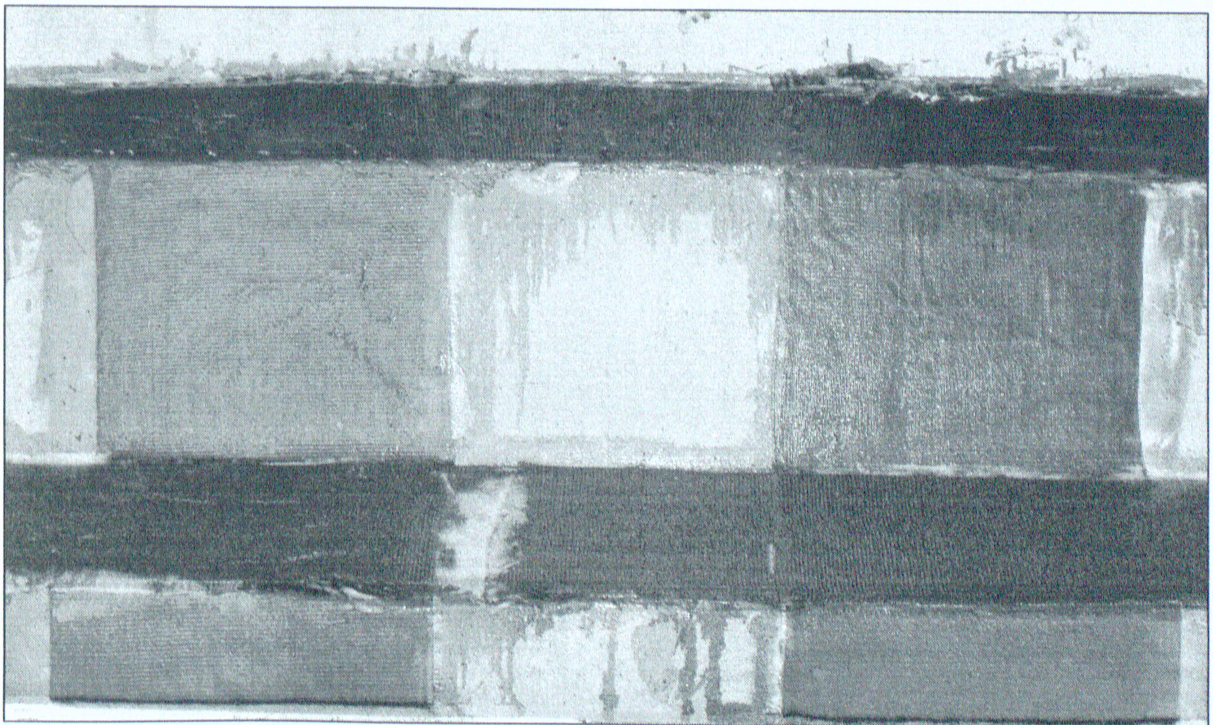


Figure 3.37 – Comparison at midspan: Completion of CFRP system

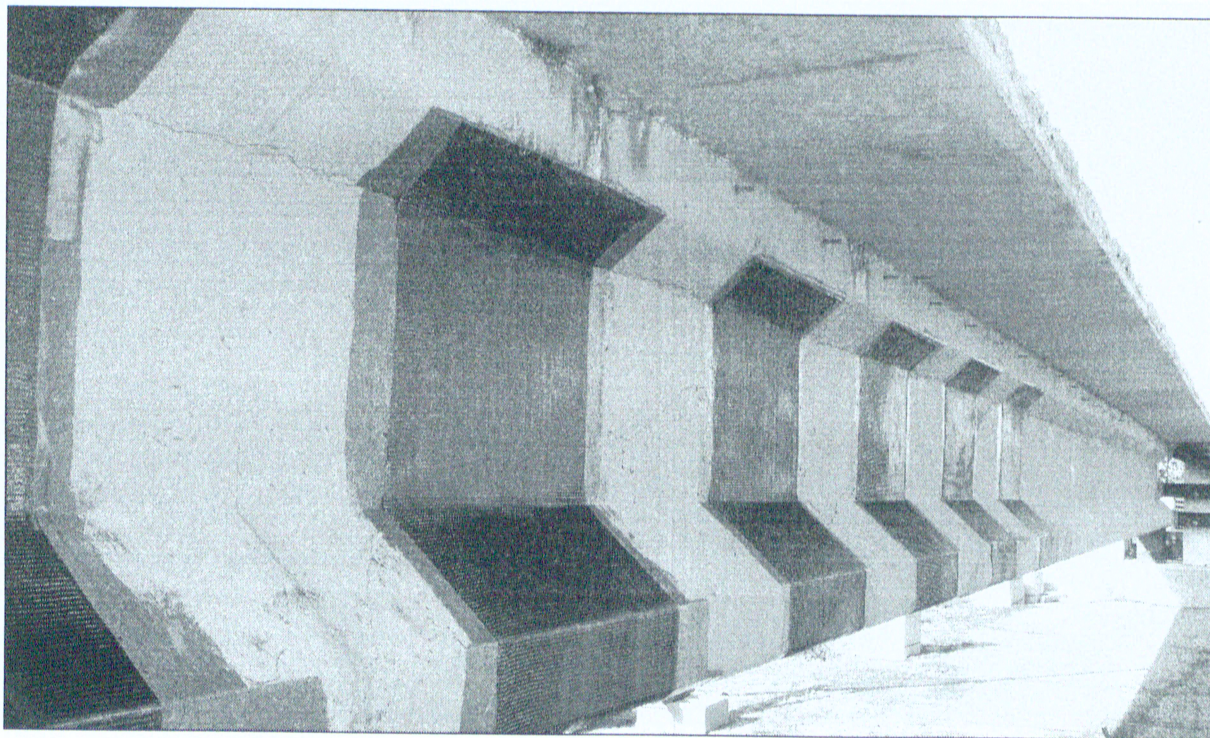


Figure 3.38 – First layer of CFRP U-wraps on one half the girder

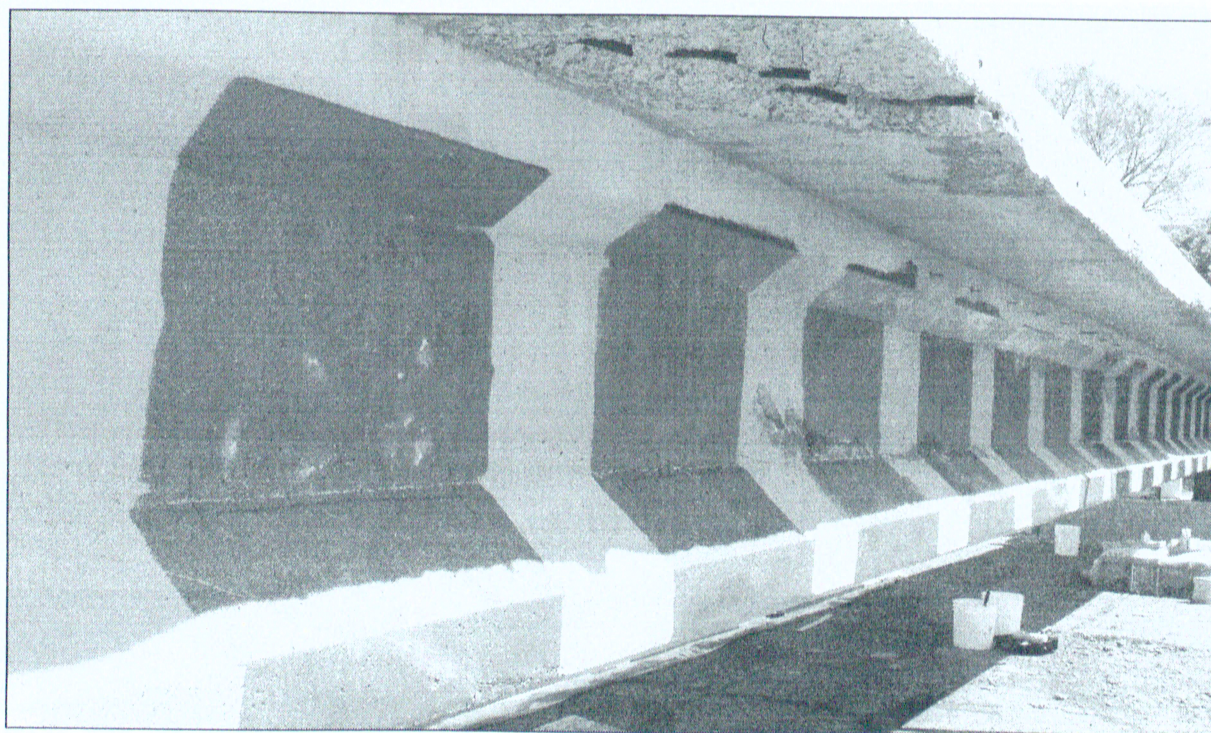


Figure 3.39 – First application of Saturant Epoxy

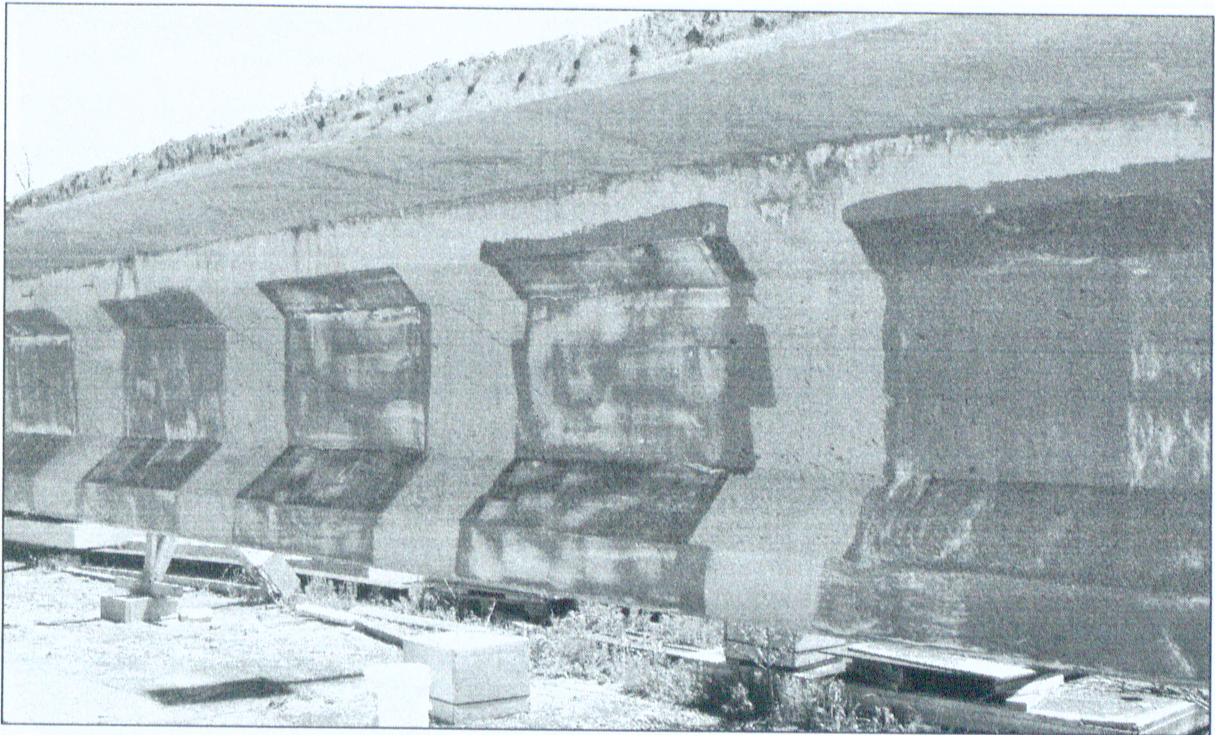


Figure 3.40 – First application of Tack Coat Epoxy

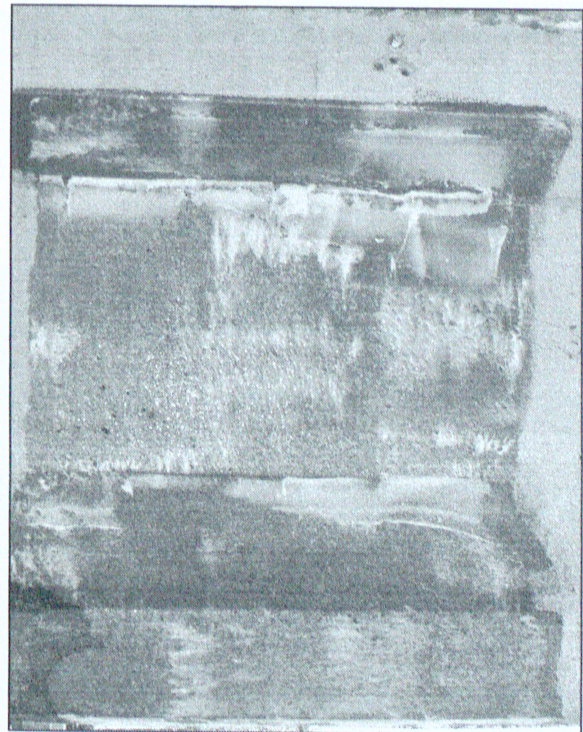
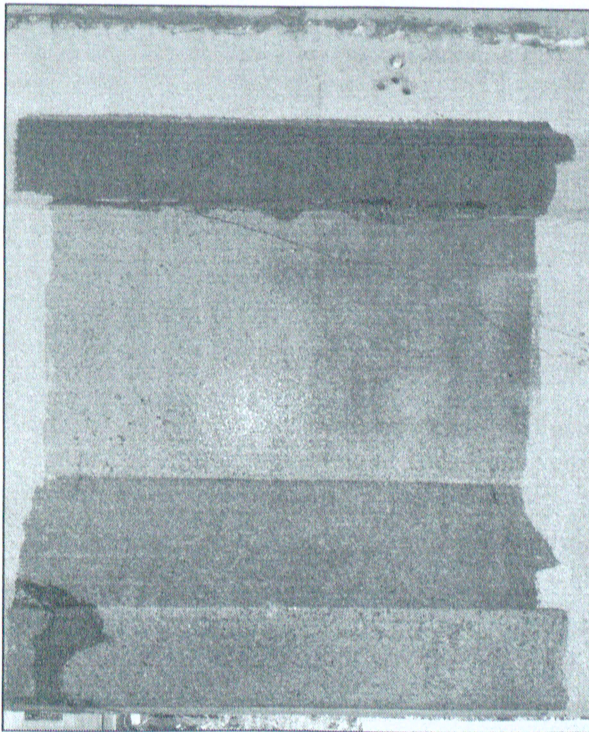


Figure 3.41 – Saturant and Tack Coat Epoxy application on a girder section

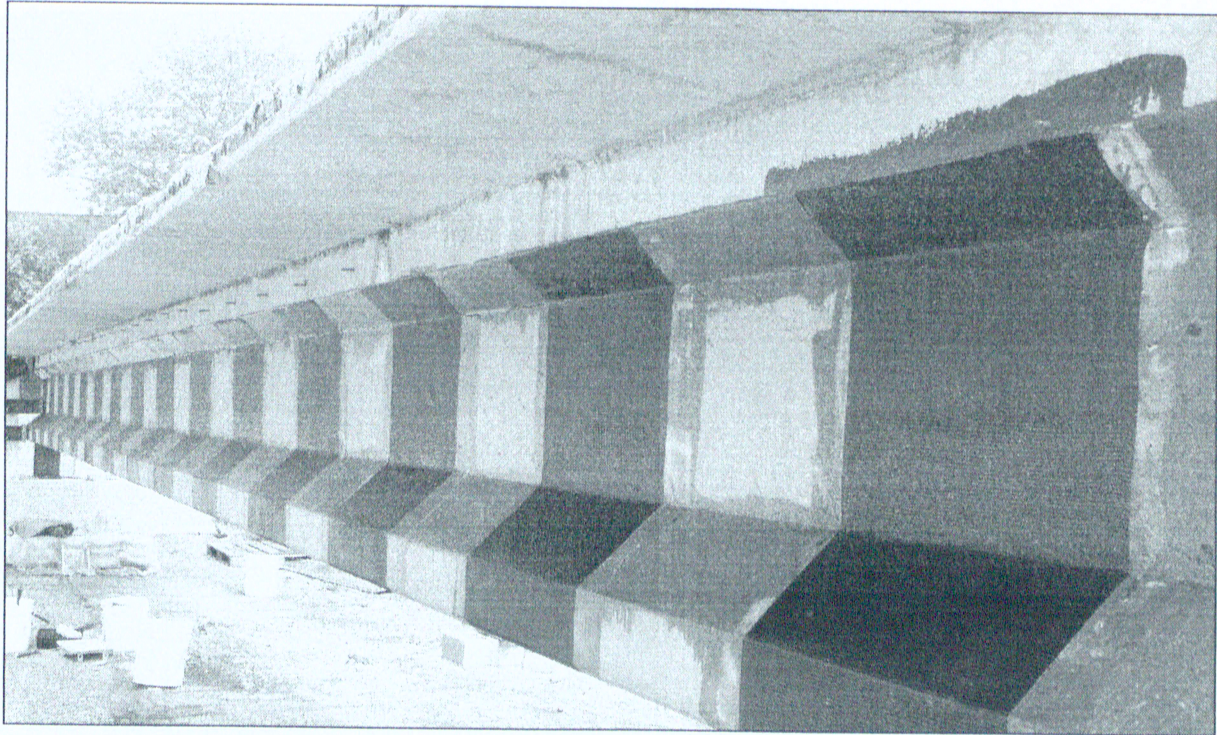


Figure 3.42 – Completion of first CFRP U-wrap layer on entire girder

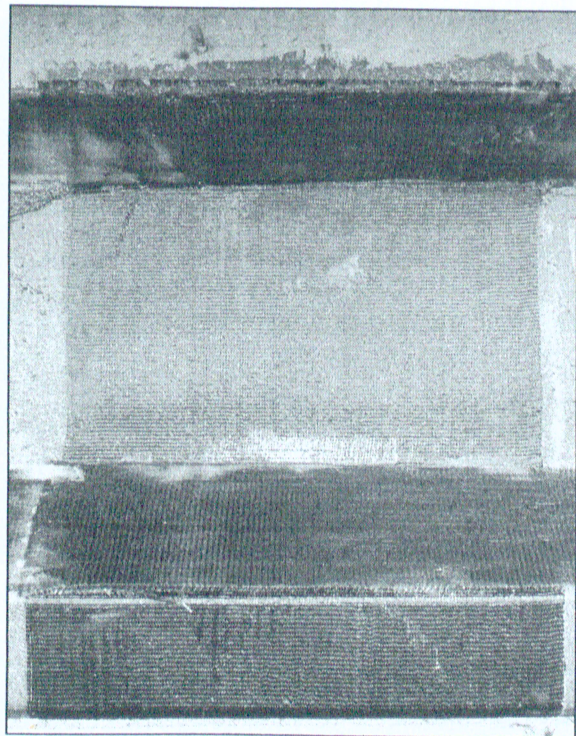
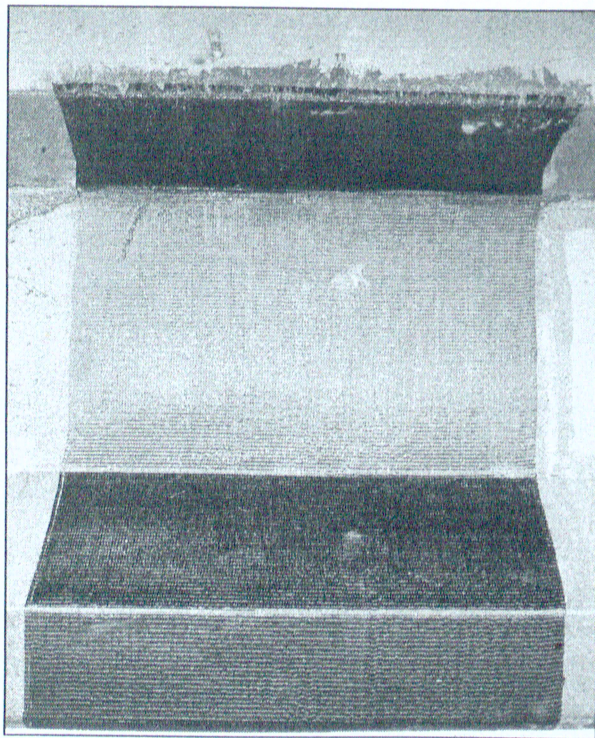


Figure 3.43 – First and second CFRP U-wrap layers with longitudinal anchor strips



Figure 3.44 – Completion of one full layer of the CFRP system for entire girder length

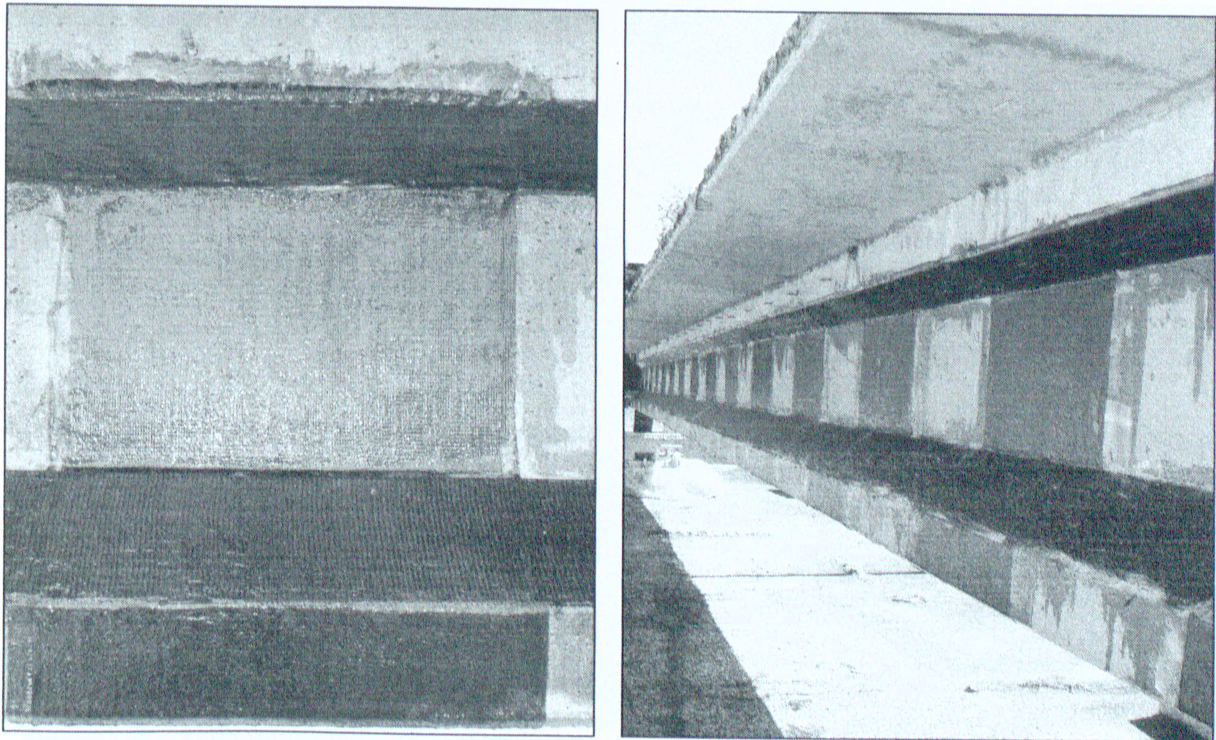


Figure 3.45 – Completion of entire CFRP system; shown for one section and entire girder

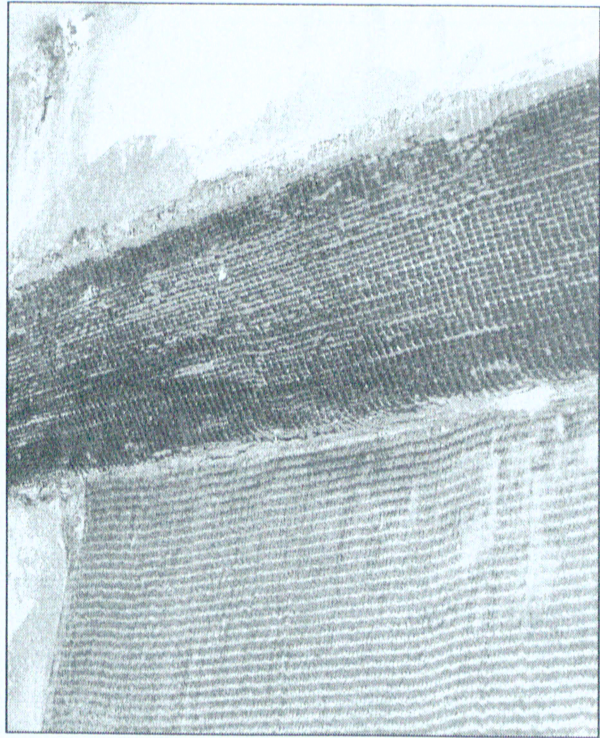
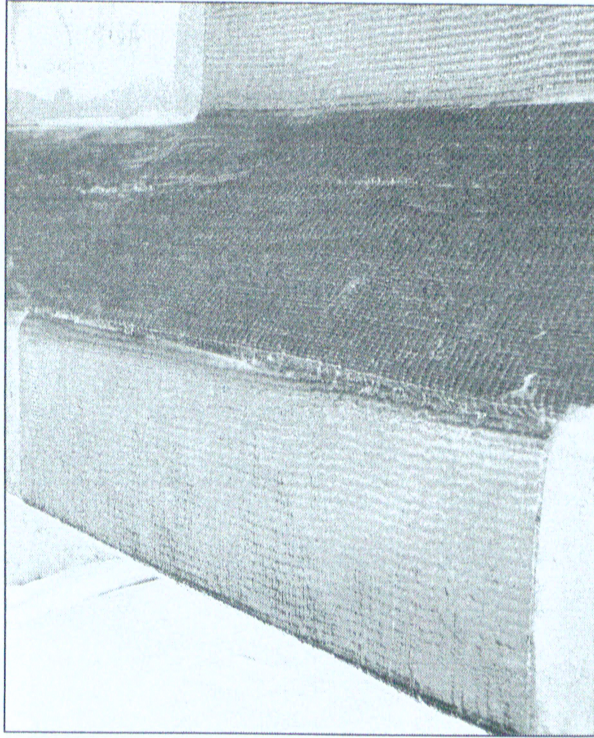


Figure 3.46 – Bottom and top chamfers after CFRP strengthening

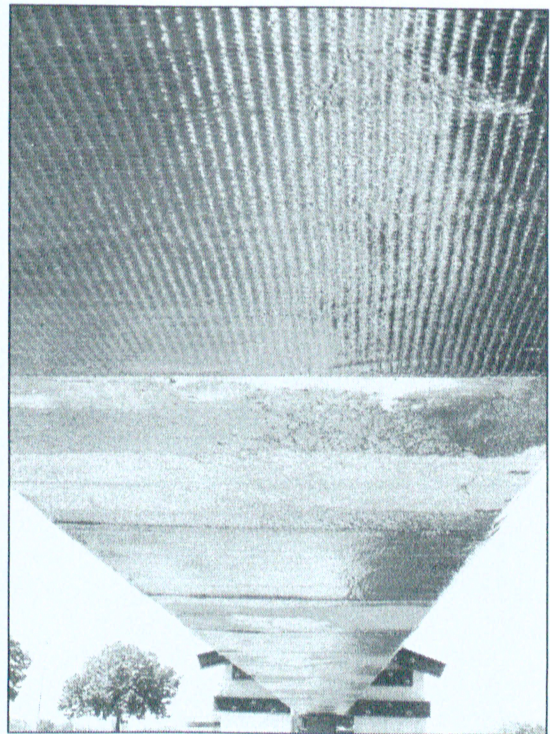
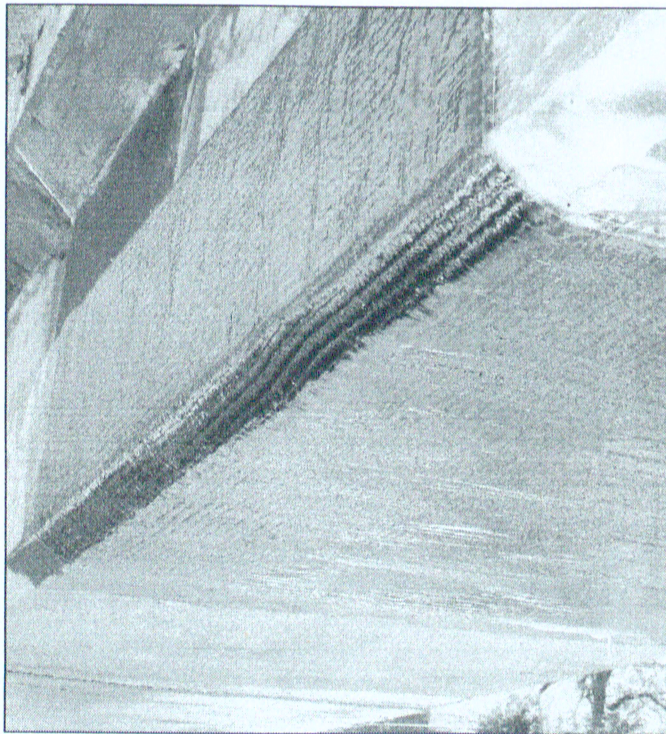


Figure 3.47 – Bottom flange underside after CFRP strengthening

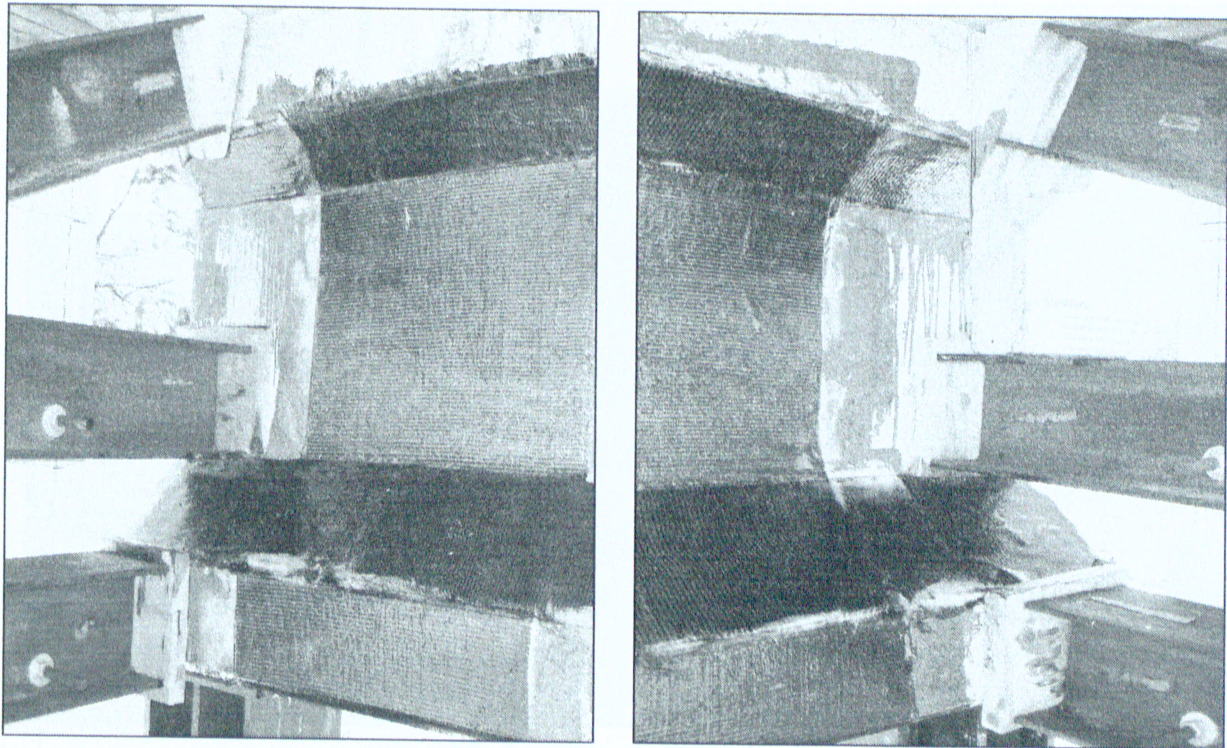


Figure 3.48 – CFRP anchoring to lateral support locations

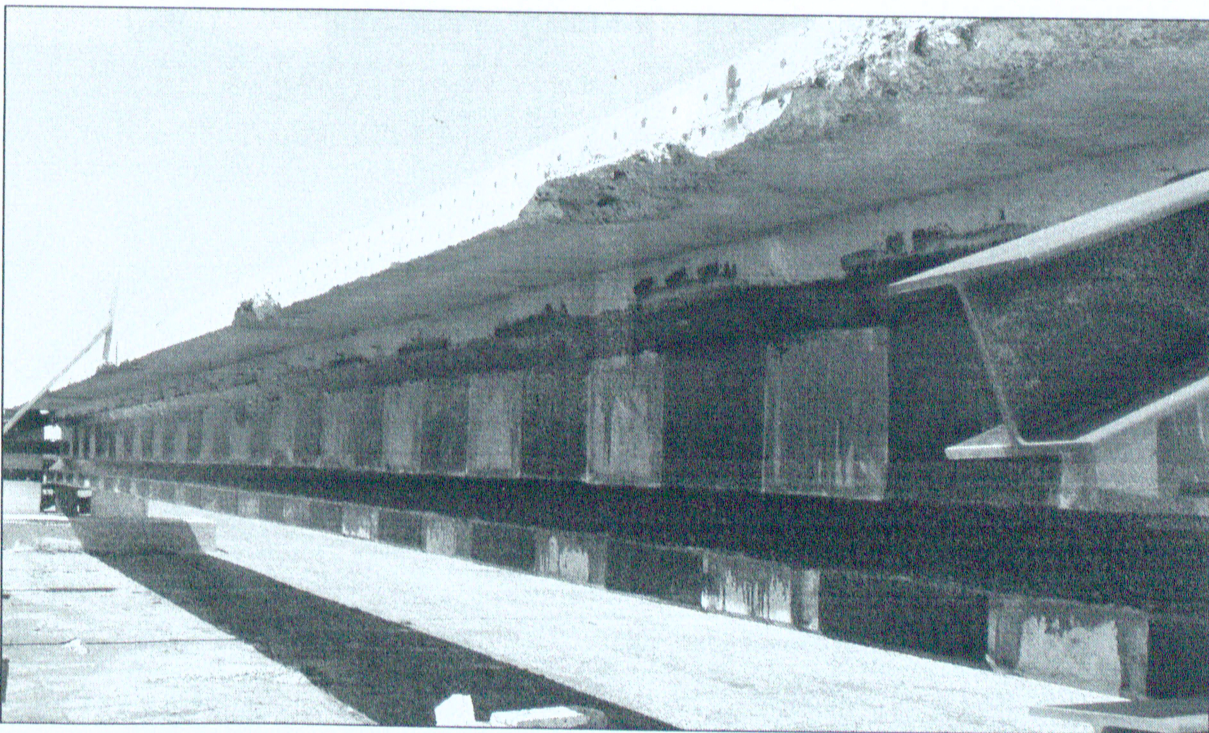


Figure 3.49 – Fully completed CFRP strengthened girder

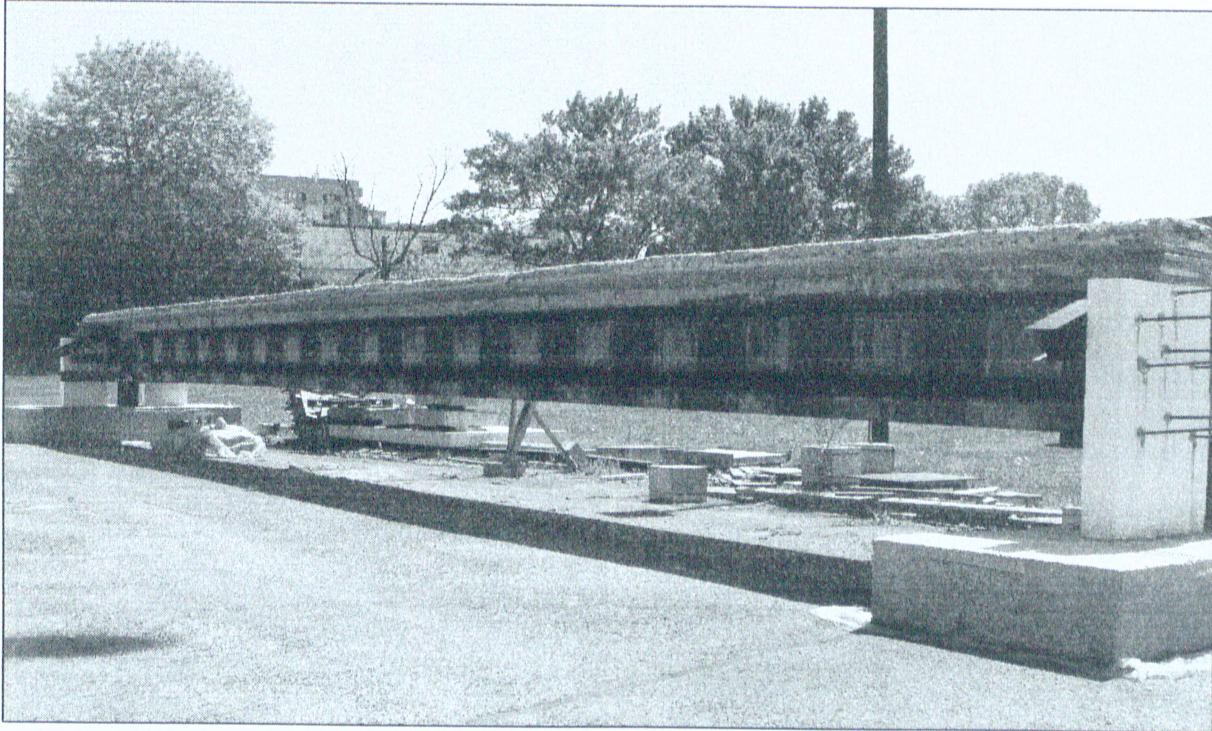


Figure 3.50 – Full view of fully completed, CFRP strengthened girder

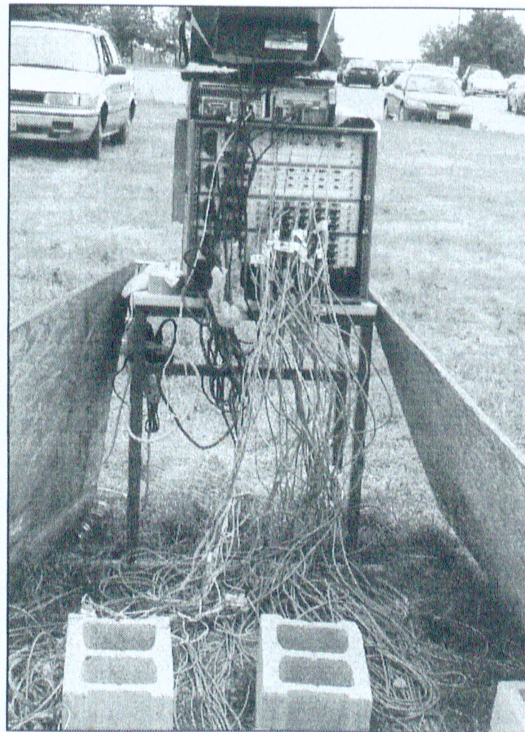
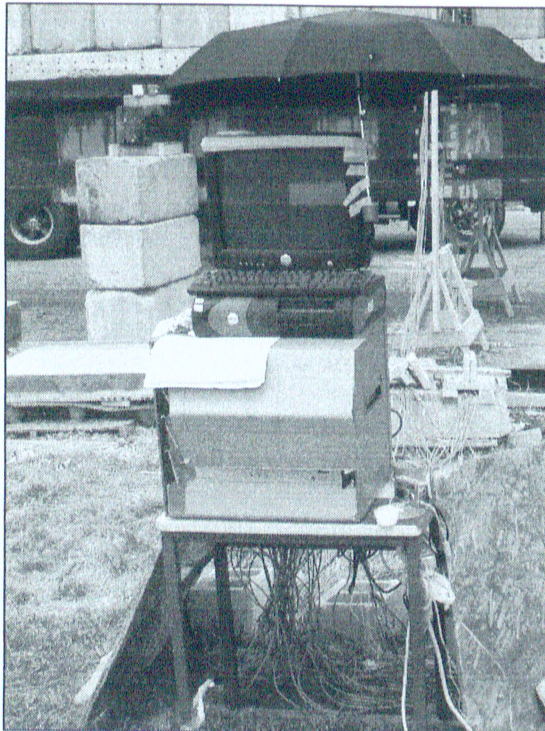


Figure 3.51 – Data acquisition system test control software (TCS) SYSTEM 6000 unit

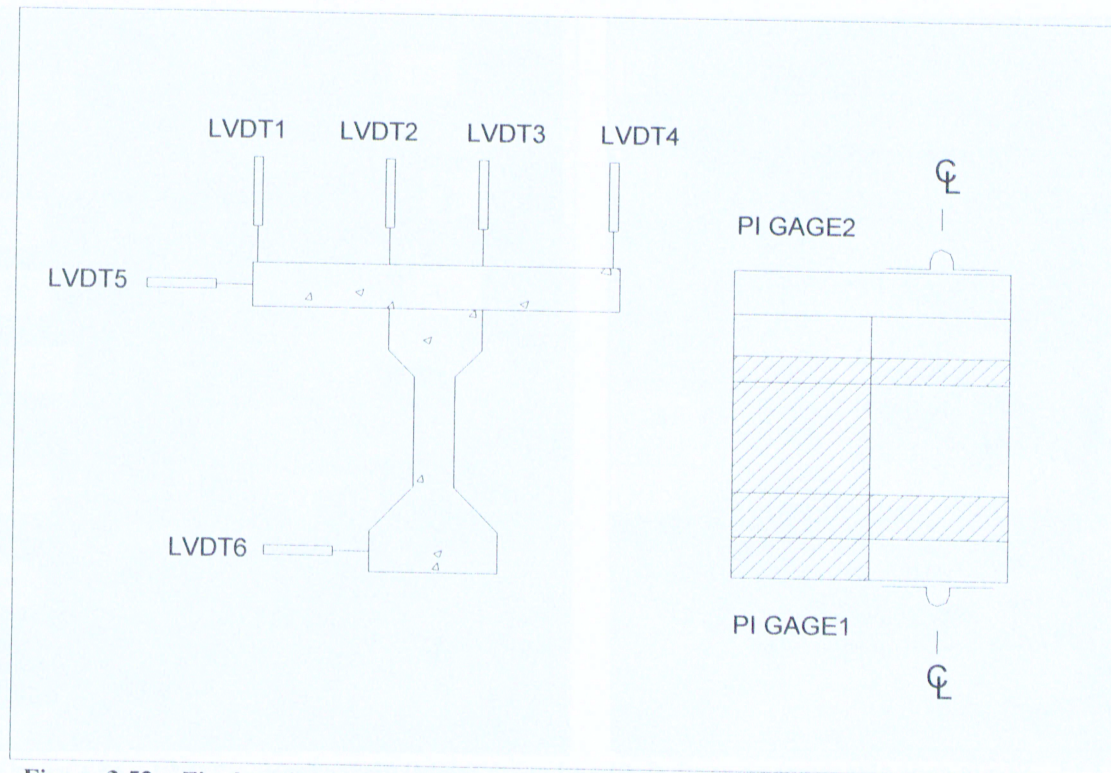


Figure 3.52 – Final testing instrumentation location for LVDTs and PI gages

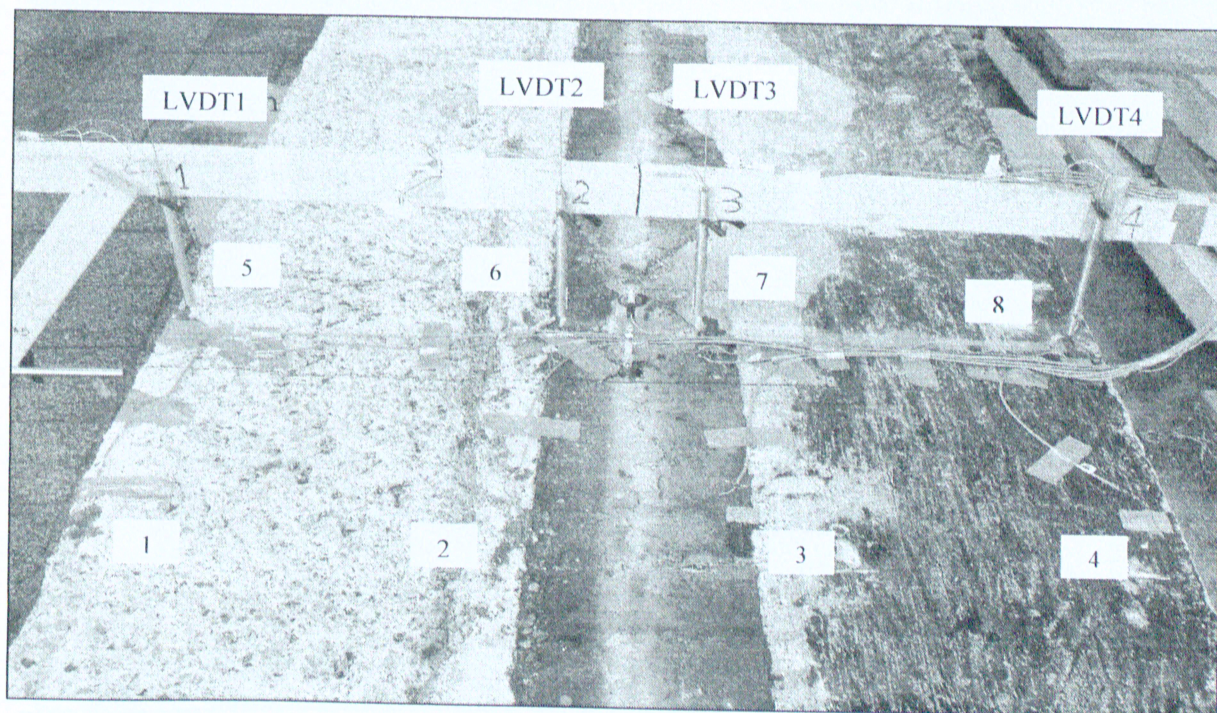


Figure 3.53 – Strain gages and LVDTs on top slab

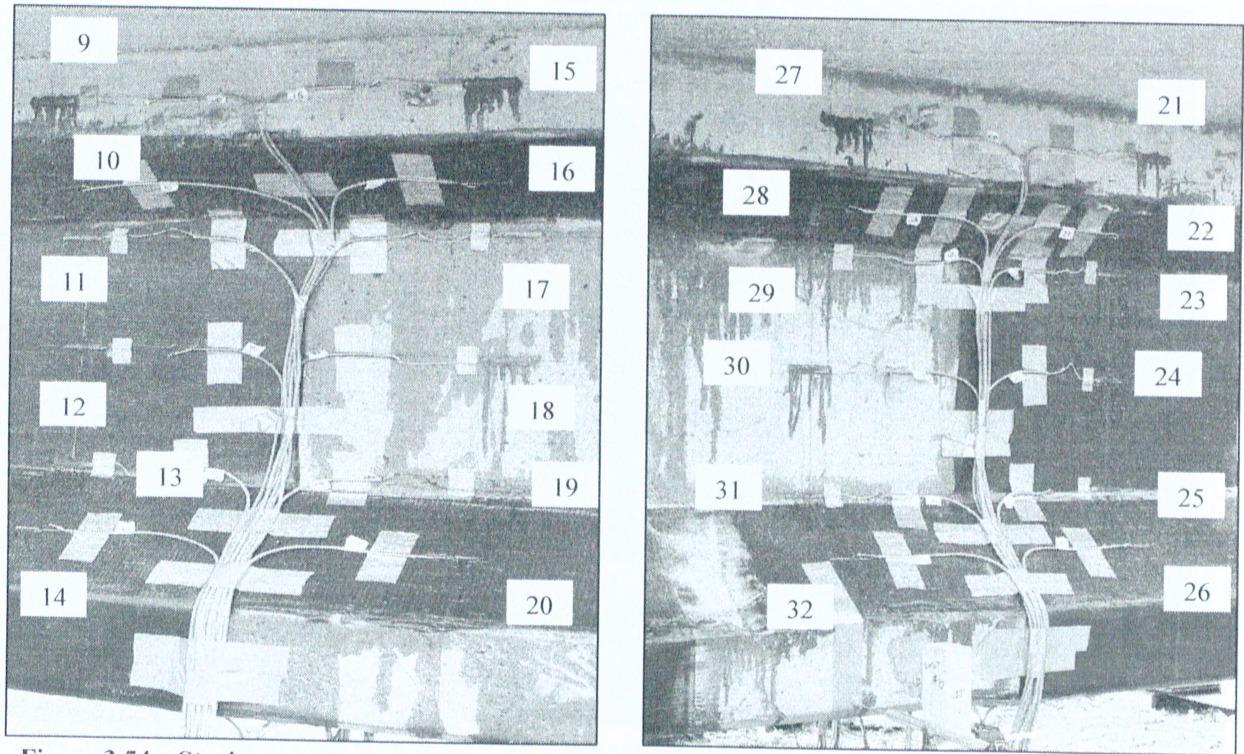


Figure 3.54 – Strain gage placement on south (left) and north (right) girder faces

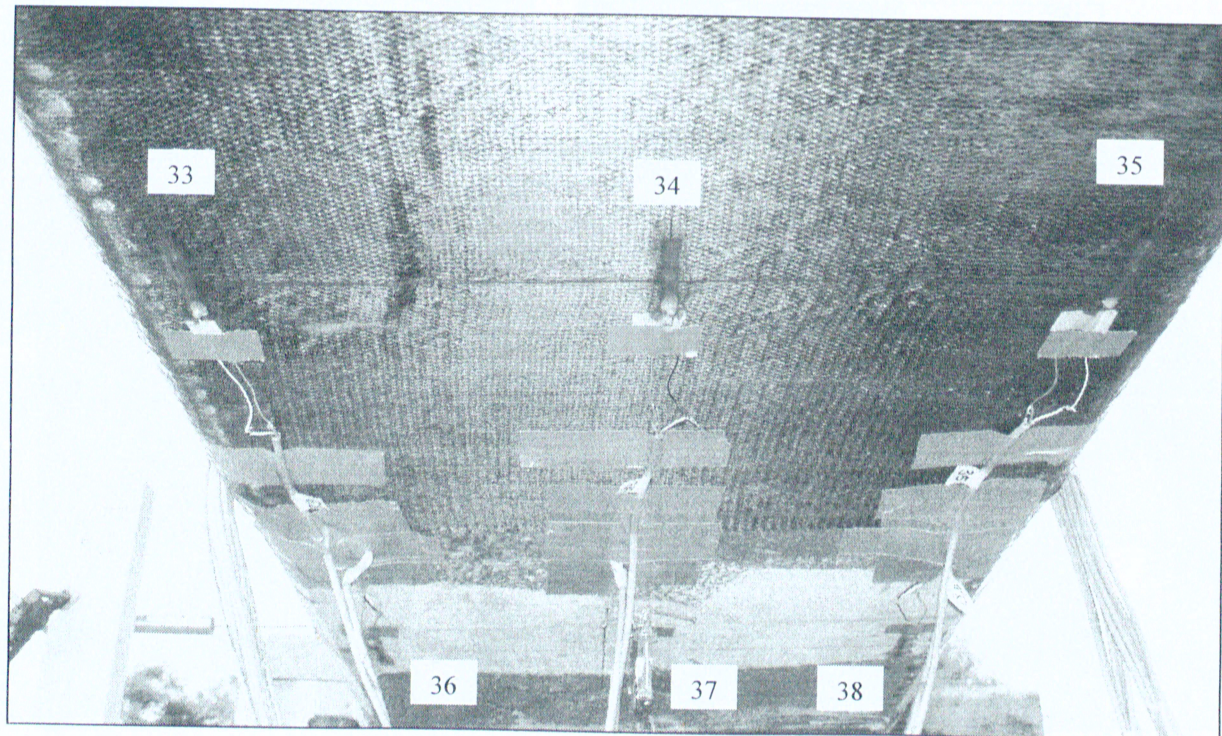


Figure 3.55 – Strain gages on the underside of the bottom flange

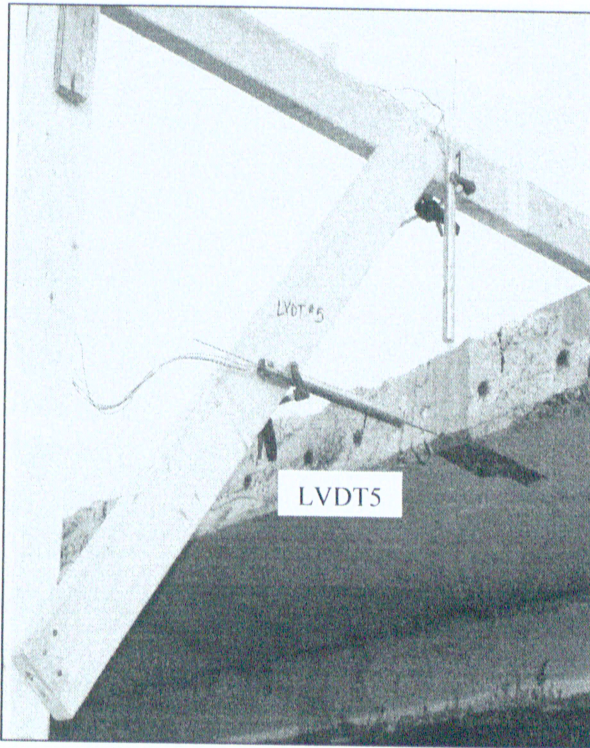


Figure 3.56 – LVDTs setup for lateral deflection

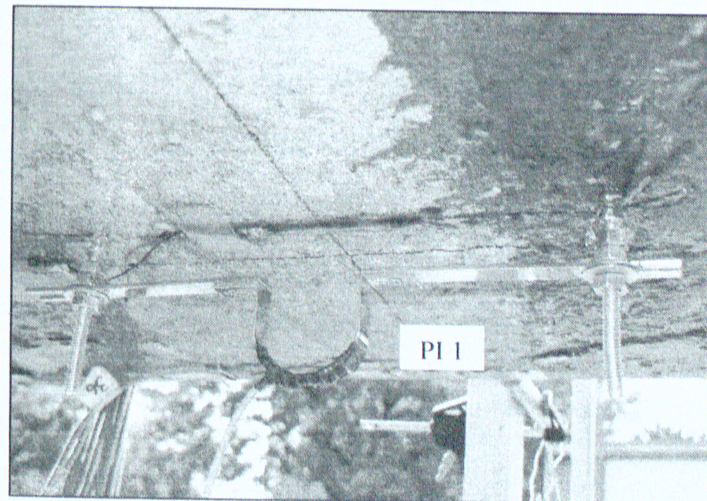
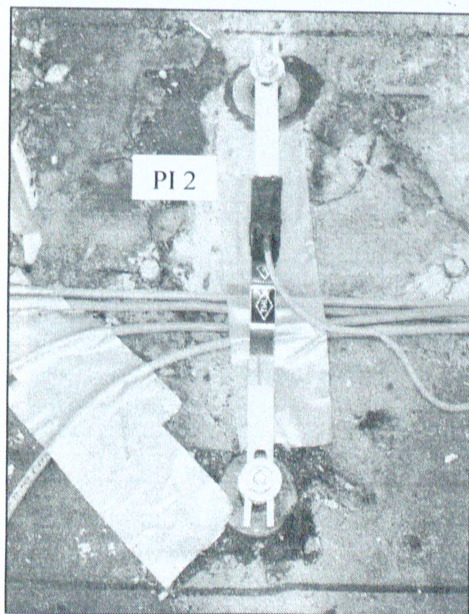


Figure 3.57 – PI gages setup on the top slab (left) and underside of bottom flange (right)

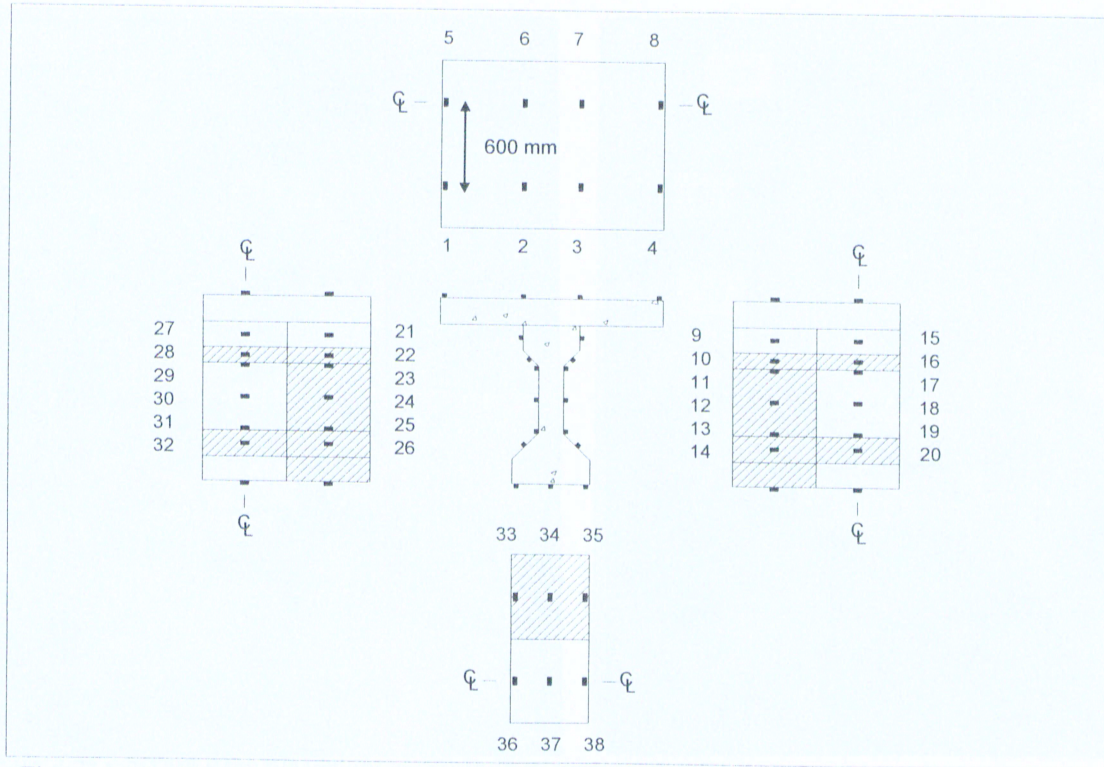


Figure 3.58 – Final testing instrumentation location for strain gages



Figure 3.59 – Mechanical dial gages, at supports, for bearing pad (left) and foundation (right) settlement

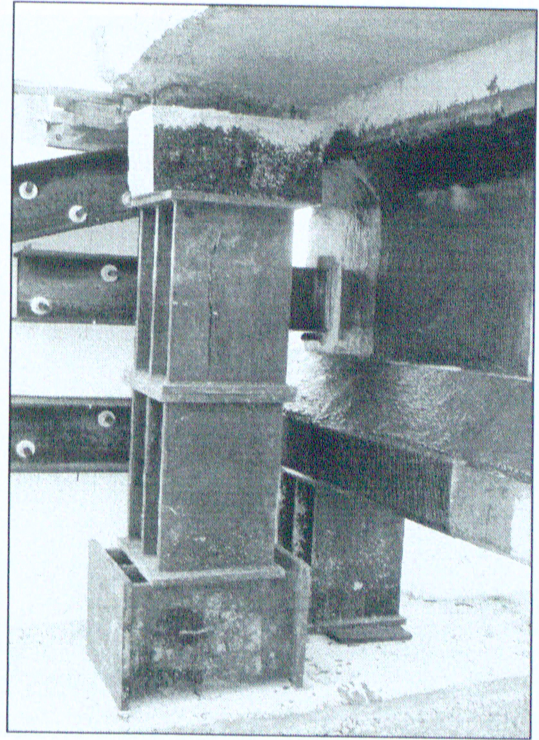
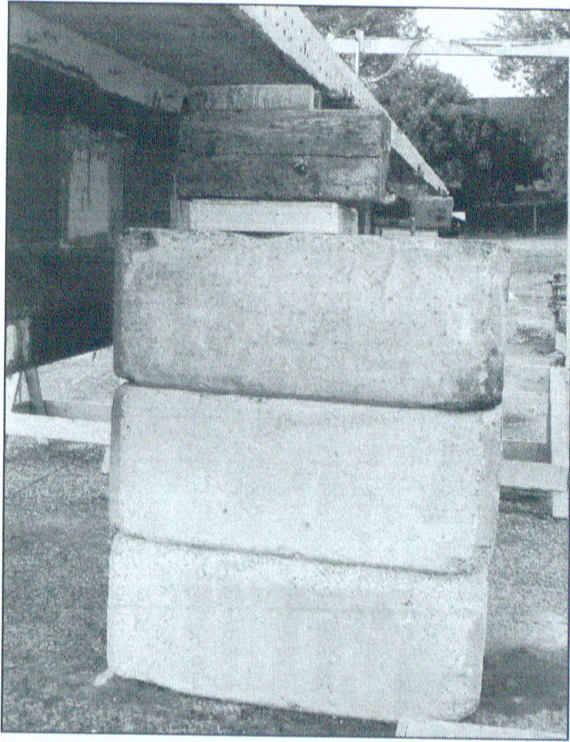


Figure 3.60 – Torsion supports (left) near midspan, and at support (right)

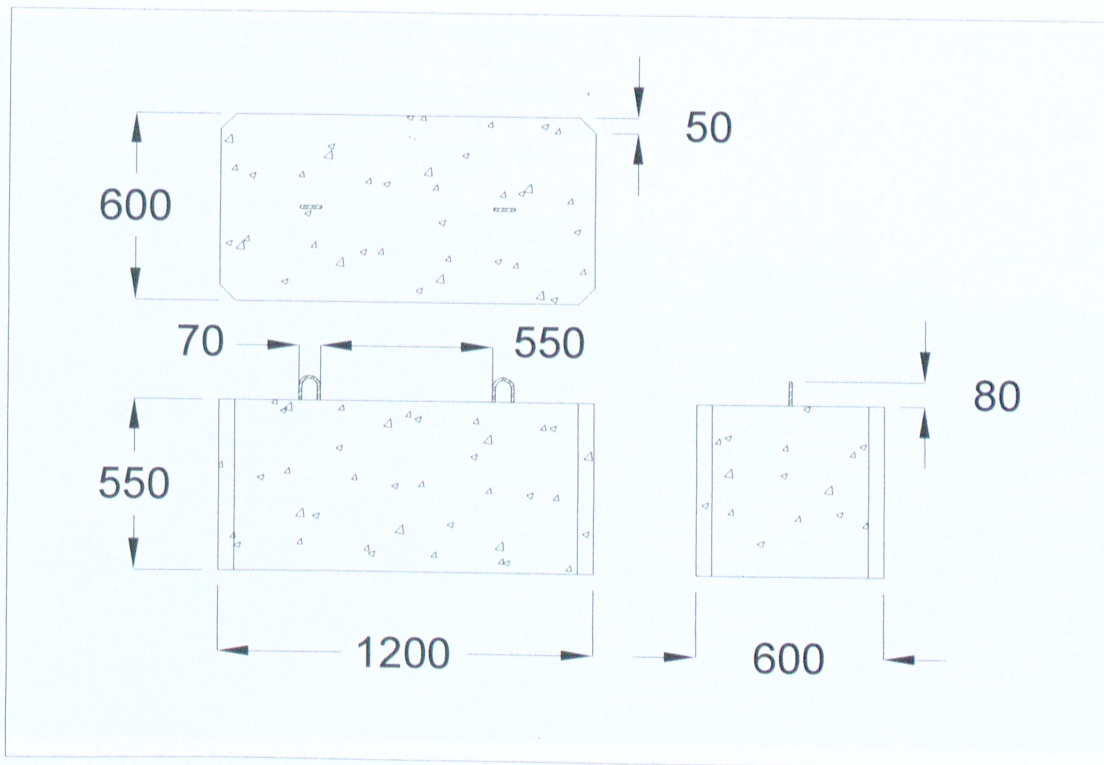


Figure 3.61 – One ton block dimensions

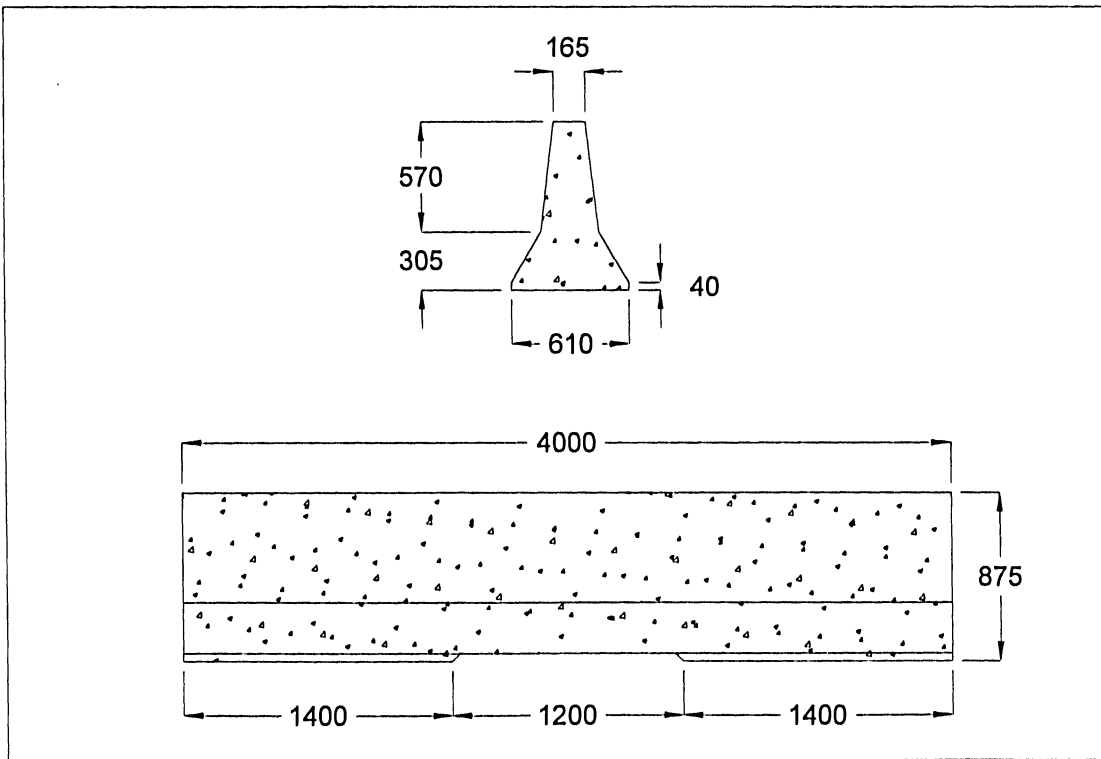


Figure 3.62 – Jersey barrier dimensions

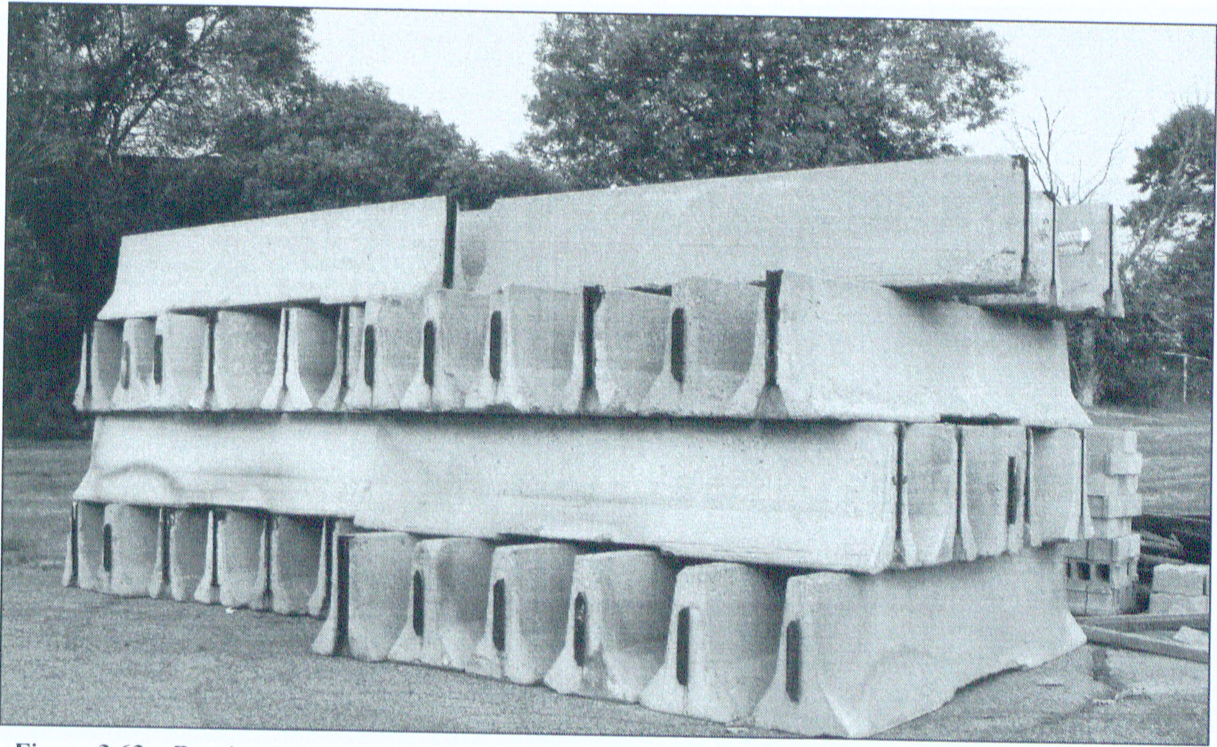


Figure 3.63 – Barrier deposit

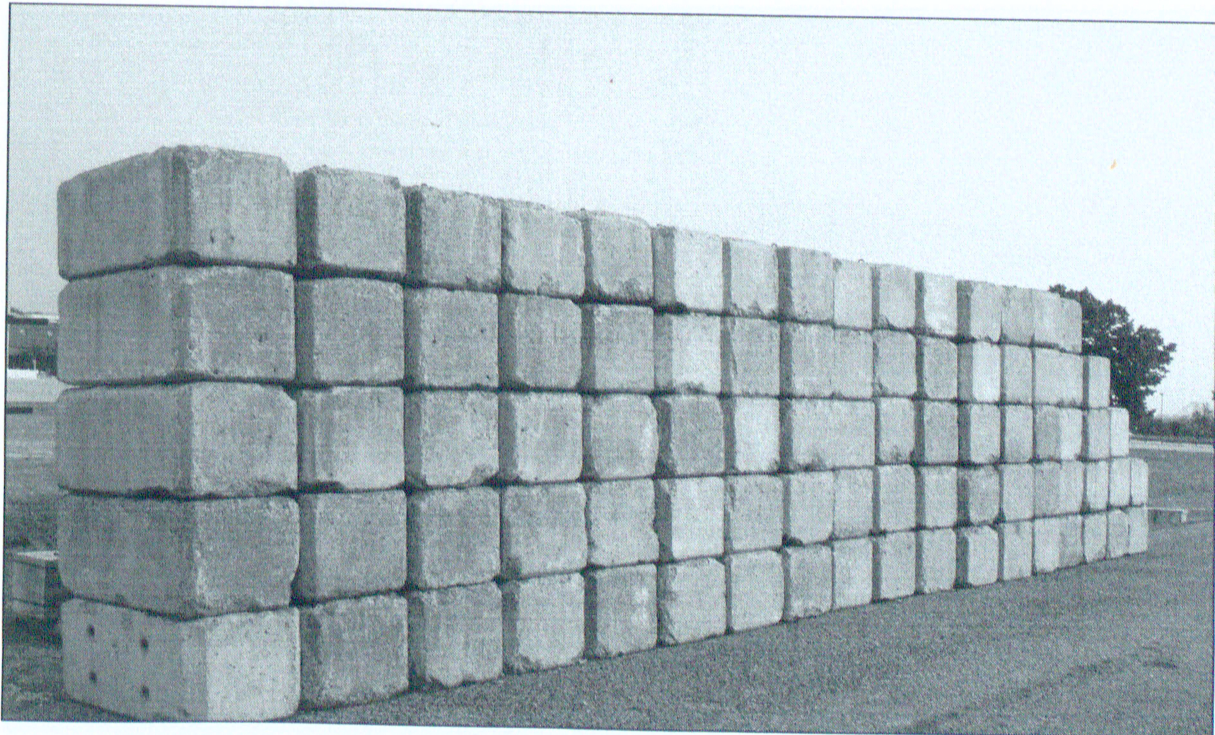


Figure 3.64 – One ton block deposit

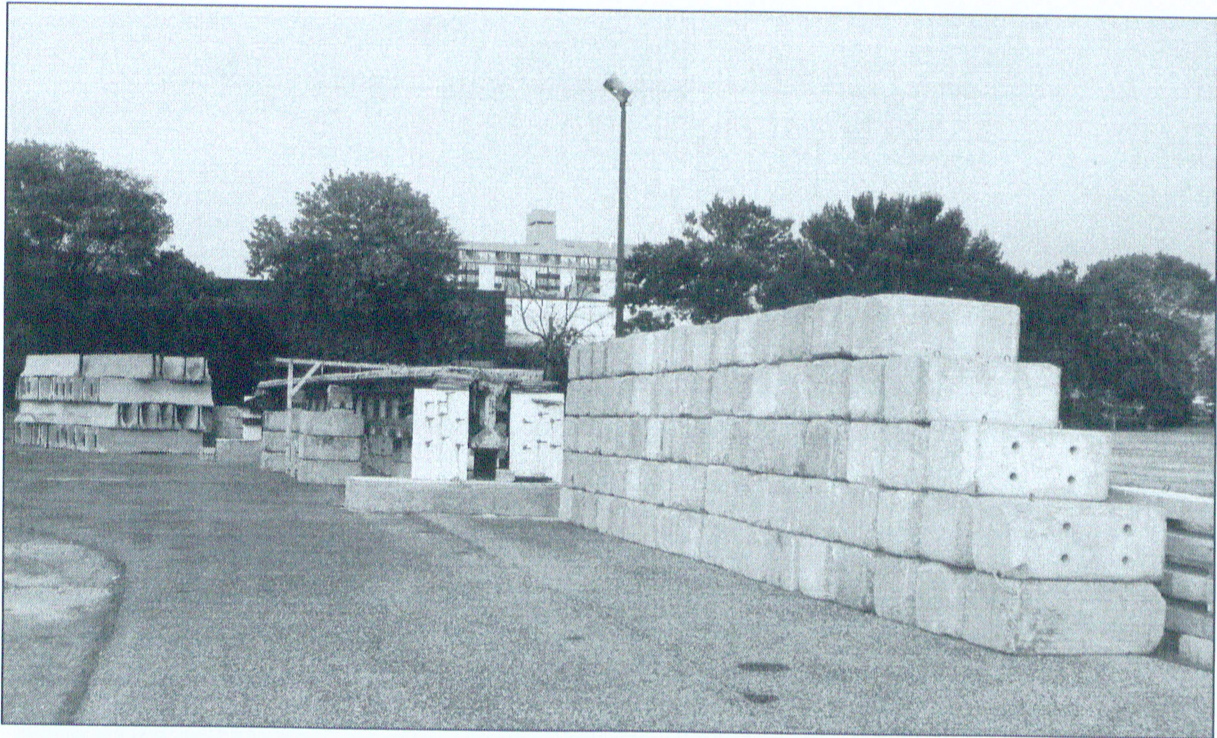


Figure 3.65 – Barriers and one ton blocks at girder test site



Figure 3.66 – First row of loading: one ton blocks

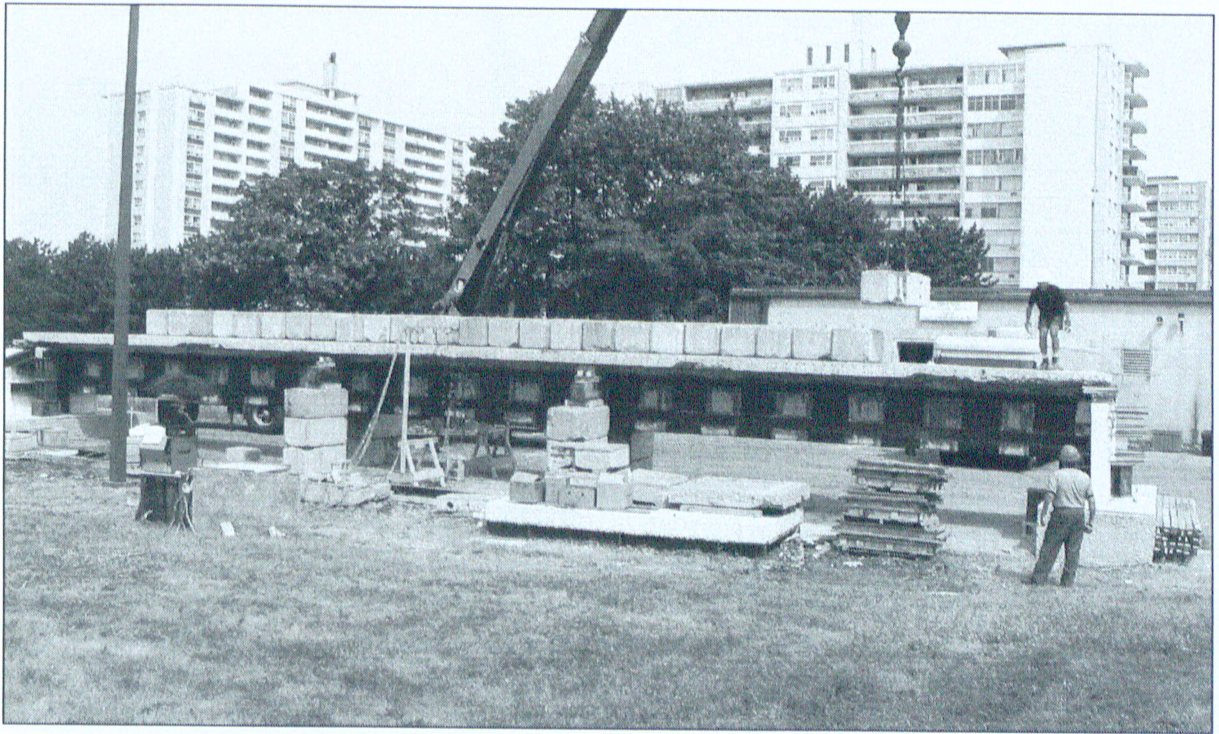


Figure 3.67 – Nearing completion for the first row of loading



Figure 3.68 – Second row of loading (left), and positioning (right)

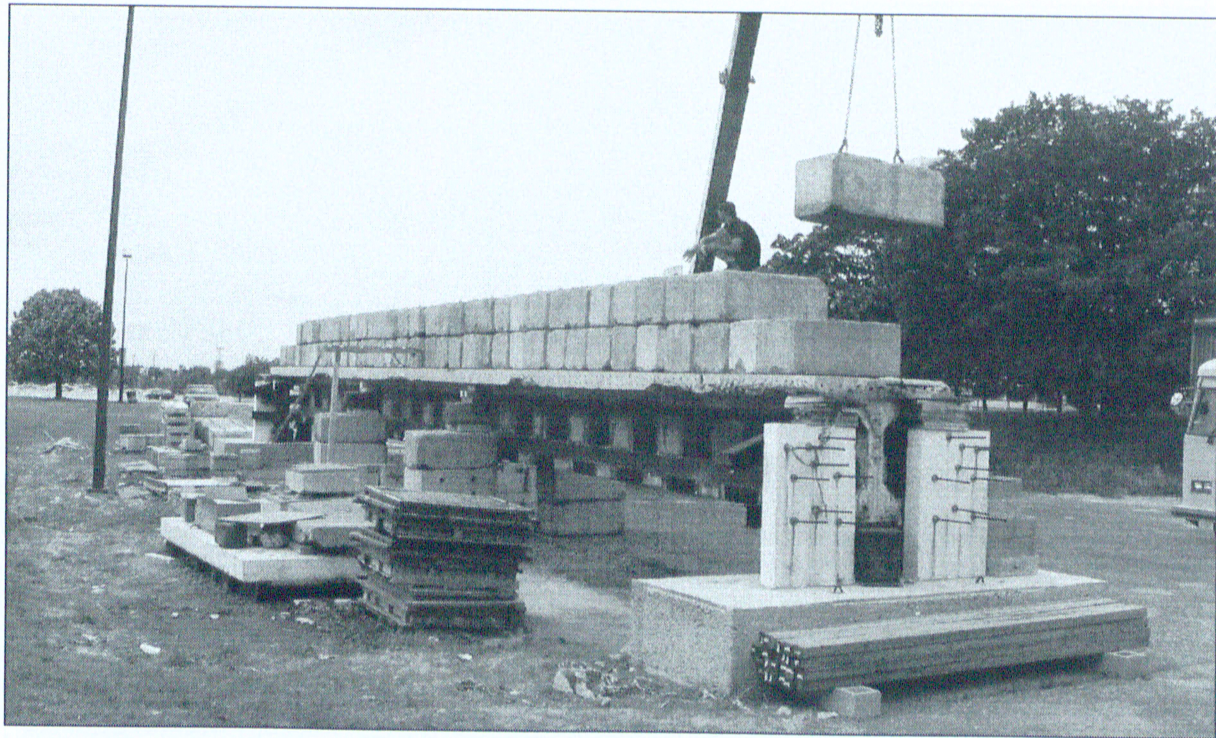


Figure 3.69 – Nearing completion of the second row of loading



Figure 3.70 – Completion of first two rows of one ton block loading



Figure 3.71 – Third and fourth rows of loading: one ton blocks



Figure 3.72 – Nearing completion of third and fourth rows of loading



Figure 3.73 – Installation and layout (inset) of wooden posts for barrier stability

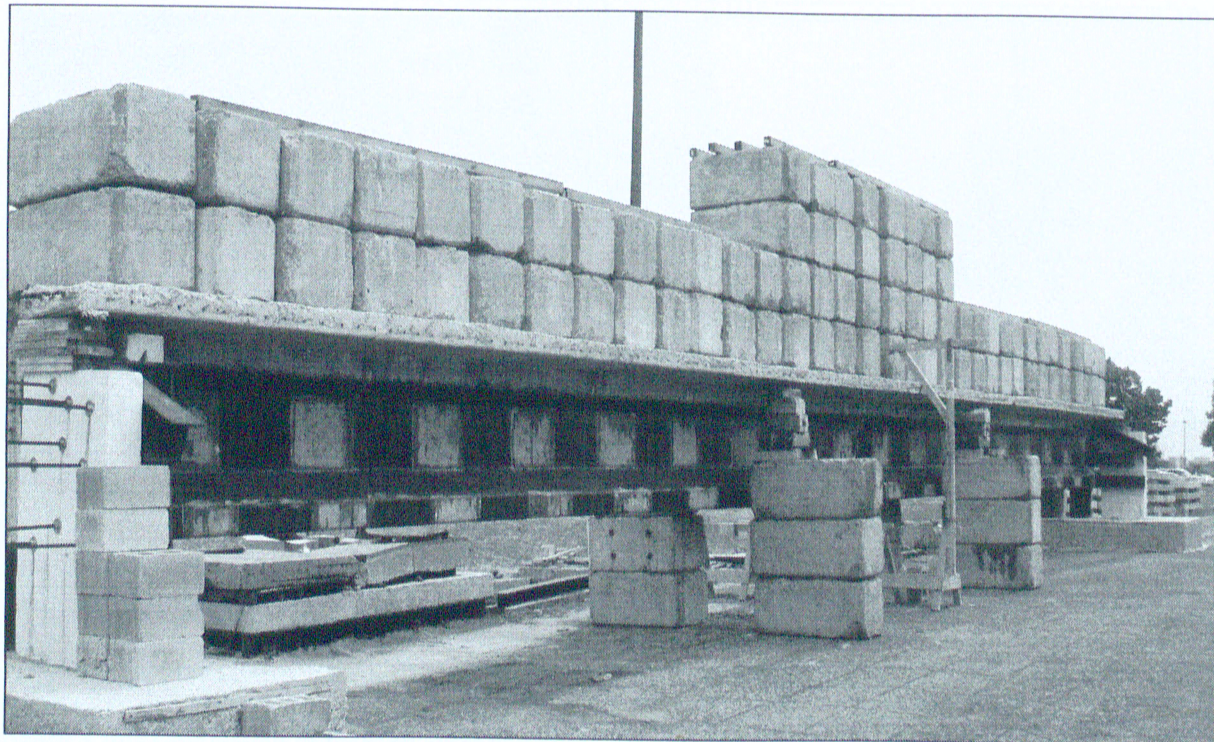


Figure 3.74 – Completion of all loading concerning the one ton blocks



Figure 3.75 – Placement of first Jersey barrier

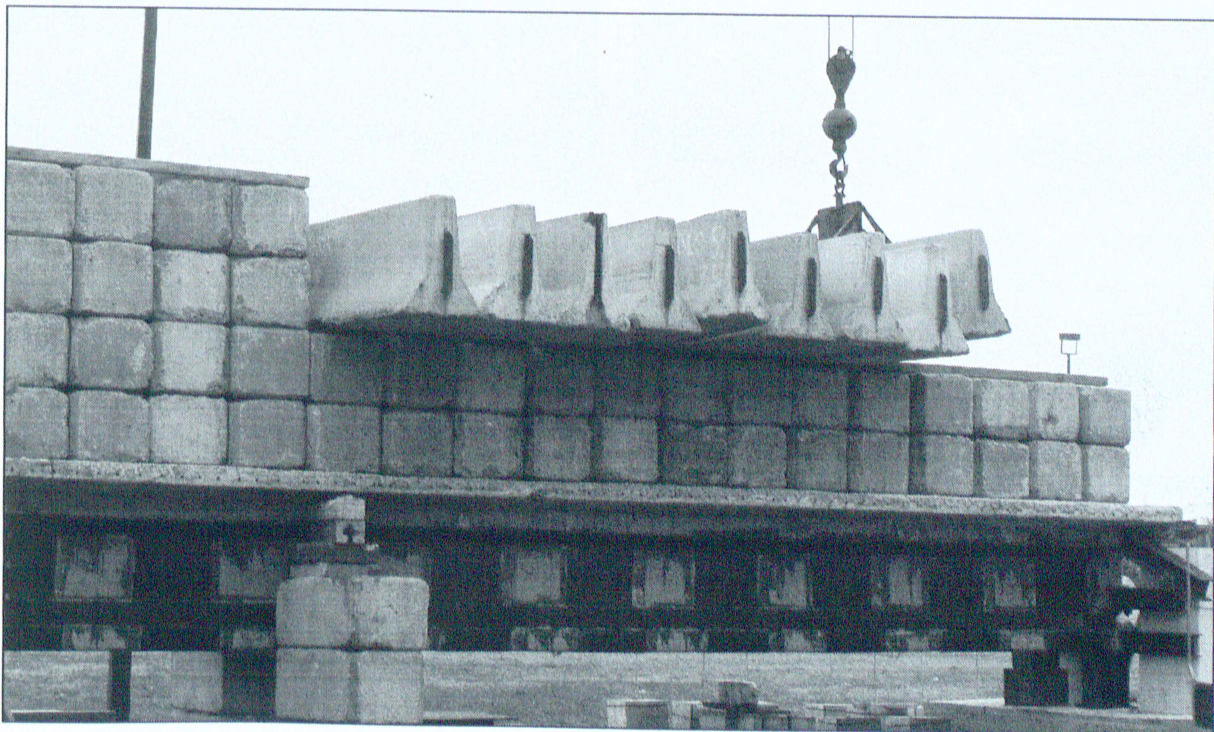


Figure 3.76 – Jersey barrier loading on one half the girder span

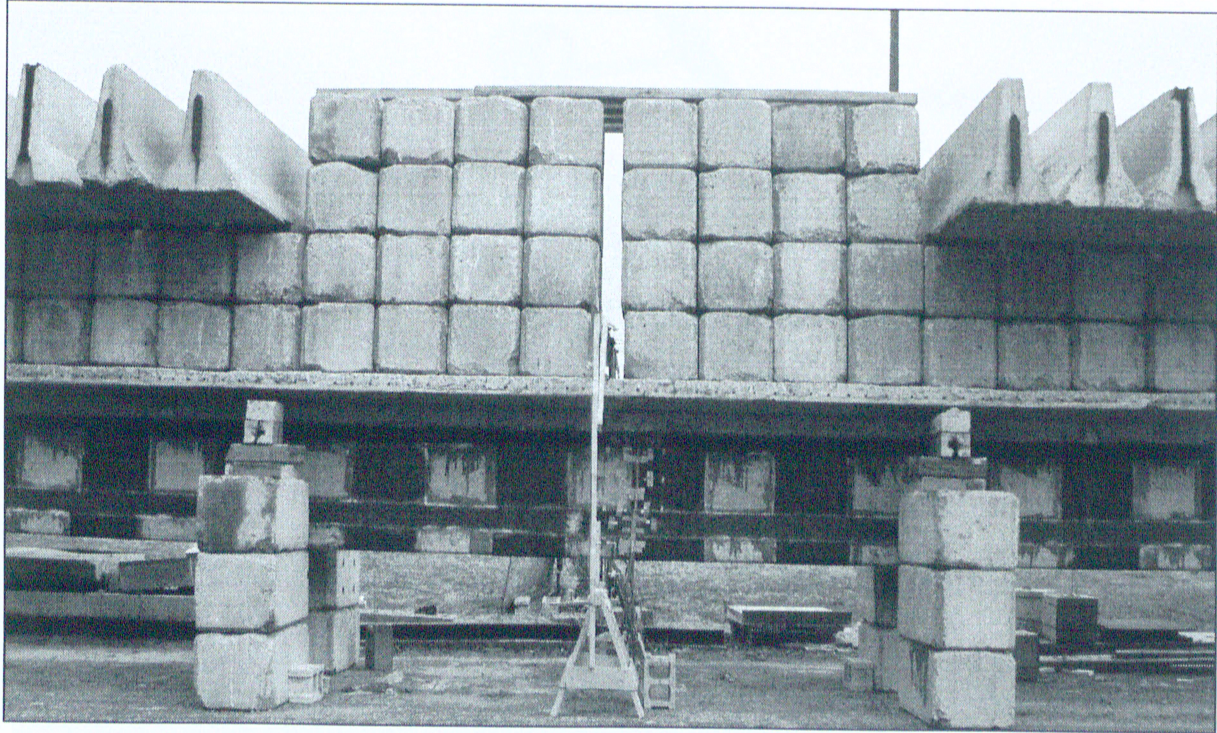


Figure 3.77 – Midspan view of final loading configuration

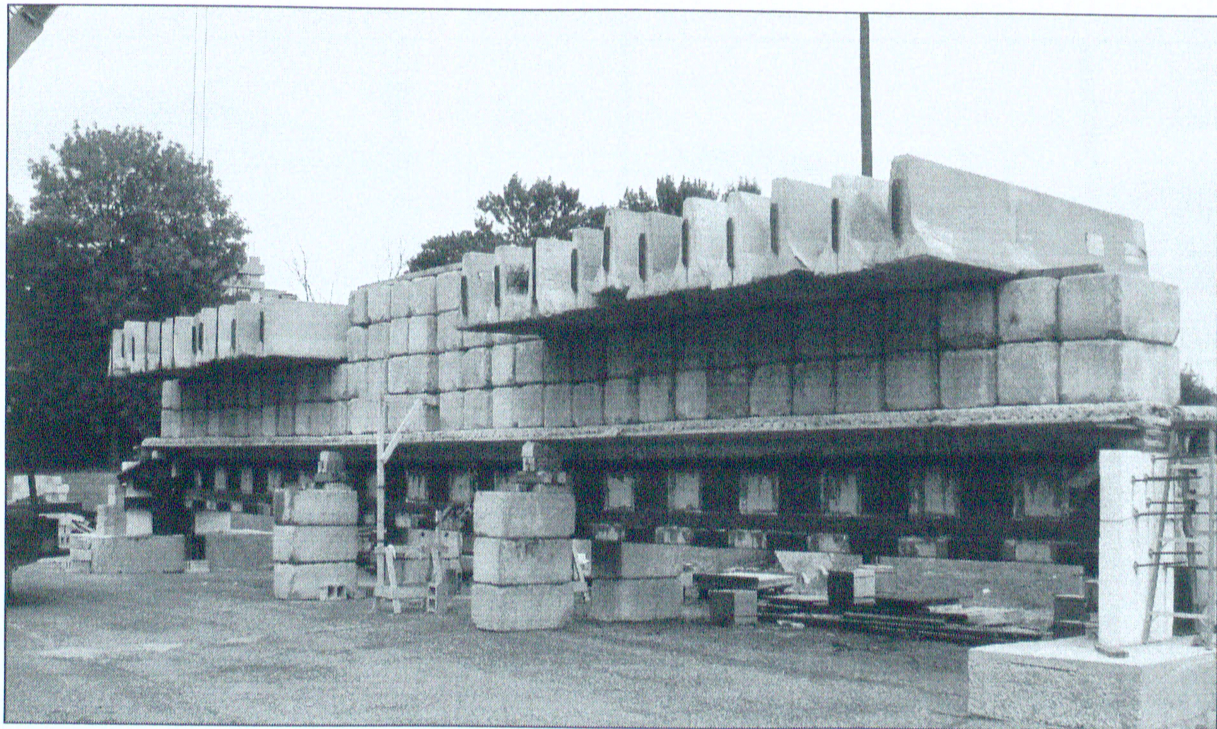


Figure 3.78 – Final loading

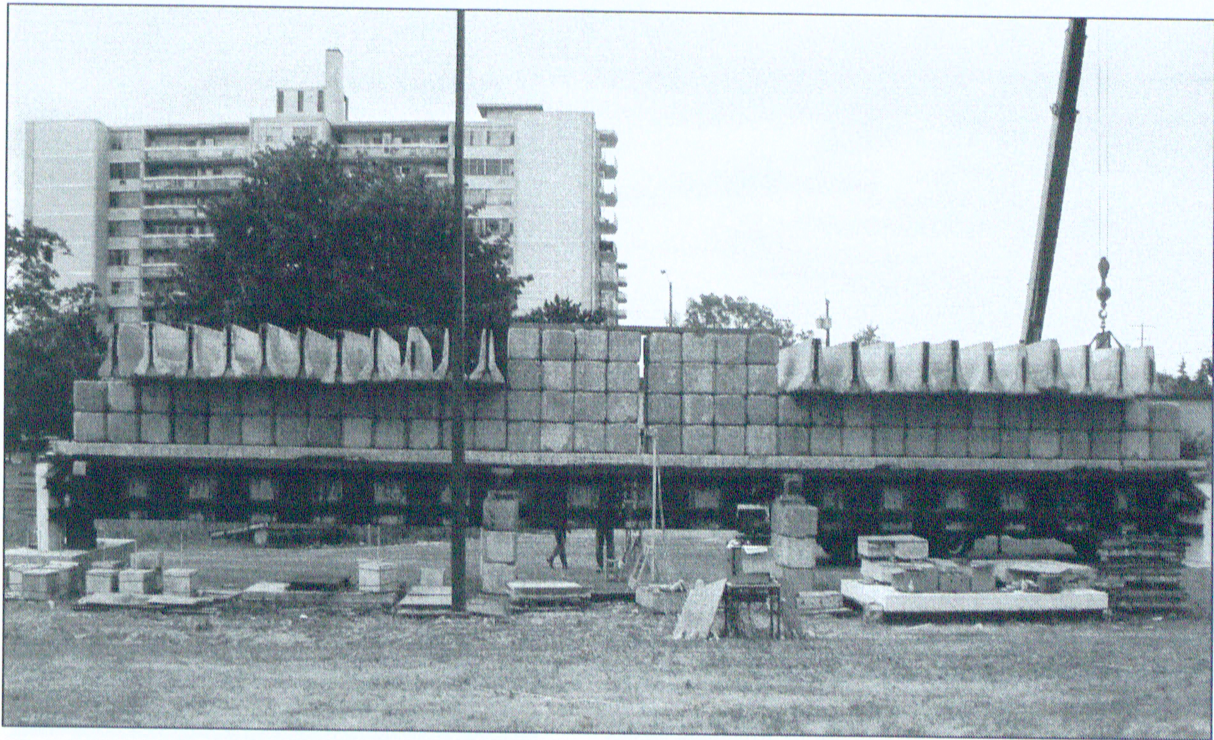


Figure 3.79 – Elevation view of final loading configuration



Figure 3.80 – Cracks at midspan portion on south (left) and north (right) faces

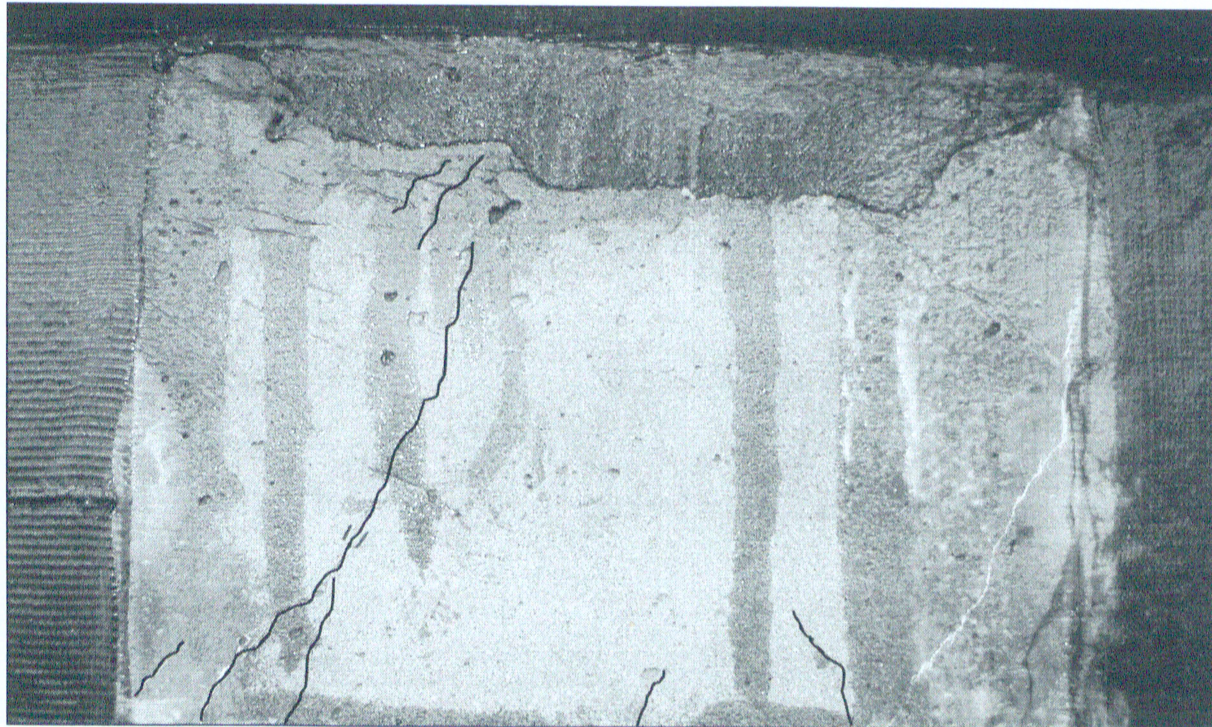


Figure 3.81 – Web section near midspan, south face

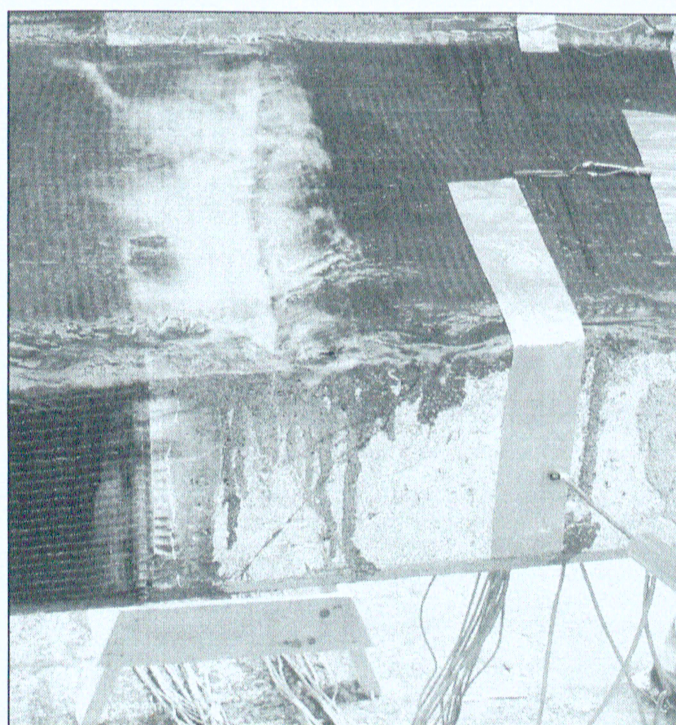


Figure 3.82 – Web section near midspan on south face (left), and bottom flange at midspan on north face

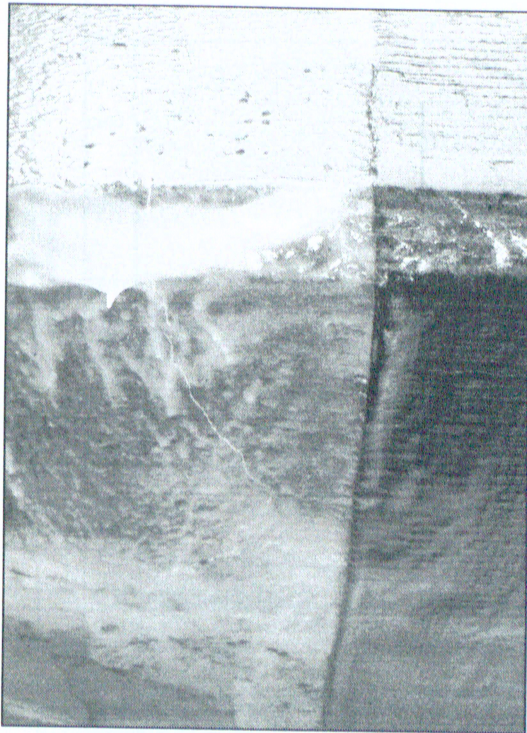


Figure 3.83 – Crack propagation through epoxy on south face

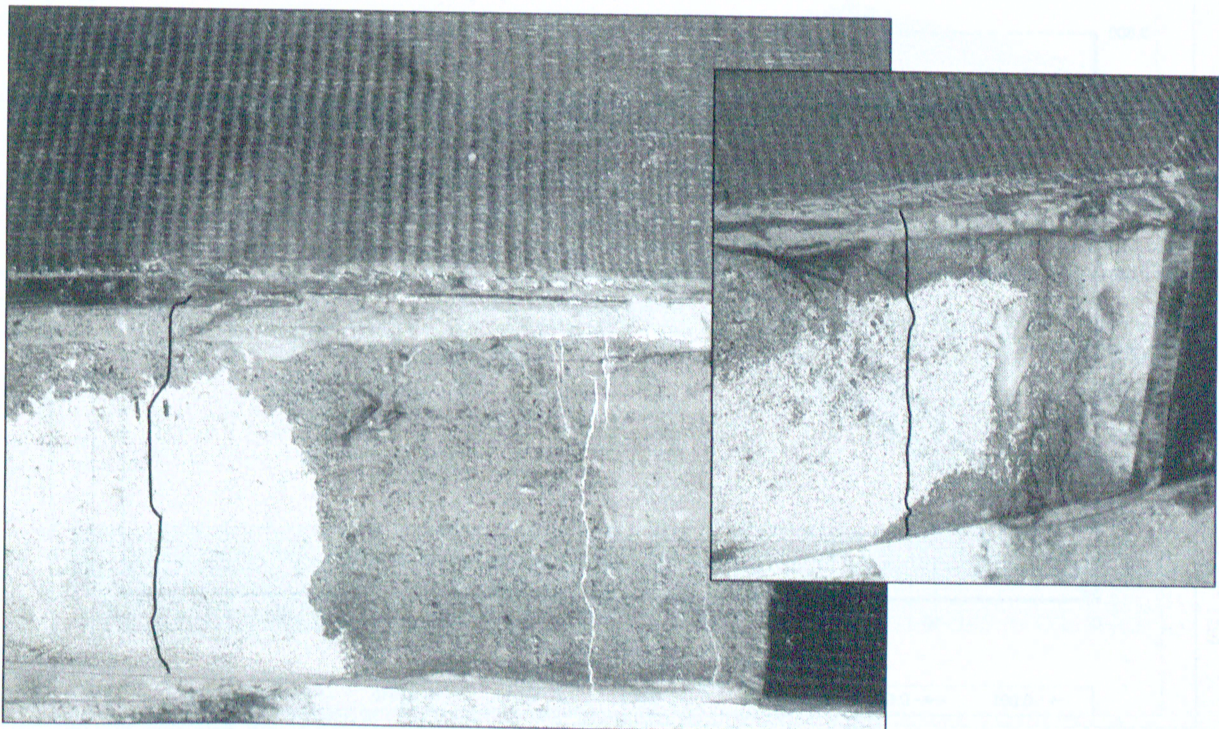


Figure 3.84 – South face cracks on bottom flange

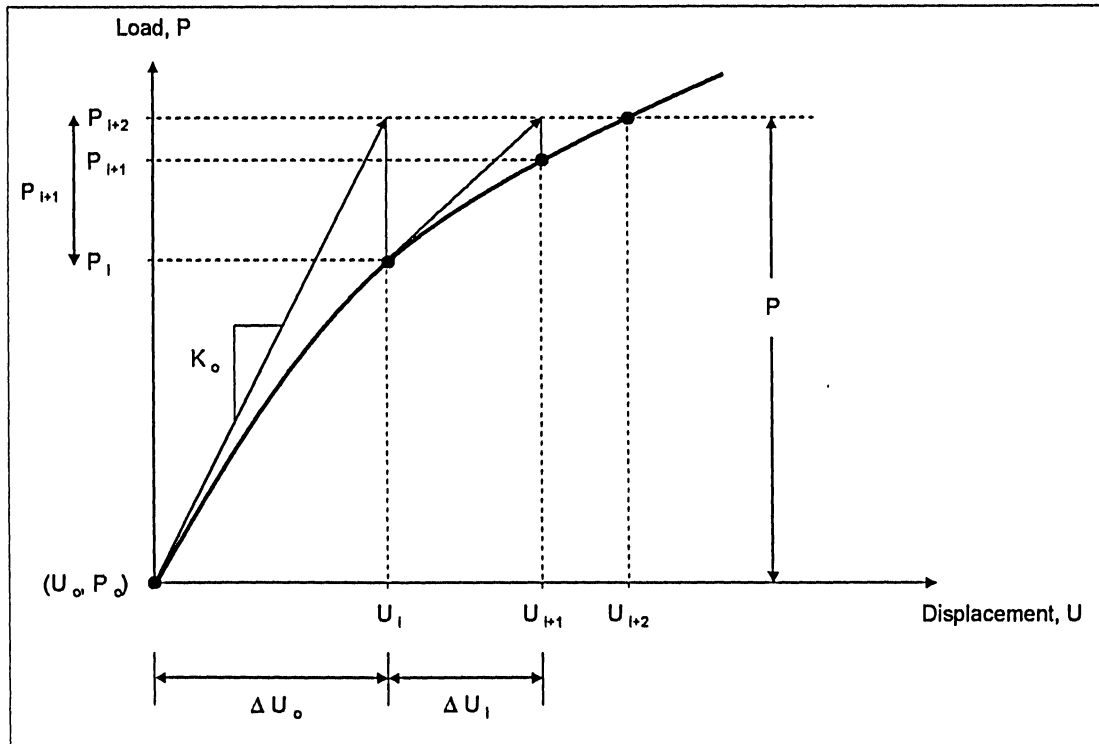


Figure 4.1 – Newton's method for tangent stiffness determination

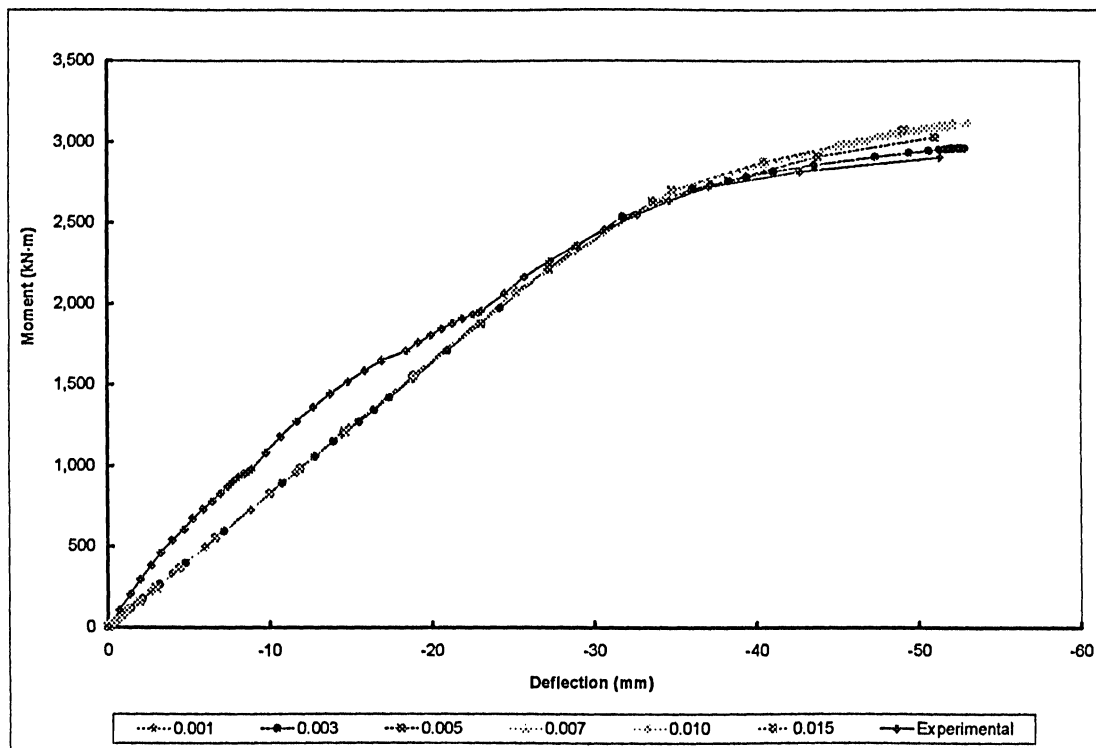


Figure 4.2 – Moment-deflection curves for the Type III girder for various tension stiffening values

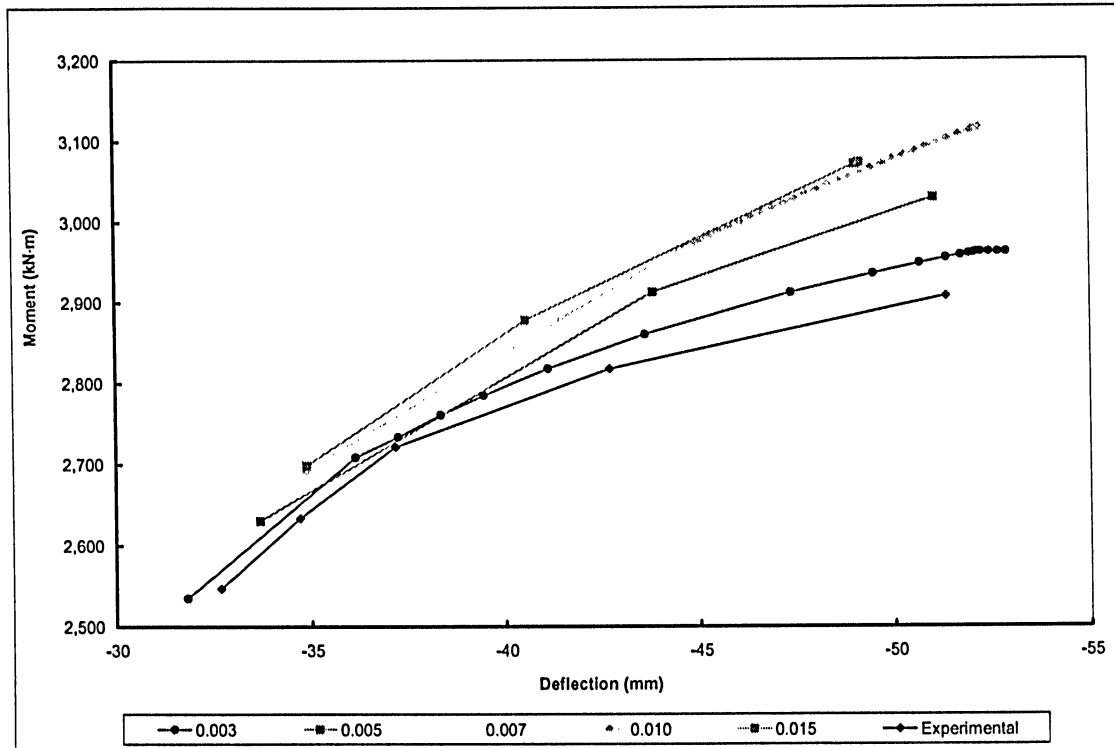


Figure 4.3 – Enlarged view of Figure 4.2 in the nonlinear range for clarity

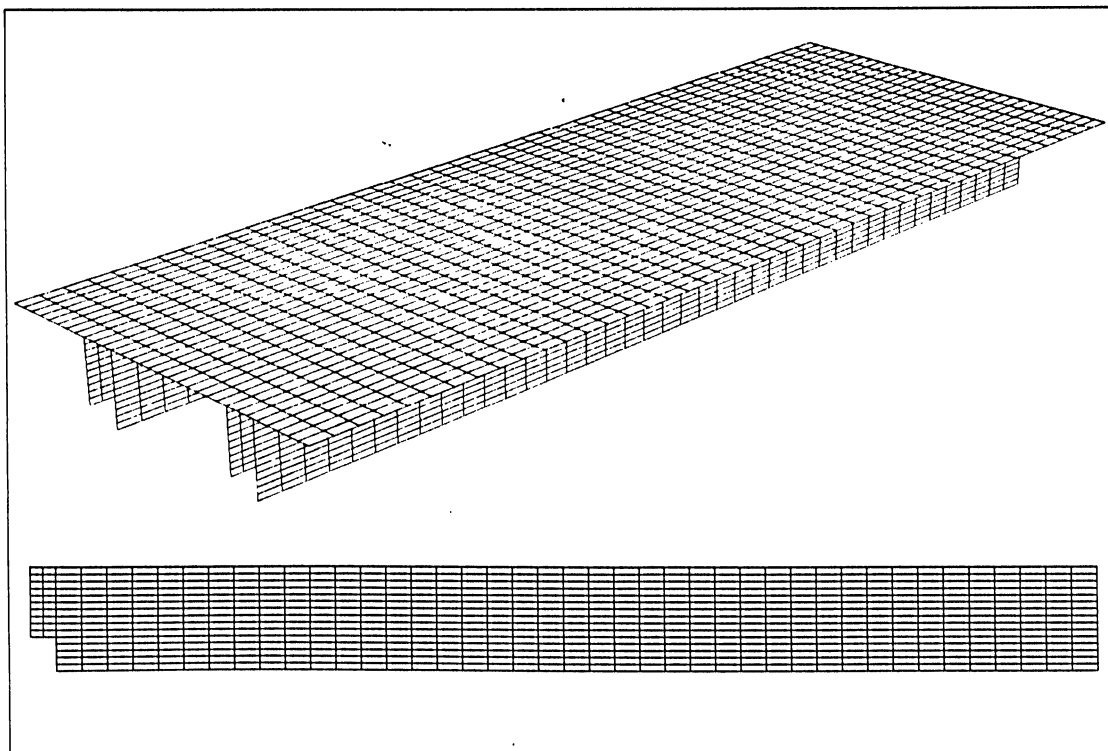


Figure 4.4 – Finite element mesh for the DT-41 girder; full view (top) and elevation (below)

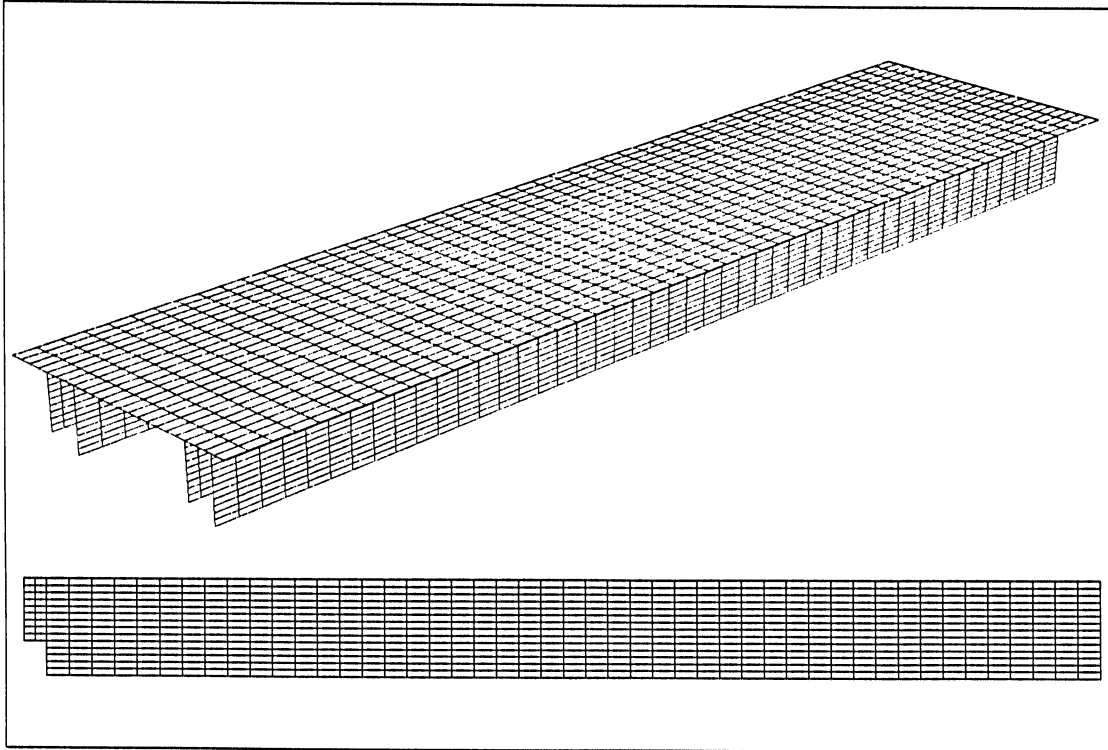


Figure 4.5 – Finite element mesh for the DT-100 girder; full view (top) and elevation (below)

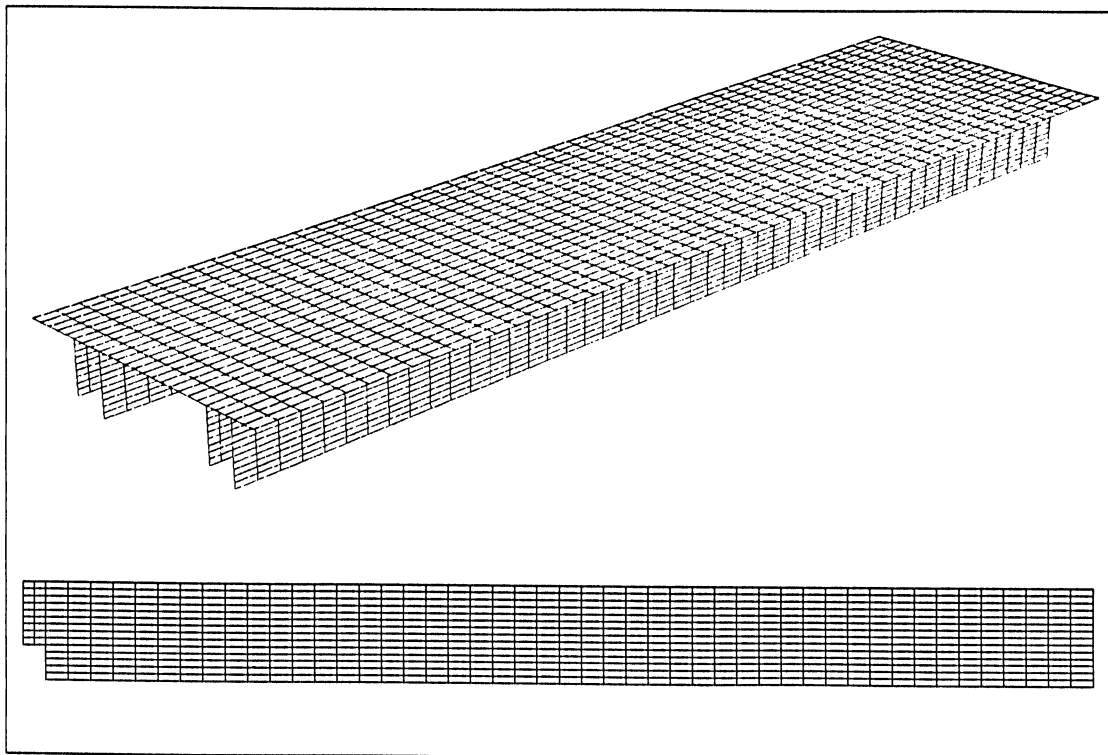


Figure 4.6 – Finite element mesh for the DT-102A girder; full view (top) and elevation (below)

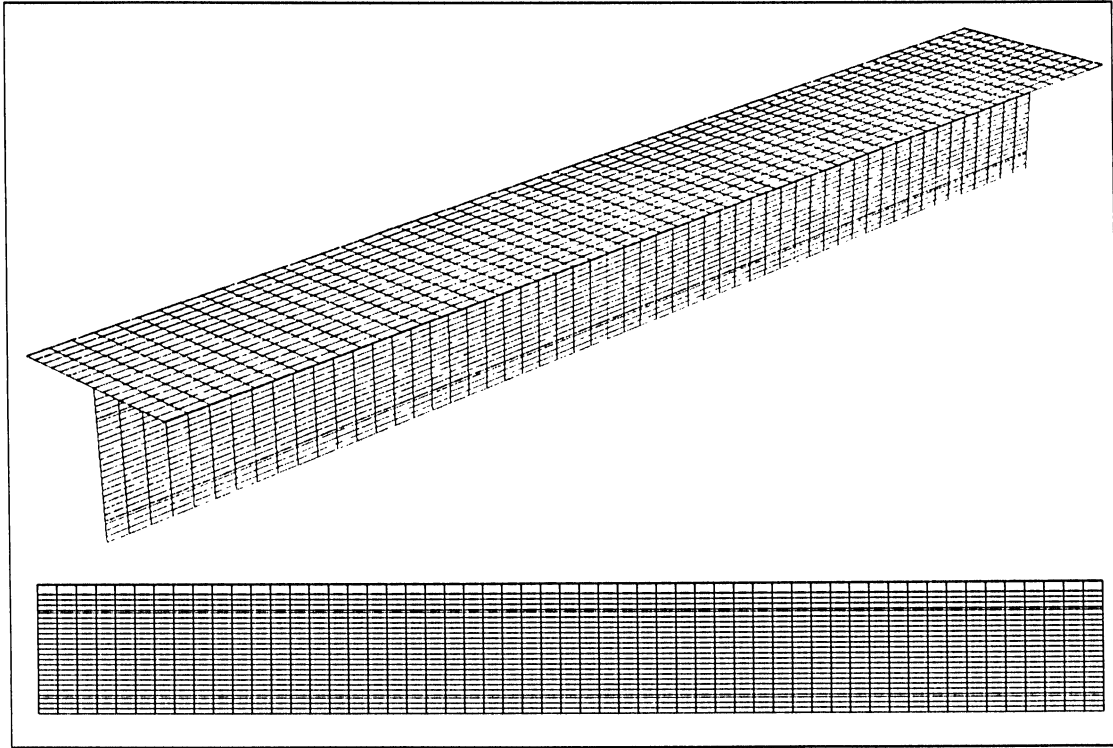


Figure 4.7 – Finite element mesh for the Type III girder; full view (top) and elevation (below)

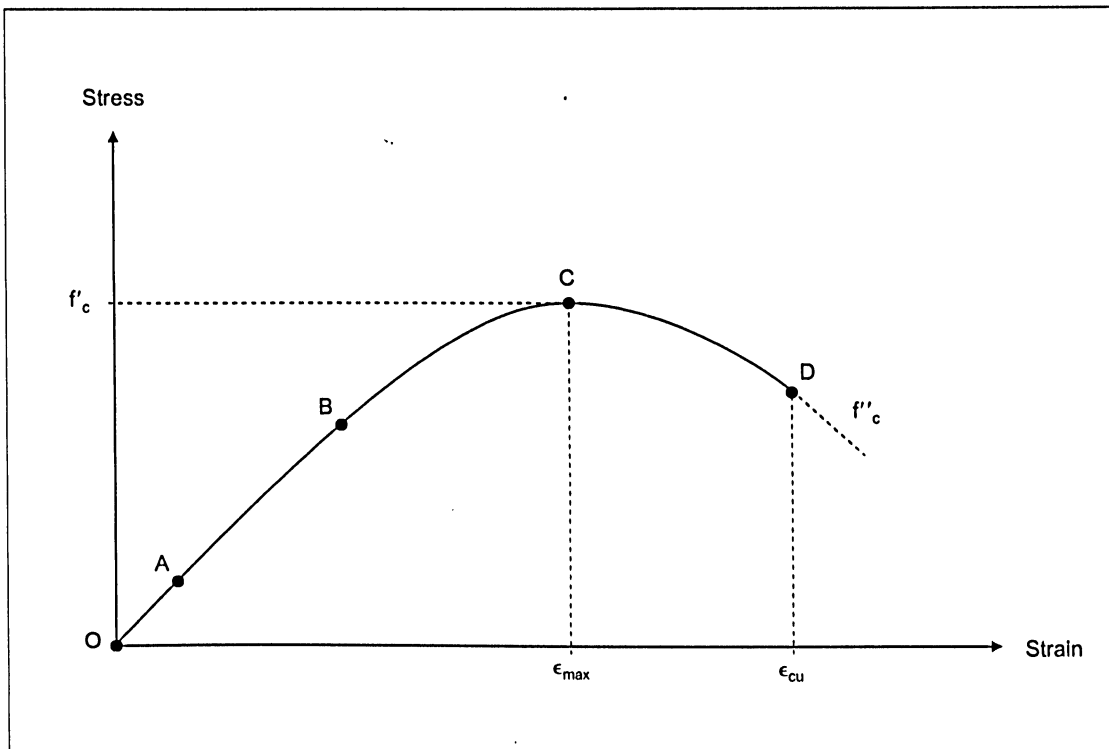


Figure 4.8 – Typical stress vs. strain curve for concrete

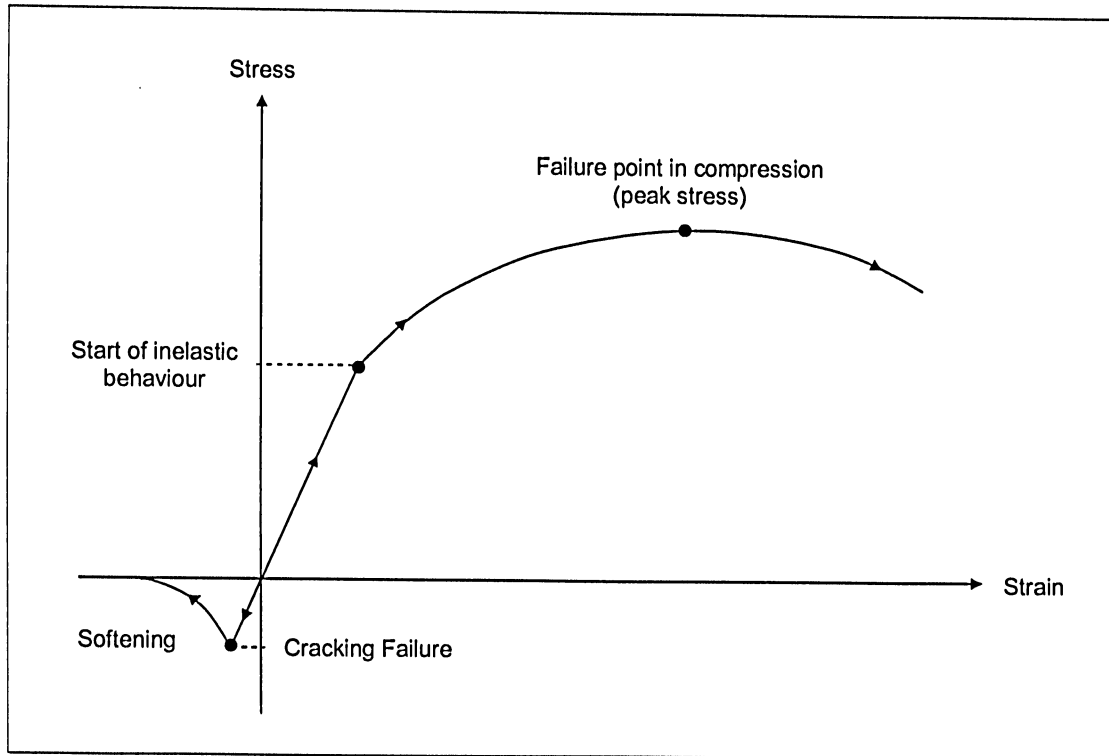


Figure 4.9 – Stress-strain relationship for plain concrete

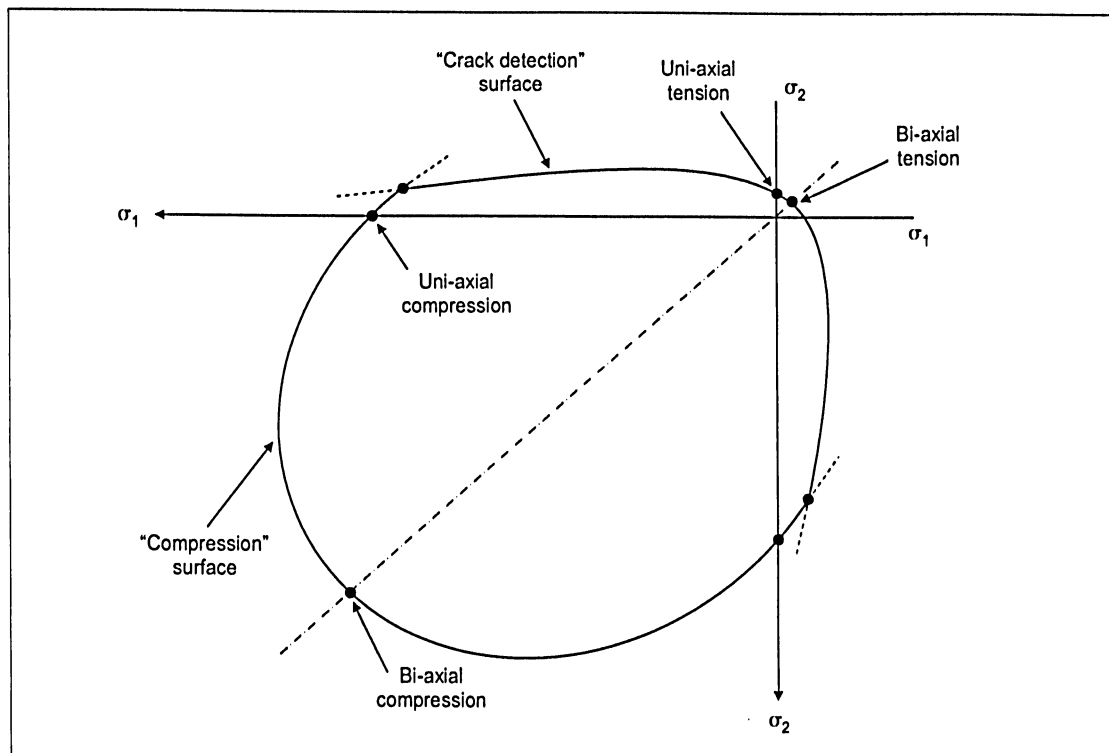


Figure 4.10 – Plane stress failure surfaces for concrete

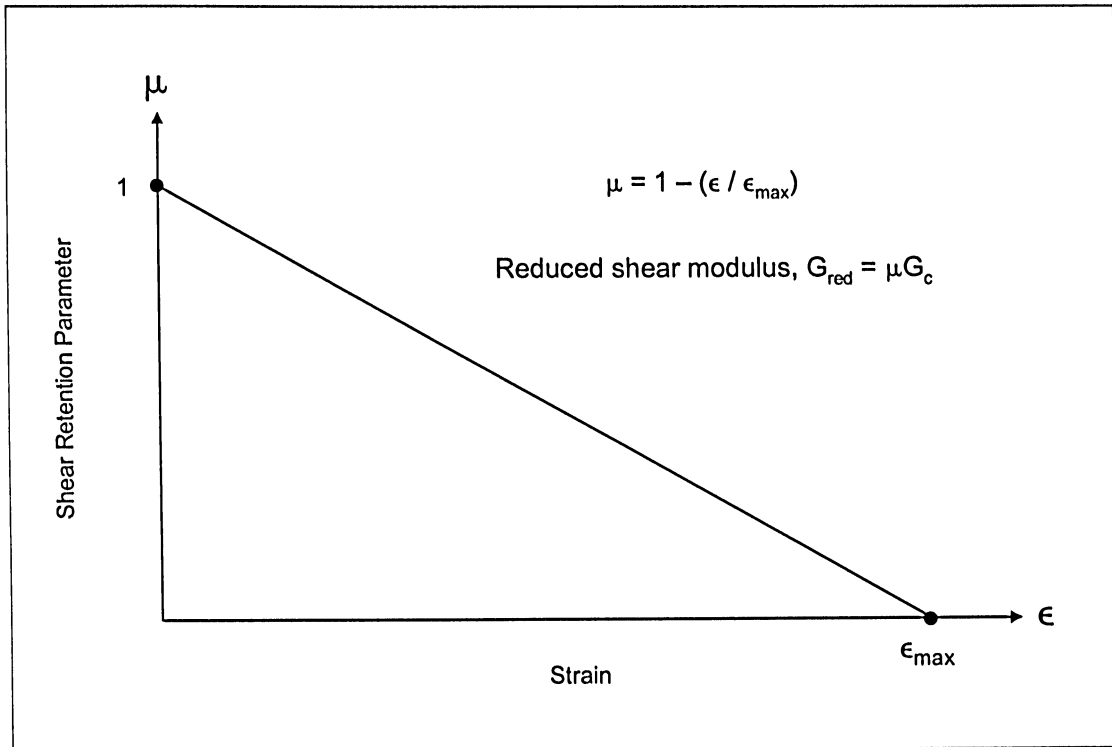


Figure 4.11 – Shear retention model for reinforced concrete

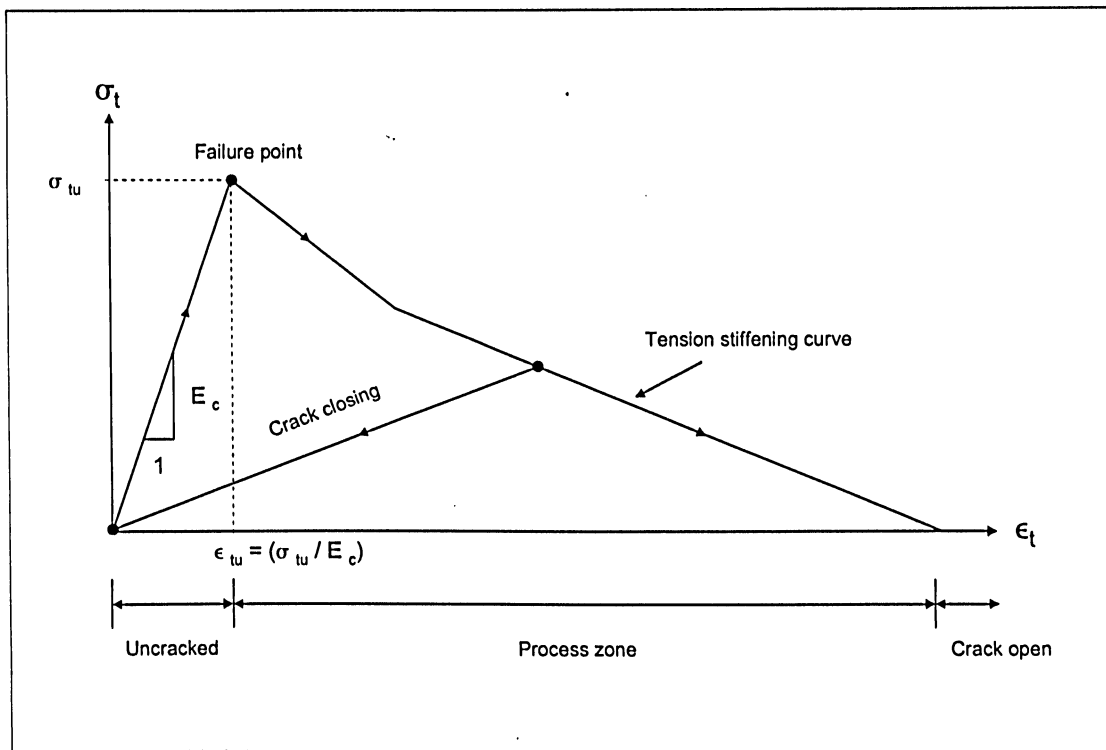


Figure 4.12 – Tension stiffening model; reinforced concrete

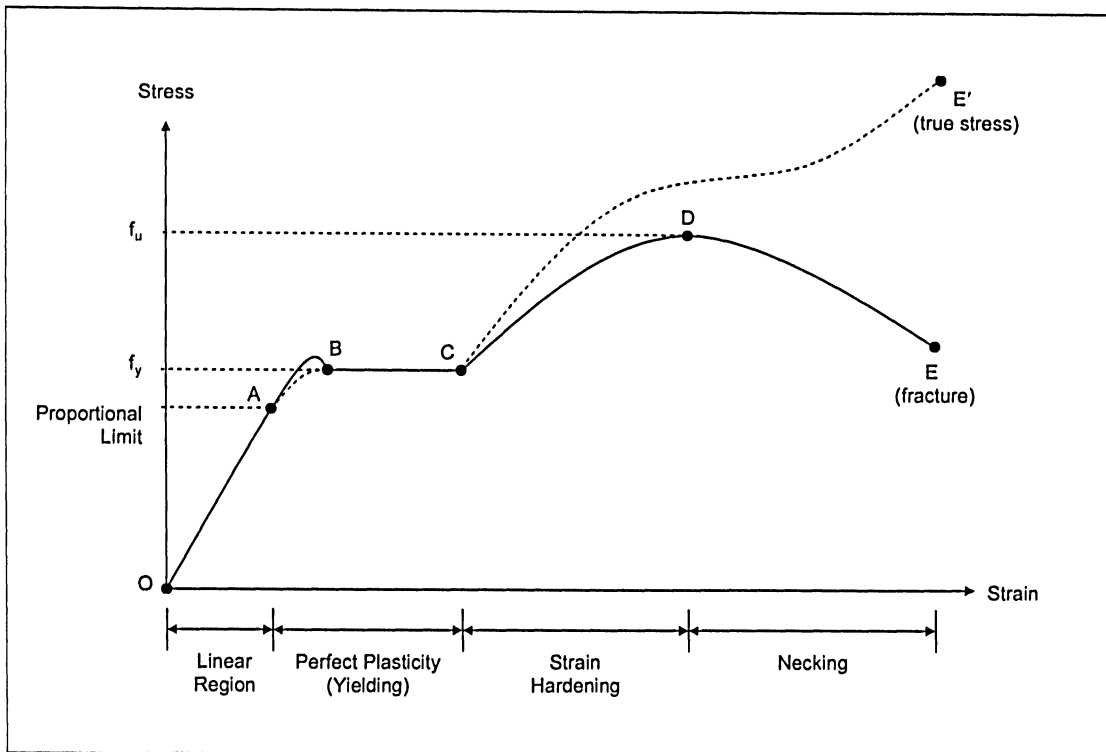


Figure 4.13 – Typical stress vs. strain curve for steel

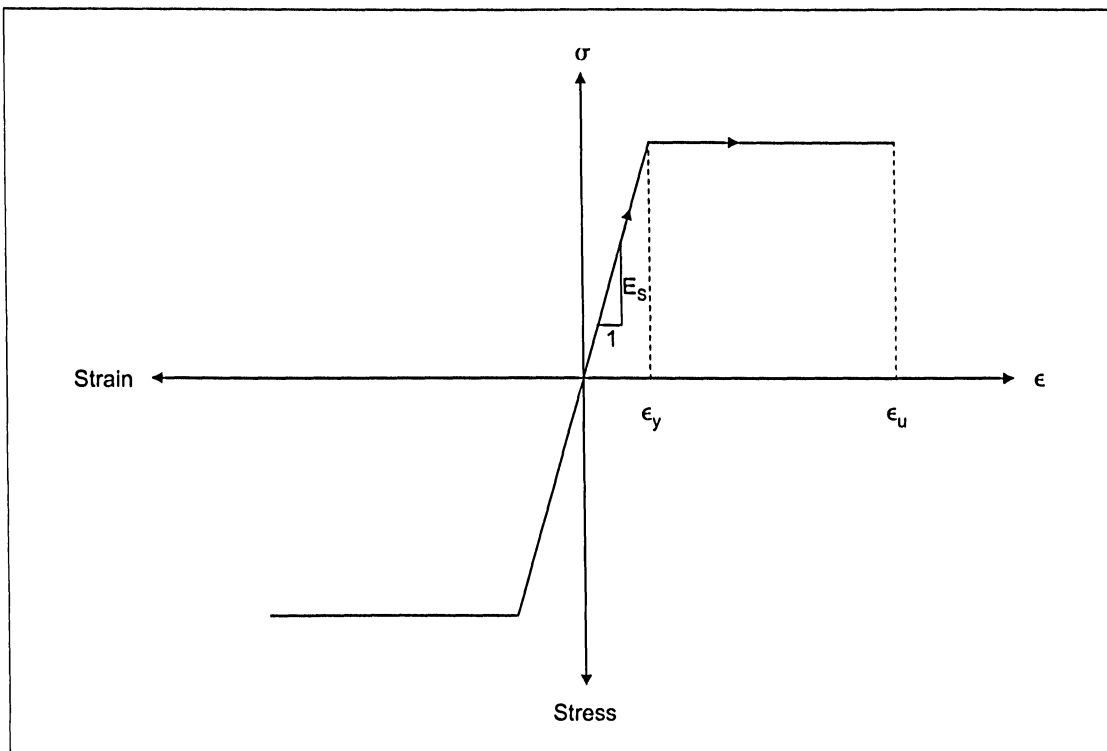


Figure 4.14 – Idealized stress-strain relation for steel

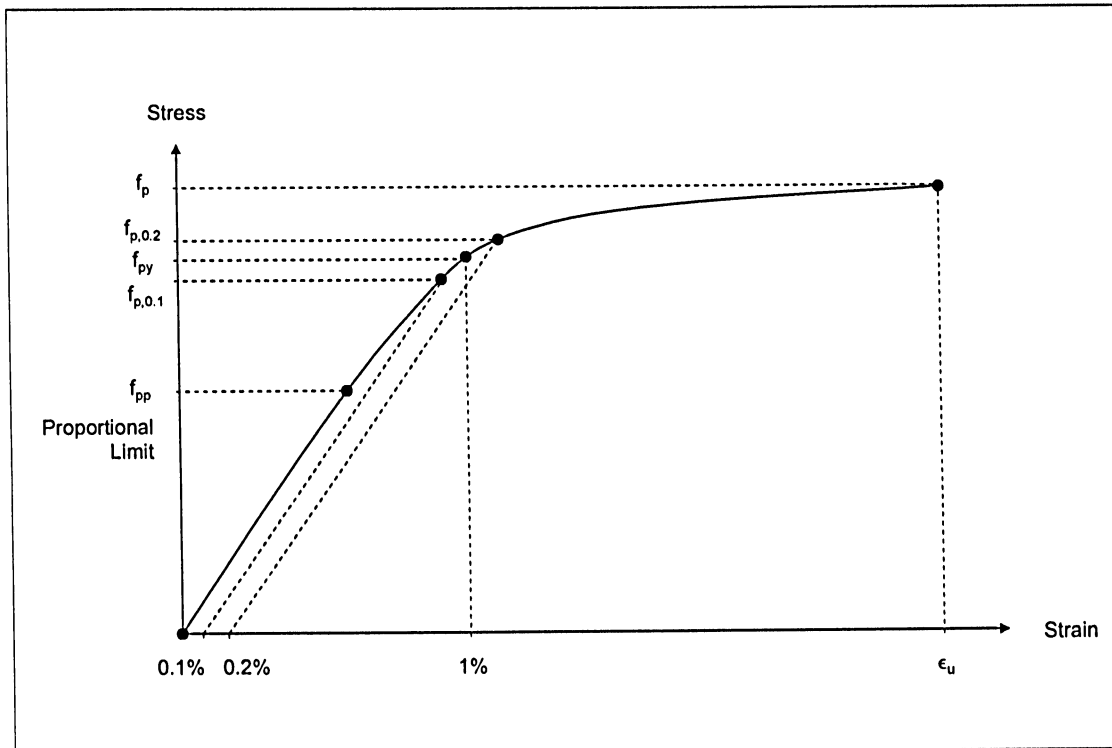


Figure 4.15 – Typical stress vs. strain curve for prestressing steel

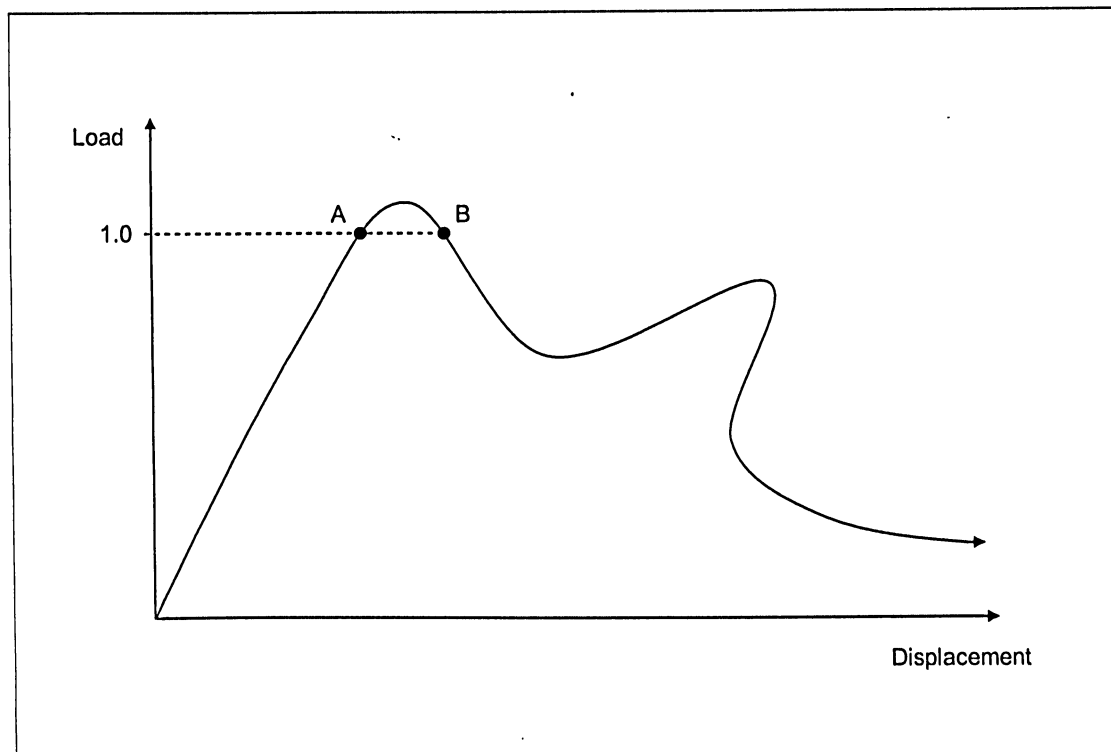


Figure 4.16 – Riks method application

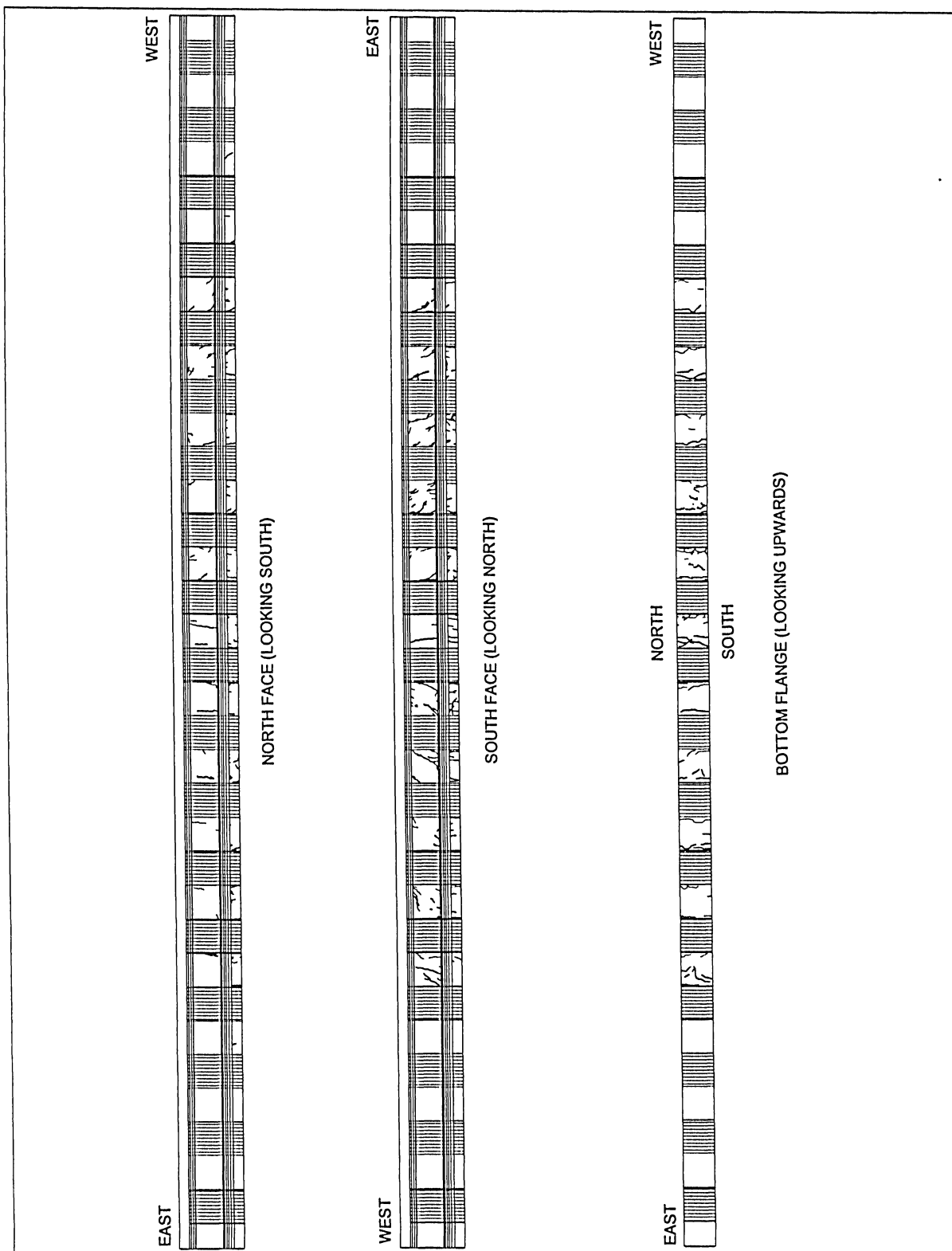


Figure 5.1 – Crack mapping due to final test loading

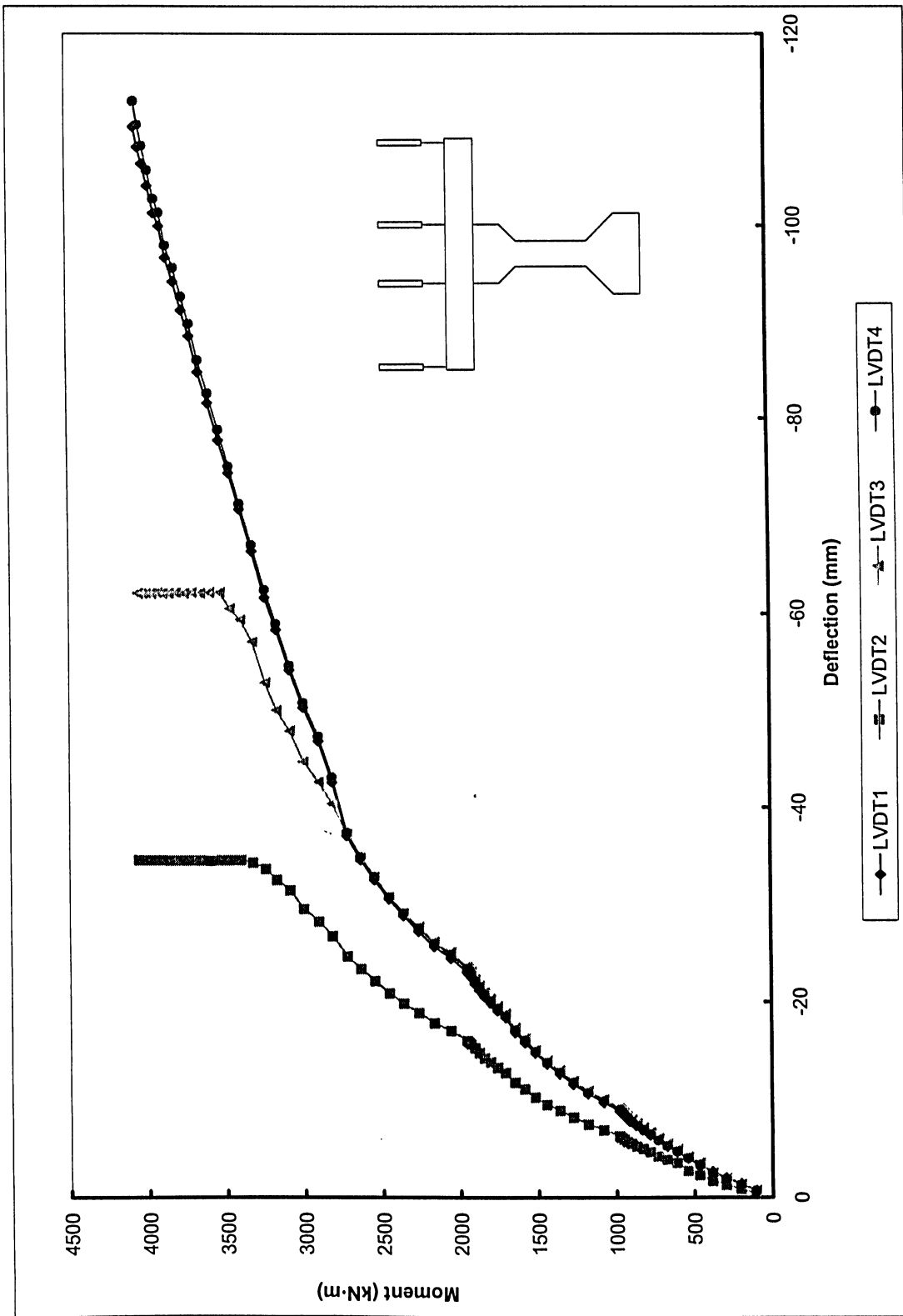


Figure 5.2 – Moment vs. vertical deflection for Type III girder (LVDT1 and 4 at the exterior; LVDT2 and 3 are central)

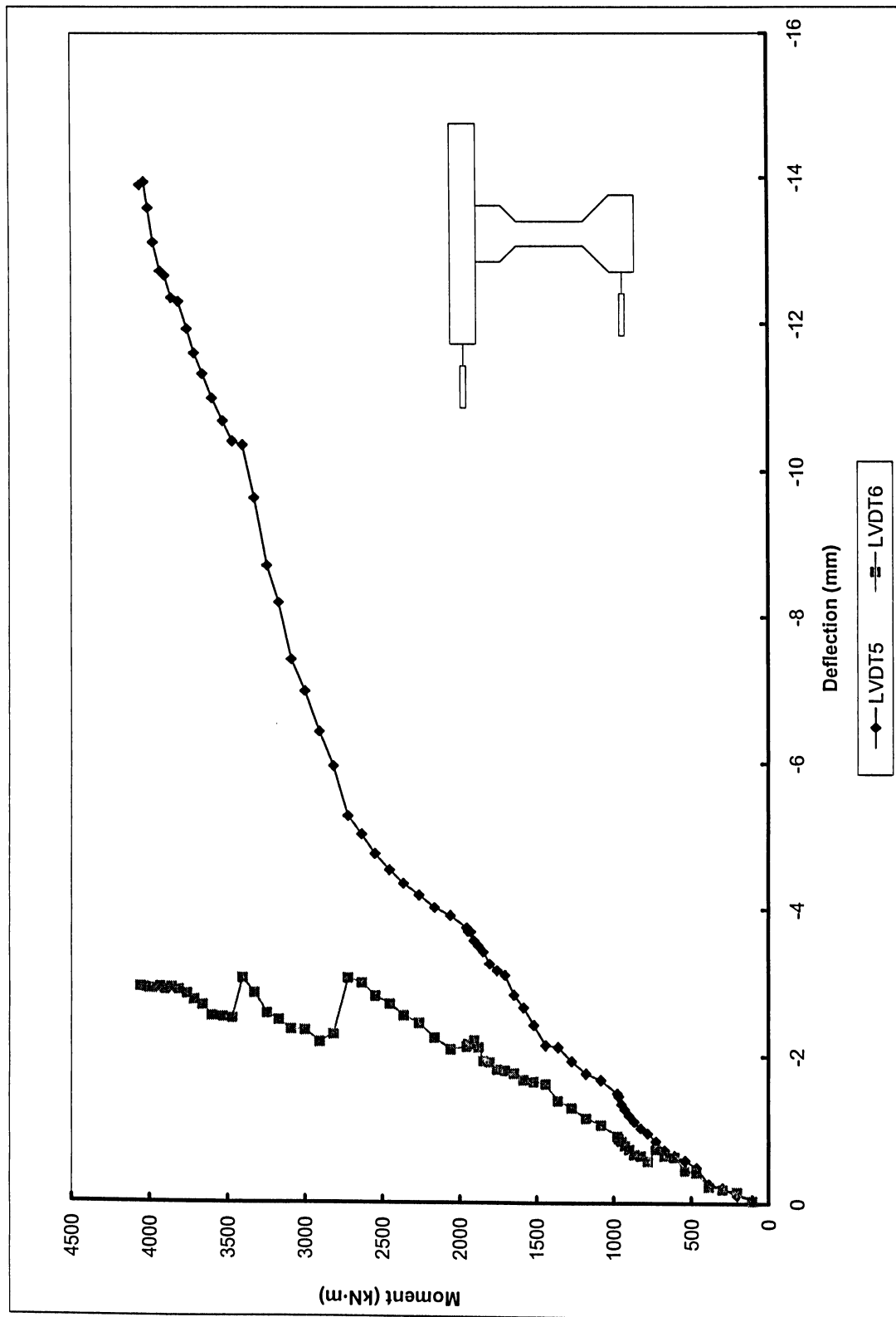


Figure 5.3 – Moment vs. lateral deflection for Type III girder (LVDT5 at the top slab; LVDT6 at the bottom flange)

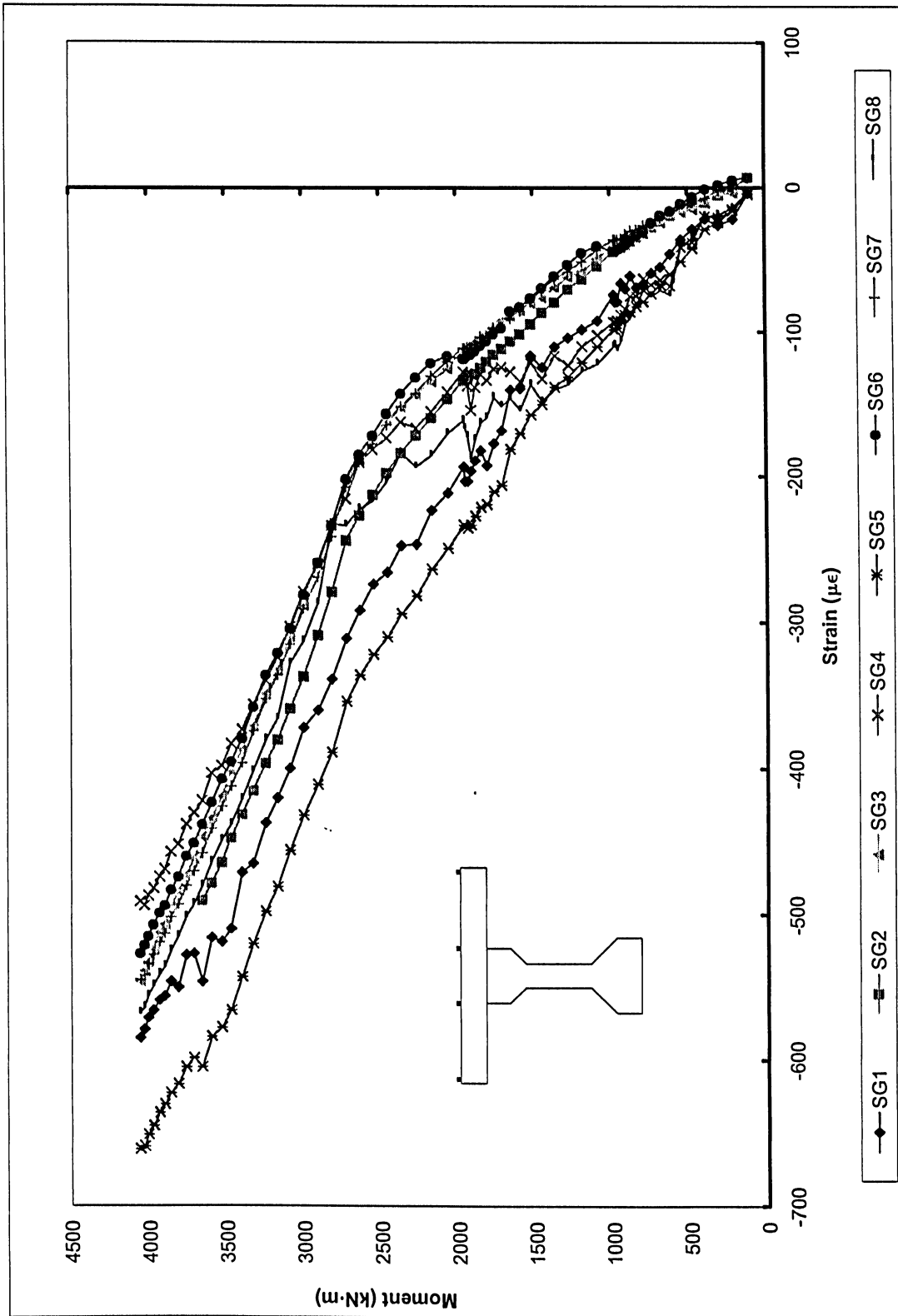


Figure 5.4 – Moment vs. slab strain for Type III girder (SG1 to SG4 600 mm from midspan; SG5 to SG8 at midspan)

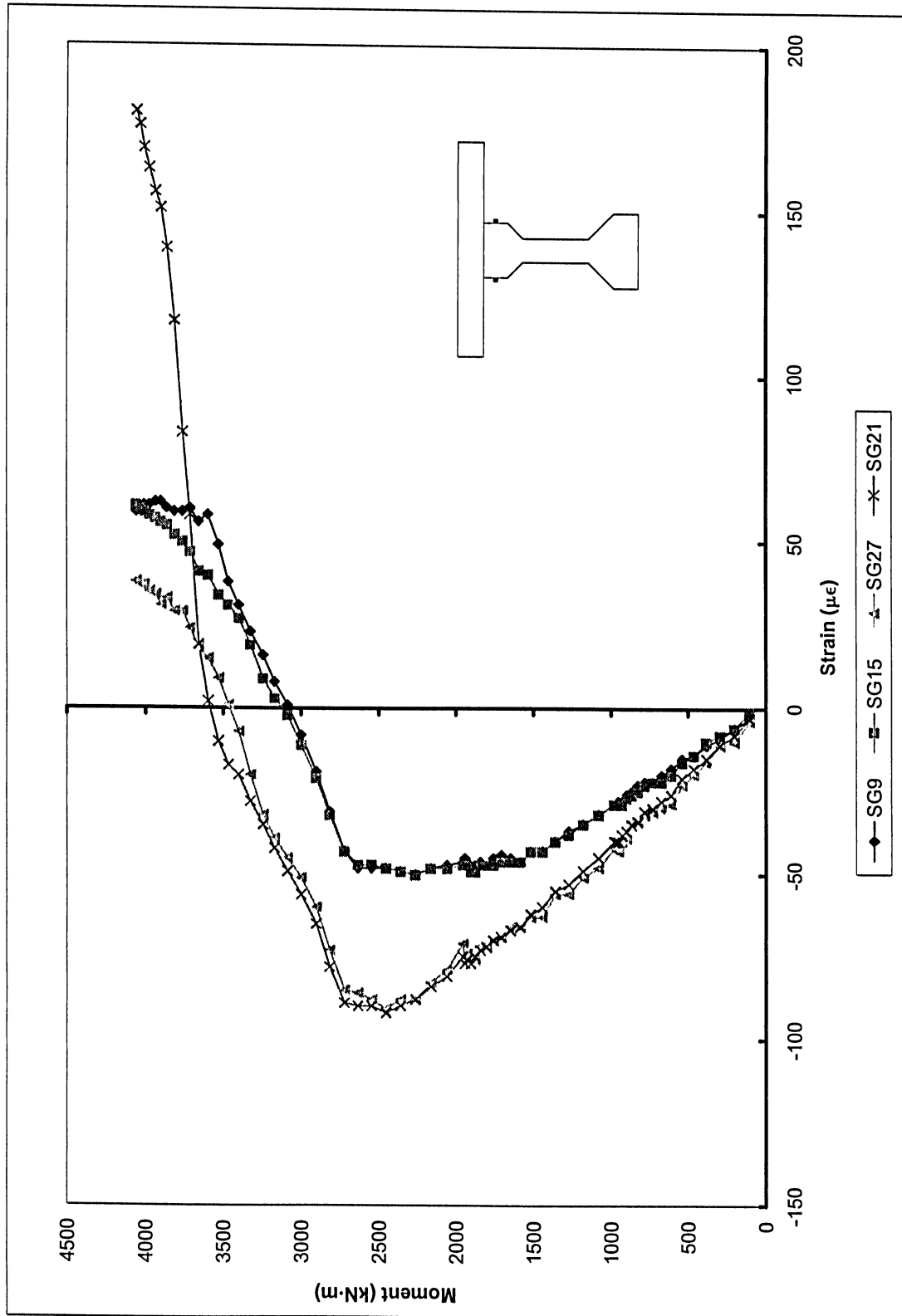


Figure 5.5 – Moment vs. top flange strain for Type III girder (SG9 & SG21 600 mm from midspan; SG15 & SG27 at midspan)

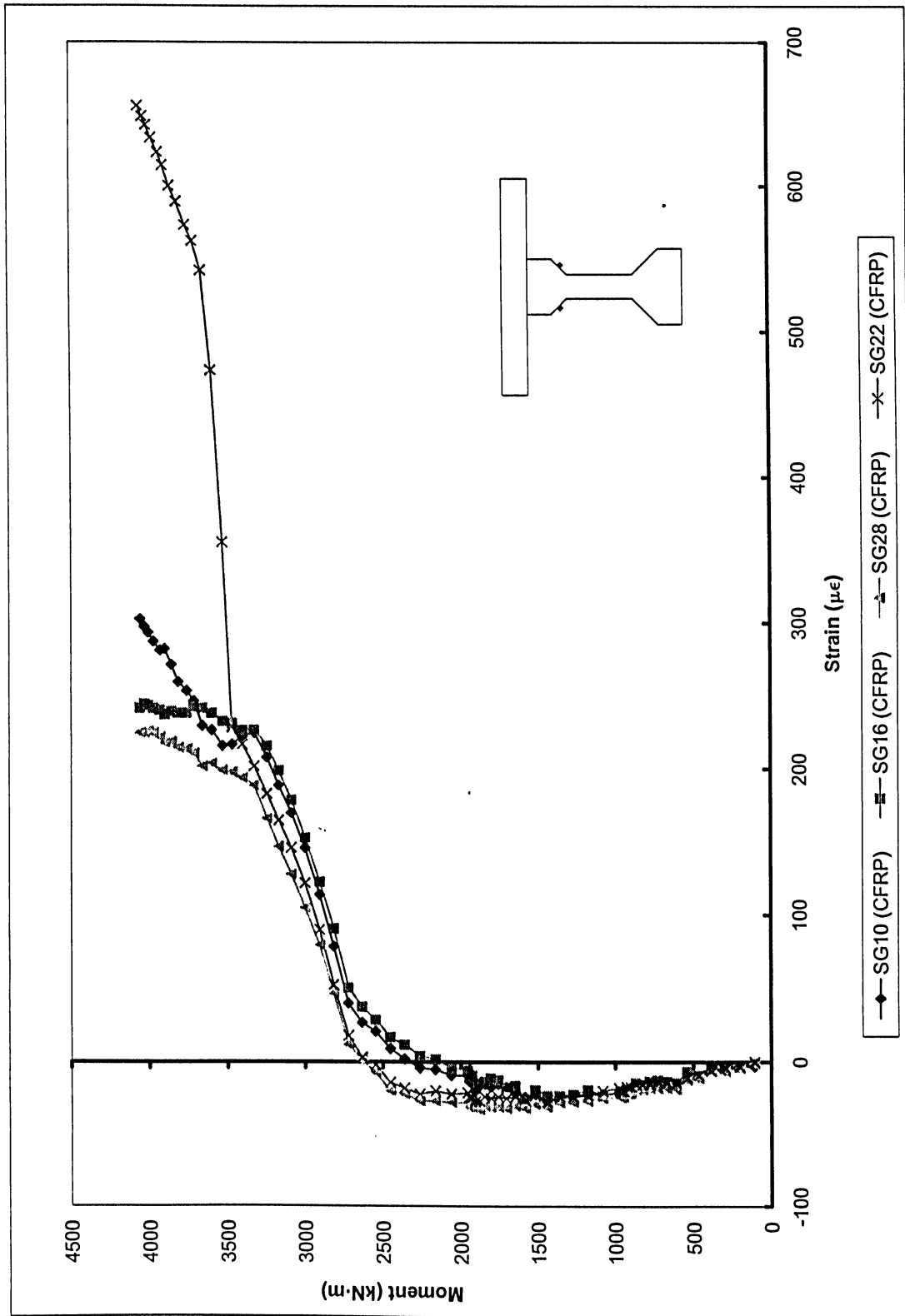


Figure 5.6 – Moment vs. top chamfer strain for Type III girder (SG10 & SG22 600 mm from midspan; SG16 & SG28 at midspan)

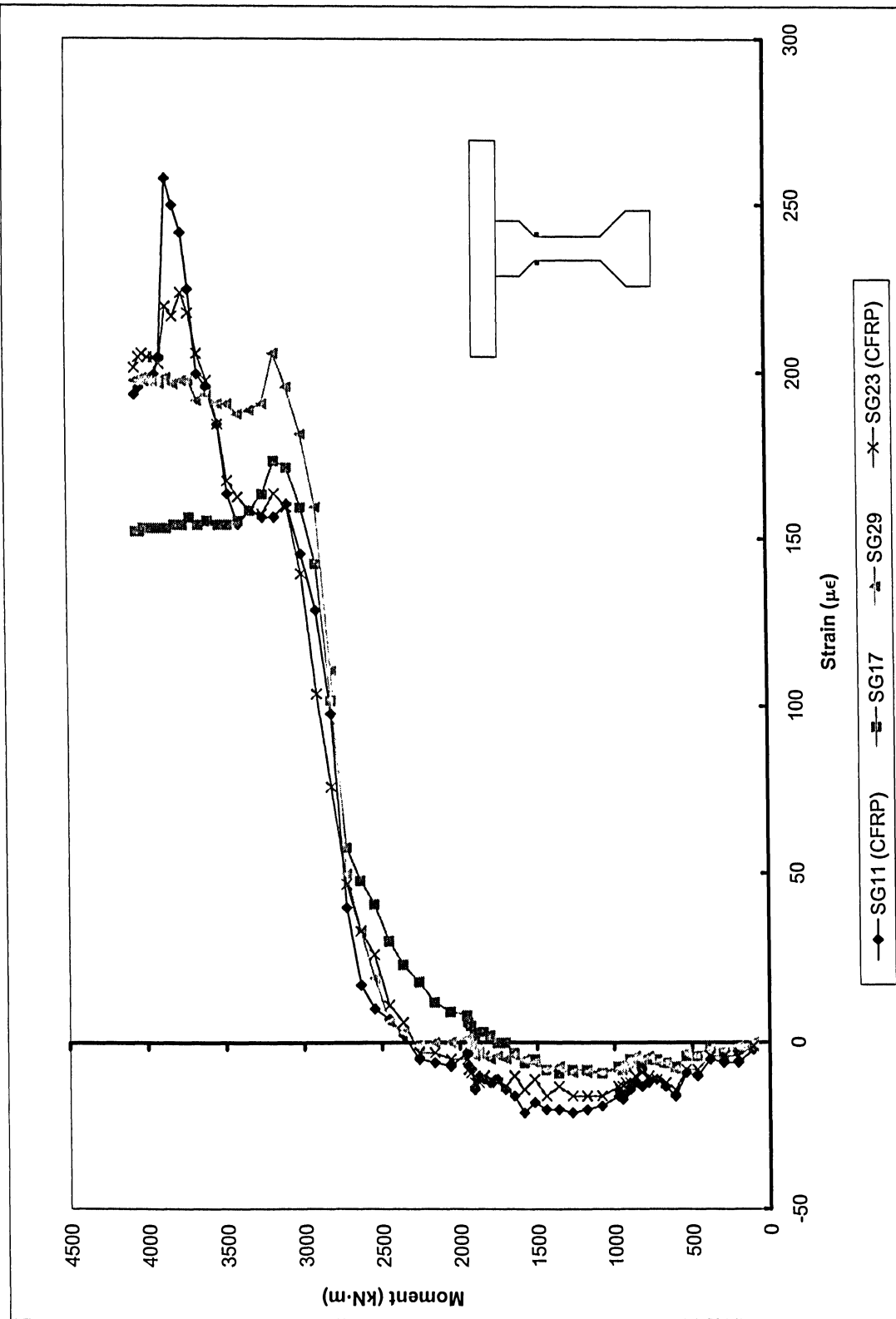


Figure 5.7 – Moment vs. top web strain for Type III girder (SG11 & SG23 600 mm from midspan; SG17 & SG29 at midspan)

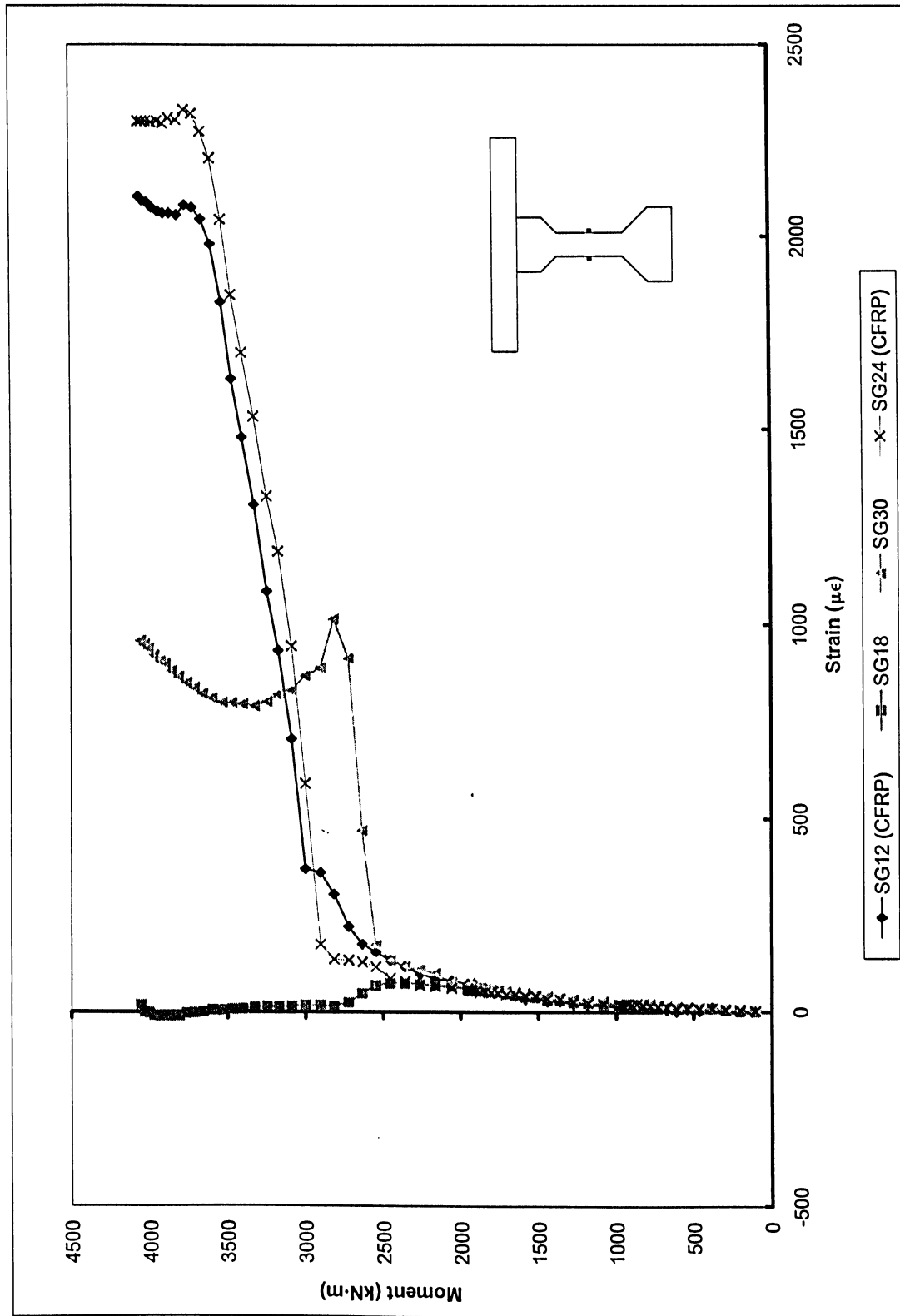


Figure 5.8 – Moment vs. mid web strain for Type III girder (SG12 & SG24 600 mm from midspan; SG18 & SG30 at midspan)

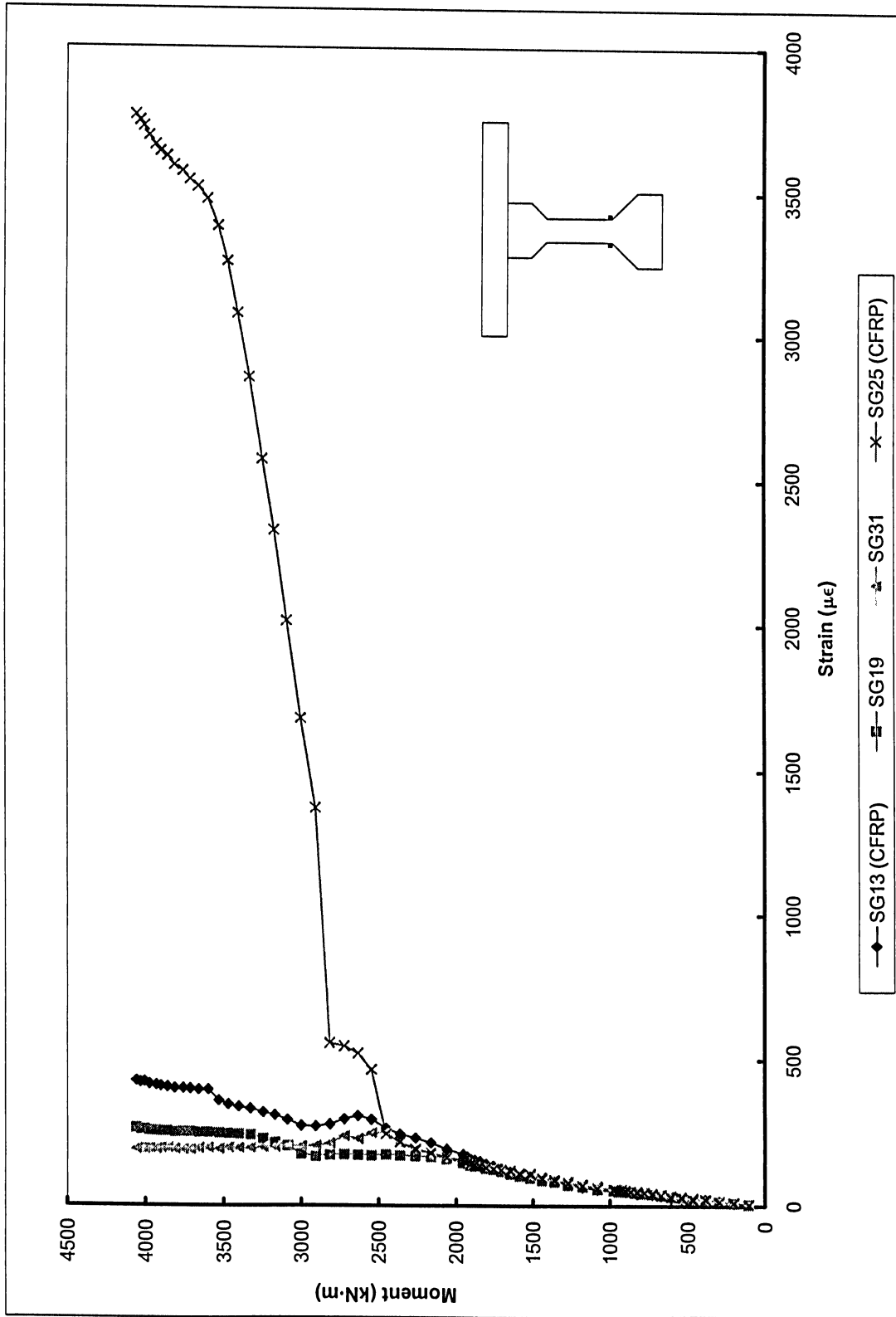


Figure 5.9 – Moment vs. bottom web strain for Type III girder (SG13 & SG25 600 mm from midspan; SG19 & SG31 at midspan)

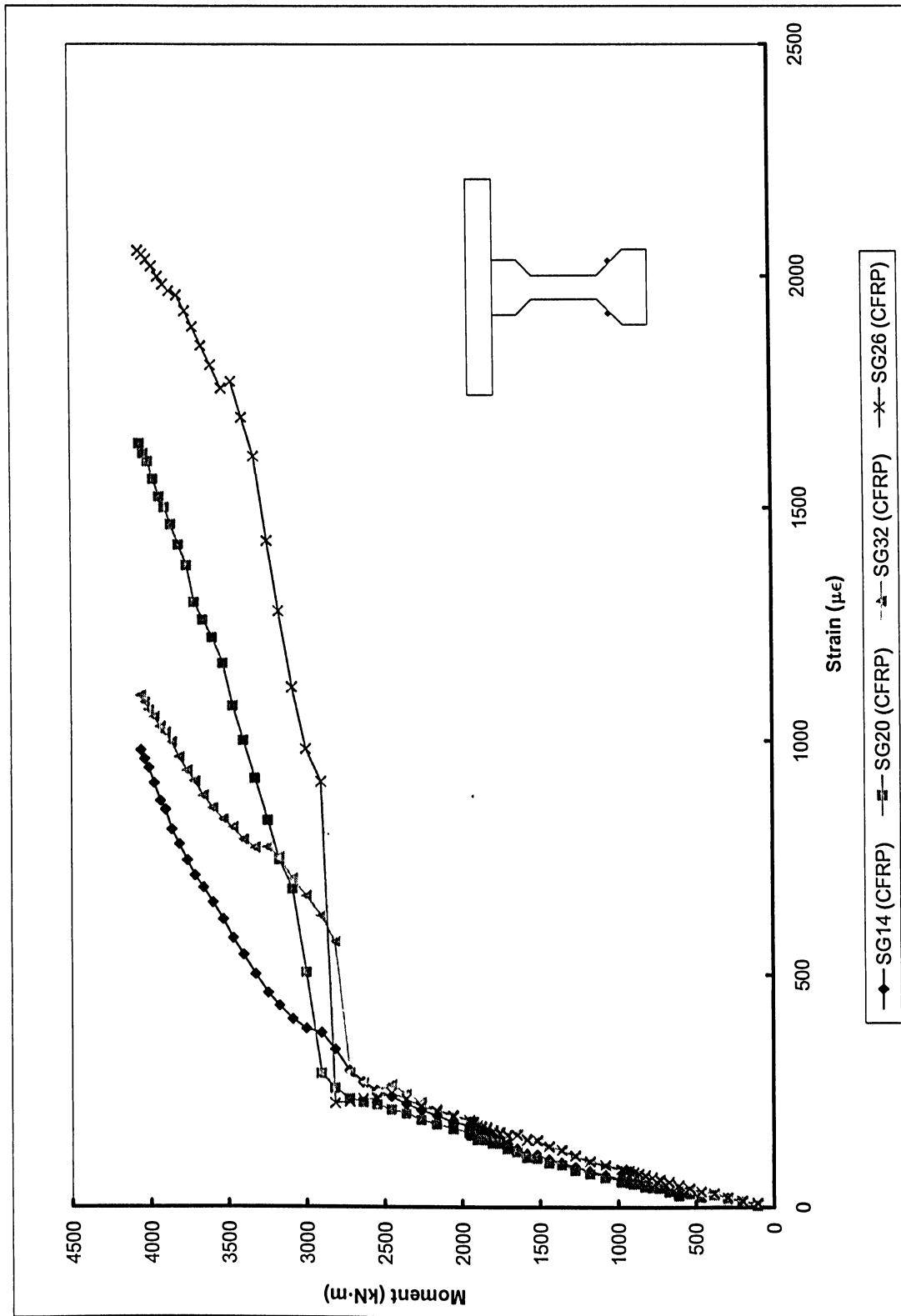


Figure 5.10 – Moment vs. bottom chamfer strain for Type III girder (SG14 & SG26 600 mm from midspan; SG20 & SG32 at midspan)

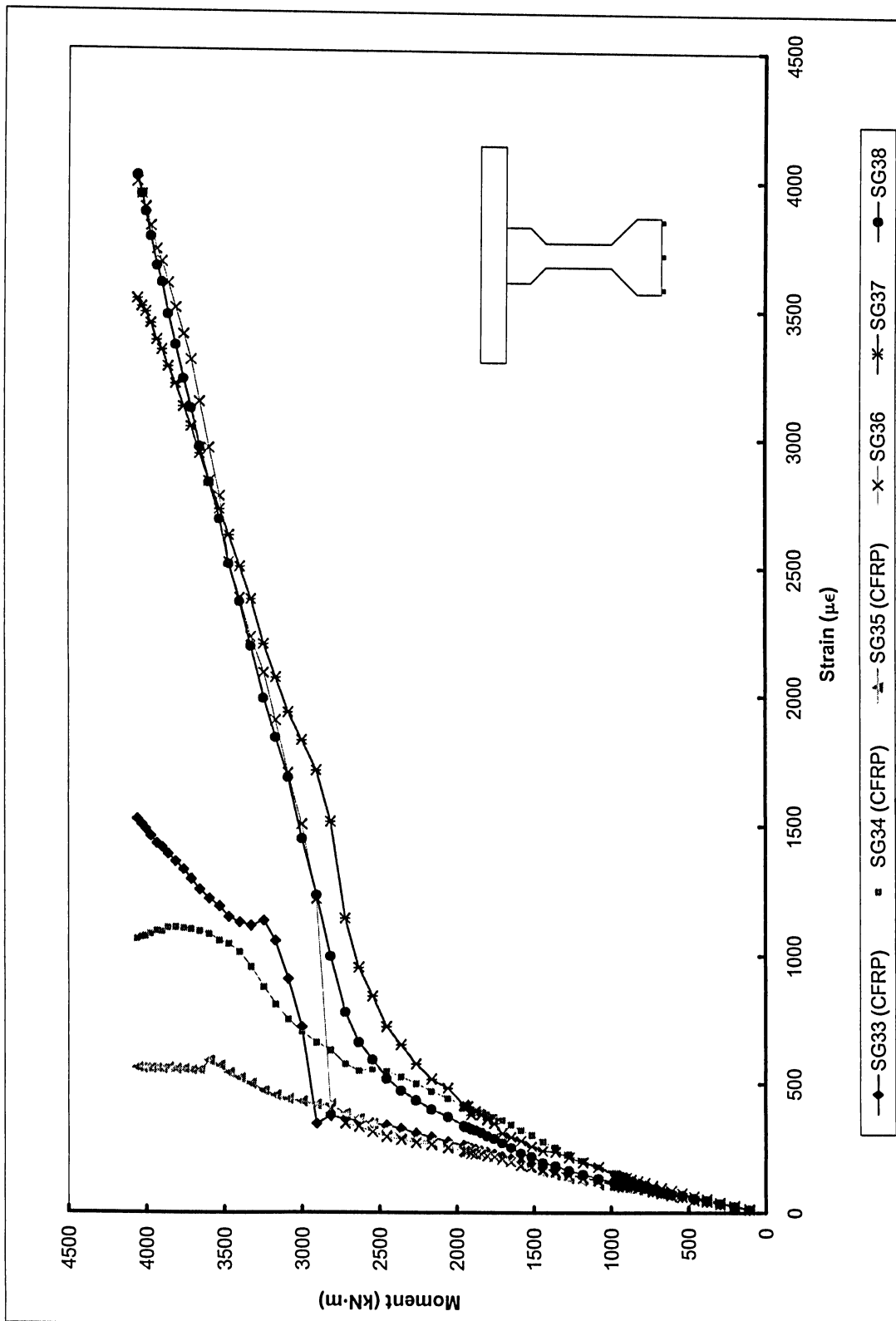


Figure 5.11 – Moment vs. bottom flange underside strain for Type III girder (SG33 to 35, 600 mm from midspan; SG36 to 38 at midspan)

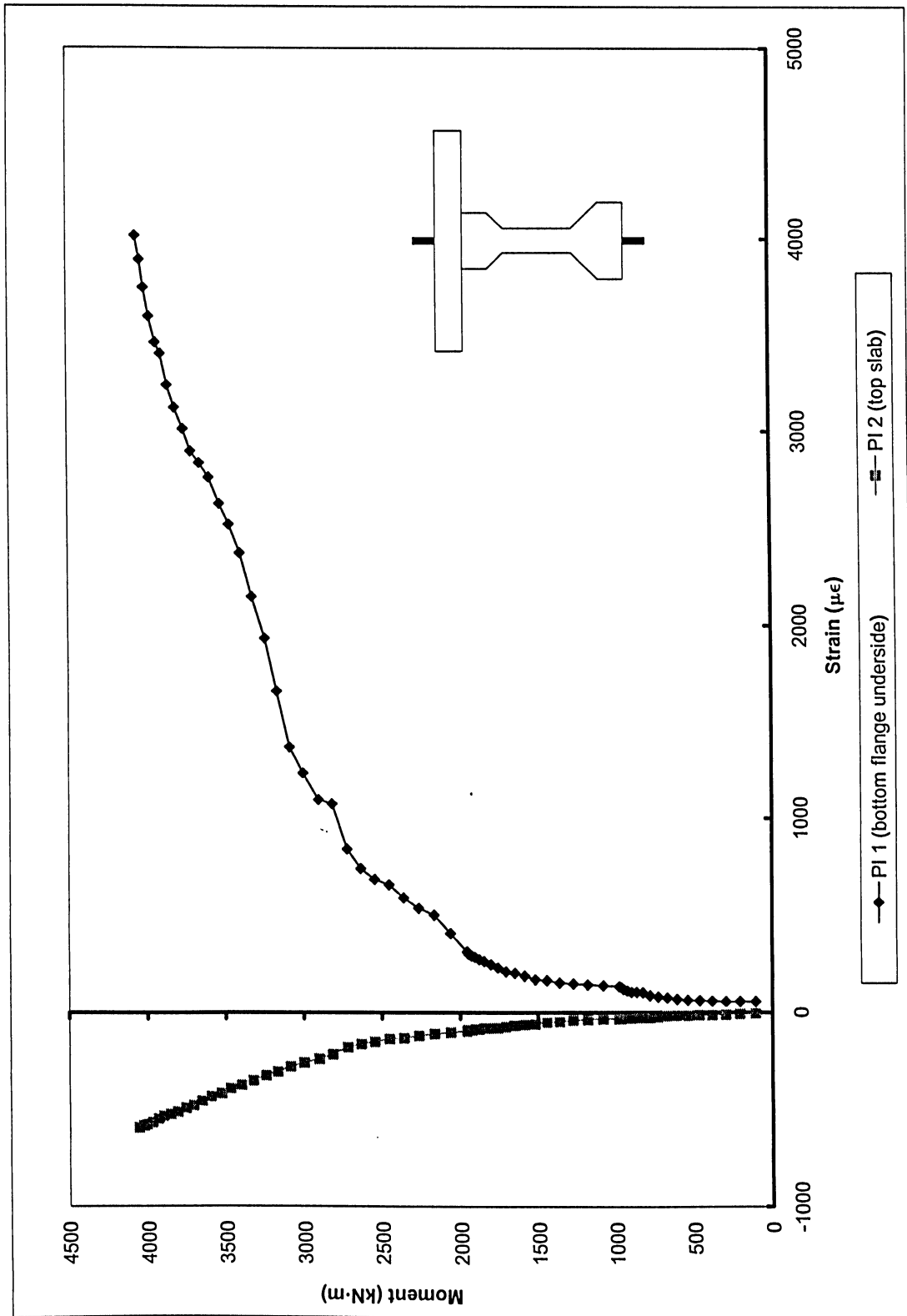


Figure 5.12 – Moment vs. PI gage strain for Type III girder (PI 1 on the bottom flange underside; PI 2 on the top slab)

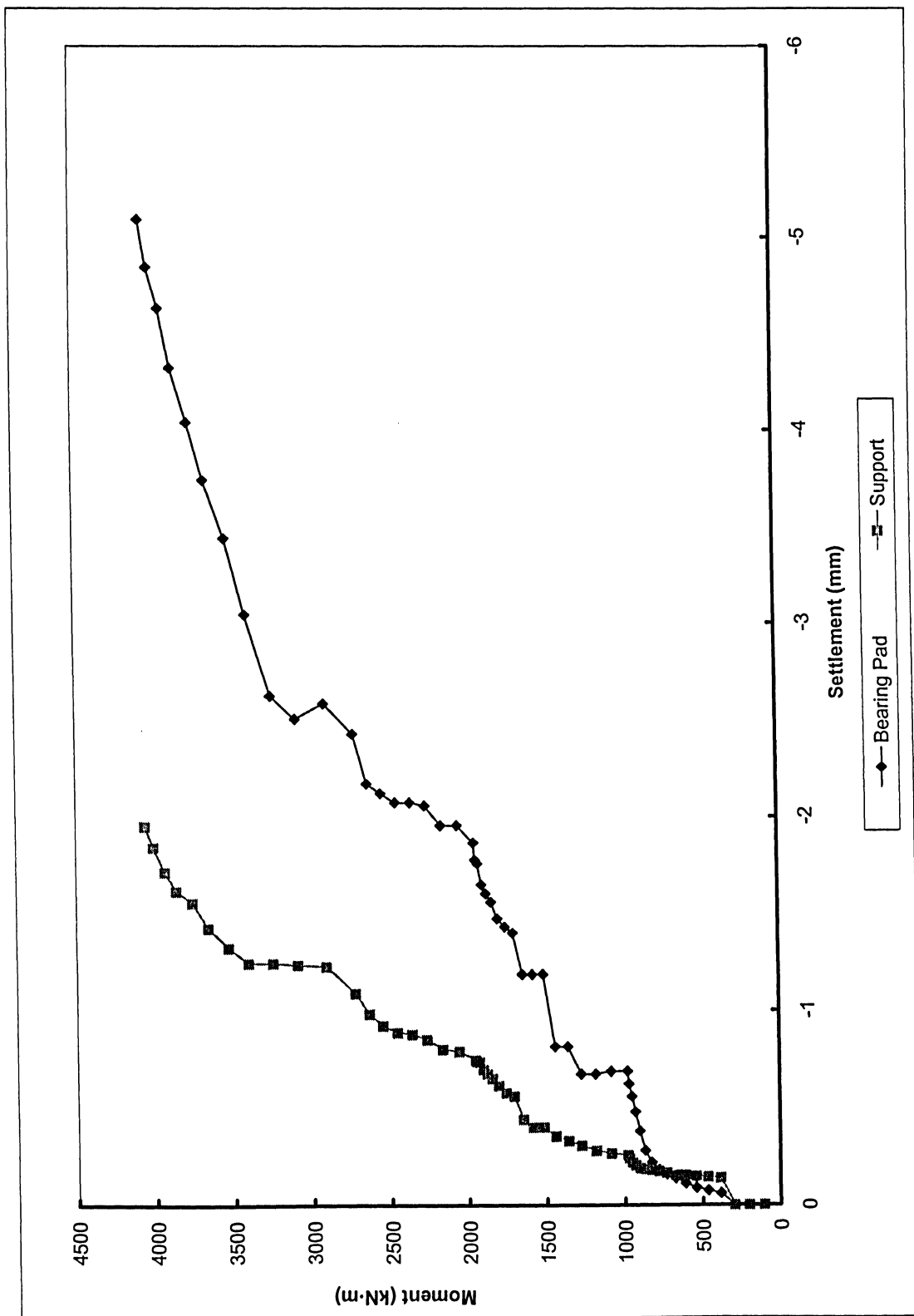


Figure 5.13 – Moment vs. settlement for Type III girder

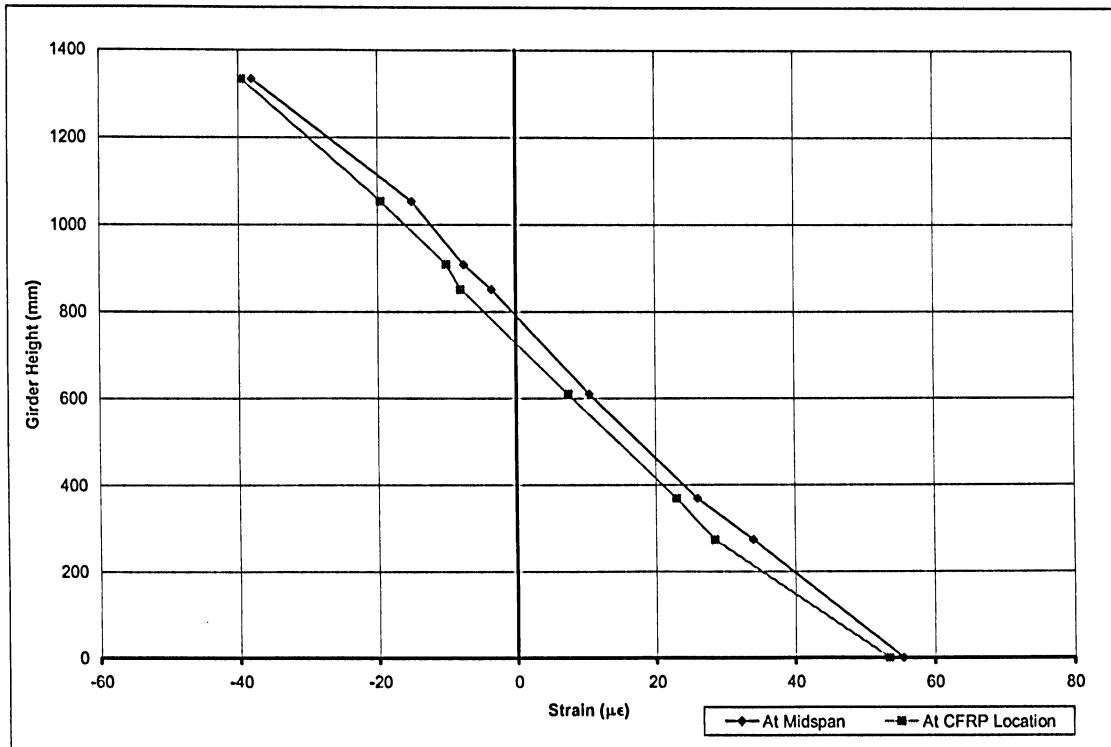


Figure 5.14 – Cross sectional Type III girder strain at 500 kN·m

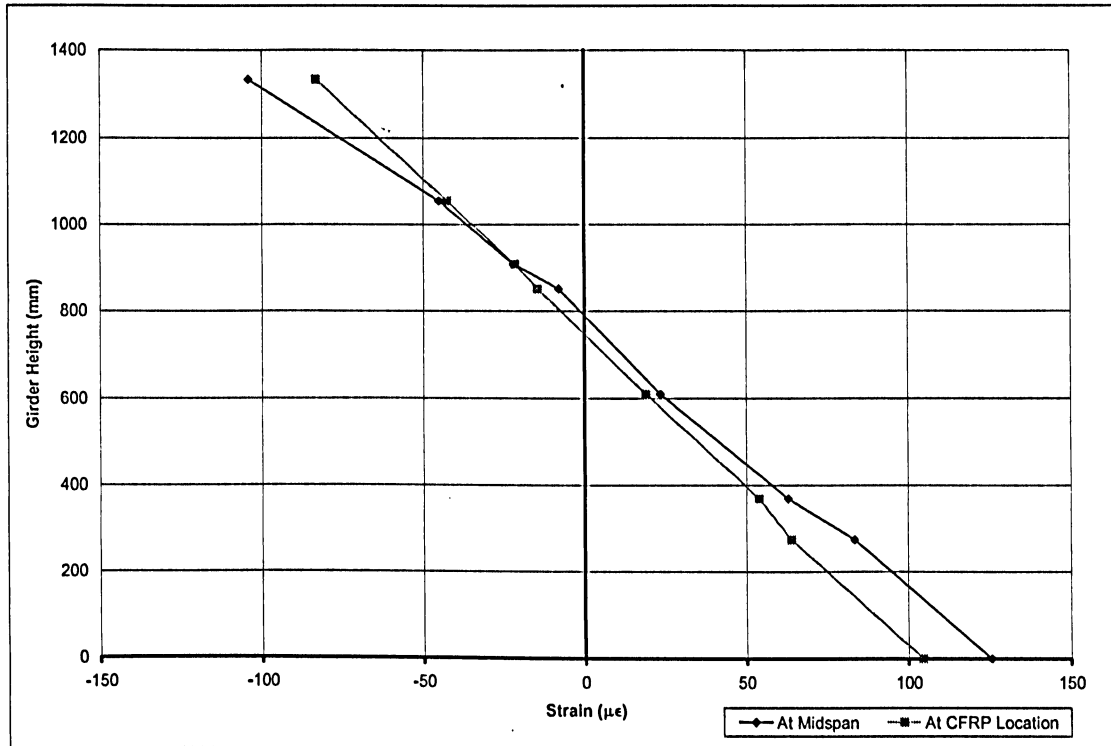


Figure 5.15 – Cross sectional Type III girder strain at 1000 kN·m

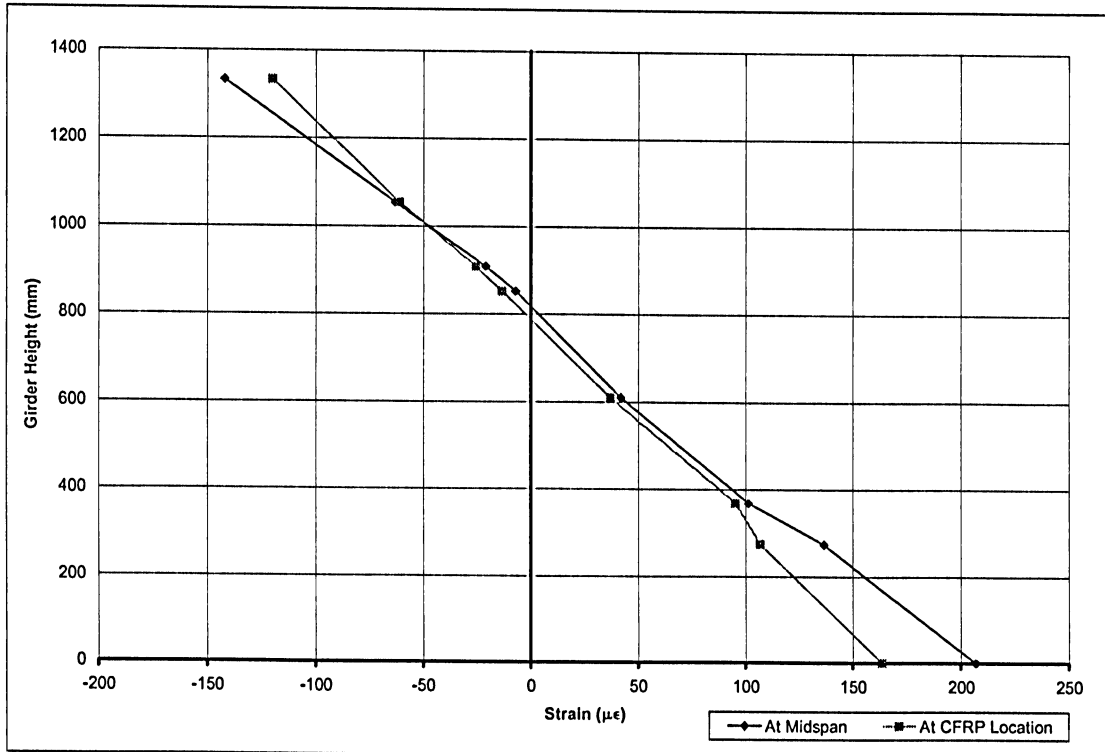


Figure 5.16 – Cross sectional Type III girder strain at 1500 kN·m

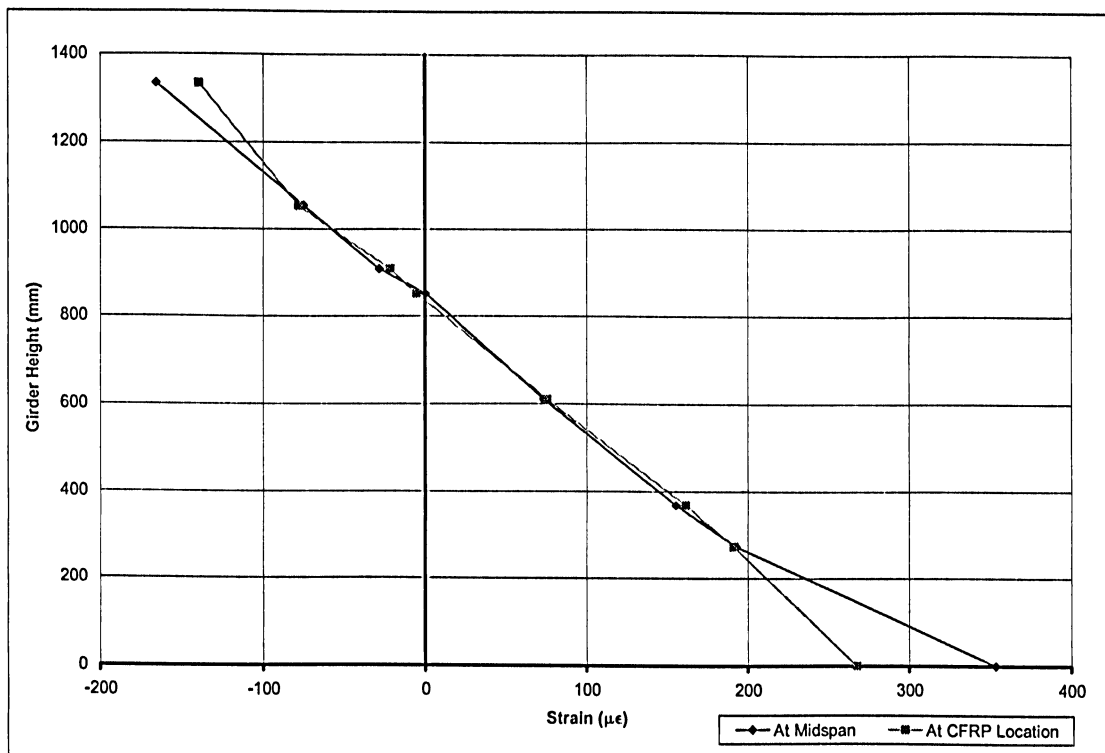


Figure 5.17 – Cross sectional Type III girder strain at 2000 kN·m

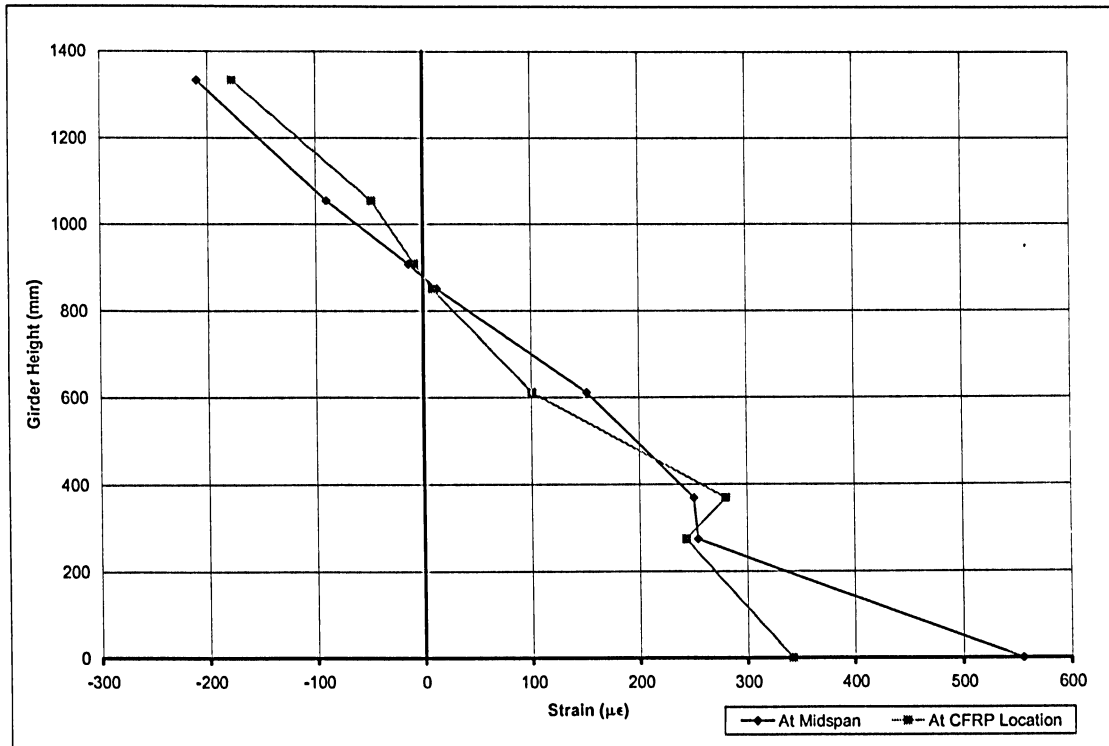


Figure 5.18 – Cross sectional Type III girder strain at 2500 kN·m

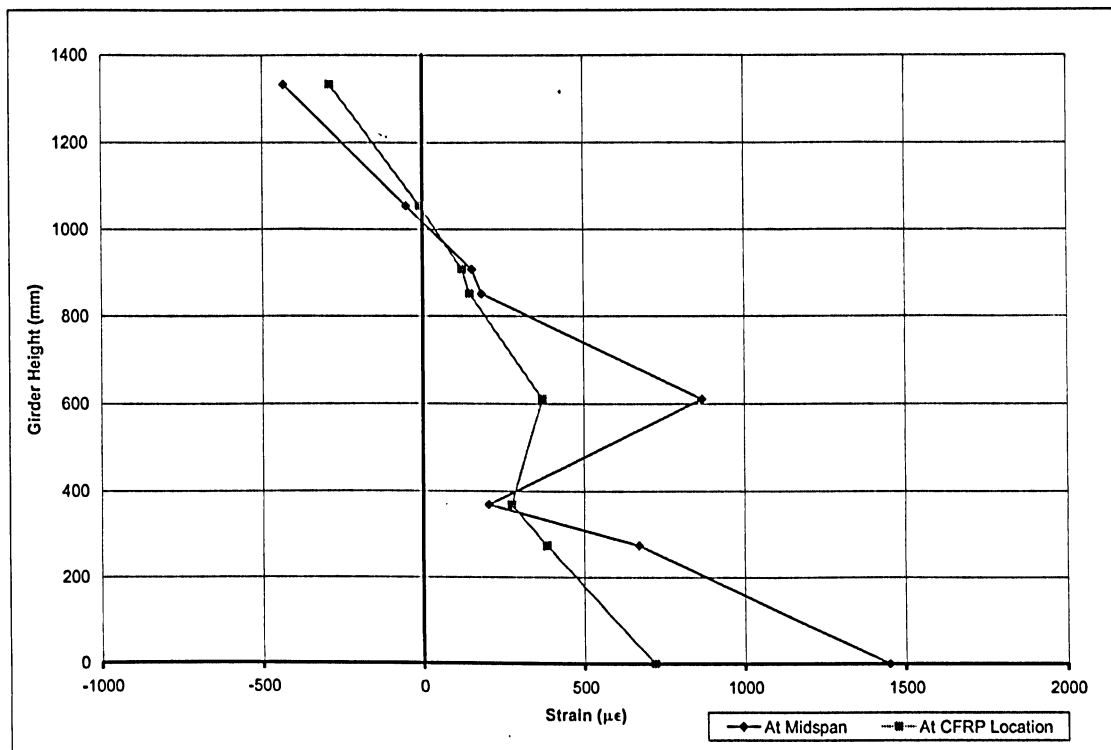


Figure 5.19 – Cross sectional Type III girder strain at 3000 kN·m

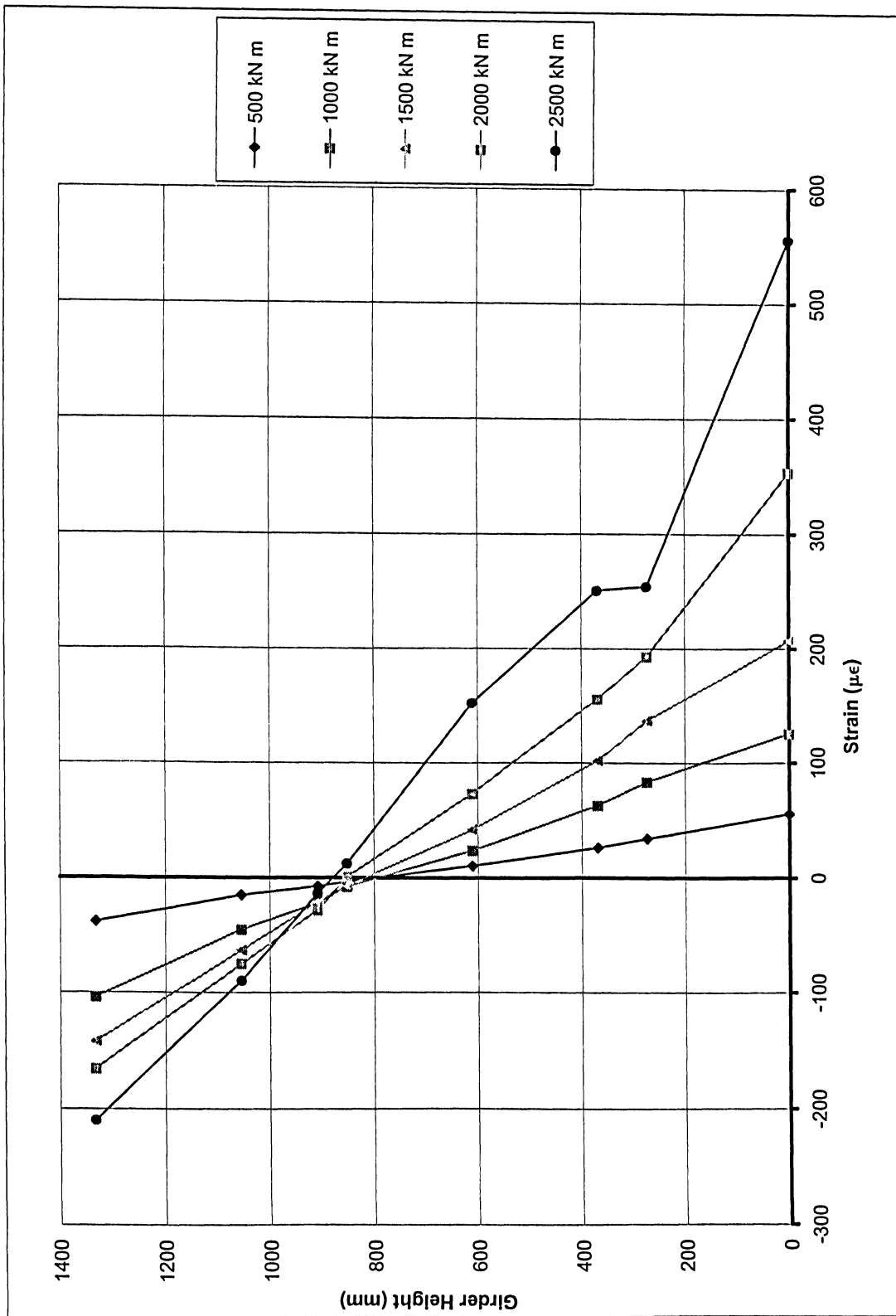


Figure 5.20 – Cross sectional girder strain, at midspan, for various values of moment

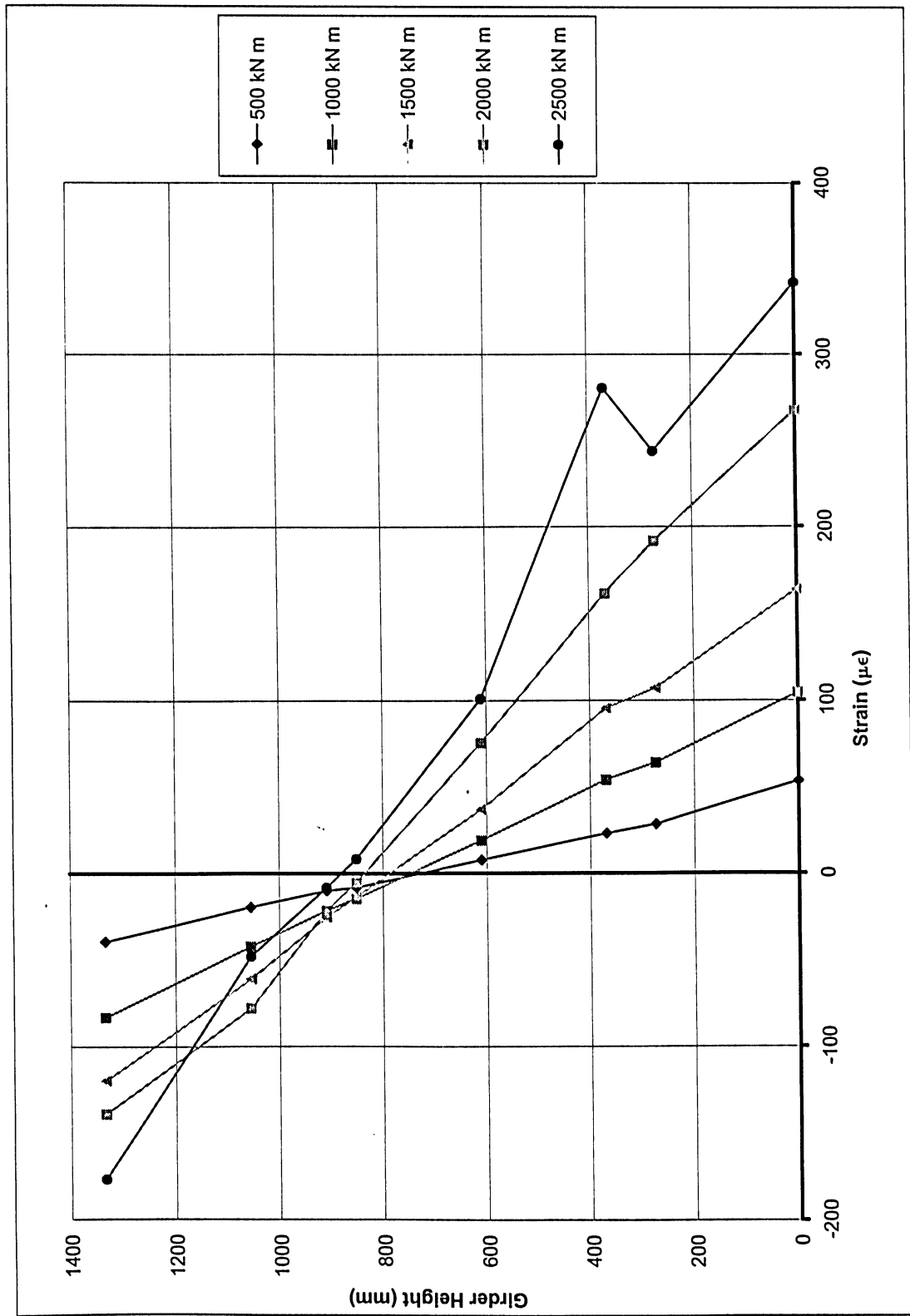


Figure 5.21 – Cross sectional girder strain, on CFRP, for various values of moment

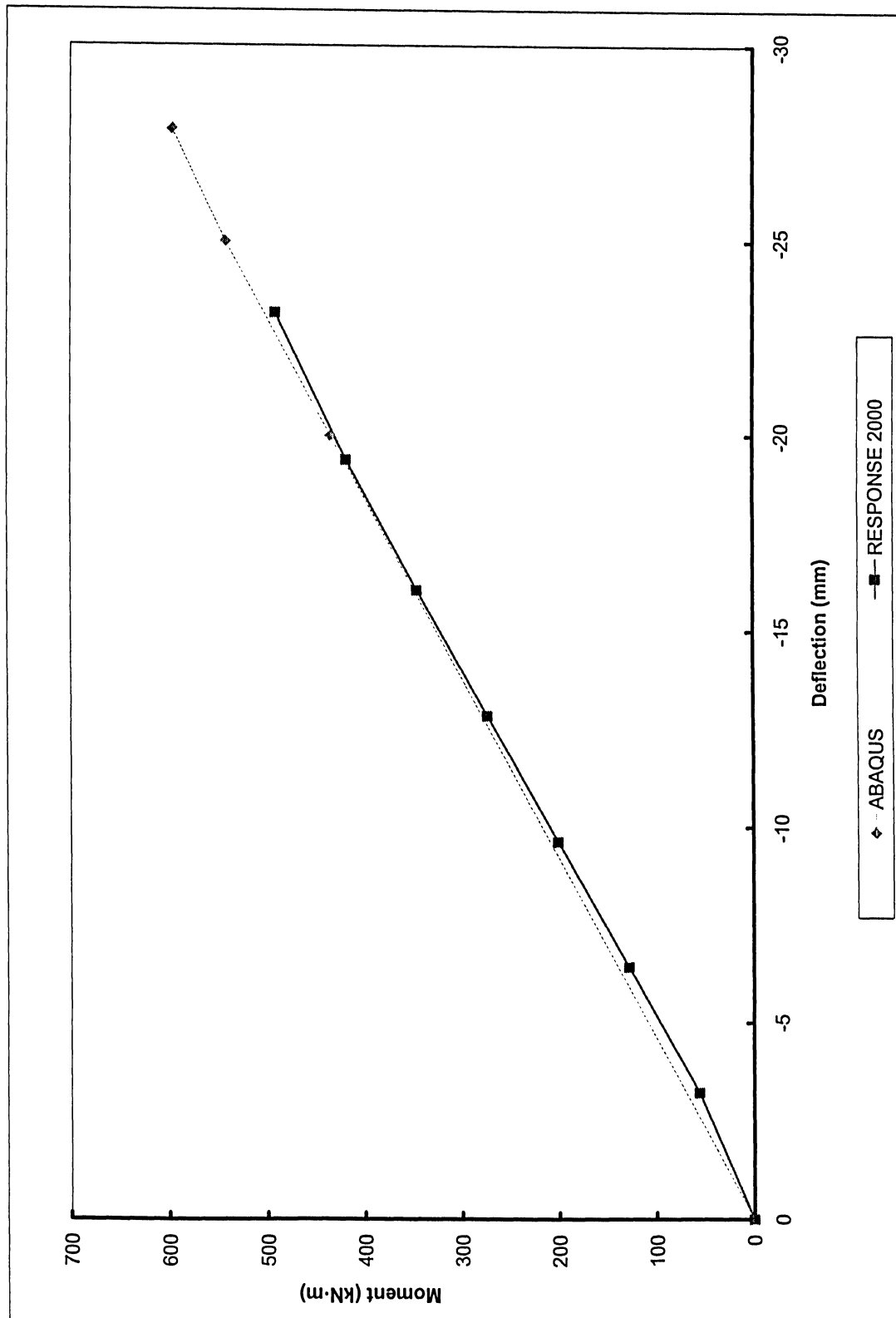


Figure 5.22 – DT-41 girder verification of modeling results in the linear-elastic range

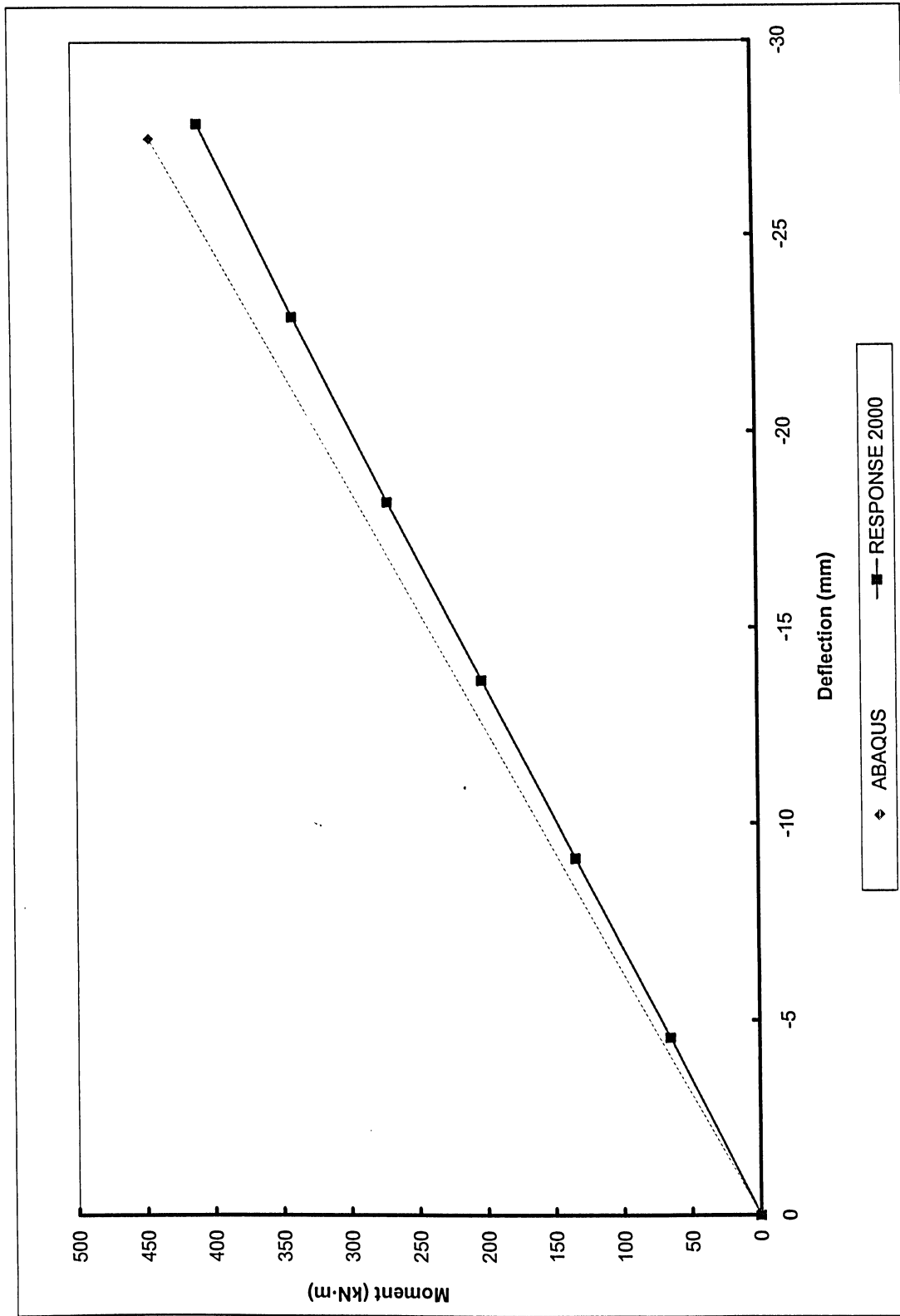


Figure 5.23 – DT-100 girder verification of modeling results in the linear-elastic range

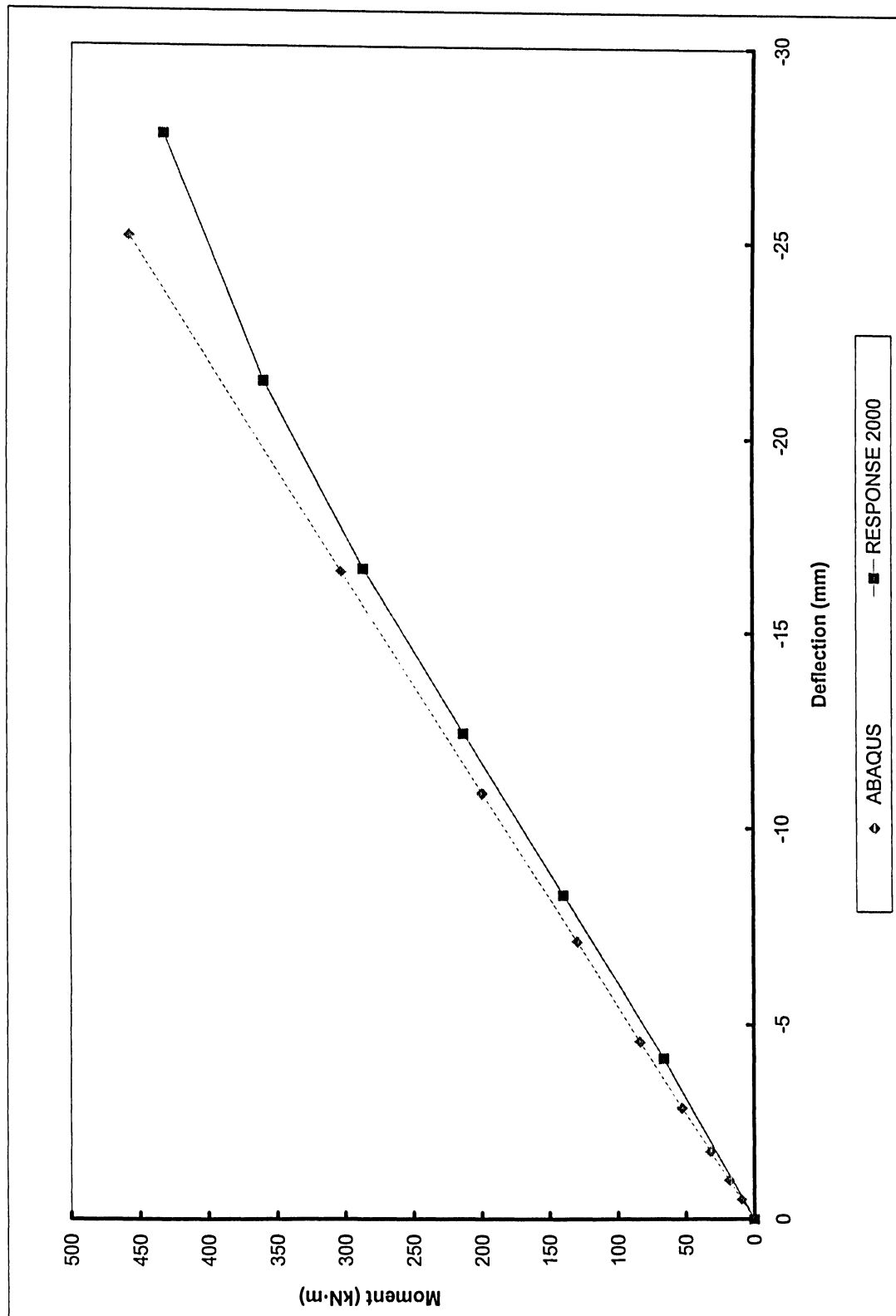


Figure 5.24 – DT-102A girder verification of modeling results in the linear-elastic range

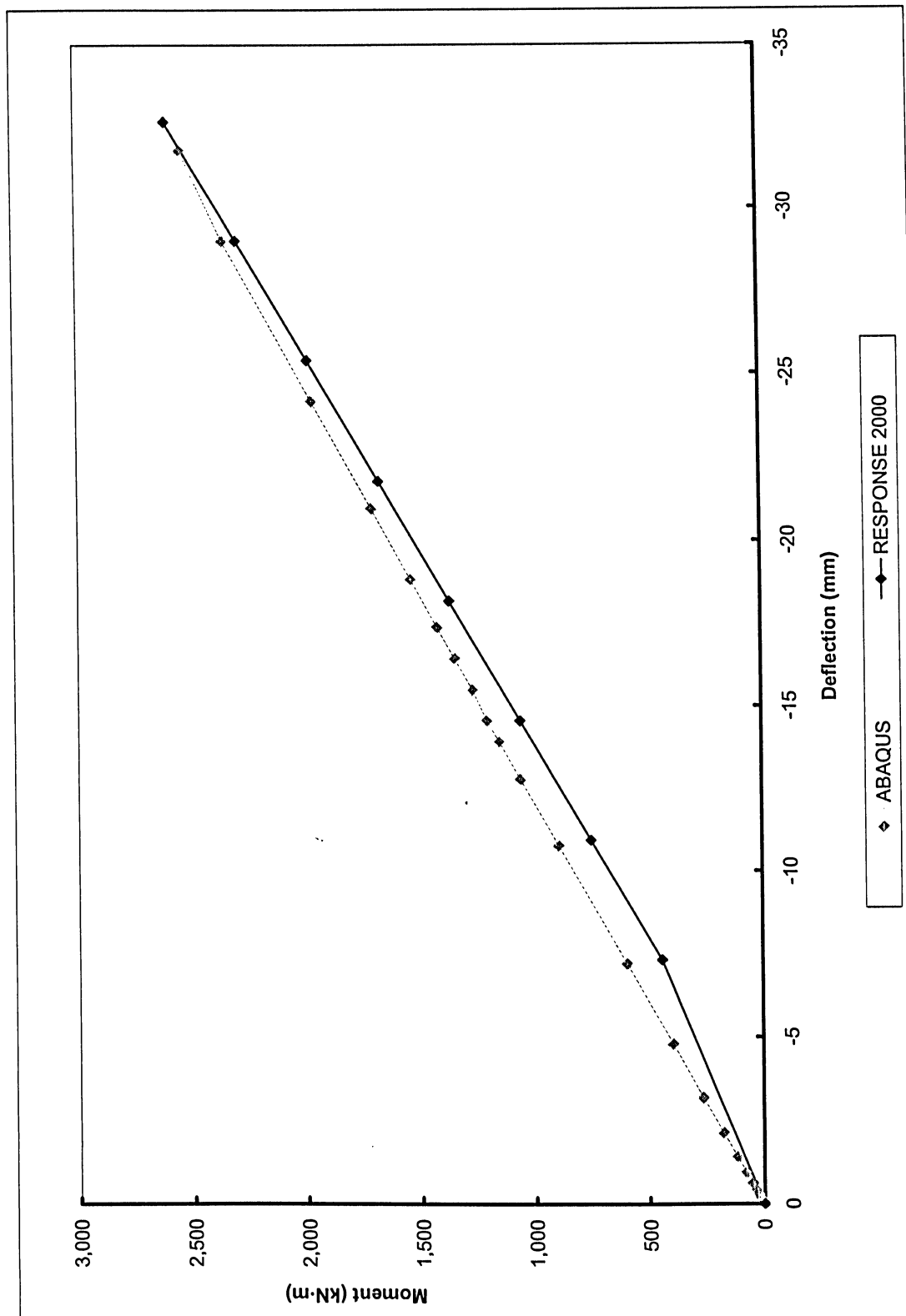


Figure 5.25 – Type III girder verification of modeling results in the linear-elastic range

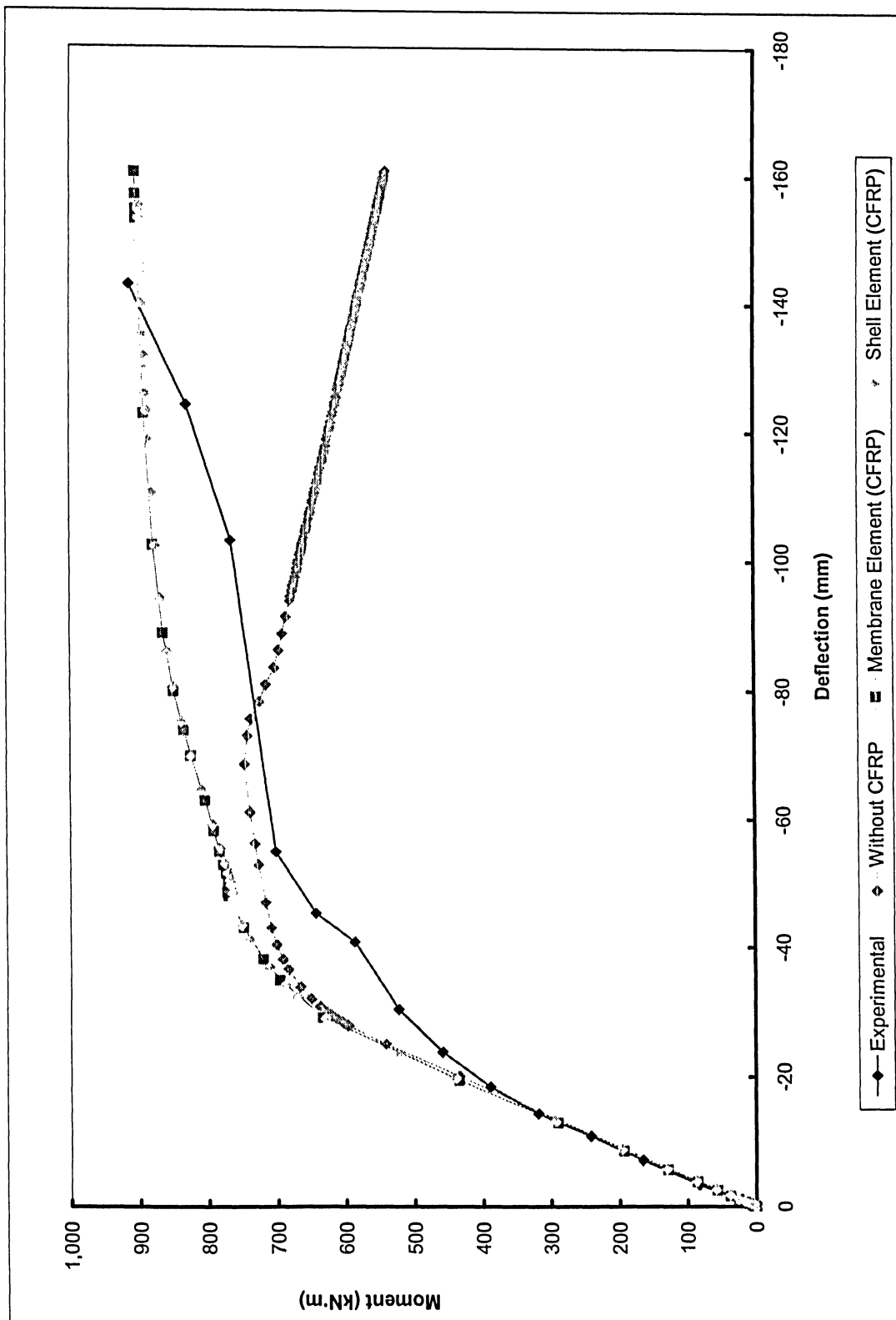


Figure 5.26 – DT-41 moment-deflection relation for different CFRP element types

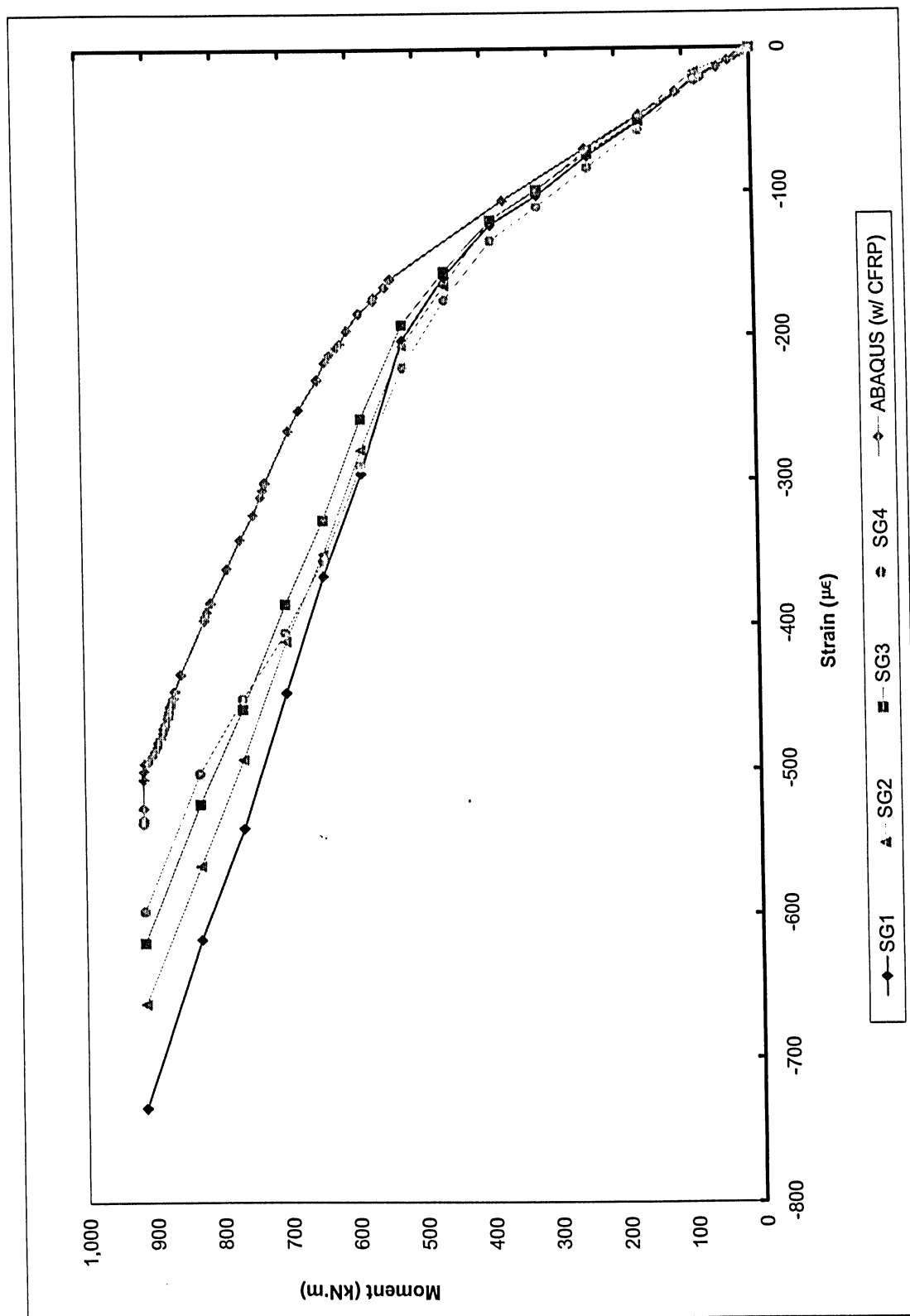


Figure 5.27 – DT-41 moment-strain relation between experimental and finite element findings

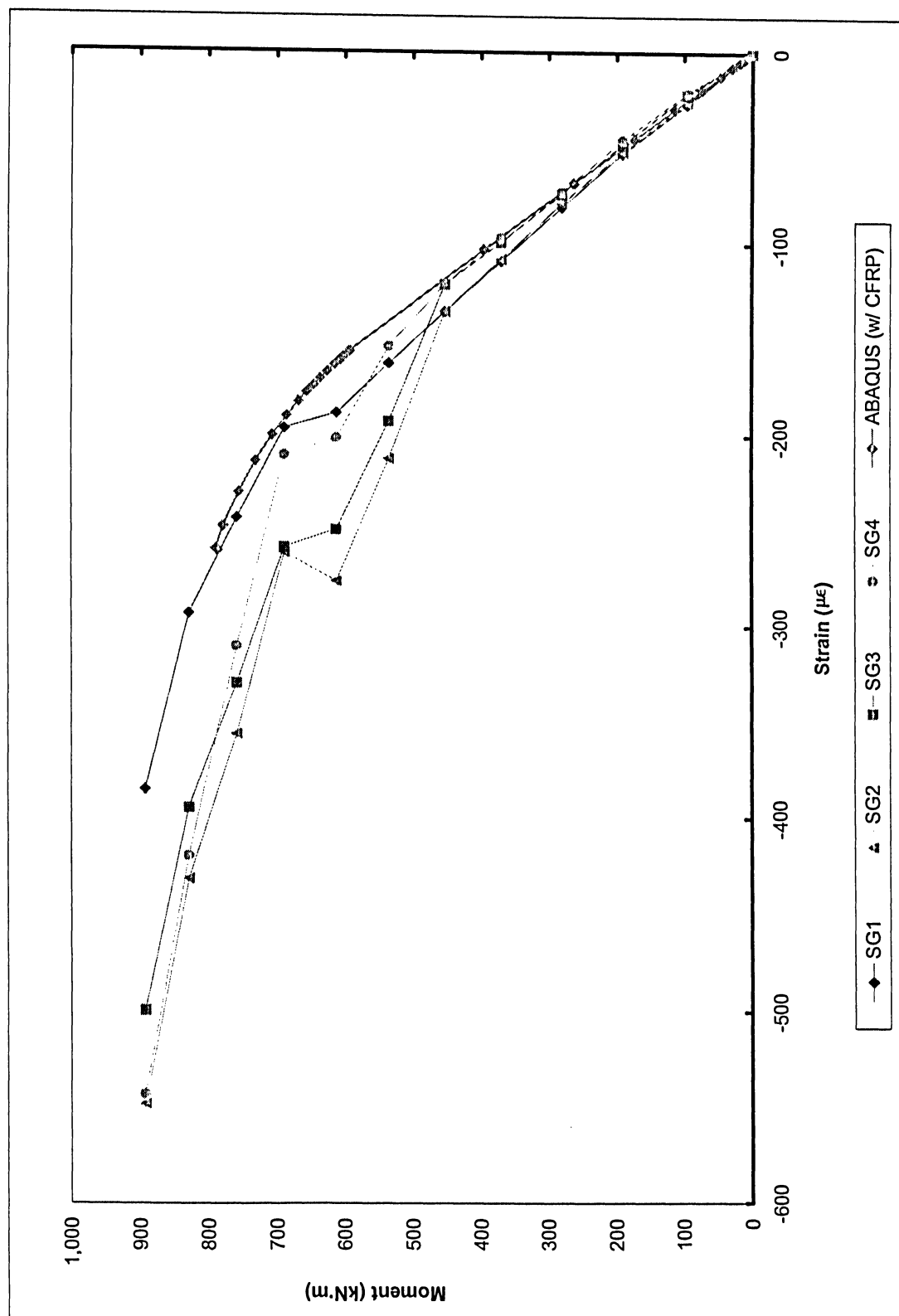


Figure 5.28 – DT-100 moment-strain relation between experimental and finite element findings

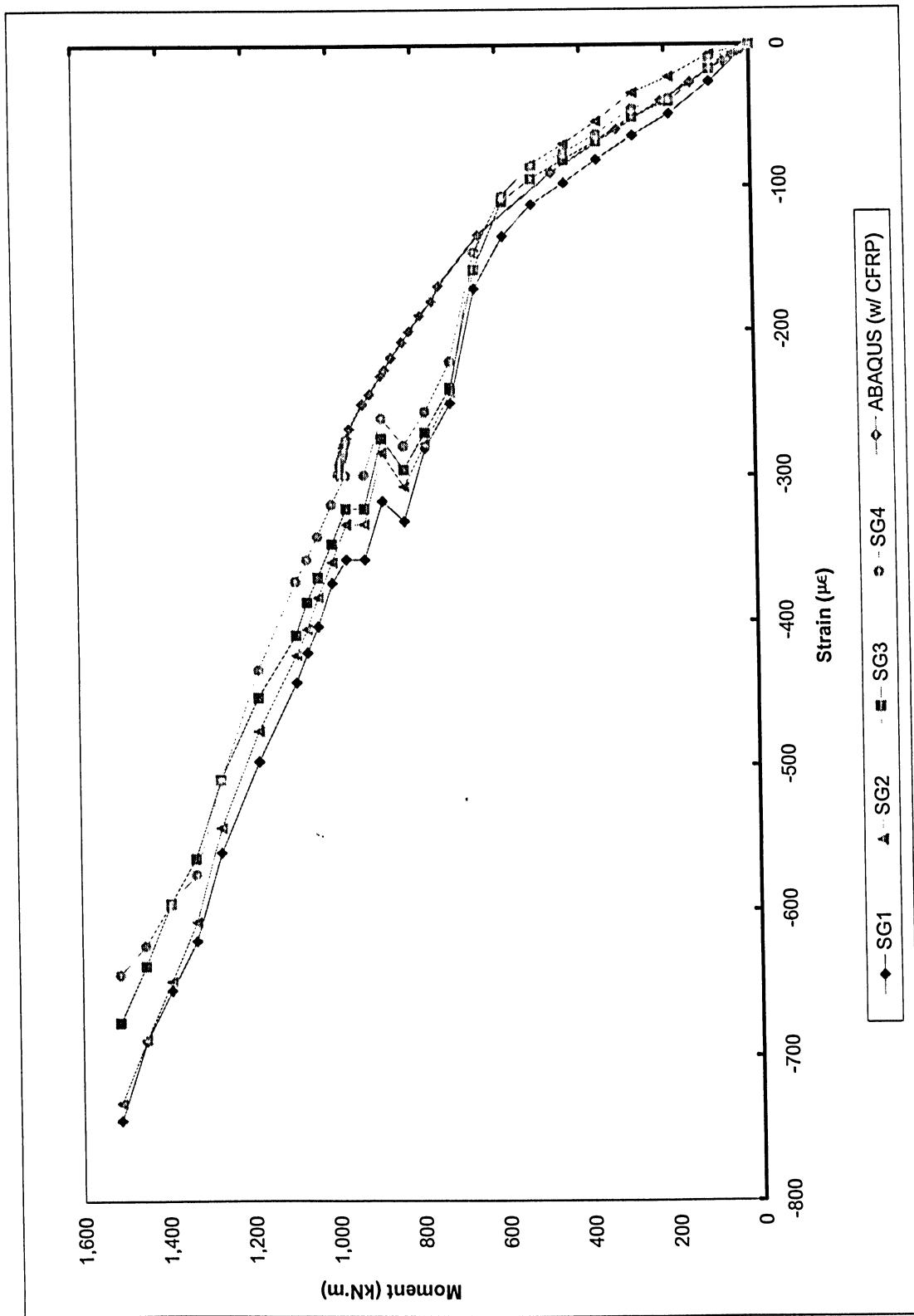


Figure 5.29 – DT-102A moment-strain relation between experimental and finite element findings

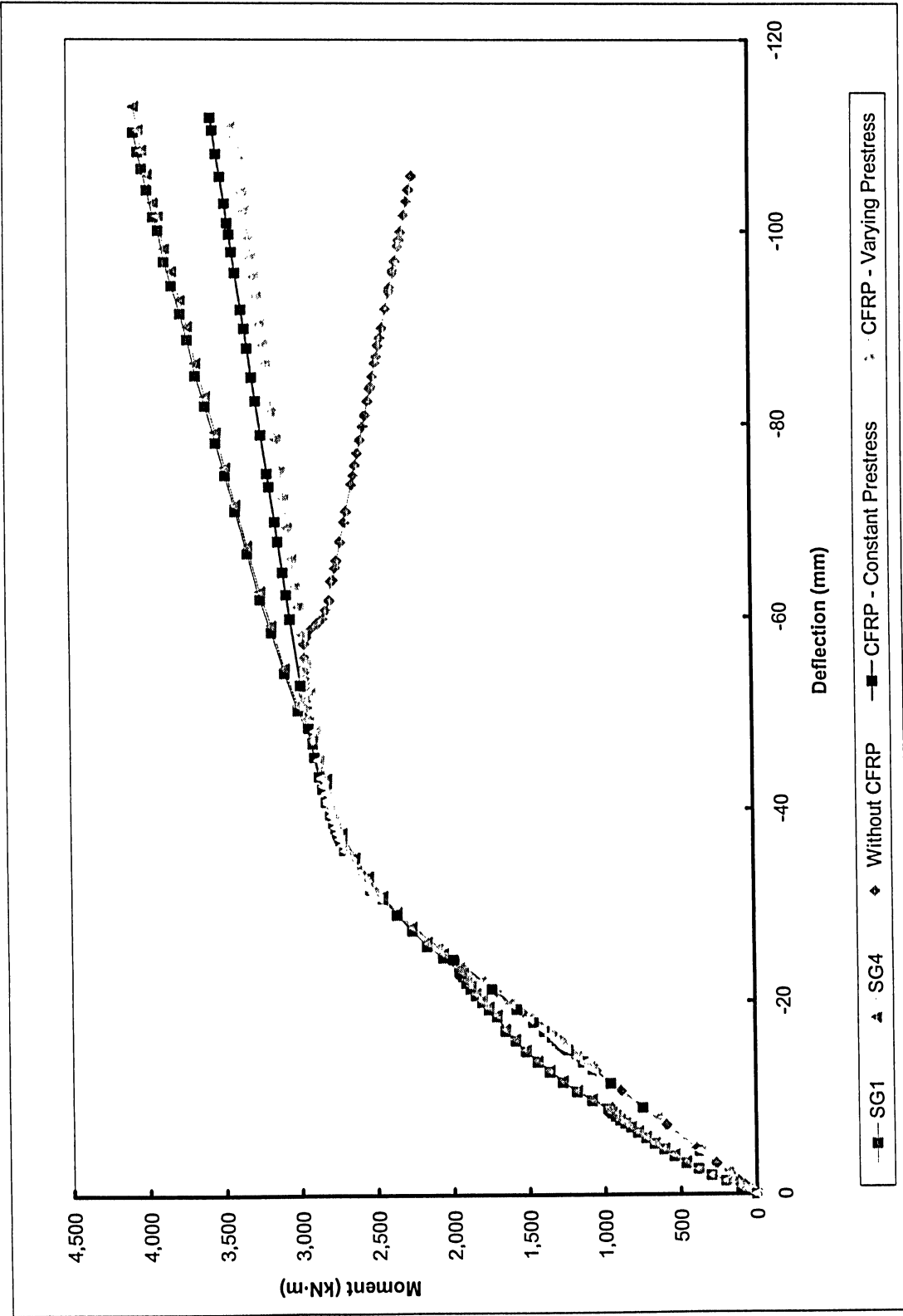


Figure 5.30 – Type III girder moment-deflection relation for finite element models exhibiting constant and varying prestress

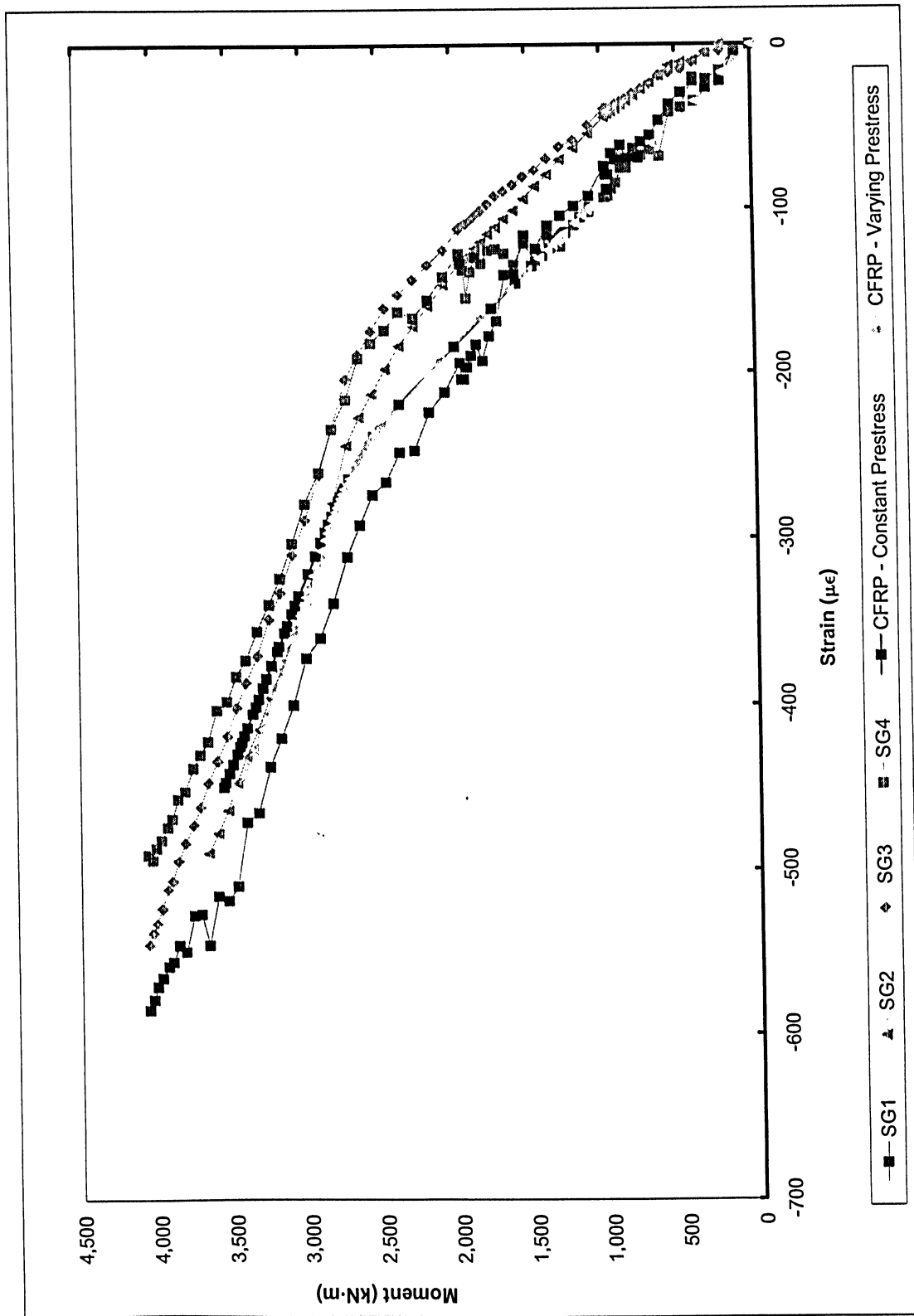


Figure 5.31 – Type III girder moment-strain relation for finite element models exhibiting constant and varying prestress

APPENDIX A

INPUT FILES FOR ABAQUS FINITE ELEMENT MODELS

AASHTO TYPE III GIRDER ABAQUS INPUT FILE

ABAQUS input file for the Type III girder strengthened with CFRP, using membrane elements, and constant prestress.

```

*HEADING
2D LINE MODEL OF PRESTRESSED CONCRETE TYPE-III I-GIRDER (N,mm) MEMBRANE CFRP FILE
**
*PREPRINT,ECHO=YES,MODEL=NO,HISTORY=NO
**RESTART,WRITE
**
*****REFERENCE NODAL COORDINATES - SLAB,GIRDER*****
**
*NODE
2,      -11000,      0,      0
34,     -11000,     1600,      0
5502,      0,      0,      0
5534,      0,     1600,      0
*****
5618,     -11000,      800,     -95
11119,    -11000,      800,    -145
16620,    -11000,      800,    -195
22121,    -11000,      800,    -245
27622,    -11000,      800,    -270
33123,    -11000,      800,    -320
38624,    -11000,      800,    -370
44125,    -11000,      800,    -420
49626,    -11000,      800,    -470
55127,    -11000,      800,    -520
60628,    -11000,      800,    -570
66129,    -11000,      800,    -620
71630,    -11000,      800,    -670
77131,    -11000,      800,    -720
82632,    -11000,      800,    -770
88133,    -11000,      800,    -820
93634,    -11000,      800,    -870
99135,    -11000,      800,    -920
104636,   -11000,      800,    -970
110137,   -11000,      800,   -1020
115638,   -11000,      800,   -1070
121139,   -11000,      800,   -1095
126640,   -11000,      800,   -1145
132141,   -11000,      800,   -1195
137642,   -11000,      800,   -1245
*****
11118,      0,      800,     -95
16619,      0,      800,    -145
22120,      0,      800,    -195
27621,      0,      800,    -245
33122,      0,      800,    -270
38623,      0,      800,    -320
44124,      0,      800,    -370
49625,      0,      800,    -420
55126,      0,      800,    -470
60627,      0,      800,    -520
66128,      0,      800,    -570
71629,      0,      800,    -620
77130,      0,      800,    -670
82631,      0,      800,    -720
88132,      0,      800,    -770
93633,      0,      800,    -820
99134,      0,      800,    -870
104635,     0,      800,    -920
110136,     0,      800,    -970
115637,     0,      800,   -1020
121138,     0,      800,   -1070
126639,     0,      800,   -1095
132140,     0,      800,   -1145
137641,     0,      800,   -1195
143142,     0,      800,   -1245
**
*****NODE GENERATION FOR TOP SLAB*****
**

```

```

*NGEN,NSET=END
2,34,2
5502,5534,2
*NGEN,NSET=NSLAB
2,5502,100
4,5504,100
6,5506,100
8,5508,100
10,5510,100
12,5512,100
14,5514,100
16,5516,100
18,5518,100
20,5520,100
22,5522,100
24,5524,100
26,5526,100
28,5528,100
30,5530,100
32,5532,100
34,5534,100
**
*****NODE GENERATION FOR GIRDER*****
**
*NGEN,NSET=NLONG
5618,11118,100
11119,16619,100
16620,22120,100
22121,27621,100
27622,33122,100
33123,38623,100
38624,44124,100
44125,49625,100
49626,55126,100
55127,60627,100
60628,66128,100
66129,71629,100
71630,77130,100
77131,82631,100
82632,88132,100
88133,93633,100
93634,99134,100
99135,104635,100
104636,110136,100
110137,115637,100
115638,121138,100
121139,126639,100
126640,132140,100
132141,137641,100
137642,143142,100
**
*****ELEMENT GENERATION FOR THE SLAB*****
**
*ELEMENT,TYPE=S4R
1,2,102,104,4
*ELGEN,ELSET=SLAB
1,55,100,16,16,2,1
**
*****ELEMENT GENERATION FOR THE GIRDER*****
**
*ELEMENT,TYPE=S4R
881,5618,5718,118,18
*ELGEN,ELSET=SLABGIRDER
881,55,100,1
**
*ELEMENT,TYPE=S4R
936,11119,11219,5718,5618
991,16620,16720,11219,11119
1046,22121,22221,16720,16620
1101,27622,27722,22221,22121
*ELGEN,ELSET=TOPFLANGE
936,55,100,1
991,55,100,1
1046,55,100,1
1101,55,100,1
**
*ELEMENT,TYPE=S4R
1156,33123,33223,27722,27622
1211,38624,38724,33223,33123
*ELGEN,ELSET=TOPCHAM
1156,55,100,1

```

```

1211,55,100,1
**
*ELEMENT,TYPE=S4R
1266,44125,44225,38724,38624
1321,49626,49726,44225,44125
1376,55127,55227,49726,49626
1431,60628,60728,55227,55127
1486,66129,66229,60728,60628
1541,71630,71730,66229,66129
1596,77131,77231,71730,71630
1651,82632,82732,77231,77131
1706,88133,88233,82732,82632
1761,93634,93734,88233,88133
*ELGEN,ELSET=WEB
1266,55,100,1
1321,55,100,1
1376,55,100,1
1431,55,100,1
1486,55,100,1
1541,55,100,1
1596,55,100,1
1651,55,100,1
1706,55,100,1
1761,55,100,1
**
*ELEMENT,TYPE=S4R
1816,99135,99235,93734,93634
1871,104636,104736,99235,99135
1926,110137,110237,104736,104636
1981,115638,115738,110237,110137
*ELGEN,ELSET=BOTCHAM
1816,55,100,1
1871,55,100,1
1926,55,100,1
1981,55,100,1
**
*ELEMENT,TYPE=S4R
2036,121139,121239,115738,115638
2091,126640,126740,121239,121139
2146,132141,132241,126740,126640
2201,137642,137742,132241,132141
*ELGEN,ELSET=BOTFLANGE
2036,55,100,1
2091,55,100,1
2146,55,100,1
2201,55,100,1
**
*****ELEMENT GENERATION FOR PRESTRESSING TENDONS*****
**
*ELEMENT,TYPE=T2D2
2256,104636,104736
*ELGEN,ELSET=PRE1
2256,55,100,1
**
*ELEMENT,TYPE=T2D2
2311,126640,126740
*ELGEN,ELSET=PRE2
2311,55,100,1
**
*ELEMENT,TYPE=T2D2
2366,132141,132241
*ELGEN,ELSET=PRE3
2366,55,100,1
**
*****ELEMENT SET ASSIGNMENT*****
**
*****R-LONG REBAR
*****S-STIRRUP
**
*****ELEMENT SET ASSIGNMENT FOR SLAB-GIRDER*****
**
*ELSET,ELSET=SLABGIRDER,GENERATE
881,935,1
**
*****ELEMENT SET ASSIGNMENT - SEC1 (S,R)*****
**
*ELSET,ELSET=TOPFLANGESEC1,GENERATE
936,1101,55
*ELSET,ELSET=TOPCHAMSEC1,GENERATE
1156,1211,55
*ELSET,ELSET=WEBSEC1,GENERATE

```

```

1266,1761,55
*ELSET,ELSET=BOTCHAMSEC1,GENERATE
1816,1981,55
*ELSET,ELSET=BOTFLANGESEC1,GENERATE
2036,2201,55
**
*****ELEMENT SET ASSIGNMENT - SEC2 (R)*****
**
*ELSET,ELSET=TOPFLANGESEC2,GENERATE
937,1102,55
*ELSET,ELSET=TOPCHAMSEC2,GENERATE
1157,1212,55
*ELSET,ELSET=WEBSEC2,GENERATE
1267,1762,55
*ELSET,ELSET=BOTCHAMSEC2,GENERATE
1817,1982,55
*ELSET,ELSET=BOTFLANGESEC2,GENERATE
2037,2202,55
**
*****ELEMENT SET ASSIGNMENT - SEC3 (S,R)*****
**
*ELSET,ELSET=TOPFLANGESEC3,GENERATE
938,1103,55
939,1104,55
940,1105,55
941,1106,55
942,1107,55
943,1108,55
*ELSET,ELSET=TOPCHAMSEC3,GENERATE
1158,1213,55
1159,1214,55
1160,1215,55
1161,1216,55
1162,1217,55
1163,1218,55
*ELSET,ELSET=WEBSEC3,GENERATE
1268,1763,55
1269,1764,55
1270,1765,55
1271,1766,55
1272,1767,55
1273,1768,55
*ELSET,ELSET=BOTCHAMSEC3,GENERATE
1818,1983,55
1819,1984,55
1820,1985,55
1821,1986,55
1822,1987,55
1823,1988,55
*ELSET,ELSET=BOTFLANGESEC3,GENERATE
2038,2203,55
2039,2204,55
2040,2205,55
2041,2206,55
2042,2207,55
2043,2208,55
**
*****ELEMENT SET ASSIGNMENT - SEC4 (R)*****
**
*ELSET,ELSET=TOPFLANGESEC4,GENERATE
944,1109,55
*ELSET,ELSET=TOPCHAMSEC4,GENERATE
1164,1219,55
*ELSET,ELSET=WEBSEC4,GENERATE
1274,1769,55
*ELSET,ELSET=BOTCHAMSEC4,GENERATE
1824,1989,55
*ELSET,ELSET=BOTFLANGESEC4,GENERATE
2044,2209,55
**
*****ELEMENT SET ASSIGNMENT - SEC5 (S,R)*****
**
*ELSET,ELSET=TOPFLANGESEC5,GENERATE
945,1110,55
946,1111,55
947,1112,55
948,1113,55
949,1114,55
950,1115,55
951,1116,55
*ELSET,ELSET=TOPCHAMSEC5,GENERATE

```

```

1165,1220,55
1166,1221,55
1167,1222,55
1168,1223,55
1169,1224,55
1170,1225,55
1171,1226,55
*ELSET,ELSET=WEBSEC5,GENERATE
1275,1770,55
1276,1771,55
1277,1772,55
1278,1773,55
1279,1774,55
1280,1775,55
1281,1776,55
*ELSET,ELSET=BOTCHAMSEC5,GENERATE
1825,1990,55
1826,1991,55
1827,1992,55
1828,1993,55
1829,1994,55
1830,1995,55
1831,1996,55
*ELSET,ELSET=BOTFLANGESEC5,GENERATE
2045,2210,55
2046,2211,55
2047,2212,55
2048,2213,55
2049,2214,55
2050,2215,55
2051,2216,55
**
*****ELEMENT SET ASSIGNMENT - SEC6 (R)*****
**
*ELSET,ELSET=TOPFLANGESEC6,GENERATE
952,1117,55
953,1118,55
954,1119,55
*ELSET,ELSET=TOPCHAMSEC6,GENERATE
1172,1227,55
1173,1228,55
1174,1229,55
*ELSET,ELSET=WEBSEC6,GENERATE
1282,1777,55
1283,1778,55
1284,1779,55
*ELSET,ELSET=BOTCHAMSEC6,GENERATE
1832,1997,55
1833,1998,55
1834,1999,55
*ELSET,ELSET=BOTFLANGESEC6,GENERATE
2052,2217,55
2053,2218,55
2054,2219,55
**
*****ELEMENT SET ASSIGNMENT - SEC7 (S,R)*****
**
*ELSET,ELSET=TOPFLANGESEC7,GENERATE
955,1120,55
956,1121,55
957,1122,55
958,1123,55
959,1124,55
960,1125,55
961,1126,55
962,1127,55
963,1128,55
964,1129,55
965,1130,55
966,1131,55
967,1132,55
968,1133,55
969,1134,55
970,1135,55
971,1136,55
972,1137,55
973,1138,55
974,1139,55
975,1140,55
976,1141,55
977,1142,55

```



```

978,1143,55
979,1144,55
980,1145,55
981,1146,55
982,1147,55
983,1148,55
984,1149,55
985,1150,55
986,1151,55
987,1152,55
988,1153,55
*ELSET,ELSET=TOPCHAMSEC7,GENERATE
1175,1230,55
1176,1231,55
1177,1232,55
1178,1233,55
1179,1234,55
1180,1235,55
1181,1236,55
1182,1237,55
1183,1238,55
1184,1239,55
1185,1240,55
1186,1241,55
1187,1242,55
1188,1243,55
1189,1244,55
1190,1245,55
1191,1246,55
1192,1247,55
1193,1248,55
1194,1249,55
1195,1250,55
1196,1251,55
1197,1252,55
1198,1253,55
1199,1254,55
1200,1255,55
1201,1256,55
1202,1257,55
1203,1258,55
1204,1259,55
1205,1260,55
1206,1261,55
1207,1262,55
1208,1263,55
*ELSET,ELSET=WEBSEC7,GENERATE
1285,1780,55
1286,1781,55
1287,1782,55
1288,1783,55
1289,1784,55
1290,1785,55
1291,1786,55
1292,1787,55
1293,1788,55
1294,1789,55
1295,1790,55
1296,1791,55
1297,1792,55
1298,1793,55
1299,1794,55
1300,1795,55
1301,1796,55
1302,1797,55
1303,1798,55
1304,1799,55
1305,1800,55
1306,1801,55
1307,1802,55
1308,1803,55
1309,1804,55
1310,1805,55
1311,1806,55
1312,1807,55
1313,1808,55
1314,1809,55
1315,1810,55
1316,1811,55
1317,1812,55
1318,1813,55

```

```

*ELSET,ELSET=BOTCHAMSEC7,GENERATE
1835,2000,55
1836,2001,55
1837,2002,55
1838,2003,55
1839,2004,55
1840,2005,55
1841,2006,55
1842,2007,55
1843,2008,55
1844,2009,55
1845,2010,55
1846,2011,55
1847,2012,55
1848,2013,55
1849,2014,55
1850,2015,55
1851,2016,55
1852,2017,55
1853,2018,55
1854,2019,55
1855,2020,55
1856,2021,55
1857,2022,55
1858,2023,55
1859,2024,55
1860,2025,55
1861,2026,55
1862,2027,55
1863,2028,55
1864,2029,55
1865,2030,55
1866,2031,55
1867,2032,55
1868,2033,55
*ELSET,ELSET=BOTFLANGESEC7,GENERATE
2055,2220,55
2056,2221,55
2057,2222,55
2058,2223,55
2059,2224,55
2060,2225,55
2061,2226,55
2062,2227,55
2063,2228,55
2064,2229,55
2065,2230,55
2066,2231,55
2067,2232,55
2068,2233,55
2069,2234,55
2070,2235,55
2071,2236,55
2072,2237,55
2073,2238,55
2074,2239,55
2075,2240,55
2076,2241,55
2077,2242,55
2078,2243,55
2079,2244,55
2080,2245,55
2081,2246,55
2082,2247,55
2083,2248,55
2084,2249,55
2085,2250,55
2086,2251,55
2087,2252,55
2088,2253,55
**
*****ELEMENT SET ASSIGNMENT - SEC8 (R)*****
**
*ELSET,ELSET=TOPFLANGESEC8,GENERATE
989,1154,55
990,1155,55
*ELSET,ELSET=TOPCHAMSEC8,GENERATE
1209,1264,55
1210,1265,55
*ELSET,ELSET=WEBSEC8,GENERATE
1319,1814,55

```

```

1320,1815,55
*ELSET,ELSET=BOTCHAMSEC8,GENERATE
1869,2034,55
1870,2035,55
*ELSET,ELSET=BOTFLANGESEC8,GENERATE
2089,2254,55
2090,2255,55
**
*****ELEMENT SET ASSIGNMENT (VERIFICATION)*****
**
*ELSET,ELSET=TOPFLANGE
TOPFLANGESEC1
TOPFLANGESEC2
TOPFLANGESEC3
TOPFLANGESEC4
TOPFLANGESEC5
TOPFLANGESEC6
TOPFLANGESEC7
TOPFLANGESEC8
**
*ELSET,ELSET=TOPCHAM
TOPCHAMSEC1
TOPCHAMSEC2
TOPCHAMSEC3
TOPCHAMSEC4
TOPCHAMSEC5
TOPCHAMSEC6
TOPCHAMSEC7
TOPCHAMSEC8
**
*ELSET,ELSET=WEB
WEBSEC1
WEBSEC2
WEBSEC3
WEBSEC4
WEBSEC5
WEBSEC6
WEBSEC7
WEBSEC8
**
*ELSET,ELSET=BOTCHAM
BOTCHAMSEC1
BOTCHAMSEC2
BOTCHAMSEC3
BOTCHAMSEC4
BOTCHAMSEC5
BOTCHAMSEC6
BOTCHAMSEC7
BOTCHAMSEC8
**
*ELSET,ELSET=BOTFLANGE
BOTFLANGESEC1
BOTFLANGESEC2
BOTFLANGESEC3
BOTFLANGESEC4
BOTFLANGESEC5
BOTFLANGESEC6
BOTFLANGESEC7
BOTFLANGESEC8
**
*****ELEMENT GENERATION FOR CFRP LONGITUDINAL STRIPS*****
**
*****Elements are the same as those defined for the concrete, but with*****
*****FRP properties, same nodes and different names*****
*****The number 9 is added to signify longitudinal strip elements.*****
*****
**
*ELEMENT,TYPE=M3D4R
91156,33123,33223,27722,27622
91211,38624,38724,33223,33123
*ELGEN,ELSET=FRPTOPCHAM
91156,55,100,1
91211,55,100,1
**
*ELEMENT,TYPE=M3D4R
91816,99135,99235,93734,93634
91871,104636,104736,99235,99135
91926,110137,110237,104736,104636
91981,115638,115738,110237,110137
*ELGEN,ELSET=FRPBOTCHAM

```

```

91816,55,100,1
91871,55,100,1
91926,55,100,1
91981,55,100,1
**
*****ELEMENT GENERATION FOR CFRP U-WRAP*****
**
*****
*****Elements are the same as those defined for the concrete, but with*****
*****FRP properties, same nodes and different names*****
*****The number 8 is added to signify U-wrap elements.*****
*****
**
*ELEMENT,TYPE=M3D4R
81206,38123,38223,32722,32622
*ELGEN,ELSET=FRPUWRAP1
81206,3,100,1,20,5501,55
**
*ELEMENT,TYPE=M3D4R
81200,37523,37623,32122,32022
*ELGEN,ELSET=FRPUWRAP2
81200,3,100,1,20,5501,55
**
*ELEMENT,TYPE=M3D4R
81194,36923,37023,31522,31422
*ELGEN,ELSET=FRPUWRAP3
81194,3,100,1,20,5501,55
**
*ELEMENT,TYPE=M3D4R
81188,36323,36423,30922,30822
*ELGEN,ELSET=FRPUWRAP4
81188,3,100,1,20,5501,55
**
*ELEMENT,TYPE=M3D4R
81182,35723,35823,30322,30222
*ELGEN,ELSET=FRPUWRAP5
81182,3,100,1,20,5501,55
**
*ELEMENT,TYPE=M3D4R
81176,35123,35223,29722,29622
*ELGEN,ELSET=FRPUWRAP6
81176,3,100,1,20,5501,55
**
*ELEMENT,TYPE=M3D4R
81170,34523,34623,29122,29022
*ELGEN,ELSET=FRPUWRAP7
81170,3,100,1,20,5501,55
**
*ELEMENT,TYPE=M3D4R
81164,33923,34023,28522,28422
*ELGEN,ELSET=FRPUWRAP8
81164,3,100,1,20,5501,55
**
*ELEMENT,TYPE=M3D4R
81158,33323,33423,27922,27822
*ELGEN,ELSET=FRPUWRAP9
81158,3,100,1,20,5501,55
**
*ELSET,ELSET=FRPUWRAPS
FRPUWRAP1
FRPUWRAP2
FRPUWRAP3
FRPUWRAP4
FRPUWRAP5
FRPUWRAP6
FRPUWRAP7
FRPUWRAP8
FRPUWRAP9
**
*****MATERIAL PROPERTIES*****
**
*SHELL SECTION,ELSET=SLAB,MATERIAL=CONSLAB
190,5
*REBAR LAYER
LTOP,500,225,12.5,REINF,0,1
LBOT,300,225,-28.25,REINF,0,1
TTOP,300,150,34.65,REINF,90,1
TBOT,300,150,-47.35,REINF,90,1
*MATERIAL,NAME=REINF
*DENSITY
7850E-9

```

```

*ELASTIC
20000,0.3
*PLASTIC
400
**
*MATERIAL,NAME=CONSLAB
*DENSITY
2400E-9
*ELASTIC
24200,0.2
*CONCRETE
11,0
27.6,0.0015
*FAILURE RATIOS
1.16,0.0836
*TENSION STIFFENING
1,0
0,0.002
*SHEAR RETENTION
1,1E+6
**
*MATERIAL,NAME=CONGIR
*DENSITY
2400E-9
*ELASTIC
26300,0.2
*CONCRETE
13.8,0
34.5,0.0015
*FAILURE RATIOS
1.16,0.0836
*TENSION STIFFENING
1,0
0,0.002
*SHEAR RETENTION
1,1E+6
**
*****SLAB-GIRDER CONNECTION*****
**
*SHELL SECTION,ELSET=SLABGIRDER,MATERIAL=CONGIR
406.4,5
**
*****SECTION1*****
**
*SHELL SECTION,ELSET=TOPFLANGESEC1,MATERIAL=CONGIR
406.4,5
*REBAR LAYER
STIR1,400,76.2,0,REINF,90,1
*SHELL SECTION,ELSET=TOPCHAMSEC1,MATERIAL=CONGIR
292.1,5
*REBAR LAYER
STIR1,400,76.2,0,REINF,90,1
*SHELL SECTION,ELSET=WEBSEC1,MATERIAL=CONGIR
177.8,5
*REBAR LAYER
STIR1,400,76.2,0,REINF,90,1
*SHELL SECTION,ELSET=BOTCHAMSEC1,MATERIAL=CONGIR
368.3,5
*REBAR LAYER
STIR1,400,76.2,0,REINF,90,1
*SHELL SECTION,ELSET=BOTFLANGESEC1,MATERIAL=CONGIR
558.8,5
*REBAR LAYER
STIR1,400,76.2,0,REINF,90,1
**
*****SECTION2*****
**
*SHELL SECTION,ELSET=TOPFLANGESEC2,MATERIAL=CONGIR
406.4,5
*SHELL SECTION,ELSET=TOPCHAMSEC2,MATERIAL=CONGIR
292.1,5
*SHELL SECTION,ELSET=WEBSEC2,MATERIAL=CONGIR
177.8,5
*SHELL SECTION,ELSET=BOTCHAMSEC2,MATERIAL=CONGIR
368.3,5
*SHELL SECTION,ELSET=BOTFLANGESEC2,MATERIAL=CONGIR
558.8,5
**
*****SECTION3*****
**
*SHELL SECTION,ELSET=TOPFLANGESEC3,MATERIAL=CONGIR

```

```

406.4,5
*REBAR LAYER
STIR3,400,177.8,0,REINF,90,1
*SHELL SECTION,ELSET=TOPCHAMSEC3,MATERIAL=CONGIR
292.1,5
*REBAR LAYER
STIR3,400,177.8,0,REINF,90,1
*SHELL SECTION,ELSET=WEBSEC3,MATERIAL=CONGIR
177.8,5
*REBAR LAYER
STIR3,400,177.8,0,REINF,90,1
*SHELL SECTION,ELSET=BOTCHAMSEC3,MATERIAL=CONGIR
368.3,5
*REBAR LAYER
STIR3,400,177.8,0,REINF,90,1
*SHELL SECTION,ELSET=BOTFLANGESEC3,MATERIAL=CONGIR
558.8,5
*REBAR LAYER
STIR3,400,177.8,0,REINF,90,1
**
*****SECTION4*****
**
*SHELL SECTION,ELSET=TOPFLANGESEC4,MATERIAL=CONGIR
406.4,5
*SHELL SECTION,ELSET=TOPCHAMSEC4,MATERIAL=CONGIR
292.1,5
*SHELL SECTION,ELSET=WEBSEC4,MATERIAL=CONGIR
177.8,5
*SHELL SECTION,ELSET=BOTCHAMSEC4,MATERIAL=CONGIR
368.3,5
*SHELL SECTION,ELSET=BOTFLANGESEC4,MATERIAL=CONGIR
558.8,5
**
*****SECTION5*****
**
*SHELL SECTION,ELSET=TOPFLANGESEC5,MATERIAL=CONGIR
406.4,5
*REBAR LAYER
STIR5,400,355.6,0,REINF,90,1
*SHELL SECTION,ELSET=TOPCHAMSEC5,MATERIAL=CONGIR
292.1,5
*REBAR LAYER
STIR5,400,355.6,0,REINF,90,1
*SHELL SECTION,ELSET=WEBSEC5,MATERIAL=CONGIR
177.8,5
*REBAR LAYER
STIR5,400,355.6,0,REINF,90,1
*SHELL SECTION,ELSET=BOTCHAMSEC5,MATERIAL=CONGIR
368.3,5
*REBAR LAYER
STIR5,400,355.6,0,REINF,90,1
*SHELL SECTION,ELSET=BOTFLANGESEC5,MATERIAL=CONGIR
558.8,5
*REBAR LAYER
STIR5,400,355.6,0,REINF,90,1
**
*****SECTION6*****
**
*SHELL SECTION,ELSET=TOPFLANGESEC6,MATERIAL=CONGIR
406.4,5
*SHELL SECTION,ELSET=TOPCHAMSEC6,MATERIAL=CONGIR
292.1,5
*SHELL SECTION,ELSET=WEBSEC6,MATERIAL=CONGIR
177.8,5
*SHELL SECTION,ELSET=BOTCHAMSEC6,MATERIAL=CONGIR
368.3,5
*SHELL SECTION,ELSET=BOTFLANGESEC6,MATERIAL=CONGIR
558.8,5
**
*****SECTION7*****
**
*SHELL SECTION,ELSET=TOPFLANGESEC7,MATERIAL=CONGIR
406.4,5
*REBAR LAYER
STIR7,400,609.6,0,REINF,90,1
*SHELL SECTION,ELSET=TOPCHAMSEC7,MATERIAL=CONGIR
292.1,5
*REBAR LAYER
STIR7,400,609.6,0,REINF,90,1
*SHELL SECTION,ELSET=WEBSEC7,MATERIAL=CONGIR
177.8,5

```

```

*REBAR LAYER
STIR7,400,609.6,0,REINF,90,1
*SHELL SECTION,ELSET=BOTCHAMSEC7,MATERIAL=CONGIR
368.3,5
*REBAR LAYER
STIR7,400,609.6,0,REINF,90,1
*SHELL SECTION,ELSET=BOTFLANGESEC7,MATERIAL=CONGIR
558.8,5
*REBAR LAYER
STIR7,400,609.6,0,REINF,90,1
**
*****SECTION8*****
**
*SHELL SECTION,ELSET=TOPFLANGESEC8,MATERIAL=CONGIR
406.4,5
*SHELL SECTION,ELSET=TOPCHAMSEC8,MATERIAL=CONGIR
292.1,5
*SHELL SECTION,ELSET=WEBSEC8,MATERIAL=CONGIR
177.8,5
*SHELL SECTION,ELSET=BOTCHAMSEC8,MATERIAL=CONGIR
368.3,5
*SHELL SECTION,ELSET=BOTFLANGESEC8,MATERIAL=CONGIR
558.8,5
**
*****PRESTRESSING STEEL*****
**
*SOLID SECTION,ELSET=PRE1,MATERIAL=PRESTEEL
594
*SOLID SECTION,ELSET=PRE2,MATERIAL=PRESTEEL
792
*SOLID SECTION,ELSET=PRE3,MATERIAL=PRESTEEL
1188
**
*MATERIAL,NAME=PRESTEEL
*DENSITY
7850E-9
*ELASTIC
200000,0.3
*PLASTIC
1690
**
*****CARBON FRP*****
**
*MEMBRANE SECTION,ELSET=FRPTOPCHAM,MATERIAL=FRP1
1
*MEMBRANE SECTION,ELSET=FRPBOTCHAM,MATERIAL=FRP1
1
*MEMBRANE SECTION,ELSET=FRPUWRAPS,MATERIAL=FRP2
1
*MATERIAL,NAME=FRP1
*ELASTIC,TYPE=LAMINA
102000,0.01,0.0001,0.0001,0.0001,0.0001,0,0
*PLASTIC
1062,0
**
*MATERIAL,NAME=FRP2
*ELASTIC,TYPE=LAMINA
0.01,102000,0.0001,0.0001,0.0001,0.0001,0,0
*PLASTIC
1062,0
**
*****PRESTRESSING OF TENDONS*****
**
*INITIAL CONDITIONS,TYPE=STRESS
PRE1,1060
PRE2,1060
PRE3,1060
**
*****BOUNDARY CONDITIONS*****
**
*NGEN,NSET=SYMMSLABSUPP
5502,5534,2
*NGEN,NSET=SYMMGIRDSUPP
11118,143142,5501
*NSET,NSET=BOTTOMENDSUPP
137742
*BOUNDARY
SYMMSLABSUPP,1
SYMMSLABSUPP,4
SYMMGIRDSUPP,1
SYMMGIRDSUPP,4

```

```

BOTTOMENDSUPP,2,3
**
*****DEAD LOAD*****
**
*ELSET,ELSET=ENTIREGIRDER,GENERATE
881,2255,1
**
*NSET,NSET=RE1
137742
*NSET,NSET=RE2
143142
**
*ELSET,ELSET=EBOTTOMFLANGE,GENERATE
1977,1980,1
2032,2035,1
2087,2090,1
2142,2145,1
2197,2200,1
2252,2255,1
**
*STEP,NLGEOM
*STATIC
*DLOAD
SLAB,GRAV,9.81,0,0,-1
ENTIREGIRDER,GRAV,9.81,0,0,-1
*ELPRINT,POSITION=AVERAGED AT NODES,ELSET=EBOTTOMFLANGE
S11
*ENDSTEP
**
*****BLOCK AND BARRIER LOADING*****
**
*NGEN,NSET=LOADNODES
318,5418,100
**
*NSET,NSET=NOUTPUT
5418
**
*ELSET,ELSET=EOUTPUT,GENERATE
840,841,1
856,857,1
**
*STEP,INC=5000
*STATIC,RIKS
0.1,1.0,1E-40,0.5
*CLOAD
LOADNODES,3,-13000
**
*OUTPUT,HISTORY,OP=ADD
*NODE, OUTPUT,NSET=NOUTPUT
U3,CF3
*ELEMENT OUTPUT,ELSET=EOUTPUT
SE1
*ENDSTEP
**

```

DT-41 GIRDER ABAQUS INPUT FILE

ABAQUS input file for DT-41 strengthened with CFRP, using membrane elements.

```

*HEADING
2D LINE MODEL OF PRESTRESSED DT-41 GIRDER (N,mm);NLGEOM, CFRP MEMBRANE
*PREPRINT,ECHO=YES,MODEL=NO,HISTORY=NO
**RESTART,WRITE
**
*****REFERENCE NODAL COORDINATES - SLAB,GIRDER WEBS*****
**
*NODE
2,      -8400,      0,      0
64,      -8400,      3100,      0
4202,      0,      0,      0
4264,      0,      3100,      0
*****
68,      -8300,      800,      0
118,      -8200,      800,      0
4368,      -8300,      800,      -50
4418,      -8200,      800,      -50
42177,      -8300,      800,      -500
**
98,      -8300,      2300,      0
148,      -8200,      2300,      0
4398,      -8300,      2300,      -50
4448,      -8200,      2300,      -50
42207,      -8300,      2300,      -500
*****
4318,      -8400,      800,      -50
42127,      -8400,      800,      -500
8518,      0,      800,      -50
67332,      0,      800,      -750
*****
42227,      -8200,      800,      -500
63232,      -8200,      800,      -750
*****
4348,      -8400,      2300,      -50
42157,      -8400,      2300,      -500
8548,      0,      2300,      -50
67362,      0,      2300,      -750
*****
42257,      -8200,      2300,      -500
63262,      -8200,      2300,      -750
**
*****NODE GENERATION FOR SLAB*****
**
*NGEN,NSET=NEND
2,64,2
4202,4264,2
*NGEN,NSET=NSLAB
2,4202,100
4,4204,100
6,4206,100
8,4208,100
10,4210,100
12,4212,100
14,4214,100
16,4216,100
18,4218,100
20,4220,100
22,4222,100
24,4224,100
26,4226,100
28,4228,100
30,4230,100
32,4232,100
34,4234,100
36,4236,100
38,4238,100
40,4240,100
42,4242,100
44,4244,100

```

```

46,4246,100
48,4248,100
50,4250,100
52,4252,100
54,4254,100
56,4256,100
58,4258,100
60,4260,100
62,4262,100
64,4264,100
**
*****NODE GENERATION FOR WEBS (ENDS)*****
**
*NGEN,NSET=NWEBENDS1
18,4318,4300
4218,8518,4300
48,4348,4300
4248,8548,4300
*****
4318,42127,4201
8518,67332,4201
4348,42157,4201
8548,67362,4201
*****
42227,63232,4201
42257,63262,4201
**
*****NODE GENERATION FOR WEBS (SUPPORT LINE)*****
**
*NGEN,NSET=NMIDSUPP1
68,4368,4300
4368,42177,4201
118,4418,4300
4418,42227,4201
*****
98,4398,4300
4398,42207,4201
148,4448,4300
4448,42257,4201
**
*****NODE GENERATION FOR WEBS (LONG)*****
**
*NGEN,NSET=NWEBLONG
4318,4418,50
4418,8518,100
8519,8619,50
8619,12719,100
12720,12820,50
12820,16920,100
16921,17021,50
17021,21121,100
21122,21222,50
21222,25322,100
25323,25423,50
25423,29523,100
29524,29624,50
29624,33724,100
33725,33825,50
33825,37925,100
37926,38026,50
38026,42126,100
42127,42227,50
42227,46327,100
**
46428,50528,100
50629,54729,100
54830,58930,100
59031,63131,100
63232,67332,100
*****
4348,4448,50
4448,8548,100
8549,8649,50
8649,12749,100
12750,12850,50
12850,16950,100
16951,17051,50
17051,21151,100
21152,21252,50
21252,25352,100
25353,25453,50

```

```

25453,29553,100
29554,29654,50
29654,33754,100
33755,33855,50
33855,37955,100
37956,38056,50
38056,42156,100
42157,42257,50
42257,46357,100
**
46458,50558,100
50659,54759,100
54860,58960,100
59061,63161,100
63262,67362,100
**
*****ELEMENT GENERATION FOR THE SLAB*****
**
*ELEMENT,TYPE=S4R
1,2,102,104,4
*ELGEN,ELSET=SLAB
1,42,100,31,31,2,1
**
*****ELEMENT GENERATION FOR GIRDER WEBS*****
**
*ELEMENT,TYPE=S4R
1303,4318,4368,68,18
1305,8519,8569,4368,4318
1323,4418,4518,218,118
1364,8619,8719,4518,4418
*ELGEN,ELSET=WEB1
1303,2,50,1
1305,2,50,9,9,4201,1
1323,41,100,1
1364,41,100,14,14,4201,1
**
*ELEMENT,TYPE=S4R
1938,4348,4398,98,48
1940,8549,8599,4398,4348
1958,4448,4548,248,148
1999,8649,8749,4548,4448
*ELGEN,ELSET=WEB2
1938,2,50,1
1940,2,50,9,9,4201,1
1958,41,100,1
1999,41,100,14,14,4201,1
**
*****ELEMENT GENERATION FOR CFRP*****
**
*ELEMENT,TYPE=M3D4R
3155,12720,12770,8569,8519
*ELGEN,ELSET=FRP1WEB1
3155,2,50,8,8,4201,1
*ELEMENT,TYPE=M3D4R
3173,12720,12770,8569,8519
3191,12820,12920,8719,8619
*ELGEN,ELSET=FRP2WEB1
3173,2,50,8,8,4201,1
3191,7,100,13,13,4201,1
*ELEMENT,TYPE=M3D4R
3282,35725,35825,31624,31524
*ELGEN,ELSET=FRP3WEB1
3282,22,100,8,8,4201,1
*****
*ELEMENT,TYPE=M3D4R
3458,12750,12800,8599,8549
*ELGEN,ELSET=FRP1WEB2
3458,2,50,8,8,4201,1
*ELEMENT,TYPE=M3D4R
3476,12750,12800,8599,8549
3494,12850,12950,8749,8649
*ELGEN,ELSET=FRP2WEB2
3476,2,50,8,8,4201,1
3494,7,100,13,13,4201,1
*ELEMENT,TYPE=M3D4R
3585,35755,35855,31654,31554
*ELGEN,ELSET=FRP3WEB2
3585,22,100,8,8,4201,1
**
*****ELEMENT SET ASSIGNMENT*****
*****R-LONG REBAR

```

```

*****S-VERT REBAR
*****W-MESH
*****ELEMENT SET ASSIGNMENT - SEC1 (NO MESH-AT SUPPORT)*****
**
*ELSET,ELSET=WEB1A1,GENERATE
1303,1304,1
*ELSET,ELSET=WEB1RSB1,GENERATE
1305,1314,9
*ELSET,ELSET=WEB1SC1,GENERATE
1306,1315,9
*ELSET,ELSET=WEB1SD1,GENERATE
1307,1316,9
*ELSET,ELSET=WEB1SE1,GENERATE
1308,1317,9
*ELSET,ELSET=WEB1RSF1,GENERATE
1309,1318,9
*ELSET,ELSET=WEB1SG1,GENERATE
1310,1319,9
*ELSET,ELSET=WEB1SH1,GENERATE
1311,1320,9
*ELSET,ELSET=WEB1SI1,GENERATE
1312,1321,9
*ELSET,ELSET=WEB1RSJ1,GENERATE
1313,1322,9
*****
*ELSET,ELSET=WEB2A1,GENERATE
1938,1939,1
*ELSET,ELSET=WEB2RSB1,GENERATE
1940,1949,9
*ELSET,ELSET=WEB2SC1,GENERATE
1941,1950,9
*ELSET,ELSET=WEB2SD1,GENERATE
1942,1951,9
*ELSET,ELSET=WEB2SE1,GENERATE
1943,1952,9
*ELSET,ELSET=WEB2RSF1,GENERATE
1944,1953,9
*ELSET,ELSET=WEB2SG1,GENERATE
1945,1954,9
*ELSET,ELSET=WEB2SH1,GENERATE
1946,1955,9
*ELSET,ELSET=WEB2SI1,GENERATE
1947,1956,9
*ELSET,ELSET=WEB2RSJ1,GENERATE
1948,1957,9
**
*****ELEMENT SET ASSIGNMENT - SEC2 (MESH)*****
**
*ELSET,ELSET=WEB1RSWB2
1364
*ELSET,ELSET=WEB1SWC2
1365
*ELSET,ELSET=WEB1SWD2
1366
*ELSET,ELSET=WEB1SWE2
1367
*ELSET,ELSET=WEB1RSWF2
1368
*ELSET,ELSET=WEB1SWG2
1369
*ELSET,ELSET=WEB1SWH2
1370
*ELSET,ELSET=WEB1SWI2
1371
*ELSET,ELSET=WEB1RSWJ2
1372
*ELSET,ELSET=WEB1SWK2
1373
*ELSET,ELSET=WEB1SWL2
1374
*ELSET,ELSET=WEB1SWM2
1375
*ELSET,ELSET=WEB1RSWN2
1376
**
*ELSET,ELSET=WEB1WA2,GENERATE
1323,1353,1
*ELSET,ELSET=WEB1RWB2,GENERATE
1378,1406,14
*ELSET,ELSET=WEB1WB2,GENERATE
1420,1784,14

```

```

*ELSET,ELSET=WEB1WC2,GENERATE
1379,1785,14
*ELSET,ELSET=WEB1WD2,GENERATE
1380,1786,14
*ELSET,ELSET=WEB1WE2,GENERATE
1381,1787,14
*ELSET,ELSET=WEB1RWF2,GENERATE
1382,1410,14
*ELSET,ELSET=WEB1WF2,GENERATE
1424,1788,14
*ELSET,ELSET=WEB1WG2,GENERATE
1383,1789,14
*ELSET,ELSET=WEB1WH2,GENERATE
1384,1790,14
*ELSET,ELSET=WEB1WI2,GENERATE
1385,1791,14
*ELSET,ELSET=WEB1RWJ2,GENERATE
1386,1456,14
*ELSET,ELSET=WEB1WJ2,GENERATE
1470,1792,14
*ELSET,ELSET=WEB1WK2,GENERATE
1387,1793,14
*ELSET,ELSET=WEB1WL2,GENERATE
1388,1794,14
*ELSET,ELSET=WEB1WM2,GENERATE
1389,1795,14
*ELSET,ELSET=WEB1RWN2
1390
*ELSET,ELSET=WEB1WN2,GENERATE
1404,1796,14
*ELSET,ELSET=WEB1WO2,GENERATE
1377,1797,14
*****
*ELSET,ELSET=WEB2RSWB2
1999
*ELSET,ELSET=WEB2SWC2
2000
*ELSET,ELSET=WEB2SWD2
2001
*ELSET,ELSET=WEB2SWE2
2002
*ELSET,ELSET=WEB2RSWF2
2003
*ELSET,ELSET=WEB2SWG2
2004
*ELSET,ELSET=WEB2SWH2
2005
*ELSET,ELSET=WEB2SWI2
2006
*ELSET,ELSET=WEB2RSWJ2
2007
*ELSET,ELSET=WEB2SWK2
2008
*ELSET,ELSET=WEB2SWL2
2009
*ELSET,ELSET=WEB2SWM2
2010
*ELSET,ELSET=WEB2RSWN2
2011
**
*ELSET,ELSET=WEB2WA2,GENERATE
1958,1988,1
*ELSET,ELSET=WEB2RWB2,GENERATE
2013,2041,14
*ELSET,ELSET=WEB2WB2,GENERATE
2055,2419,14
*ELSET,ELSET=WEB2WC2,GENERATE
2014,2420,14
*ELSET,ELSET=WEB2WD2,GENERATE
2015,2421,14
*ELSET,ELSET=WEB2WE2,GENERATE
2016,2422,14
*ELSET,ELSET=WEB2RWF2,GENERATE
2017,2045,14
*ELSET,ELSET=WEB2WF2,GENERATE
2059,2423,14
*ELSET,ELSET=WEB2WG2,GENERATE
2018,2424,14
*ELSET,ELSET=WEB2WH2,GENERATE
2019,2425,14
*ELSET,ELSET=WEB2WI2,GENERATE

```

```

2020,2426,14
*ELSET,ELSET=WEB2RWJ2,GENERATE
2021,2091,14
*ELSET,ELSET=WEB2WJ2,GENERATE
2105,2427,14
*ELSET,ELSET=WEB2WK2,GENERATE
2022,2428,14
*ELSET,ELSET=WEB2WL2,GENERATE
2023,2429,14
*ELSET,ELSET=WEB2WM2,GENERATE
2024,2430,14
*ELSET,ELSET=WEB2RWN2
2025
*ELSET,ELSET=WEB2WN2,GENERATE
2039,2431,14
*ELSET,ELSET=WEB2WO2,GENERATE
2012,2432,14
**
*****ELEMENT SET ASSIGNMENT - SEC3 (END-NO MESH)*****
**
*ELSET,ELSET=WEB1A3,GENERATE
1354,1363,1
*ELSET,ELSET=WEB1B3,GENERATE
1798,1924,14
*ELSET,ELSET=WEB1C3,GENERATE
1799,1925,14
*ELSET,ELSET=WEB1D3,GENERATE
1800,1926,14
*ELSET,ELSET=WEB1E3,GENERATE
1801,1927,14
*ELSET,ELSET=WEB1F3,GENERATE
1802,1928,14
*ELSET,ELSET=WEB1G3,GENERATE
1803,1929,14
*ELSET,ELSET=WEB1H3,GENERATE
1804,1930,14
*ELSET,ELSET=WEB1I3,GENERATE
1805,1931,14
*ELSET,ELSET=WEB1J3,GENERATE
1806,1932,14
*ELSET,ELSET=WEB1K3,GENERATE
1807,1933,14
*ELSET,ELSET=WEB1L3,GENERATE
1808,1934,14
*ELSET,ELSET=WEB1M3,GENERATE
1809,1935,14
*ELSET,ELSET=WEB1N3,GENERATE
1810,1936,14
*ELSET,ELSET=WEB1O3,GENERATE
1811,1937,14
*****
*ELSET,ELSET=WEB2A3,GENERATE
1989,1998,1
*ELSET,ELSET=WEB2B3,GENERATE
2433,2559,14
*ELSET,ELSET=WEB2C3,GENERATE
2434,2560,14
*ELSET,ELSET=WEB2D3,GENERATE
2435,2561,14
*ELSET,ELSET=WEB2E3,GENERATE
2436,2562,14
*ELSET,ELSET=WEB2F3,GENERATE
2437,2563,14
*ELSET,ELSET=WEB2G3,GENERATE
2438,2564,14
*ELSET,ELSET=WEB2H3,GENERATE
2439,2565,14
*ELSET,ELSET=WEB2I3,GENERATE
2440,2566,14
*ELSET,ELSET=WEB2J3,GENERATE
2441,2567,14
*ELSET,ELSET=WEB2K3,GENERATE
2442,2568,14
*ELSET,ELSET=WEB2L3,GENERATE
2443,2569,14
*ELSET,ELSET=WEB2M3,GENERATE
2444,2570,14
*ELSET,ELSET=WEB2N3,GENERATE
2445,2571,14
*ELSET,ELSET=WEB2O3,GENERATE
2446,2572,14

```

```

**
*****ELEMENT SET ASSIGNMENT FOR WEBS (BY SEC-TO VERIFY)*****
**
*ELSET,ELSET=WEB1SEC1
WEB1A1
WEB1RSB1
WEB1SC1
WEB1SD1
WEB1SE1
WEB1RSF1
WEB1SG1
WEB1SH1
WEB1SI1
WEB1RSJ1
*ELSET,ELSET=WEB1SEC2
WEB1RSWB2
WEB1SWC2
WEB1SWD2
WEB1SWE2
WEB1RSWF2
WEB1SWG2
WEB1SWH2
WEB1SWI2
WEB1RSWJ2
WEB1SWK2
WEB1SWL2
WEB1SWM2
WEB1RSWN2
WEB1WA2
WEB1RWB2
WEB1WB2
WEB1WC2
WEB1WD2
WEB1WE2
WEB1RWF2
WEB1WF2
WEB1WG2
WEB1WH2
WEB1WI2
WEB1RWJ2
WEB1WJ2
WEB1WK2
WEB1WL2
WEB1WM2
WEB1RWN2
WEB1WN2
WEB1WO2
*ELSET,ELSET=WEB1SEC3
WEB1A3
WEB1B3
WEB1C3
WEB1D3
WEB1E3
WEB1F3
WEB1G3
WEB1H3
WEB1I3
WEB1J3
WEB1K3
WEB1L3
WEB1M3
WEB1N3
WEB1O3
*****
*ELSET,ELSET=WEB2SEC1
WEB2A1
WEB2RSB1
WEB2SC1
WEB2SD1
WEB2SE1
WEB2RSF1
WEB2SG1
WEB2SH1
WEB2SI1
WEB2RSJ1
*ELSET,ELSET=WEB2SEC2
WEB2RSWB2
WEB2SWC2
WEB2SWD2
WEB2SWE2
WEB2RSWF2

```



```

WEB2SWG2
WEB2SWH2
WEB2SWI2
WEB2RSWJ2
WEB2SWK2
WEB2SWL2
WEB2SWM2
WEB2RSWN2
WEB2WA2
WEB2RWB2
WEB2WB2
WEB2WC2
WEB2WD2
WEB2WE2
WEB2RWF2
WEB2WF2
WEB2WG2
WEB2WH2
WEB2WI2
WEB2RWJ2
WEB2WJ2
WEB2WK2
WEB2WL2
WEB2WM2
WEB2RWN2
WEB2WN2
WEB2WO2
*ELSET,ELSET=WEB2SEC3
WEB2A3
WEB2B3
WEB2C3
WEB2D3
WEB2E3
WEB2F3
WEB2G3
WEB2H3
WEB2I3
WEB2J3
WEB2K3
WEB2L3
WEB2M3
WEB2N3
WEB2O3
**
*****ELEMENT GENERATION FOR PRESTRESSING TENDONS*****
**
*ELEMENT,TYPE=T2D2
2573,59031,59131
*ELGEN,ELSET=LPRE1
2573,41,100,1
*ELEMENT,TYPE=T2D2
2614,54830,54930
*ELGEN,ELSET=LPRE2
2614,41,100,1
*ELEMENT,TYPE=T2D2
2655,50629,50729
*ELGEN,ELSET=LPRE3
2655,41,100,1
*ELEMENT,TYPE=T2D2
2696,46428,46528
*ELGEN,ELSET=LPRE4
2696,41,100,1
*ELEMENT,TYPE=T2D2
2737,42227,42327
*ELGEN,ELSET=LPRE5
2737,41,100,1
*ELEMENT,TYPE=T2D2
2778,29524,29574
2780,29624,29724
*ELGEN,ELSET=LPRE6
2778,2,50,1
2780,41,100,1
*ELEMENT,TYPE=T2D2
2821,25323,25373
2823,25423,25523
*ELGEN,ELSET=LPRE7
2821,2,50,1
2823,41,100,1
*****
*ELEMENT,TYPE=T2D2
2864,59061,59161

```

```

*ELGEN,ELSET=RPRE1
2864,41,100,1
*ELEMENT,TYPE=T2D2
2905,54860,54960
*ELGEN,ELSET=RPRE2
2905,41,100,1
*ELEMENT,TYPE=T2D2
2946,50659,50759
*ELGEN,ELSET=RPRE3
2946,41,100,1
*ELEMENT,TYPE=T2D2
2987,46458,46558
*ELGEN,ELSET=RPRE4
2987,41,100,1
*ELEMENT,TYPE=T2D2
3028,42257,42357
*ELGEN,ELSET=RPRE5
3028,41,100,1
*ELEMENT,TYPE=T2D2
3069,29554,29604
3071,29654,29754
*ELGEN,ELSET=RPRE6
3069,2,50,1
3071,41,100,1
*ELEMENT,TYPE=T2D2
3112,25353,25403
3114,25453,25553
*ELGEN,ELSET=RPRE7
3112,2,50,1
3114,41,100,1
**
*****MATERIAL PROPERTIES*****
**
*SHELL SECTION,ELSET=SLAB,MATERIAL=CON
100,5
*REBAR LAYER
LONG,25.8,102,0,WWF,0,1
TRANS,18.7,300,0,WWF,90,1
*MATERIAL,NAME=WWF
*DENSITY
7850E-9
*ELASTIC
200000,0.3
*PLASTIC
450
*MATERIAL,NAME=CON
*DENSITY
2400E-9
*ELASTIC
24000,0.2
*CONCRETE
14,0
35,0.0015
*FAILURE RATIOS
1.16,0.0836
*TENSION STIFFENING
1,0
0,0.002
*SHEAR RETENTION
1,1E+6
*MATERIAL,NAME=REINF
*DENSITY
7850E-9
*ELASTIC
200000,0.3
*PLASTIC
400
**
*****WEB1*****
**
*****SECTION1*****
**
*SHELL SECTION,ELSET=WEB1A1,MATERIAL=CON
170,5
*SHELL SECTION,ELSET=WEB1RSB1,MATERIAL=CON
167.5,5
*REBAR LAYER
LONG1,100,50,0,REINF,0,1
VERT1,100,200,0,REINF,90,1
*SHELL SECTION,ELSET=WEB1SC1,MATERIAL=CON
162.5,5

```

```

*REBAR LAYER
VERT1,100,200,0,REINF,90,1
*SHELL SECTION,ELSET=WEB1SD1,MATERIAL=CON
157.5,5
*REBAR LAYER
VERT1,100,200,0,REINF,90,1
*SHELL SECTION,ELSET=WEB1SE1,MATERIAL=CON
152.5,5
*REBAR LAYER
VERT1,100,200,0,REINF,90,1
*SHELL SECTION,ELSET=WEB1RSF1,MATERIAL=CON
147.5,5
*REBAR LAYER
LONG2,100,50,0,REINF,0,1
VERT1,100,200,0,REINF,90,1
*SHELL SECTION,ELSET=WEB1SG1,MATERIAL=CON
142.5,5
*REBAR LAYER
VERT1,100,200,0,REINF,90,1
*SHELL SECTION,ELSET=WEB1SH1,MATERIAL=CON
137.5,5
*REBAR LAYER
VERT1,100,200,0,REINF,90,1
*SHELL SECTION,ELSET=WEB1SI1,MATERIAL=CON
132.5,5
*REBAR LAYER
VERT1,100,200,0,REINF,90,1
*SHELL SECTION,ELSET=WEB1RSJ1,MATERIAL=CON
127.5,5
*REBAR LAYER
LONG3,300,50,0,REINF,0,1
VERT1,100,200,0,REINF,90,1
**
*****WEB1 SECTION2 - 1ST COLUMN*****
**
*SHELL SECTION,ELSET=WEB1RSWB2,MATERIAL=CON
167.5,5
*REBAR LAYER
LONG1,100,50,0,REINF,0,1
VERT2,600,200,0,REINF,90,1
HORIZ,25.8,102,0,WWF,0,1
VERT,25.8,102,0,WWF,90,1
*SHELL SECTION,ELSET=WEB1SWC2,MATERIAL=CON
162.5,5
*REBAR LAYER
VERT2,600,200,0,REINF,90,1
HORIZ,25.8,102,0,WWF,0,1
VERT,25.8,102,0,WWF,90,1
*SHELL SECTION,ELSET=WEB1SWD2,MATERIAL=CON
157.5,5
*REBAR LAYER
VERT2,600,200,0,REINF,90,1
HORIZ,25.8,102,0,WWF,0,1
VERT,25.8,102,0,WWF,90,1
*SHELL SECTION,ELSET=WEB1SWE2,MATERIAL=CON
152.5,5
*REBAR LAYER
VERT2,600,200,0,REINF,90,1
HORIZ,25.8,102,0,WWF,0,1
VERT,25.8,102,0,WWF,90,1
*SHELL SECTION,ELSET=WEB1RSWF2,MATERIAL=CON
147.5,5
*REBAR LAYER
LONG2,100,50,0,REINF,0,1
VERT2,600,200,0,REINF,90,1
HORIZ,25.8,102,0,WWF,0,1
VERT,25.8,102,0,WWF,90,1
*SHELL SECTION,ELSET=WEB1SWG2,MATERIAL=CON
142.5,5
*REBAR LAYER
VERT2,600,200,0,REINF,90,1
HORIZ,25.8,102,0,WWF,0,1
VERT,25.8,102,0,WWF,90,1
*SHELL SECTION,ELSET=WEB1SWH2,MATERIAL=CON
137.5,5
*REBAR LAYER
VERT2,600,200,0,REINF,90,1
HORIZ,25.8,102,0,WWF,0,1
VERT,25.8,102,0,WWF,90,1
*SHELL SECTION,ELSET=WEB1SWI2,MATERIAL=CON
132.5,5

```

```

*REBAR LAYER
VERT2,600,200,0,REINF,90,1
HORIZ,25.8,102,0,WWF,0,1
VERT,25.8,102,0,WWF,90,1
*SHELL SECTION,ELSET=WEB1RSWJ2,MATERIAL=CON
127.5,5
*REBAR LAYER
LONG3,300,50,0,REINF,0,1
VERT2,600,200,0,REINF,90,1
HORIZ,25.8,102,0,WWF,0,1
VERT,25.8,102,0,WWF,90,1
*SHELL SECTION,ELSET=WEB1SWK2,MATERIAL=CON
122.5,5
*REBAR LAYER
VERT2,600,200,0,REINF,90,1
HORIZ,25.8,102,0,WWF,0,1
VERT,25.8,102,0,WWF,90,1
*SHELL SECTION,ELSET=WEB1SWL2,MATERIAL=CON
117.5,5
*REBAR LAYER
VERT2,600,200,0,REINF,90,1
HORIZ,25.8,102,0,WWF,0,1
VERT,25.8,102,0,WWF,90,1
*SHELL SECTION,ELSET=WEB1SWM2,MATERIAL=CON
112.5,5
*REBAR LAYER
VERT2,600,200,0,REINF,90,1
HORIZ,25.8,102,0,WWF,0,1
VERT,25.8,102,0,WWF,90,1
*SHELL SECTION,ELSET=WEB1RSWN2,MATERIAL=CON
107.5,5
*REBAR LAYER
LONG4,600,50,0,REINF,0,1
VERT2,600,200,0,REINF,90,1
HORIZ,25.8,102,0,WWF,0,1
VERT,25.8,102,0,WWF,90,1
**
*****WEB1 SECTION2 - MESH*****
**
*SHELL SECTION,ELSET=WEB1WA2,MATERIAL=CON
170,5
*REBAR LAYER
HORIZ,25.8,102,0,WWF,0,1
VERT,25.8,102,0,WWF,90,1
*SHELL SECTION,ELSET=WEB1RWB2,MATERIAL=CON
167.5,5
*REBAR LAYER
LONG1,100,50,0,REINF,0,1
HORIZ,25.8,102,0,WWF,0,1
VERT,25.8,102,0,WWF,90,1
*SHELL SECTION,ELSET=WEB1WB2,MATERIAL=CON
167.5,5
*REBAR LAYER
HORIZ,25.8,102,0,WWF,0,1
VERT,25.8,102,0,WWF,90,1
*SHELL SECTION,ELSET=WEB1WC2,MATERIAL=CON
162.5,5
*REBAR LAYER
HORIZ,25.8,102,0,WWF,0,1
VERT,25.8,102,0,WWF,90,1
*SHELL SECTION,ELSET=WEB1WD2,MATERIAL=CON
157.5,5
*REBAR LAYER
HORIZ,25.8,102,0,WWF,0,1
VERT,25.8,102,0,WWF,90,1
*SHELL SECTION,ELSET=WEB1WE2,MATERIAL=CON
152.5,5
*REBAR LAYER
HORIZ,25.8,102,0,WWF,0,1
VERT,25.8,102,0,WWF,90,1
*SHELL SECTION,ELSET=WEB1RWF2,MATERIAL=CON
147.5,5
*REBAR LAYER
LONG2,100,50,0,REINF,0,1
HORIZ,25.8,102,0,WWF,0,1
VERT,25.8,102,0,WWF,90,1
*SHELL SECTION,ELSET=WEB1WF2,MATERIAL=CON
147.5,5
*REBAR LAYER
HORIZ,25.8,102,0,WWF,0,1
VERT,25.8,102,0,WWF,90,1

```

```

*SHELL SECTION,ELSET=WEB1WG2,MATERIAL=CON
142.5,5
*REBAR LAYER
HORIZ,25.8,102,0,WWF,0,1
VERT,25.8,102,0,WWF,90,1
*SHELL SECTION,ELSET=WEB1WH2,MATERIAL=CON
137.5,5
*REBAR LAYER
HORIZ,25.8,102,0,WWF,0,1
VERT,25.8,102,0,WWF,90,1
*SHELL SECTION,ELSET=WEB1WI2,MATERIAL=CON
132.5,5
*REBAR LAYER
HORIZ,25.8,102,0,WWF,0,1
VERT,25.8,102,0,WWF,90,1
*SHELL SECTION,ELSET=WEB1RWJ2,MATERIAL=CON
127.5,5
*REBAR LAYER
LONG3,300,50,0,REINF,0,1
HORIZ,25.8,102,0,WWF,0,1
VERT,25.8,102,0,WWF,90,1
*SHELL SECTION,ELSET=WEB1WJ2,MATERIAL=CON
127.5,5
*REBAR LAYER
HORIZ,25.8,102,0,WWF,0,1
VERT,25.8,102,0,WWF,90,1
*SHELL SECTION,ELSET=WEB1WK2,MATERIAL=CON
122.5,5
*REBAR LAYER
HORIZ,25.8,102,0,WWF,0,1
VERT,25.8,102,0,WWF,90,1
*SHELL SECTION,ELSET=WEB1WL2,MATERIAL=CON
117.5,5
*REBAR LAYER
HORIZ,25.8,102,0,WWF,0,1
VERT,25.8,102,0,WWF,90,1
*SHELL SECTION,ELSET=WEB1WM2,MATERIAL=CON
112.5,5
*REBAR LAYER
HORIZ,25.8,102,0,WWF,0,1
VERT,25.8,102,0,WWF,90,1
*SHELL SECTION,ELSET=WEB1RWN2,MATERIAL=CON
107.5,5
*REBAR LAYER
LONG4,600,50,0,REINF,0,1
HORIZ,25.8,102,0,WWF,0,1
VERT,25.8,102,0,WWF,90,1
*SHELL SECTION,ELSET=WEB1WN2,MATERIAL=CON
107.5,5
*REBAR LAYER
HORIZ,25.8,102,0,WWF,0,1
VERT,25.8,102,0,WWF,90,1
*SHELL SECTION,ELSET=WEB1WO2,MATERIAL=CON
102.5,5
*REBAR LAYER
HORIZ,25.8,102,0,WWF,0,1
VERT,25.8,102,0,WWF,90,1
**
*****WEB1 SECTION3 - NO MESH*****
**
*SHELL SECTION,ELSET=WEB1A3,MATERIAL=CON
170,5
*SHELL SECTION,ELSET=WEB1B3,MATERIAL=CON
167.5,5
*SHELL SECTION,ELSET=WEB1C3,MATERIAL=CON
162.5,5
*SHELL SECTION,ELSET=WEB1D3,MATERIAL=CON
157.5,5
*SHELL SECTION,ELSET=WEB1E3,MATERIAL=CON
152.5,5
*SHELL SECTION,ELSET=WEB1F3,MATERIAL=CON
147.5,5
*SHELL SECTION,ELSET=WEB1G3,MATERIAL=CON
142.5,5
*SHELL SECTION,ELSET=WEB1H3,MATERIAL=CON
137.5,5
*SHELL SECTION,ELSET=WEB1I3,MATERIAL=CON
132.5,5
*SHELL SECTION,ELSET=WEB1J3,MATERIAL=CON
127.5,5
*SHELL SECTION,ELSET=WEB1K3,MATERIAL=CON

```



```

122.5,5
*SHELL SECTION,ELSET=WEB1L3,MATERIAL=CON
117.5,5
*SHELL SECTION,ELSET=WEB1M3,MATERIAL=CON
112.5,5
*SHELL SECTION,ELSET=WEB1N3,MATERIAL=CON
107.5,5
*SHELL SECTION,ELSET=WEB1O3,MATERIAL=CON
102.5,5
**
*****WEB2*****
**
*****SECTION1*****
**
*SHELL SECTION,ELSET=WEB2A1,MATERIAL=CON
170,5
*SHELL SECTION,ELSET=WEB2RSB1,MATERIAL=CON
167.5,5
*REBAR LAYER
LONG1,100,50,0,REINF,0,1
VERT1,100,200,0,REINF,90,1
*SHELL SECTION,ELSET=WEB2SC1,MATERIAL=CON
162.5,5
*REBAR LAYER
VERT1,100,200,0,REINF,90,1
*SHELL SECTION,ELSET=WEB2SD1,MATERIAL=CON
157.5,5
*REBAR LAYER
VERT1,100,200,0,REINF,90,1
*SHELL SECTION,ELSET=WEB2SE1,MATERIAL=CON
152.5,5
*REBAR LAYER
VERT1,100,200,0,REINF,90,1
*SHELL SECTION,ELSET=WEB2RSF1,MATERIAL=CON
147.5,5
*REBAR LAYER
LONG2,100,50,0,REINF,0,1
VERT1,100,200,0,REINF,90,1
*SHELL SECTION,ELSET=WEB2SG1,MATERIAL=CON
142.5,5
*REBAR LAYER
VERT1,100,200,0,REINF,90,1
*SHELL SECTION,ELSET=WEB2SH1,MATERIAL=CON
137.5,5
*REBAR LAYER
VERT1,100,200,0,REINF,90,1
*SHELL SECTION,ELSET=WEB2SI1,MATERIAL=CON
132.5,5
*REBAR LAYER
VERT1,100,200,0,REINF,90,1
*SHELL SECTION,ELSET=WEB2RSJ1,MATERIAL=CON
127.5,5
*REBAR LAYER
LONG3,300,50,0,REINF,0,1
VERT1,100,200,0,REINF,90,1
**
*****WEB2 SECTION2 - 1ST COLUMN*****
**
*SHELL SECTION,ELSET=WEB2RSWB2,MATERIAL=CON
167.5,5
*REBAR LAYER
LONG1,100,50,0,REINF,0,1
VERT2,600,200,0,REINF,90,1
HORIZ,25.8,102,0,WWF,0,1
VERT,25.8,102,0,WWF,90,1
*SHELL SECTION,ELSET=WEB2SWC2,MATERIAL=CON
162.5,5
*REBAR LAYER
VERT2,600,200,0,REINF,90,1
HORIZ,25.8,102,0,WWF,0,1
VERT,25.8,102,0,WWF,90,1
*SHELL SECTION,ELSET=WEB2SWD2,MATERIAL=CON
157.5,5
*REBAR LAYER
VERT2,600,200,0,REINF,90,1
HORIZ,25.8,102,0,WWF,0,1
VERT,25.8,102,0,WWF,90,1
*SHELL SECTION,ELSET=WEB2SWE2,MATERIAL=CON
152.5,5
*REBAR LAYER
VERT2,600,200,0,REINF,90,1

```

```

HORIZ,25.8,102,0,WWF,0,1
VERT,25.8,102,0,WWF,90,1
*SHELL SECTION,ELSET=WEB2RSWF2,MATERIAL=CON
147.5,5
*REBAR LAYER
LONG2,100,50,0,REINF,0,1
VERT2,600,200,0,REINF,90,1
HORIZ,25.8,102,0,WWF,0,1
VERT,25.8,102,0,WWF,90,1
*SHELL SECTION,ELSET=WEB2SWG2,MATERIAL=CON
142.5,5
*REBAR LAYER
VERT2,600,200,0,REINF,90,1
HORIZ,25.8,102,0,WWF,0,1
VERT,25.8,102,0,WWF,90,1
*SHELL SECTION,ELSET=WEB2SWH2,MATERIAL=CON
137.5,5
*REBAR LAYER
VERT2,600,200,0,REINF,90,1
HORIZ,25.8,102,0,WWF,0,1
VERT,25.8,102,0,WWF,90,1
*SHELL SECTION,ELSET=WEB2SWI2,MATERIAL=CON
132.5,5
*REBAR LAYER
VERT2,600,200,0,REINF,90,1
HORIZ,25.8,102,0,WWF,0,1
VERT,25.8,102,0,WWF,90,1
*SHELL SECTION,ELSET=WEB2RSWJ2,MATERIAL=CON
127.5,5
*REBAR LAYER
LONG3,300,50,0,REINF,0,1
VERT2,600,200,0,REINF,90,1
HORIZ,25.8,102,0,WWF,0,1
VERT,25.8,102,0,WWF,90,1
*SHELL SECTION,ELSET=WEB2SWK2,MATERIAL=CON
122.5,5
*REBAR LAYER
VERT2,600,200,0,REINF,90,1
HORIZ,25.8,102,0,WWF,0,1
VERT,25.8,102,0,WWF,90,1
*SHELL SECTION,ELSET=WEB2SWL2,MATERIAL=CON
117.5,5
*REBAR LAYER
VERT2,600,200,0,REINF,90,1
HORIZ,25.8,102,0,WWF,0,1
VERT,25.8,102,0,WWF,90,1
*SHELL SECTION,ELSET=WEB2SWM2,MATERIAL=CON
112.5,5
*REBAR LAYER
VERT2,600,200,0,REINF,90,1
HORIZ,25.8,102,0,WWF,0,1
VERT,25.8,102,0,WWF,90,1
*SHELL SECTION,ELSET=WEB2RSWN2,MATERIAL=CON
107.5,5
*REBAR LAYER
LONG4,600,50,0,REINF,0,1
VERT2,600,200,0,REINF,90,1
HORIZ,25.8,102,0,WWF,0,1
VERT,25.8,102,0,WWF,90,1
**
*****WEB2 SECTION2 - MESH*****
**
*SHELL SECTION,ELSET=WEB2WA2,MATERIAL=CON
170,5
*REBAR LAYER
HORIZ,25.8,102,0,WWF,0,1
VERT,25.8,102,0,WWF,90,1
*SHELL SECTION,ELSET=WEB2RWB2,MATERIAL=CON
167.5,5
*REBAR LAYER
LONG1,100,50,0,REINF,0,1
HORIZ,25.8,102,0,WWF,0,1
VERT,25.8,102,0,WWF,90,1
*SHELL SECTION,ELSET=WEB2WB2,MATERIAL=CON
167.5,5
*REBAR LAYER
HORIZ,25.8,102,0,WWF,0,1
VERT,25.8,102,0,WWF,90,1
*SHELL SECTION,ELSET=WEB2WC2,MATERIAL=CON
162.5,5
*REBAR LAYER

```

```

HORIZ,25.8,102,0,WWF,0,1
VERT,25.8,102,0,WWF,90,1
*SHELL SECTION,ELSET=WEB2WD2,MATERIAL=CON
157.5,5
*REBAR LAYER
HORIZ,25.8,102,0,WWF,0,1
VERT,25.8,102,0,WWF,90,1
*SHELL SECTION,ELSET=WEB2WE2,MATERIAL=CON
152.5,5
*REBAR LAYER
HORIZ,25.8,102,0,WWF,0,1
VERT,25.8,102,0,WWF,90,1
*SHELL SECTION,ELSET=WEB2RWF2,MATERIAL=CON
147.5,5
*REBAR LAYER
LONG2,100,50,0,REINF,0,1
HORIZ,25.8,102,0,WWF,0,1
VERT,25.8,102,0,WWF,90,1
*SHELL SECTION,ELSET=WEB2WF2,MATERIAL=CON
147.5,5
*REBAR LAYER
HORIZ,25.8,102,0,WWF,0,1
VERT,25.8,102,0,WWF,90,1
*SHELL SECTION,ELSET=WEB2WG2,MATERIAL=CON
142.5,5
*REBAR LAYER
HORIZ,25.8,102,0,WWF,0,1
VERT,25.8,102,0,WWF,90,1
*SHELL SECTION,ELSET=WEB2WH2,MATERIAL=CON
137.5,5
*REBAR LAYER
HORIZ,25.8,102,0,WWF,0,1
VERT,25.8,102,0,WWF,90,1
*SHELL SECTION,ELSET=WEB2WI2,MATERIAL=CON
132.5,5
*REBAR LAYER
HORIZ,25.8,102,0,WWF,0,1
VERT,25.8,102,0,WWF,90,1
*SHELL SECTION,ELSET=WEB2RWJ2,MATERIAL=CON
127.5,5
*REBAR LAYER
LONG3,300,50,0,REINF,0,1
HORIZ,25.8,102,0,WWF,0,1
VERT,25.8,102,0,WWF,90,1
*SHELL SECTION,ELSET=WEB2WJ2,MATERIAL=CON
127.5,5
*REBAR LAYER
HORIZ,25.8,102,0,WWF,0,1
VERT,25.8,102,0,WWF,90,1
*SHELL SECTION,ELSET=WEB2WK2,MATERIAL=CON
122.5,5
*REBAR LAYER
HORIZ,25.8,102,0,WWF,0,1
VERT,25.8,102,0,WWF,90,1
*SHELL SECTION,ELSET=WEB2WL2,MATERIAL=CON
117.5,5
*REBAR LAYER
HORIZ,25.8,102,0,WWF,0,1
VERT,25.8,102,0,WWF,90,1
*SHELL SECTION,ELSET=WEB2WM2,MATERIAL=CON
112.5,5
*REBAR LAYER
HORIZ,25.8,102,0,WWF,0,1
VERT,25.8,102,0,WWF,90,1
*SHELL SECTION,ELSET=WEB2RWN2,MATERIAL=CON
107.5,5
*REBAR LAYER
LONG4,600,50,0,REINF,0,1
HORIZ,25.8,102,0,WWF,0,1
VERT,25.8,102,0,WWF,90,1
*SHELL SECTION,ELSET=WEB2WN2,MATERIAL=CON
107.5,5
*REBAR LAYER
HORIZ,25.8,102,0,WWF,0,1
VERT,25.8,102,0,WWF,90,1
*SHELL SECTION,ELSET=WEB2WO2,MATERIAL=CON
102.5,5
*REBAR LAYER
HORIZ,25.8,102,0,WWF,0,1
VERT,25.8,102,0,WWF,90,1
**

```

```

*****WEB2 SECTION3 - NO MESH*****
**
*SHELL SECTION,ELSET=WEB2A3,MATERIAL=CON
170,5
*SHELL SECTION,ELSET=WEB2B3,MATERIAL=CON
167.5,5
*SHELL SECTION,ELSET=WEB2C3,MATERIAL=CON
162.5,5
*SHELL SECTION,ELSET=WEB2D3,MATERIAL=CON
157.5,5
*SHELL SECTION,ELSET=WEB2E3,MATERIAL=CON
152.5,5
*SHELL SECTION,ELSET=WEB2F3,MATERIAL=CON
147.5,5
*SHELL SECTION,ELSET=WEB2G3,MATERIAL=CON
142.5,5
*SHELL SECTION,ELSET=WEB2H3,MATERIAL=CON
137.5,5
*SHELL SECTION,ELSET=WEB2I3,MATERIAL=CON
132.5,5
*SHELL SECTION,ELSET=WEB2J3,MATERIAL=CON
127.5,5
*SHELL SECTION,ELSET=WEB2K3,MATERIAL=CON
122.5,5
*SHELL SECTION,ELSET=WEB2L3,MATERIAL=CON
117.5,5
*SHELL SECTION,ELSET=WEB2M3,MATERIAL=CON
112.5,5
*SHELL SECTION,ELSET=WEB2N3,MATERIAL=CON
107.5,5
*SHELL SECTION,ELSET=WEB2O3,MATERIAL=CON
102.5,5
**
*****PRESTRESSING STEEL*****
**
*SOLID SECTION,ELSET=LPRE1,MATERIAL=PRESTEEL
99
*SOLID SECTION,ELSET=LPRE2,MATERIAL=PRESTEEL
99
*SOLID SECTION,ELSET=LPRE3,MATERIAL=PRESTEEL
99
*SOLID SECTION,ELSET=LPRE4,MATERIAL=PRESTEEL
99
*SOLID SECTION,ELSET=LPRE5,MATERIAL=PRESTEEL
99
*SOLID SECTION,ELSET=LPRE6,MATERIAL=PRESTEEL
99
*SOLID SECTION,ELSET=LPRE7,MATERIAL=PRESTEEL
99
*SOLID SECTION,ELSET=RPRE1,MATERIAL=PRESTEEL
99
*SOLID SECTION,ELSET=RPRE2,MATERIAL=PRESTEEL
99
*SOLID SECTION,ELSET=RPRE3,MATERIAL=PRESTEEL
99
*SOLID SECTION,ELSET=RPRE4,MATERIAL=PRESTEEL
99
*SOLID SECTION,ELSET=RPRE5,MATERIAL=PRESTEEL
99
*SOLID SECTION,ELSET=RPRE6,MATERIAL=PRESTEEL
99
*SOLID SECTION,ELSET=RPRE7,MATERIAL=PRESTEEL
99
*MATERIAL,NAME=PRESTEEL
*DENSITY
7850E-9
*ELASTIC
200000,0.3
*PLASTIC
1690
**
*****CARBON FRP*****
**
*MEMBRANE SECTION,ELSET=FRP1WEB1,MATERIAL=FRP
2
*MEMBRANE SECTION,ELSET=FRP2WEB1,MATERIAL=FRP
2
*MEMBRANE SECTION,ELSET=FRP3WEB1,MATERIAL=FRP
2
*MEMBRANE SECTION,ELSET=FRP1WEB2,MATERIAL=FRP
2

```

```

*MEMBRANE SECTION,ELSET=FRP2WEB2,MATERIAL=FRP
2
*MEMBRANE SECTION,ELSET=FRP3WEB2,MATERIAL=FRP
2
*MATERIAL,NAME=FRP
*ELASTIC,TYPE=LAMINA
72400,40.6,0.0001,0.0001,0.0001,0.0001,0,0
*PLASTIC
876,0
***44,0
***44,0.012
***44,0.024
**
*****PRESTRESSING OF TENDONS*****
**
*INITIAL CONDITIONS,TYPE=STRESS
LPRE1,1302
LPRE2,1302
LPRE3,1302
LPRE4,1302
LPRE5,1302
LPRE6,1302
LPRE7,1302
RPRE1,1302
RPRE2,1302
RPRE3,1302
RPRE4,1302
RPRE5,1302
RPRE6,1302
RPRE7,1302
**
*****BOUNDARY CONDITIONS (1/2 OF DT MODELED)*****
**
*NGEN,NSET=SLABSUPP
4202,4264,2
*NGEN,NSET=WEB1SUPP
8518,67332,4201
*NGEN,NSET=WEB2SUPP
8548,67362,4201
*NSET,NSET=WEB1BOTSUPP
42177
*NSET,NSET=WEB2BOTSUPP
42207
*BOUNDARY
SLABSUPP,1
SLABSUPP,4
***SLABSUPP,5
WEB1SUPP,1
WEB1SUPP,4
***WEB1SUPP,5
WEB2SUPP,1
WEB2SUPP,4
***WEB2SUPP,5
WEB1BOTSUPP,2,3
WEB2BOTSUPP,3
**
*****DEAD LOAD*****
**
*ELSET,ELSET=ENTIREDT,GENERATE
1303,2572,1
**
*NSET,NSET=RE1
42207,42177
*NSET,NSET=RE2
67362,67332
**
*ELSET,ELSET=EBOTTOMWEBS,GENERATE
1867,1937,14
1866,1936,14
1865,1935,14
1864,1934,14
2502,2572,14
2501,2571,14
2500,2570,14
2499,2569,14
**
*STEP,NLGEOM
*STATIC
*DLOAD
SLAB,GRAV,9.81,0,0,-1
ENTIREDT,GRAV,9.81,0,0,-1

```



```

*ELPRINT, POSITION=AVERAGED AT NODES, ELSET=EBOTTOMWEBS
S11
*ENDSTEP
**
*****BARRIER LOADING*****
**
*NGEN, NSET=LOADNODES
2618, 4118, 100
2648, 4148, 100
**
*NSET, NSET=NOUTPUT
67332, 67232, 67362, 67262, 4218, 4248
LOADNODES
**
*ELSET, ELSET=EOUTPUT, GENERATE
1210, 1302, 1
**
*STEP, INC=5000
*STATIC, RIKS
0.0005, 1.0, 1E-40, 0.5
*CLOAD
LOADNODES, 3, -5000
**
*OUTPUT, HISTORY, OP=ADD
*NODE OUTPUT, NSET=NOUTPUT
U3, CF3
*ELEMENT OUTPUT, ELSET=EOUTPUT
SE1
*ENDSTEP
**

```

DT-100 GIRDER ABAQUS INPUT FILE

ABAQUS input file for DT-100 strengthened with CFRP, using membrane elements.

```

*HEADING
2D LINE MODEL OF PRESTRESSED DT-100 GIRDER (N,mm);NLGEOM, CFRP MEMBRANE
*PREPRINT,ECHO=YES,MODEL=NO,HISTORY=NO
**RESTART,WRITE
**
*****REFERENCE NODAL COORDINATES - SLAB,GIRDER WEBS*****
**
*NODE
2,      -9600,      0,      0
48,      -9600,      2300,      0
4802,      0,      0,      0
4848,      0,      2300,      0
*****
60,      -9500,      400,      0
110,      -9400,      400,      0
4960,      -9500,      400,      -50
5010,      -9400,      400,      -50
43368,      -9500,      400,      -450
**
90,      -9500,      1900,      0
140,      -9400,      1900,      0
4990,      -9500,      1900,      -50
5040,      -9400,      1900,      -50
43398,      -9500,      1900,      -450
*****
4910,      -9600,      400,      -50
43318,      -9600,      400,      -450
9710,      0,      400,      -50
72123,      0,      400,      -700
*****
43418,      -9400,      400,      -450
67423,      -9400,      400,      -700
*****
4940,      -9600,      1900,      -50
43348,      -9600,      1900,      -450
9740,      0,      1900,      -50
72153,      0,      1900,      -700
*****
43448,      -9400,      1900,      -450
67453,      -9400,      1900,      -700
**
*****NODE GENERATION FOR SLAB*****
**
*NGEN,NSET=NEND
2,48,2
4802,4848,2
*NGEN,NSET=NSLAB
2,4802,100
4,4804,100
6,4806,100
8,4808,100
10,4810,100
12,4812,100
14,4814,100
16,4816,100
18,4818,100
20,4820,100
22,4822,100
24,4824,100
26,4826,100
28,4828,100
30,4830,100
32,4832,100
34,4834,100
36,4836,100
38,4838,100
40,4840,100
42,4842,100
44,4844,100

```

```

46,4846,100
48,4848,100
**
*****NODE GENERATION FOR WEBS (ENDS)*****
**
*NGEN,NSET=NWEBENDS1
10,4910,4900
4810,9710,4900
40,4940,4900
4840,9740,4900
*****
4910,43318,4801
9710,72123,4801
4940,43348,4801
9740,72153,4801
*****
43418,67423,4801
43448,67453,4801
**
*****NODE GENERATION FOR WEBS (SUPPORT LINE)*****
**
*NGEN,NSET=NMIDSUPP1
60,4960,4900
4960,43368,4801
110,5010,4900
5010,43418,4801
*****
90,4990,4900
4990,43398,4801
140,5040,4900
5040,43448,4801
**
*****NODE GENERATION FOR WEBS (LONG)*****
**
*NGEN,NSET=NWEBLONG
4910,5010,50
5010,9710,100
9711,9811,50
9811,14511,100
14512,14612,50
14612,19312,100
19313,19413,50
19413,24113,100
24114,24214,50
24214,28914,100
28915,29015,50
29015,33715,100
33716,33816,50
33816,38516,100
38517,38617,50
38617,43317,100
43318,43418,50
43418,48118,100
**
48219,52919,100
53020,57720,100
57821,62521,100
62622,67322,100
67423,72123,100
*****
4940,5040,50
5040,9740,100
9741,9841,50
9841,14541,100
14542,14642,50
14642,19342,100
19343,19443,50
19443,24143,100
24144,24244,50
24244,28944,100
28945,29045,50
29045,33745,100
33746,33846,50
33846,38546,100
38547,38647,50
38647,43347,100
43348,43448,50
43448,48148,100
**
48249,52949,100
53050,57750,100

```

```

57851,62551,100
62652,67352,100
67453,72153,100
**
*****ELEMENT GENERATION FOR THE SLAB*****
**
*ELEMENT,TYPE=S4R
1,2,102,104,4
*ELGEN,ELSET=SLAB
1,48,100,23,23,2,1
**
*****ELEMENT GENERATION FOR GIRDER WEBS*****
**
*ELEMENT,TYPE=S4R
1105,4910,4960,60,10
1107,9711,9761,4960,4910
1123,5010,5110,210,110
1170,9811,9911,5110,5010
*ELGEN,ELSET=WEB1
1105,2,50,1
1107,2,50,8,8,4801,1
1123,47,100,1
1170,47,100,13,13,4801,1
**
*ELEMENT,TYPE=S4R
1781,4940,4990,90,40
1783,9741,9791,4990,4940
1799,5040,5140,240,140
1846,9841,9941,5140,5040
*ELGEN,ELSET=WEB2
1781,2,50,1
1783,2,50,8,8,4801,1
1799,47,100,1
1846,47,100,13,13,4801,1
**
*****ELEMENT GENERATION FOR CFRP*****
**
*ELEMENT,TYPE=M3D4R
2931,9711,9761,4960,4910
*ELGEN,ELSET=FRP1WEB1
2931,2,50,8,8,4801,1
*ELEMENT,TYPE=M3D4R
2947,9711,9761,4960,4910
2963,9811,9911,5110,5010
*ELGEN,ELSET=FRP2WEB1
2947,2,50,8,8,4801,1
2963,7,100,13,13,4801,1
*****
*ELEMENT,TYPE=M3D4R
3607,9741,9791,4990,4940
*ELGEN,ELSET=FRP1WEB2
3607,2,50,8,8,4801,1
*ELEMENT,TYPE=M3D4R
3623,9741,9791,4990,4940
3639,9841,9941,5140,5040
*ELGEN,ELSET=FRP2WEB2
3623,2,50,8,8,4801,1
3639,7,100,13,13,4801,1
**
*****ELEMENT SET ASSIGNMENT*****
*****R-LONG REBAR
*****S-VERT REBAR
*****W-MESH
*****ELEMENT SET ASSIGNMENT - SEC1 (NO MESH-AT SUPPORT)*****
**
*ELSET,ELSET=WEB1A1,GENERATE
1105,1106,1
*ELSET,ELSET=WEB1SB1,GENERATE
1107,1115,8
*ELSET,ELSET=WEB1RSC1,GENERATE
1108,1116,8
*ELSET,ELSET=WEB1RSD1,GENERATE
1109,1117,8
*ELSET,ELSET=WEB1SE1,GENERATE
1110,1118,8
*ELSET,ELSET=WEB1RSF1,GENERATE
1111,1119,8
*ELSET,ELSET=WEB1SG1,GENERATE
1112,1120,8
*ELSET,ELSET=WEB1SH1,GENERATE
1113,1121,8

```

```

*ELSET,ELSET=WEB1SI1,GENERATE
1114,1122,8
*****
*ELSET,ELSET=WEB2A1,GENERATE
1781,1782,1
*ELSET,ELSET=WEB2SB1,GENERATE
1783,1791,8
*ELSET,ELSET=WEB2RSC1,GENERATE
1784,1792,8
*ELSET,ELSET=WEB2RSD1,GENERATE
1785,1793,8
*ELSET,ELSET=WEB2SE1,GENERATE
1786,1794,8
*ELSET,ELSET=WEB2RSF1,GENERATE
1787,1795,8
*ELSET,ELSET=WEB2SG1,GENERATE
1788,1796,8
*ELSET,ELSET=WEB2SH1,GENERATE
1789,1797,8
*ELSET,ELSET=WEB2SI1,GENERATE
1790,1798,8
**
*****ELEMENT SET ASSIGNMENT - SEC2 (MESH)*****
**
*ELSET,ELSET=WEB1RSWC2
1171
*ELSET,ELSET=WEB1SWD2
1172
*ELSET,ELSET=WEB1SWE2
1173
*ELSET,ELSET=WEB1RSWF2
1174
*ELSET,ELSET=WEB1SWG2
1175
*ELSET,ELSET=WEB1SWH2
1176
*ELSET,ELSET=WEB1SWI2
1177
*ELSET,ELSET=WEB1SWJ2
1178
*ELSET,ELSET=WEB1SWK2
1179
*ELSET,ELSET=WEB1SWL2
1180
*ELSET,ELSET=WEB1SWM2
1181
*ELSET,ELSET=WEB1RSWN2
1182
**
*ELSET,ELSET=WEB1SSWWB2
1183
*ELSET,ELSET=WEB1SSWWC2
1184
*ELSET,ELSET=WEB1SSWWD2
1185
*ELSET,ELSET=WEB1SSWWE2
1186
*ELSET,ELSET=WEB1RRSSF2
1187
*ELSET,ELSET=WEB1SSWWG2
1188
**
*ELSET,ELSET=WEB1WWB2
1170
**
*ELSET,ELSET=WEB1WA2,GENERATE
1123,1158,1
*ELSET,ELSET=WEB1WB2,GENERATE
1196,1625,13
*ELSET,ELSET=WEB1WC2,GENERATE
1197,1626,13
*ELSET,ELSET=WEB1WD2,GENERATE
1198,1627,13
*ELSET,ELSET=WEB1WE2,GENERATE
1199,1628,13
*ELSET,ELSET=WEB1WF2,GENERATE
1200,1629,13
*ELSET,ELSET=WEB1WG2,GENERATE
1201,1630,13
*ELSET,ELSET=WEB1WH2,GENERATE
1189,1631,13

```

```

*ELSET,ELSET=WEB1WI2,GENERATE
1190,1632,13
*ELSET,ELSET=WEB1WJ2,GENERATE
1191,1633,13
*ELSET,ELSET=WEB1WK2,GENERATE
1192,1634,13
*ELSET,ELSET=WEB1WL2,GENERATE
1193,1635,13
*ELSET,ELSET=WEB1WM2,GENERATE
1194,1636,13
*ELSET,ELSET=WEB1RWN2,GENERATE
1195,1403,13
*ELSET,ELSET=WEB1WN2,GENERATE
1416,1637,13
*****
*ELSET,ELSET=WEB2RSWC2
1847
*ELSET,ELSET=WEB2SWD2
1848
*ELSET,ELSET=WEB2SWE2
1849
*ELSET,ELSET=WEB2RSWF2
1850
*ELSET,ELSET=WEB2SWG2
1851
*ELSET,ELSET=WEB2SWH2
1852
*ELSET,ELSET=WEB2SWI2
1853
*ELSET,ELSET=WEB2SWJ2
1854
*ELSET,ELSET=WEB2SWK2
1855
*ELSET,ELSET=WEB2SWL2
1856
*ELSET,ELSET=WEB2SWM2
1857
*ELSET,ELSET=WEB2RSWN2
1858
**
*ELSET,ELSET=WEB2SSWB2
1859
*ELSET,ELSET=WEB2SSWWC2
1860
*ELSET,ELSET=WEB2SSWWD2
1861
*ELSET,ELSET=WEB2SSWE2
1862
*ELSET,ELSET=WEB2RRSSF2
1863
*ELSET,ELSET=WEB2SSWWG2
1864
**
*ELSET,ELSET=WEB2WWB2
1846
**
*ELSET,ELSET=WEB2WA2,GENERATE
1799,1834,1
*ELSET,ELSET=WEB2WB2,GENERATE
1872,2301,13
*ELSET,ELSET=WEB2WC2,GENERATE
1873,2302,13
*ELSET,ELSET=WEB2WD2,GENERATE
1874,2303,13
*ELSET,ELSET=WEB2WE2,GENERATE
1875,2304,13
*ELSET,ELSET=WEB2WF2,GENERATE
1876,2305,13
*ELSET,ELSET=WEB2WG2,GENERATE
1877,2306,13
*ELSET,ELSET=WEB2WH2,GENERATE
1865,2307,13
*ELSET,ELSET=WEB2WI2,GENERATE
1866,2308,13
*ELSET,ELSET=WEB2WJ2,GENERATE
1867,2309,13
*ELSET,ELSET=WEB2WK2,GENERATE
1868,2310,13
*ELSET,ELSET=WEB2WL2,GENERATE
1869,2311,13
*ELSET,ELSET=WEB2WM2,GENERATE

```

```

1870,2312,13
*ELSET,ELSET=WEB2RWN2,GENERATE
1871,2079,13
*ELSET,ELSET=WEB2WN2,GENERATE
2092,2313,13
**
*****ELEMENT SET ASSIGNMENT - SEC3 (END-NO MESH)*****
**
*ELSET,ELSET=WEB1A3,GENERATE
1159,1169,1
*ELSET,ELSET=WEB1B3,GENERATE
1638,1768,13
*ELSET,ELSET=WEB1C3,GENERATE
1639,1769,13
*ELSET,ELSET=WEB1D3,GENERATE
1640,1770,13
*ELSET,ELSET=WEB1E3,GENERATE
1641,1771,13
*ELSET,ELSET=WEB1F3,GENERATE
1642,1772,13
*ELSET,ELSET=WEB1G3,GENERATE
1643,1773,13
*ELSET,ELSET=WEB1H3,GENERATE
1644,1774,13
*ELSET,ELSET=WEB1I3,GENERATE
1645,1775,13
*ELSET,ELSET=WEB1J3,GENERATE
1646,1776,13
*ELSET,ELSET=WEB1K3,GENERATE
1647,1777,13
*ELSET,ELSET=WEB1L3,GENERATE
1648,1778,13
*ELSET,ELSET=WEB1M3,GENERATE
1649,1779,13
*ELSET,ELSET=WEB1N3,GENERATE
1650,1780,13
*****
*ELSET,ELSET=WEB2A3,GENERATE
1835,1845,1
*ELSET,ELSET=WEB2B3,GENERATE
2314,2444,13
*ELSET,ELSET=WEB2C3,GENERATE
2315,2445,13
*ELSET,ELSET=WEB2D3,GENERATE
2316,2446,13
*ELSET,ELSET=WEB2E3,GENERATE
2317,2447,13
*ELSET,ELSET=WEB2F3,GENERATE
2318,2448,13
*ELSET,ELSET=WEB2G3,GENERATE
2319,2449,13
*ELSET,ELSET=WEB2H3,GENERATE
2320,2450,13
*ELSET,ELSET=WEB2I3,GENERATE
2321,2451,13
*ELSET,ELSET=WEB2J3,GENERATE
2322,2452,13
*ELSET,ELSET=WEB2K3,GENERATE
2323,2453,13
*ELSET,ELSET=WEB2L3,GENERATE
2324,2454,13
*ELSET,ELSET=WEB2M3,GENERATE
2325,2455,13
*ELSET,ELSET=WEB2N3,GENERATE
2326,2456,13
**
*****ELEMENT SET ASSIGNMENT FOR WEBS (BY SEC-TO VERIFY)*****
**
*ELSET,ELSET=WEB1SEC1
WEB1A1
WEB1SB1
WEB1RSC1
WEB1RSD1
WEB1SE1
WEB1RSF1
WEB1SG1
WEB1SH1
WEB1SI1
*ELSET,ELSET=WEB1SEC2
WEB1RSWC2
WEB1SWD2

```

```

WEB1SWE2
WEB1RSWF2
WEB1SWG2
WEB1SWH2
WEB1SWI2
WEB1SWJ2
WEB1SWK2
WEB1SWL2
WEB1SWM2
WEB1RSWN2
WEB1SSWNB2
WEB1SSWNC2
WEB1SSWWD2
WEB1SSWWE2
WEB1RRSSF2
WEB1SSWWG2
WEB1WWB2
WEB1WA2
WEB1WB2
WEB1WC2
WEB1WD2
WEB1WE2
WEB1WF2
WEB1WG2
WEB1WH2
WEB1WI2
WEB1WJ2
WEB1WK2
WEB1WL2
WEB1WM2
WEB1RWN2
WEB1WN2
*ELSET,ELSET=WEB1SEC3
WEB1A3
WEB1B3
WEB1C3
WEB1D3
WEB1E3
WEB1F3
WEB1G3
WEB1H3
WEB1I3
WEB1J3
WEB1K3
WEB1L3
WEB1M3
WEB1N3
*****
*ELSET,ELSET=WEB2SEC1
WEB2A1
WEB2SB1
WEB2RSC1
WEB2RSD1
WEB2SE1
WEB2RSF1
WEB2SG1
WEB2SH1
WEB2SI1
*ELSET,ELSET=WEB2SEC2
WEB2RSWC2
WEB2SWD2
WEB2SWE2
WEB2RSWF2
WEB2SWG2
WEB2SWH2
WEB2SWI2
WEB2SWJ2
WEB2SWK2
WEB2SWL2
WEB2SWM2
WEB2RSWN2
WEB2SSWNB2
WEB2SSWNC2
WEB2SSWWD2
WEB2SSWWE2
WEB2RRSSF2
WEB2SSWWG2
WEB2WWB2
WEB2WA2
WEB2WB2
WEB2WC2

```

```

WEB2WD2
WEB2WE2
WEB2WF2
WEB2WG2
WEB2WH2
WEB2WI2
WEB2WJ2
WEB2WK2
WEB2WL2
WEB2WM2
WEB2RWN2
WEB2WN2
*ELSET,ELSET=WEB2SEC3
WEB2A3
WEB2B3
WEB2C3
WEB2D3
WEB2E3
WEB2F3
WEB2G3
WEB2H3
WEB2I3
WEB2J3
WEB2K3
WEB2L3
WEB2M3
WEB2N3
**
*****ELEMENT GENERATION FOR PRESTRESSING TENDONS*****
**
*ELEMENT,TYPE=T2D2
2457,62622,62722
*ELGEN,ELSET=LPRE1
2457,47,100,1
*ELEMENT,TYPE=T2D2
2504,57821,57921
*ELGEN,ELSET=LPRE2
2504,47,100,1
*ELEMENT,TYPE=T2D2
2551,53020,53120
*ELGEN,ELSET=LPRE3
2551,47,100,1
*ELEMENT,TYPE=T2D2
2598,48219,48319
*ELGEN,ELSET=LPRE4
2598,47,100,1
*ELEMENT,TYPE=T2D2
2645,33716,33766
2647,33816,33916
*ELGEN,ELSET=LPRE5
2645,2,50,1
2647,47,100,1
*****
*ELEMENT,TYPE=T2D2
2694,62652,62752
*ELGEN,ELSET=RPRE1
2694,47,100,1
*ELEMENT,TYPE=T2D2
2741,57851,57951
*ELGEN,ELSET=RPRE2
2741,47,100,1
*ELEMENT,TYPE=T2D2
2788,53050,53150
*ELGEN,ELSET=RPRE3
2788,47,100,1
*ELEMENT,TYPE=T2D2
2835,48249,48349
*ELGEN,ELSET=RPRE4
2835,47,100,1
*ELEMENT,TYPE=T2D2
2882,33746,33796
2884,33846,33946
*ELGEN,ELSET=RPRE5
2882,2,50,1
2884,47,100,1
**
*****MATERIAL PROPERTIES*****
**
*SHELL SECTION,ELSET=SLAB,MATERIAL=CON
105,5
*REBAR LAYER

```

```

LONG,25.8,102,0,WWF,0,1
TRANS,13.3,300,0,WWF,90,1
*MATERIAL,NAME=WWF
*DENSITY
7850E-9
*ELASTIC
210000,0.3
*PLASTIC
450
*MATERIAL,NAME=CON
*DENSITY
2400E-9
*ELASTIC
30500,0.2
*CONCRETE
20.4,0
51,0.0022
*FAILURE RATIOS
1.16,0.0836
*TENSION STIFFENING
1,0
0,0.003
*SHEAR RETENTION
1,1E+6
*MATERIAL,NAME=REINF
*DENSITY
7850E-9
*ELASTIC
200000,0.3
*PLASTIC
400
**
*****WEB1*****
**
*****SECTION1*****
**
*SHELL SECTION,ELSET=WEB1A1,MATERIAL=CON
170,5
*SHELL SECTION,ELSET=WEB1SB1,MATERIAL=CON
167.32,5
*REBAR LAYER
VERT1,600,200,0,REINF,90,1
VERT3,100,200,0,REINF,90,1
*SHELL SECTION,ELSET=WEB1RSC1,MATERIAL=CON
161.95,5
*REBAR LAYER
LONG1,300,50,0,REINF,0,1
VERT1,600,200,0,REINF,90,1
VERT3,100,200,0,REINF,90,1
*SHELL SECTION,ELSET=WEB1RSD1,MATERIAL=CON
156.56,5
*REBAR LAYER
LONG2,300,50,0,REINF,0,1
VERT1,600,200,0,REINF,90,1
VERT3,100,200,0,REINF,90,1
*SHELL SECTION,ELSET=WEB1SE1,MATERIAL=CON
151.18,5
*REBAR LAYER
VERT1,600,200,0,REINF,90,1
VERT3,100,200,0,REINF,90,1
*SHELL SECTION,ELSET=WEB1RSF1,MATERIAL=CON
145.79,5
*REBAR LAYER
LONG3,200,50,0,REINF,0,1
VERT1,600,200,0,REINF,90,1
VERT3,100,200,0,REINF,90,1
*SHELL SECTION,ELSET=WEB1SG1,MATERIAL=CON
140.41,5
*REBAR LAYER
VERT1,600,200,0,REINF,90,1
VERT3,100,200,0,REINF,90,1
*SHELL SECTION,ELSET=WEB1SH1,MATERIAL=CON
135.02,5
*REBAR LAYER
VERT1,600,200,0,REINF,90,1
VERT3,100,200,0,REINF,90,1
*SHELL SECTION,ELSET=WEB1SI1,MATERIAL=CON
129.64,5
*REBAR LAYER
VERT1,600,200,0,REINF,90,1
VERT3,100,200,0,REINF,90,1

```

```

**
*****WEB1 SECTION2 - 1ST COLUMN*****
**
*SHELL SECTION,ELSET=WEB1RSWC2,MATERIAL=CON
161.95,5
*REBAR LAYER
LONG1,300,50,0,REINF,0,1
VERT2,600,200,0,REINF,90,1
HORIZ,25.8,102,0,WWF,0,1
VERT,25.8,102,0,WWF,90,1
*SHELL SECTION,ELSET=WEB1SWD2,MATERIAL=CON
156.56,5
*REBAR LAYER
VERT2,600,200,0,REINF,90,1
HORIZ,25.8,102,0,WWF,0,1
VERT,25.8,102,0,WWF,90,1
*SHELL SECTION,ELSET=WEB1SWE2,MATERIAL=CON
151.18,5
*REBAR LAYER
VERT2,600,200,0,REINF,90,1
HORIZ,25.8,102,0,WWF,0,1
VERT,25.8,102,0,WWF,90,1
*SHELL SECTION,ELSET=WEB1RSWF2,MATERIAL=CON
145.79,5
*REBAR LAYER
LONG3,200,50,0,REINF,0,1
VERT2,600,200,0,REINF,90,1
HORIZ,25.8,102,0,WWF,0,1
VERT,25.8,102,0,WWF,90,1
*SHELL SECTION,ELSET=WEB1SWG2,MATERIAL=CON
140.41,5
*REBAR LAYER
VERT2,600,200,0,REINF,90,1
HORIZ,25.8,102,0,WWF,0,1
VERT,25.8,102,0,WWF,90,1
*SHELL SECTION,ELSET=WEB1SWH2,MATERIAL=CON
135.02,5
*REBAR LAYER
VERT2,600,200,0,REINF,90,1
HORIZ,25.8,102,0,WWF,0,1
VERT,25.8,102,0,WWF,90,1
*SHELL SECTION,ELSET=WEB1SWI2,MATERIAL=CON
129.64,5
*REBAR LAYER
VERT2,600,200,0,REINF,90,1
HORIZ,25.8,102,0,WWF,0,1
VERT,25.8,102,0,WWF,90,1
*SHELL SECTION,ELSET=WEB1SWJ2,MATERIAL=CON
124.26,5
*REBAR LAYER
VERT2,600,200,0,REINF,90,1
HORIZ,25.8,102,0,WWF,0,1
VERT,25.8,102,0,WWF,90,1
*SHELL SECTION,ELSET=WEB1SWK2,MATERIAL=CON
118.87,5
*REBAR LAYER
VERT2,600,200,0,REINF,90,1
HORIZ,25.8,102,0,WWF,0,1
VERT,25.8,102,0,WWF,90,1
*SHELL SECTION,ELSET=WEB1SWL2,MATERIAL=CON
113.49,5
*REBAR LAYER
VERT2,600,200,0,REINF,90,1
HORIZ,25.8,102,0,WWF,0,1
VERT,25.8,102,0,WWF,90,1
*SHELL SECTION,ELSET=WEB1SWM2,MATERIAL=CON
108.1,5
*REBAR LAYER
VERT2,600,200,0,REINF,90,1
HORIZ,25.8,102,0,WWF,0,1
VERT,25.8,102,0,WWF,90,1
*SHELL SECTION,ELSET=WEB1RSWN2,MATERIAL=CON
102.7,5
*REBAR LAYER
LONG4,600,50,0,REINF,0,1
VERT2,600,200,0,REINF,90,1
HORIZ,25.8,102,0,WWF,0,1
VERT,25.8,102,0,WWF,90,1
**
*****WEB1 SECTION2 - 2ND COLUMN*****
**

```



```

*SHELL SECTION,ELSET=WEB1SSWB2,MATERIAL=CON
167.32,5
*REBAR LAYER
VERT4,100,200,0,REINF,90,1
HORIZ,25.8,102,0,WWF,0,1
VERT,25.8,102,0,WWF,90,1
*SHELL SECTION,ELSET=WEB1SSWC2,MATERIAL=CON
161.95,5
*REBAR LAYER
VERT4,100,200,0,REINF,90,1
HORIZ,25.8,102,0,WWF,0,1
VERT,25.8,102,0,WWF,90,1
*SHELL SECTION,ELSET=WEB1SSWD2,MATERIAL=CON
156.56,5
*REBAR LAYER
VERT4,100,200,0,REINF,90,1
HORIZ,25.8,102,0,WWF,0,1
VERT,25.8,102,0,WWF,90,1
*SHELL SECTION,ELSET=WEB1SSWE2,MATERIAL=CON
151.18,5
*REBAR LAYER
VERT4,100,200,0,REINF,90,1
HORIZ,25.8,102,0,WWF,0,1
VERT,25.8,102,0,WWF,90,1
*SHELL SECTION,ELSET=WEB1RRSSF2,MATERIAL=CON
145.79,5
*REBAR LAYER
LONG3,200,50,0,REINF,0,1
VERT4,100,200,0,REINF,90,1
HORIZ,25.8,102,0,WWF,0,1
VERT,25.8,102,0,WWF,90,1
*SHELL SECTION,ELSET=WEB1SSWVG2,MATERIAL=CON
140.41,5
*REBAR LAYER
VERT4,100,200,0,REINF,90,1
HORIZ,25.8,102,0,WWF,0,1
VERT,25.8,102,0,WWF,90,1
**
*****WEB1 SECTION2 - MESH*****
**
*SHELL SECTION,ELSET=WEB1WB2,MATERIAL=CON
167.32,5
*REBAR LAYER
HORIZ,25.8,102,0,WWF,0,1
VERT,25.8,102,0,WWF,90,1
*****
*SHELL SECTION,ELSET=WEB1WA2,MATERIAL=CON
170,5
*REBAR LAYER
HORIZ,25.8,102,0,WWF,0,1
VERT,25.8,102,0,WWF,90,1
*SHELL SECTION,ELSET=WEB1WB2,MATERIAL=CON
167.32,5
*REBAR LAYER
HORIZ,25.8,102,0,WWF,0,1
VERT,25.8,102,0,WWF,90,1
*SHELL SECTION,ELSET=WEB1WC2,MATERIAL=CON
161.95,5
*REBAR LAYER
HORIZ,25.8,102,0,WWF,0,1
VERT,25.8,102,0,WWF,90,1
*SHELL SECTION,ELSET=WEB1WD2,MATERIAL=CON
156.56,5
*REBAR LAYER
HORIZ,25.8,102,0,WWF,0,1
VERT,25.8,102,0,WWF,90,1
*SHELL SECTION,ELSET=WEB1WE2,MATERIAL=CON
151.18,5
*REBAR LAYER
HORIZ,25.8,102,0,WWF,0,1
VERT,25.8,102,0,WWF,90,1
*SHELL SECTION,ELSET=WEB1WF2,MATERIAL=CON
145.79,5
*REBAR LAYER
HORIZ,25.8,102,0,WWF,0,1
VERT,25.8,102,0,WWF,90,1
*SHELL SECTION,ELSET=WEB1WG2,MATERIAL=CON
140.41,5
*REBAR LAYER
HORIZ,25.8,102,0,WWF,0,1
VERT,25.8,102,0,WWF,90,1

```

```

*SHELL SECTION,ELSET=WEB1WH2,MATERIAL=CON
135.02,5
*REBAR LAYER
HORIZ,25.8,102,0,WWF,0,1
VERT,25.8,102,0,WWF,90,1
*SHELL SECTION,ELSET=WEB1WI2,MATERIAL=CON
129.64,5
*REBAR LAYER
HORIZ,25.8,102,0,WWF,0,1
VERT,25.8,102,0,WWF,90,1
*SHELL SECTION,ELSET=WEB1WJ2,MATERIAL=CON
124.26,5
*REBAR LAYER
HORIZ,25.8,102,0,WWF,0,1
VERT,25.8,102,0,WWF,90,1
*SHELL SECTION,ELSET=WEB1WK2,MATERIAL=CON
118.87,5
*REBAR LAYER
HORIZ,25.8,102,0,WWF,0,1
VERT,25.8,102,0,WWF,90,1
*SHELL SECTION,ELSET=WEB1WL2,MATERIAL=CON
113.49,5
*REBAR LAYER
HORIZ,25.8,102,0,WWF,0,1
VERT,25.8,102,0,WWF,90,1
*SHELL SECTION,ELSET=WEB1WM2,MATERIAL=CON
108.1,5
*REBAR LAYER
HORIZ,25.8,102,0,WWF,0,1
VERT,25.8,102,0,WWF,90,1
*SHELL SECTION,ELSET=WEB1RWN2,MATERIAL=CON
102.7,5
*REBAR LAYER
LONG4,600,50,0,REINF,0,1
HORIZ,25.8,102,0,WWF,0,1
VERT,25.8,102,0,WWF,90,1
*SHELL SECTION,ELSET=WEB1WN2,MATERIAL=CON
102.7,5
*REBAR LAYER
HORIZ,25.8,102,0,WWF,0,1
VERT,25.8,102,0,WWF,90,1
**
*****WEB1 SECTION3 - NO MESH*****
**
*SHELL SECTION,ELSET=WEB1A3,MATERIAL=CON
170,5
*SHELL SECTION,ELSET=WEB1B3,MATERIAL=CON
167.32,5
*SHELL SECTION,ELSET=WEB1C3,MATERIAL=CON
161.95,5
*SHELL SECTION,ELSET=WEB1D3,MATERIAL=CON
156.56,5
*SHELL SECTION,ELSET=WEB1E3,MATERIAL=CON
151.18,5
*SHELL SECTION,ELSET=WEB1F3,MATERIAL=CON
145.79,5
*SHELL SECTION,ELSET=WEB1G3,MATERIAL=CON
140.41,5
*SHELL SECTION,ELSET=WEB1H3,MATERIAL=CON
135.02,5
*SHELL SECTION,ELSET=WEB1I3,MATERIAL=CON
129.64,5
*SHELL SECTION,ELSET=WEB1J3,MATERIAL=CON
124.26,5
*SHELL SECTION,ELSET=WEB1K3,MATERIAL=CON
118.87,5
*SHELL SECTION,ELSET=WEB1L3,MATERIAL=CON
113.49,5
*SHELL SECTION,ELSET=WEB1M3,MATERIAL=CON
108.1,5
*SHELL SECTION,ELSET=WEB1N3,MATERIAL=CON
102.7,5
**
*****WEB2*****
**
*****SECTION1*****
**
*SHELL SECTION,ELSET=WEB2A1,MATERIAL=CON
170,5
*SHELL SECTION,ELSET=WEB2SB1,MATERIAL=CON
167.32,5

```

```

*REBAR LAYER
VERT1,600,200,0,REINF,90,1
VERT3,100,200,0,REINF,90,1
*SHELL SECTION,ELSET=WEB2RSC1,MATERIAL=CON
161.95,5
*REBAR LAYER
LONG1,300,50,0,REINF,0,1
VERT1,600,200,0,REINF,90,1
VERT3,100,200,0,REINF,90,1
*SHELL SECTION,ELSET=WEB2RSD1,MATERIAL=CON
156.56,5
*REBAR LAYER
LONG2,300,50,0,REINF,0,1
VERT1,600,200,0,REINF,90,1
VERT3,100,200,0,REINF,90,1
*SHELL SECTION,ELSET=WEB2SE1,MATERIAL=CON
151.18,5
*REBAR LAYER
VERT1,600,200,0,REINF,90,1
VERT3,100,200,0,REINF,90,1
*SHELL SECTION,ELSET=WEB2RSF1,MATERIAL=CON
145.79,5
*REBAR LAYER
LONG3,200,50,0,REINF,0,1
VERT1,600,200,0,REINF,90,1
VERT3,100,200,0,REINF,90,1
*SHELL SECTION,ELSET=WEB2SG1,MATERIAL=CON
140.41,5
*REBAR LAYER
VERT1,600,200,0,REINF,90,1
VERT3,100,200,0,REINF,90,1
*SHELL SECTION,ELSET=WEB2SH1,MATERIAL=CON
135.02,5
*REBAR LAYER
VERT1,600,200,0,REINF,90,1
VERT3,100,200,0,REINF,90,1
*SHELL SECTION,ELSET=WEB2SI1,MATERIAL=CON
129.64,5
*REBAR LAYER
VERT1,600,200,0,REINF,90,1
VERT3,100,200,0,REINF,90,1
**
*****WEB2 SECTION2 - 1ST COLUMN*****
**
*SHELL SECTION,ELSET=WEB2RSWC2,MATERIAL=CON
161.95,5
*REBAR LAYER
LONG1,300,50,0,REINF,0,1
VERT2,600,200,0,REINF,90,1
HORIZ,25.8,102,0,WWF,0,1
VERT,25.8,102,0,WWF,90,1
*SHELL SECTION,ELSET=WEB2SWD2,MATERIAL=CON
156.56,5
*REBAR LAYER
VERT2,600,200,0,REINF,90,1
HORIZ,25.8,102,0,WWF,0,1
VERT,25.8,102,0,WWF,90,1
*SHELL SECTION,ELSET=WEB2SWE2,MATERIAL=CON
151.18,5
*REBAR LAYER
VERT2,600,200,0,REINF,90,1
HORIZ,25.8,102,0,WWF,0,1
VERT,25.8,102,0,WWF,90,1
*SHELL SECTION,ELSET=WEB2RSWF2,MATERIAL=CON
145.79,5
*REBAR LAYER
LONG3,200,50,0,REINF,0,1
VERT2,600,200,0,REINF,90,1
HORIZ,25.8,102,0,WWF,0,1
VERT,25.8,102,0,WWF,90,1
*SHELL SECTION,ELSET=WEB2SWG2,MATERIAL=CON
140.41,5
*REBAR LAYER
VERT2,600,200,0,REINF,90,1
HORIZ,25.8,102,0,WWF,0,1
VERT,25.8,102,0,WWF,90,1
*SHELL SECTION,ELSET=WEB2SWH2,MATERIAL=CON
135.02,5
*REBAR LAYER
VERT2,600,200,0,REINF,90,1
HORIZ,25.8,102,0,WWF,0,1

```

```

VERT,25.8,102,0,WWF,90,1
*SHELL SECTION,ELSET=WEB2SWI2,MATERIAL=CON
129.64,5
*REBAR LAYER
VERT2,600,200,0,REINF,90,1
HORIZ,25.8,102,0,WWF,0,1
VERT,25.8,102,0,WWF,90,1
*SHELL SECTION,ELSET=WEB2SWJ2,MATERIAL=CON
124.26,5
*REBAR LAYER
VERT2,600,200,0,REINF,90,1
HORIZ,25.8,102,0,WWF,0,1
VERT,25.8,102,0,WWF,90,1
*SHELL SECTION,ELSET=WEB2SWK2,MATERIAL=CON
118.87,5
*REBAR LAYER
VERT2,600,200,0,REINF,90,1
HORIZ,25.8,102,0,WWF,0,1
VERT,25.8,102,0,WWF,90,1
*SHELL SECTION,ELSET=WEB2SWL2,MATERIAL=CON
113.49,5
*REBAR LAYER
VERT2,600,200,0,REINF,90,1
HORIZ,25.8,102,0,WWF,0,1
VERT,25.8,102,0,WWF,90,1
*SHELL SECTION,ELSET=WEB2SWM2,MATERIAL=CON
108.1,5
*REBAR LAYER
VERT2,600,200,0,REINF,90,1
HORIZ,25.8,102,0,WWF,0,1
VERT,25.8,102,0,WWF,90,1
*SHELL SECTION,ELSET=WEB2RSWN2,MATERIAL=CON
102.7,5
*REBAR LAYER
LONG4,600,50,0,REINF,0,1
VERT2,600,200,0,REINF,90,1
HORIZ,25.8,102,0,WWF,0,1
VERT,25.8,102,0,WWF,90,1
**
*****WEB2 SECTION2 - 2ND COLUMN*****
**
*SHELL SECTION,ELSET=WEB2SSWWB2,MATERIAL=CON
167.32,5
*REBAR LAYER
VERT4,100,200,0,REINF,90,1
HORIZ,25.8,102,0,WWF,0,1
VERT,25.8,102,0,WWF,90,1
*SHELL SECTION,ELSET=WEB2SSWWC2,MATERIAL=CON
161.95,5
*REBAR LAYER
VERT4,100,200,0,REINF,90,1
HORIZ,25.8,102,0,WWF,0,1
VERT,25.8,102,0,WWF,90,1
*SHELL SECTION,ELSET=WEB2SSWWD2,MATERIAL=CON
156.56,5
*REBAR LAYER
VERT4,100,200,0,REINF,90,1
HORIZ,25.8,102,0,WWF,0,1
VERT,25.8,102,0,WWF,90,1
*SHELL SECTION,ELSET=WEB2SSWWE2,MATERIAL=CON
151.18,5
*REBAR LAYER
VERT4,100,200,0,REINF,90,1
HORIZ,25.8,102,0,WWF,0,1
VERT,25.8,102,0,WWF,90,1
*SHELL SECTION,ELSET=WEB2RRSSF2,MATERIAL=CON
145.79,5
*REBAR LAYER
LONG3,200,50,0,REINF,0,1
VERT4,100,200,0,REINF,90,1
HORIZ,25.8,102,0,WWF,0,1
VERT,25.8,102,0,WWF,90,1
*SHELL SECTION,ELSET=WEB2SSWWG2,MATERIAL=CON
140.41,5
*REBAR LAYER
VERT4,100,200,0,REINF,90,1
HORIZ,25.8,102,0,WWF,0,1
VERT,25.8,102,0,WWF,90,1
**
*****WEB2 SECTION2 - MESH*****
**

```

```

*SHELL SECTION,ELSET=WEB2WVB2,MATERIAL=CON
167.32,5
*REBAR LAYER
HORIZ,25.8,102,0,WWF,0,1
VERT,25.8,102,0,WWF,90,1
*****
*SHELL SECTION,ELSET=WEB2WA2,MATERIAL=CON
170,5
*REBAR LAYER
HORIZ,25.8,102,0,WWF,0,1
VERT,25.8,102,0,WWF,90,1
*SHELL SECTION,ELSET=WEB2WB2,MATERIAL=CON
167.32,5
*REBAR LAYER
HORIZ,25.8,102,0,WWF,0,1
VERT,25.8,102,0,WWF,90,1
*SHELL SECTION,ELSET=WEB2WC2,MATERIAL=CON
161.95,5
*REBAR LAYER
HORIZ,25.8,102,0,WWF,0,1
VERT,25.8,102,0,WWF,90,1
*SHELL SECTION,ELSET=WEB2WD2,MATERIAL=CON
156.56,5
*REBAR LAYER
HORIZ,25.8,102,0,WWF,0,1
VERT,25.8,102,0,WWF,90,1
*SHELL SECTION,ELSET=WEB2WE2,MATERIAL=CON
151.18,5
*REBAR LAYER
HORIZ,25.8,102,0,WWF,0,1
VERT,25.8,102,0,WWF,90,1
*SHELL SECTION,ELSET=WEB2WF2,MATERIAL=CON
145.79,5
*REBAR LAYER
HORIZ,25.8,102,0,WWF,0,1
VERT,25.8,102,0,WWF,90,1
*SHELL SECTION,ELSET=WEB2WG2,MATERIAL=CON
140.41,5
*REBAR LAYER
HORIZ,25.8,102,0,WWF,0,1
VERT,25.8,102,0,WWF,90,1
*SHELL SECTION,ELSET=WEB2WH2,MATERIAL=CON
135.02,5
*REBAR LAYER
HORIZ,25.8,102,0,WWF,0,1
VERT,25.8,102,0,WWF,90,1
*SHELL SECTION,ELSET=WEB2WI2,MATERIAL=CON
129.64,5
*REBAR LAYER
HORIZ,25.8,102,0,WWF,0,1
VERT,25.8,102,0,WWF,90,1
*SHELL SECTION,ELSET=WEB2WJ2,MATERIAL=CON
124.26,5
*REBAR LAYER
HORIZ,25.8,102,0,WWF,0,1
VERT,25.8,102,0,WWF,90,1
*SHELL SECTION,ELSET=WEB2WK2,MATERIAL=CON
118.87,5
*REBAR LAYER
HORIZ,25.8,102,0,WWF,0,1
VERT,25.8,102,0,WWF,90,1
*SHELL SECTION,ELSET=WEB2WL2,MATERIAL=CON
113.49,5
*REBAR LAYER
HORIZ,25.8,102,0,WWF,0,1
VERT,25.8,102,0,WWF,90,1
*SHELL SECTION,ELSET=WEB2WM2,MATERIAL=CON
108.1,5
*REBAR LAYER
HORIZ,25.8,102,0,WWF,0,1
VERT,25.8,102,0,WWF,90,1
*SHELL SECTION,ELSET=WEB2RWN2,MATERIAL=CON
102.7,5
*REBAR LAYER
LONG4,600,50,0,REINF,0,1
HORIZ,25.8,102,0,WWF,0,1
VERT,25.8,102,0,WWF,90,1
*SHELL SECTION,ELSET=WEB2WN2,MATERIAL=CON
102.7,5
*REBAR LAYER
HORIZ,25.8,102,0,WWF,0,1

```

```

VERT,25.8,102,0,WWF,90,1
**
*****WEB2 SECTION3 - NO MESH*****
**
*SHELL SECTION,ELSET=WEB2A3,MATERIAL=CON
170,5
*SHELL SECTION,ELSET=WEB2B3,MATERIAL=CON
167.32,5
*SHELL SECTION,ELSET=WEB2C3,MATERIAL=CON
161.95,5
*SHELL SECTION,ELSET=WEB2D3,MATERIAL=CON
156.56,5
*SHELL SECTION,ELSET=WEB2E3,MATERIAL=CON
151.18,5
*SHELL SECTION,ELSET=WEB2F3,MATERIAL=CON
145.79,5
*SHELL SECTION,ELSET=WEB2G3,MATERIAL=CON
140.41,5
*SHELL SECTION,ELSET=WEB2H3,MATERIAL=CON
135.02,5
*SHELL SECTION,ELSET=WEB2I3,MATERIAL=CON
129.64,5
*SHELL SECTION,ELSET=WEB2J3,MATERIAL=CON
124.26,5
*SHELL SECTION,ELSET=WEB2K3,MATERIAL=CON
118.87,5
*SHELL SECTION,ELSET=WEB2L3,MATERIAL=CON
113.49,5
*SHELL SECTION,ELSET=WEB2M3,MATERIAL=CON
108.1,5
*SHELL SECTION,ELSET=WEB2N3,MATERIAL=CON
102.7,5
**
*****PRESTRESSING STEEL *****
**
*SOLID SECTION,ELSET=LPRE1,MATERIAL=PRESTEEL
148
*SOLID SECTION,ELSET=LPRE2,MATERIAL=PRESTEEL
148
*SOLID SECTION,ELSET=LPRE3,MATERIAL=PRESTEEL
148
*SOLID SECTION,ELSET=LPRE4,MATERIAL=PRESTEEL
148
*SOLID SECTION,ELSET=LPRE5,MATERIAL=PRESTEEL
148
*SOLID SECTION,ELSET=RPRE1,MATERIAL=PRESTEEL
148
*SOLID SECTION,ELSET=RPRE2,MATERIAL=PRESTEEL
148
*SOLID SECTION,ELSET=RPRE3,MATERIAL=PRESTEEL
148
*SOLID SECTION,ELSET=RPRE4,MATERIAL=PRESTEEL
148
*SOLID SECTION,ELSET=RPRE5,MATERIAL=PRESTEEL
148
*MATERIAL,NAME=PRESTEEL
*DENSITY
7850E-9
*ELASTIC
200000,0.3
*PLASTIC
1580
**
*****CARBON FRP*****
**
*MEMBRANE SECTION,ELSET=FRP1WEB1,MATERIAL=FRP
2
*MEMBRANE SECTION,ELSET=FRP2WEB1,MATERIAL=FRP
2
*MEMBRANE SECTION,ELSET=FRP3WEB1,MATERIAL=FRP
2
*MEMBRANE SECTION,ELSET=FRP1WEB2,MATERIAL=FRP
2
*MEMBRANE SECTION,ELSET=FRP2WEB2,MATERIAL=FRP
2
*MEMBRANE SECTION,ELSET=FRP3WEB2,MATERIAL=FRP
2
*MATERIAL,NAME=FRP
*ELASTIC,TYPE=LAMINA
72400,40.6,0.0001,0.0001,0.0001,0,0
*PLASTIC

```



```

876,0
****44,0
****44,0.012
****44,0.024
**
*****PRESTRESSING OF TENDONS*****
**
*INITIAL CONDITIONS,TYPE=STRESS
LPRE1,1267
LPRE2,1267
LPRE3,1267
LPRE4,1267
LPRE5,1267
RPRE1,1267
RPRE2,1267
RPRE3,1267
RPRE4,1267
RPRE5,1267
**
*****BOUNDARY CONDITIONS (1/2 OF DT MODELED)*****
**
*NGEN,NSET=SLABSUPP
4802,4848,2
*NGEN,NSET=WEB1SUPP
9710,72123,4801
*NGEN,NSET=WEB2SUPP
9740,72153,4801
*NSET,NSET=WEB1BOTSUPP
43368
*NSET,NSET=WEB2BOTSUPP
43398
*BOUNDARY
SLABSUPP,1
SLABSUPP,4
***SLABSUPP,5
WEB1SUPP,1
WEB1SUPP,4
***WEB1SUPP,5
WEB2SUPP,1
WEB2SUPP,4
***WEB2SUPP,5
WEB1BOTSUPP,2,3
WEB2BOTSUPP,3
**
*****DEAD LOAD*****
**
*ELSET,ELSET=ENTIREDT,GENERATE
1105,2456,1
**
*NSET,NSET=RE1
43398,43368
*NSET,NSET=RE2
72153,72123
**
*STEP,NLGEOM
*STATIC
*DLOAD
SLAB,GRAV,9.81,0,0,-1
ENTIREDT,GRAV,9.81,0,0,-1
***ELPRINT,POSITION=AVERAGED AT NODES,ELSET=ENTIREDT
***S11
*ENDSTEP
**
*****BARRIER LOADING*****
**
*NGEN,NSET=LOADNODES
2910,4710,100
2940,4740,100
**
*NSET,NSET=NOUTPUT
72153,72053,72123,72023,4810,4840
LOADNODES
**
*ELSET,ELSET=EOUTPUT,GENERATE
1036,1104,1
**
*STEP,INC=5000
*STATIC,RIKS
0.005,1.0,1E-40,0.5
*CLOAD
LOADNODES,3,-4000

```

```
**  
*OUTPUT,HISTORY,OP=ADD  
*NODE OUTPUT,NSET=NOUTPUT  
U3,CF3  
*ELEMENT OUTPUT,ELSET=EOUTPUT  
SE1  
*ENDSTEP  
**
```

DT-102A GIRDER ABAQUS INPUT FILE

ABAQUS input file for DT-102A strengthened with CFRP, using membrane elements.

```

*HEADING
2D LINE MODEL OF PRESTRESSED DT-102A GIRDER (N,mm);NLGEOM, CFRP MEMBRANE
*PREPRINT,ECHO=YES,MODEL=NO,HISTORY=NO
**RESTART,WRITE
**
*****REFERENCE NODAL COORDINATES - SLAB,GIRDER WEBS*****
**
*NODE
2,      -9600,      0,      0
52,     -9600,     2500,     0
4802,    0,         0,      0
4852,    0,     2500,     0
*****
62,     -9500,     500,     0
112,    -9400,     500,     0
4962,   -9500,     500,    -50
5012,   -9400,     500,    -50
43370,  -9500,     500,   -450
*****
92,     -9500,     2000,     0
142,    -9400,     2000,     0
4992,   -9500,     2000,    -50
5042,   -9400,     2000,    -50
43400,  -9500,     2000,   -450
*****
4912,   -9600,     500,    -50
43320,  -9600,     500,   -450
9712,    0,       500,    -50
72125,   0,       500,   -700
*****
43420,  -9400,     500,   -450
67425,  -9400,     500,   -700
*****
4942,   -9600,     2000,    -50
43350,  -9600,     2000,   -450
9742,    0,       2000,    -50
72155,   0,       2000,   -700
*****
43450,  -9400,     2000,   -450
67455,  -9400,     2000,   -700
**
*****NODE GENERATION FOR SLAB*****
**
*NGEN,NSET=NEND
2,52,2
4802,4852,2
*NGEN,NSET=NSLAB
2,4802,100
4,4804,100
6,4806,100
8,4808,100
10,4810,100
12,4812,100
14,4814,100
16,4816,100
18,4818,100
20,4820,100
22,4822,100
24,4824,100
26,4826,100
28,4828,100
30,4830,100
32,4832,100
34,4834,100
36,4836,100
38,4838,100
40,4840,100
42,4842,100
44,4844,100

```

```

46,4846,100
48,4848,100
50,4850,100
52,4852,100
**
*****NODE GENERATION FOR WEBS (ENDS)*****
**
*NGEN,NSET=NWEBENDS1
12,4912,4900
4812,9712,4900
42,4942,4900
4842,9742,4900
*****
4912,43320,4801
9712,72125,4801
4942,43350,4801
9742,72155,4801
*****
43420,67425,4801
43450,67455,4801
**
*****NODE GENERATION FOR WEBS (SUPPORT LINE)*****
**
*NGEN,NSET=NMIDSUPP1
62,4962,4900
4962,43370,4801
112,5012,4900
5012,43420,4801
*****
92,4992,4900
4992,43400,4801
142,5042,4900
5042,43450,4801
**
*****NODE GENERATION FOR WEBS (LONG)*****
**
*NGEN,NSET=NWEBLONG
4912,5012,50
5012,9712,100
9713,9813,50
9813,14513,100
14514,14614,50
14614,19314,100
19315,19415,50
19415,24115,100
24116,24216,50
24216,28916,100
28917,29017,50
29017,33717,100
33718,33818,50
33818,38518,100
38519,38619,50
38619,43319,100
43320,43420,50
43420,48120,100
**
48221,52921,100
53022,57722,100
57823,62523,100
62624,67324,100
67425,72125,100
*****
4942,5042,50
5042,9742,100
9743,9843,50
9843,14543,100
14544,14644,50
14644,19344,100
19345,19445,50
19445,24145,100
24146,24246,50
24246,28946,100
28947,29047,50
29047,33747,100
33748,33848,50
33848,38548,100
38549,38649,50
38649,43349,100
43350,43450,50
43450,48150,100
**

```

```

48251,52951,100
53052,57752,100
57853,62553,100
62654,67354,100
67455,72155,100
**
*****ELEMENT GENERATION FOR THE SLAB*****
**
*ELEMENT,TYPE=S4R
1,2,102,104,4
*ELGEN,ELSET=SLAB
1,48,100,25,25,2,1
**
*****ELEMENT GENERATION FOR GIRDER WEBS*****
**
*ELEMENT,TYPE=S4R
1201,4912,4962,62,12
1203,9713,9763,4962,4912
1219,5012,5112,212,112
1266,9813,9913,5112,5012
*ELGEN,ELSET=WEB1
1201,2,50,1
1203,2,50,8,8,4801,1
1219,47,100,1
1266,47,100,13,13,4801,1
**
*ELEMENT,TYPE=S4R
1877,4942,4992,92,42
1879,9743,9793,4992,4942
1895,5042,5142,242,142
1942,9843,9943,5142,5042
*ELGEN,ELSET=WEB2
1877,2,50,1
1879,2,50,8,8,4801,1
1895,47,100,1
1942,47,100,13,13,4801,1
**
*****ELEMENT GENERATION FOR CFRP*****
**
*ELEMENT,TYPE=M3D4R
3027,9713,9763,4962,4912
*ELGEN,ELSET=FRP1WEB1
3027,2,50,8,8,4801,1
*ELEMENT,TYPE=M3D4R
3043,9713,9763,4962,4912
3059,9813,9913,5112,5012
*ELGEN,ELSET=FRP2WEB1
3043,2,50,8,8,4801,1
3059,7,100,13,13,4801,1
*ELEMENT,TYPE=M3D4R
3150,36318,36418,31617,31517
*ELGEN,ELSET=FRP3WEB1
3150,22,100,8,8,4801,1
*****
*ELEMENT,TYPE=M3D4R
3703,9743,9793,4992,4942
*ELGEN,ELSET=FRP1WEB2
3703,2,50,8,8,4801,1
*ELEMENT,TYPE=M3D4R
3719,9743,9793,4992,4942
3735,9843,9943,5142,5042
*ELGEN,ELSET=FRP2WEB2
3719,2,50,8,8,4801,1
3735,7,100,13,13,4801,1
*ELEMENT,TYPE=M3D4R
3826,36348,36448,31647,31547
*ELGEN,ELSET=FRP3WEB2
3826,22,100,8,8,4801,1
**
*****ELEMENT SET ASSIGNMENT*****
*****R-LONG REBAR
*****S-VERT REBAR
*****W-MESH
*****ELEMENT SET ASSIGNMENT - SEC1 (NO MESH-AT SUPPORT)*****
**
*ELSET,ELSET=WEB1A1,GENERATE
1201,1202,1
*ELSET,ELSET=WEB1SB1,GENERATE
1203,1211,8
*ELSET,ELSET=WEB1RSC1,GENERATE
1204,1212,8

```

```

*ELSET,ELSET=WEB1RSD1,GENERATE
1205,1213,8
*ELSET,ELSET=WEB1SE1,GENERATE
1206,1214,8
*ELSET,ELSET=WEB1RSF1,GENERATE
1207,1215,8
*ELSET,ELSET=WEB1SG1,GENERATE
1208,1216,8
*ELSET,ELSET=WEB1SH1,GENERATE
1209,1217,8
*ELSET,ELSET=WEB1SI1,GENERATE
1210,1218,8
*****
*ELSET,ELSET=WEB2A1,GENERATE
1877,1878,1
*ELSET,ELSET=WEB2SB1,GENERATE
1879,1887,8
*ELSET,ELSET=WEB2RSC1,GENERATE
1880,1888,8
*ELSET,ELSET=WEB2RSD1,GENERATE
1881,1889,8
*ELSET,ELSET=WEB2SE1,GENERATE
1882,1890,8
*ELSET,ELSET=WEB2RSF1,GENERATE
1883,1891,8
*ELSET,ELSET=WEB2SG1,GENERATE
1884,1892,8
*ELSET,ELSET=WEB2SH1,GENERATE
1885,1893,8
*ELSET,ELSET=WEB2SI1,GENERATE
1886,1894,8
**
*****ELEMENT SET ASSIGNMENT - SEC2 (MESH)*****
**
*ELSET,ELSET=WEB1RSWC2
1267
*ELSET,ELSET=WEB1SWD2
1268
*ELSET,ELSET=WEB1SWE2
1269
*ELSET,ELSET=WEB1RSWF2
1270
*ELSET,ELSET=WEB1SWG2
1271
*ELSET,ELSET=WEB1SWH2
1272
*ELSET,ELSET=WEB1SWI2
1273
*ELSET,ELSET=WEB1SWJ2
1274
*ELSET,ELSET=WEB1SWK2
1275
*ELSET,ELSET=WEB1SWL2
1276
*ELSET,ELSET=WEB1SWM2
1277
*ELSET,ELSET=WEB1RSWN2
1278
**
*ELSET,ELSET=WEB1SSWWB2
1279
*ELSET,ELSET=WEB1SSWWC2
1280
*ELSET,ELSET=WEB1SSWWD2
1281
*ELSET,ELSET=WEB1SSWWE2
1282
*ELSET,ELSET=WEB1RRSSF2
1283
*ELSET,ELSET=WEB1SSWWG2
1284
**
*ELSET,ELSET=WEB1WWB2
1266
**
*ELSET,ELSET=WEB1WA2,GENERATE
1219,1254,1
*ELSET,ELSET=WEB1WB2,GENERATE
1292,1271,13
*ELSET,ELSET=WEB1WC2,GENERATE
1293,1272,13

```

```

*ELSET,ELSET=WEB1WD2,GENERATE
1294,1723,13
*ELSET,ELSET=WEB1WE2,GENERATE
1295,1724,13
*ELSET,ELSET=WEB1WF2,GENERATE
1296,1725,13
*ELSET,ELSET=WEB1WG2,GENERATE
1297,1726,13
*ELSET,ELSET=WEB1WH2,GENERATE
1285,1727,13
*ELSET,ELSET=WEB1WI2,GENERATE
1286,1728,13
*ELSET,ELSET=WEB1WJ2,GENERATE
1287,1729,13
*ELSET,ELSET=WEB1WK2,GENERATE
1288,1730,13
*ELSET,ELSET=WEB1WL2,GENERATE
1289,1731,13
*ELSET,ELSET=WEB1WM2,GENERATE
1290,1732,13
*ELSET,ELSET=WEB1RWN2,GENERATE
1291,1499,13
*ELSET,ELSET=WEB1WN2,GENERATE
1512,1733,13
*****
*ELSET,ELSET=WEB2RSWC2
1943
*ELSET,ELSET=WEB2SWD2
1944
*ELSET,ELSET=WEB2SWE2
1945
*ELSET,ELSET=WEB2RSWF2
1946
*ELSET,ELSET=WEB2SWG2
1947
*ELSET,ELSET=WEB2SWH2
1948
*ELSET,ELSET=WEB2SWI2
1949
*ELSET,ELSET=WEB2SWJ2
1950
*ELSET,ELSET=WEB2SWK2
1951
*ELSET,ELSET=WEB2SWL2
1952
*ELSET,ELSET=WEB2SWM2
1953
*ELSET,ELSET=WEB2RSWN2
1954
**
*ELSET,ELSET=WEB2SSWNB2
1955
*ELSET,ELSET=WEB2SSWNC2
1956
*ELSET,ELSET=WEB2SSWWD2
1957
*ELSET,ELSET=WEB2SSWWE2
1958
*ELSET,ELSET=WEB2RRSSF2
1959
*ELSET,ELSET=WEB2SSWWG2
1960
**
*ELSET,ELSET=WEB2WWB2
1942
**
*ELSET,ELSET=WEB2WA2,GENERATE
1895,1930,1
*ELSET,ELSET=WEB2WB2,GENERATE
1968,2397,13
*ELSET,ELSET=WEB2WC2,GENERATE
1969,2398,13
*ELSET,ELSET=WEB2WD2,GENERATE
1970,2399,13
*ELSET,ELSET=WEB2WE2,GENERATE
1971,2400,13
*ELSET,ELSET=WEB2WF2,GENERATE
1972,2401,13
*ELSET,ELSET=WEB2WG2,GENERATE
1973,2402,13
*ELSET,ELSET=WEB2WH2,GENERATE

```

```

1961,2403,13
*ELSET,ELSET=WEB2WI2,GENERATE
1962,2404,13
*ELSET,ELSET=WEB2WJ2,GENERATE
1963,2405,13
*ELSET,ELSET=WEB2WK2,GENERATE
1964,2406,13
*ELSET,ELSET=WEB2WL2,GENERATE
1965,2407,13
*ELSET,ELSET=WEB2WM2,GENERATE
1966,2408,13
*ELSET,ELSET=WEB2RWN2,GENERATE
1967,2175,13
*ELSET,ELSET=WEB2WN2,GENERATE
2188,2409,13
**
*****ELEMENT SET ASSIGNMENT - SEC3 (END-NO MESH)*****
**
*ELSET,ELSET=WEB1A3,GENERATE
1255,1265,1
*ELSET,ELSET=WEB1B3,GENERATE
1734,1864,13
*ELSET,ELSET=WEB1C3,GENERATE
1735,1865,13
*ELSET,ELSET=WEB1D3,GENERATE
1736,1866,13
*ELSET,ELSET=WEB1E3,GENERATE
1737,1867,13
*ELSET,ELSET=WEB1F3,GENERATE
1738,1868,13
*ELSET,ELSET=WEB1G3,GENERATE
1739,1869,13
*ELSET,ELSET=WEB1H3,GENERATE
1740,1870,13
*ELSET,ELSET=WEB1I3,GENERATE
1741,1871,13
*ELSET,ELSET=WEB1J3,GENERATE
1742,1872,13
*ELSET,ELSET=WEB1K3,GENERATE
1743,1873,13
*ELSET,ELSET=WEB1L3,GENERATE
1744,1874,13
*ELSET,ELSET=WEB1M3,GENERATE
1745,1875,13
*ELSET,ELSET=WEB1N3,GENERATE
1746,1876,13
*****
*ELSET,ELSET=WEB2A3,GENERATE
1931,1941,1
*ELSET,ELSET=WEB2B3,GENERATE
2410,2540,13
*ELSET,ELSET=WEB2C3,GENERATE
2411,2541,13
*ELSET,ELSET=WEB2D3,GENERATE
2412,2542,13
*ELSET,ELSET=WEB2E3,GENERATE
2413,2543,13
*ELSET,ELSET=WEB2F3,GENERATE
2414,2544,13
*ELSET,ELSET=WEB2G3,GENERATE
2415,2545,13
*ELSET,ELSET=WEB2H3,GENERATE
2416,2546,13
*ELSET,ELSET=WEB2I3,GENERATE
2417,2547,13
*ELSET,ELSET=WEB2J3,GENERATE
2418,2548,13
*ELSET,ELSET=WEB2K3,GENERATE
2419,2549,13
*ELSET,ELSET=WEB2L3,GENERATE
2420,2550,13
*ELSET,ELSET=WEB2M3,GENERATE
2421,2551,13
*ELSET,ELSET=WEB2N3,GENERATE
2422,2552,13
**
*****ELEMENT SET ASSIGNMENT FOR WEBS (BY SEC-TO VERIFY)*****
**
*ELSET,ELSET=WEB1SEC1
WEB1A1
WEB1SB1

```

```

WEB1RSC1
WEB1RSD1
WEB1SE1
WEB1RSF1
WEB1SG1
WEB1SH1
WEB1SI1
*ELSET,ELSET=WEB1SEC2
WEB1RSWC2
WEB1SWD2
WEB1SWE2
WEB1RSWF2
WEB1SWG2
WEB1SWH2
WEB1SWI2
WEB1SWJ2
WEB1SWK2
WEB1SWL2
WEB1SWM2
WEB1RSWN2
WEB1SSWNB2
WEB1SSWNC2
WEB1SSWWD2
WEB1SSWWE2
WEB1RRSSF2
WEB1SSWWG2
WEB1WWB2
WEB1WA2
WEB1WB2
WEB1WC2
WEB1WD2
WEB1WE2
WEB1WF2
WEB1WG2
WEB1WH2
WEB1WI2
WEB1WJ2
WEB1WK2
WEB1WL2
WEB1WM2
WEB1RWN2
WEB1WN2
*ELSET,ELSET=WEB1SEC3
WEB1A3
WEB1B3
WEB1C3
WEB1D3
WEB1E3
WEB1F3
WEB1G3
WEB1H3
WEB1I3
WEB1J3
WEB1K3
WEB1L3
WEB1M3
WEB1N3
*****
*ELSET,ELSET=WEB2SEC1
WEB2A1
WEB2SB1
WEB2RSC1
WEB2RSD1
WEB2SE1
WEB2RSF1
WEB2SG1
WEB2SH1
WEB2SI1
*ELSET,ELSET=WEB2SEC2
WEB2RSWC2
WEB2SWD2
WEB2SWE2
WEB2RSWF2
WEB2SWG2
WEB2SWH2
WEB2SWI2
WEB2SWJ2
WEB2SWK2
WEB2SWL2
WEB2SWM2
WEB2RSWN2

```

```

WEB2SSWB2
WEB2SSWC2
WEB2SSWD2
WEB2SSWE2
WEB2RRSSF2
WEB2SSWG2
WEB2WNB2
WEB2WA2
WEB2WB2
WEB2WC2
WEB2WD2
WEB2WE2
WEB2WF2
WEB2WG2
WEB2WH2
WEB2WI2
WEB2WJ2
WEB2WK2
WEB2WL2
WEB2WM2
WEB2RWN2
WEB2WN2
*ELSET,ELSET=WEB2SEC3
WEB2A3
WEB2B3
WEB2C3
WEB2D3
WEB2E3
WEB2F3
WEB2G3
WEB2H3
WEB2I3
WEB2J3
WEB2K3
WEB2L3
WEB2M3
WEB2N3
**
*****ELEMENT GENERATION FOR PRESTRESSING TENDONS*****
**
*ELEMENT,TYPE=T2D2
2553,62624,62724
*ELGEN,ELSET=LPRE1
2553,47,100,1
*ELEMENT,TYPE=T2D2
2600,57823,57923
*ELGEN,ELSET=LPRE2
2600,47,100,1
*ELEMENT,TYPE=T2D2
2647,53022,53122
*ELGEN,ELSET=LPRE3
2647,47,100,1
*ELEMENT,TYPE=T2D2
2694,48221,48321
*ELGEN,ELSET=LPRE4
2694,47,100,1
*ELEMENT,TYPE=T2D2
2741,33718,33768
2743,33818,33918
*ELGEN,ELSET=LPRE5
2741,2,50,1
2743,47,100,1
*****
*ELEMENT,TYPE=T2D2
2790,62654,62754
*ELGEN,ELSET=RPRE1
2790,47,100,1
*ELEMENT,TYPE=T2D2
2837,57853,57953
*ELGEN,ELSET=RPRE2
2837,47,100,1
*ELEMENT,TYPE=T2D2
2884,53052,53152
*ELGEN,ELSET=RPRE3
2884,47,100,1
*ELEMENT,TYPE=T2D2
2931,48251,48351
*ELGEN,ELSET=RPRE4
2931,47,100,1
*ELEMENT,TYPE=T2D2
2978,33748,33798

```

```

2980,33848,33948
*ELGEN,ELSET=RPRES
2978,2,50,1
2980,47,100,1
**
*****MATERIAL PROPERTIES*****
**
*SHELL SECTION,ELSET=SLAB,MATERIAL=CON
136,5
*REBAR LAYER
LONG,25.8,102,0,WWF,0,1
TRANS,13.3,300,0,WWF,90,1
*MATERIAL,NAME=WWF
*DENSITY
7850E-9
*ELASTIC
210000,0.3
*PLASTIC
450
*MATERIAL,NAME=CON
*DENSITY
2400E-9
*ELASTIC
30500,0.2
*CONCRETE
20.4,0
51,0.0022
*FAILURE RATIOS
1.16,0.0836
*TENSION STIFFENING
1,0
0,0.003
*SHEAR RETENTION
1,1E+6
*MATERIAL,NAME=REINF
*DENSITY
7850E-9
*ELASTIC
200000,0.3
*PLASTIC
400
**
*****WEB1*****
**
*****SECTION1*****
**
*SHELL SECTION,ELSET=WEB1A1,MATERIAL=CON
170,5
*SHELL SECTION,ELSET=WEB1SB1,MATERIAL=CON
167.32,5
*REBAR LAYER
VERT1,600,200,0,REINF,90,1
VERT3,100,200,0,REINF,90,1
*SHELL SECTION,ELSET=WEB1RSC1,MATERIAL=CON
161.95,5
*REBAR LAYER
LONG1,300,50,0,REINF,0,1
VERT1,600,200,0,REINF,90,1
VERT3,100,200,0,REINF,90,1
*SHELL SECTION,ELSET=WEB1RSD1,MATERIAL=CON
156.56,5
*REBAR LAYER
LONG2,300,50,0,REINF,0,1
VERT1,600,200,0,REINF,90,1
VERT3,100,200,0,REINF,90,1
*SHELL SECTION,ELSET=WEB1SE1,MATERIAL=CON
151.18,5
*REBAR LAYER
VERT1,600,200,0,REINF,90,1
VERT3,100,200,0,REINF,90,1
*SHELL SECTION,ELSET=WEB1RSF1,MATERIAL=CON
145.79,5
*REBAR LAYER
LONG3,200,50,0,REINF,0,1
VERT1,600,200,0,REINF,90,1
VERT3,100,200,0,REINF,90,1
*SHELL SECTION,ELSET=WEB1SG1,MATERIAL=CON
140.41,5
*REBAR LAYER
VERT1,600,200,0,REINF,90,1
VERT3,100,200,0,REINF,90,1

```

```

*SHELL SECTION,ELSET=WEB1SH1,MATERIAL=CON
135.02,5
*REBAR LAYER
VERT1,600,200,0,REINF,90,1
VERT3,100,200,0,REINF,90,1
*SHELL SECTION,ELSET=WEB1SI1,MATERIAL=CON
129.64,5
*REBAR LAYER
VERT1,600,200,0,REINF,90,1
VERT3,100,200,0,REINF,90,1
**
*****WEB1 SECTION2 - 1ST COLUMN*****
**
*SHELL SECTION,ELSET=WEB1RSWC2,MATERIAL=CON
161.95,5
*REBAR LAYER
LONG1,300,50,0,REINF,0,1
VERT2,600,200,0,REINF,90,1
HORIZ,25.8,102,0,WWF,0,1
VERT,25.8,102,0,WWF,90,1
*SHELL SECTION,ELSET=WEB1SWD2,MATERIAL=CON
156.56,5
*REBAR LAYER
VERT2,600,200,0,REINF,90,1
HORIZ,25.8,102,0,WWF,0,1
VERT,25.8,102,0,WWF,90,1
*SHELL SECTION,ELSET=WEB1SWE2,MATERIAL=CON
151.18,5
*REBAR LAYER
VERT2,600,200,0,REINF,90,1
HORIZ,25.8,102,0,WWF,0,1
VERT,25.8,102,0,WWF,90,1
*SHELL SECTION,ELSET=WEB1RSWF2,MATERIAL=CON
145.79,5
*REBAR LAYER
LONG3,200,50,0,REINF,0,1
VERT2,600,200,0,REINF,90,1
HORIZ,25.8,102,0,WWF,0,1
VERT,25.8,102,0,WWF,90,1
*SHELL SECTION,ELSET=WEB1SWG2,MATERIAL=CON
140.41,5
*REBAR LAYER
VERT2,600,200,0,REINF,90,1
HORIZ,25.8,102,0,WWF,0,1
VERT,25.8,102,0,WWF,90,1
*SHELL SECTION,ELSET=WEB1SWH2,MATERIAL=CON
135.02,5
*REBAR LAYER
VERT2,600,200,0,REINF,90,1
HORIZ,25.8,102,0,WWF,0,1
VERT,25.8,102,0,WWF,90,1
*SHELL SECTION,ELSET=WEB1SWI2,MATERIAL=CON
129.64,5
*REBAR LAYER
VERT2,600,200,0,REINF,90,1
HORIZ,25.8,102,0,WWF,0,1
VERT,25.8,102,0,WWF,90,1
*SHELL SECTION,ELSET=WEB1SWJ2,MATERIAL=CON
124.26,5
*REBAR LAYER
VERT2,600,200,0,REINF,90,1
HORIZ,25.8,102,0,WWF,0,1
VERT,25.8,102,0,WWF,90,1
*SHELL SECTION,ELSET=WEB1SWK2,MATERIAL=CON
118.87,5
*REBAR LAYER
VERT2,600,200,0,REINF,90,1
HORIZ,25.8,102,0,WWF,0,1
VERT,25.8,102,0,WWF,90,1
*SHELL SECTION,ELSET=WEB1SWL2,MATERIAL=CON
113.49,5
*REBAR LAYER
VERT2,600,200,0,REINF,90,1
HORIZ,25.8,102,0,WWF,0,1
VERT,25.8,102,0,WWF,90,1
*SHELL SECTION,ELSET=WEB1SWM2,MATERIAL=CON
108.1,5
*REBAR LAYER
VERT2,600,200,0,REINF,90,1
HORIZ,25.8,102,0,WWF,0,1
VERT,25.8,102,0,WWF,90,1

```



```

*SHELL SECTION,ELSET=WEB1RSWN2,MATERIAL=CON
102.7,5
*REBAR LAYER
LONG4,600,50,0,REINF,0,1
VERT2,600,200,0,REINF,90,1
HORIZ,25.8,102,0,WWF,0,1
VERT,25.8,102,0,WWF,90,1
**
*****WEB1 SECTION2 - 2ND COLUMN*****
**
*SHELL SECTION,ELSET=WEB1SSWB2,MATERIAL=CON
167.32,5
*REBAR LAYER
VERT4,100,200,0,REINF,90,1
HORIZ,25.8,102,0,WWF,0,1
VERT,25.8,102,0,WWF,90,1
*SHELL SECTION,ELSET=WEB1SSWWC2,MATERIAL=CON
161.95,5
*REBAR LAYER
VERT4,100,200,0,REINF,90,1
HORIZ,25.8,102,0,WWF,0,1
VERT,25.8,102,0,WWF,90,1
*SHELL SECTION,ELSET=WEB1SSWWD2,MATERIAL=CON
156.56,5
*REBAR LAYER
VERT4,100,200,0,REINF,90,1
HORIZ,25.8,102,0,WWF,0,1
VERT,25.8,102,0,WWF,90,1
*SHELL SECTION,ELSET=WEB1SSWWE2,MATERIAL=CON
151.18,5
*REBAR LAYER
VERT4,100,200,0,REINF,90,1
HORIZ,25.8,102,0,WWF,0,1
VERT,25.8,102,0,WWF,90,1
*SHELL SECTION,ELSET=WEB1RRSSF2,MATERIAL=CON
145.79,5
*REBAR LAYER
LONG3,200,50,0,REINF,0,1
VERT4,100,200,0,REINF,90,1
HORIZ,25.8,102,0,WWF,0,1
VERT,25.8,102,0,WWF,90,1
*SHELL SECTION,ELSET=WEB1SSWWG2,MATERIAL=CON
140.41,5
*REBAR LAYER
VERT4,100,200,0,REINF,90,1
HORIZ,25.8,102,0,WWF,0,1
VERT,25.8,102,0,WWF,90,1
**
*****WEB1 SECTION2 - MESH*****
**
*SHELL SECTION,ELSET=WEB1WWB2,MATERIAL=CON
167.32,5
*REBAR LAYER
HORIZ,25.8,102,0,WWF,0,1
VERT,25.8,102,0,WWF,90,1
*****
*SHELL SECTION,ELSET=WEB1WA2,MATERIAL=CON
170,5
*REBAR LAYER
HORIZ,25.8,102,0,WWF,0,1
VERT,25.8,102,0,WWF,90,1
*SHELL SECTION,ELSET=WEB1WB2,MATERIAL=CON
167.32,5
*REBAR LAYER
HORIZ,25.8,102,0,WWF,0,1
VERT,25.8,102,0,WWF,90,1
*SHELL SECTION,ELSET=WEB1WC2,MATERIAL=CON
161.95,5
*REBAR LAYER
HORIZ,25.8,102,0,WWF,0,1
VERT,25.8,102,0,WWF,90,1
*SHELL SECTION,ELSET=WEB1WD2,MATERIAL=CON
156.56,5
*REBAR LAYER
HORIZ,25.8,102,0,WWF,0,1
VERT,25.8,102,0,WWF,90,1
*SHELL SECTION,ELSET=WEB1WE2,MATERIAL=CON
151.18,5
*REBAR LAYER
HORIZ,25.8,102,0,WWF,0,1
VERT,25.8,102,0,WWF,90,1

```

```

*SHELL SECTION,ELSET=WEB1WF2,MATERIAL=CON
145.79,5
*REBAR LAYER
HORIZ,25.8,102,0,WWF,0,1
VERT,25.8,102,0,WWF,90,1
*SHELL SECTION,ELSET=WEB1WG2,MATERIAL=CON
140.41,5
*REBAR LAYER
HORIZ,25.8,102,0,WWF,0,1
VERT,25.8,102,0,WWF,90,1
*SHELL SECTION,ELSET=WEB1WH2,MATERIAL=CON
135.02,5
*REBAR LAYER
HORIZ,25.8,102,0,WWF,0,1
VERT,25.8,102,0,WWF,90,1
*SHELL SECTION,ELSET=WEB1WI2,MATERIAL=CON
129.64,5
*REBAR LAYER
HORIZ,25.8,102,0,WWF,0,1
VERT,25.8,102,0,WWF,90,1
*SHELL SECTION,ELSET=WEB1WJ2,MATERIAL=CON
124.26,5
*REBAR LAYER
HORIZ,25.8,102,0,WWF,0,1
VERT,25.8,102,0,WWF,90,1
*SHELL SECTION,ELSET=WEB1WK2,MATERIAL=CON
118.87,5
*REBAR LAYER
HORIZ,25.8,102,0,WWF,0,1
VERT,25.8,102,0,WWF,90,1
*SHELL SECTION,ELSET=WEB1WL2,MATERIAL=CON
113.49,5
*REBAR LAYER
HORIZ,25.8,102,0,WWF,0,1
VERT,25.8,102,0,WWF,90,1
*SHELL SECTION,ELSET=WEB1WM2,MATERIAL=CON
108.1,5
*REBAR LAYER
HORIZ,25.8,102,0,WWF,0,1
VERT,25.8,102,0,WWF,90,1
*SHELL SECTION,ELSET=WEB1RWN2,MATERIAL=CON
102.7,5
*REBAR LAYER
LONG4,600,50,0,REINF,0,1
HORIZ,25.8,102,0,WWF,0,1
VERT,25.8,102,0,WWF,90,1
*SHELL SECTION,ELSET=WEB1WN2,MATERIAL=CON
102.7,5
*REBAR LAYER
HORIZ,25.8,102,0,WWF,0,1
VERT,25.8,102,0,WWF,90,1
**
*****WEB1 SECTION3 - NO MESH*****
**
*SHELL SECTION,ELSET=WEB1A3,MATERIAL=CON
170,5
*SHELL SECTION,ELSET=WEB1B3,MATERIAL=CON
167.32,5
*SHELL SECTION,ELSET=WEB1C3,MATERIAL=CON
161.95,5
*SHELL SECTION,ELSET=WEB1D3,MATERIAL=CON
156.56,5
*SHELL SECTION,ELSET=WEB1E3,MATERIAL=CON
151.18,5
*SHELL SECTION,ELSET=WEB1F3,MATERIAL=CON
145.79,5
*SHELL SECTION,ELSET=WEB1G3,MATERIAL=CON
140.41,5
*SHELL SECTION,ELSET=WEB1H3,MATERIAL=CON
135.02,5
*SHELL SECTION,ELSET=WEB1I3,MATERIAL=CON
129.64,5
*SHELL SECTION,ELSET=WEB1J3,MATERIAL=CON
124.26,5
*SHELL SECTION,ELSET=WEB1K3,MATERIAL=CON
118.87,5
*SHELL SECTION,ELSET=WEB1L3,MATERIAL=CON
113.49,5
*SHELL SECTION,ELSET=WEB1M3,MATERIAL=CON
108.1,5
*SHELL SECTION,ELSET=WEB1N3,MATERIAL=CON

```

```

102.7,5
**
*****WEB2*****
**
*****SECTION1*****
**
*SHELL SECTION,ELSET=WEB2A1,MATERIAL=CON
170,5
*SHELL SECTION,ELSET=WEB2SB1,MATERIAL=CON
167.32,5
*REBAR LAYER
VERT1,600,200,0,REINF,90,1
VERT3,100,200,0,REINF,90,1
*SHELL SECTION,ELSET=WEB2RSC1,MATERIAL=CON
161.95,5
*REBAR LAYER
LONG1,300,50,0,REINF,0,1
VERT1,600,200,0,REINF,90,1
VERT3,100,200,0,REINF,90,1
*SHELL SECTION,ELSET=WEB2RSD1,MATERIAL=CON
156.56,5
*REBAR LAYER
LONG2,300,50,0,REINF,0,1
VERT1,600,200,0,REINF,90,1
VERT3,100,200,0,REINF,90,1
*SHELL SECTION,ELSET=WEB2SE1,MATERIAL=CON
151.18,5
*REBAR LAYER
VERT1,600,200,0,REINF,90,1
VERT3,100,200,0,REINF,90,1
*SHELL SECTION,ELSET=WEB2RSF1,MATERIAL=CON
145.79,5
*REBAR LAYER
LONG3,200,50,0,REINF,0,1
VERT1,600,200,0,REINF,90,1
VERT3,100,200,0,REINF,90,1
*SHELL SECTION,ELSET=WEB2SG1,MATERIAL=CON
140.41,5
*REBAR LAYER
VERT1,600,200,0,REINF,90,1
VERT3,100,200,0,REINF,90,1
*SHELL SECTION,ELSET=WEB2SH1,MATERIAL=CON
135.02,5
*REBAR LAYER
VERT1,600,200,0,REINF,90,1
VERT3,100,200,0,REINF,90,1
*SHELL SECTION,ELSET=WEB2SI1,MATERIAL=CON
129.64,5
*REBAR LAYER
VERT1,600,200,0,REINF,90,1
VERT3,100,200,0,REINF,90,1
**
*****WEB2 SECTION2 - 1ST COLUMN*****
**
*SHELL SECTION,ELSET=WEB2RSWC2,MATERIAL=CON
161.95,5
*REBAR LAYER
LONG1,300,50,0,REINF,0,1
VERT2,600,200,0,REINF,90,1
HORIZ,25.8,102,0,WWF,0,1
VERT,25.8,102,0,WWF,90,1
*SHELL SECTION,ELSET=WEB2SWD2,MATERIAL=CON
156.56,5
*REBAR LAYER
VERT2,600,200,0,REINF,90,1
HORIZ,25.8,102,0,WWF,0,1
VERT,25.8,102,0,WWF,90,1
*SHELL SECTION,ELSET=WEB2SWE2,MATERIAL=CON
151.18,5
*REBAR LAYER
VERT2,600,200,0,REINF,90,1
HORIZ,25.8,102,0,WWF,0,1
VERT,25.8,102,0,WWF,90,1
*SHELL SECTION,ELSET=WEB2RSWF2,MATERIAL=CON
145.79,5
*REBAR LAYER
LONG3,200,50,0,REINF,0,1
VERT2,600,200,0,REINF,90,1
HORIZ,25.8,102,0,WWF,0,1
VERT,25.8,102,0,WWF,90,1
*SHELL SECTION,ELSET=WEB2SWG2,MATERIAL=CON

```

```

140.41,5
*REBAR LAYER
VERT2,600,200,0,REINF,90,1
HORIZ,25.8,102,0,WWF,0,1
VERT,25.8,102,0,WWF,90,1
*SHELL SECTION,ELSET=WEB2SWH2,MATERIAL=CON
135.02,5
*REBAR LAYER
VERT2,600,200,0,REINF,90,1
HORIZ,25.8,102,0,WWF,0,1
VERT,25.8,102,0,WWF,90,1
*SHELL SECTION,ELSET=WEB2SWI2,MATERIAL=CON
129.64,5
*REBAR LAYER
VERT2,600,200,0,REINF,90,1
HORIZ,25.8,102,0,WWF,0,1
VERT,25.8,102,0,WWF,90,1
*SHELL SECTION,ELSET=WEB2SWJ2,MATERIAL=CON
124.26,5
*REBAR LAYER
VERT2,600,200,0,REINF,90,1
HORIZ,25.8,102,0,WWF,0,1
VERT,25.8,102,0,WWF,90,1
*SHELL SECTION,ELSET=WEB2SWK2,MATERIAL=CON
118.87,5
*REBAR LAYER
VERT2,600,200,0,REINF,90,1
HORIZ,25.8,102,0,WWF,0,1
VERT,25.8,102,0,WWF,90,1
*SHELL SECTION,ELSET=WEB2SWL2,MATERIAL=CON
113.49,5
*REBAR LAYER
VERT2,600,200,0,REINF,90,1
HORIZ,25.8,102,0,WWF,0,1
VERT,25.8,102,0,WWF,90,1
*SHELL SECTION,ELSET=WEB2SWM2,MATERIAL=CON
108.1,5
*REBAR LAYER
VERT2,600,200,0,REINF,90,1
HORIZ,25.8,102,0,WWF,0,1
VERT,25.8,102,0,WWF,90,1
*SHELL SECTION,ELSET=WEB2RSWN2,MATERIAL=CON
102.7,5
*REBAR LAYER
LONG4,600,50,0,REINF,0,1
VERT2,600,200,0,REINF,90,1
HORIZ,25.8,102,0,WWF,0,1
VERT,25.8,102,0,WWF,90,1
**
*****WEB2 SECTION2 - 2ND COLUMN*****
**
*SHELL SECTION,ELSET=WEB2SSWB2,MATERIAL=CON
167.32,5
*REBAR LAYER
VERT4,100,200,0,REINF,90,1
HORIZ,25.8,102,0,WWF,0,1
VERT,25.8,102,0,WWF,90,1
*SHELL SECTION,ELSET=WEB2SSWWC2,MATERIAL=CON
161.95,5
*REBAR LAYER
VERT4,100,200,0,REINF,90,1
HORIZ,25.8,102,0,WWF,0,1
VERT,25.8,102,0,WWF,90,1
*SHELL SECTION,ELSET=WEB2SSWWD2,MATERIAL=CON
156.56,5
*REBAR LAYER
VERT4,100,200,0,REINF,90,1
HORIZ,25.8,102,0,WWF,0,1
VERT,25.8,102,0,WWF,90,1
*SHELL SECTION,ELSET=WEB2SSWWE2,MATERIAL=CON
151.18,5
*REBAR LAYER
VERT4,100,200,0,REINF,90,1
HORIZ,25.8,102,0,WWF,0,1
VERT,25.8,102,0,WWF,90,1
*SHELL SECTION,ELSET=WEB2RRSSF2,MATERIAL=CON
145.79,5
*REBAR LAYER
LONG3,200,50,0,REINF,0,1
VERT4,100,200,0,REINF,90,1
HORIZ,25.8,102,0,WWF,0,1

```

```

VERT,25.8,102,0,WWF,90,1
*SHELL SECTION,ELSET=WEB2SSWWG2,MATERIAL=CON
140.41,5
*REBAR LAYER
VERT,100,200,0,REINF,90,1
HORIZ,25.8,102,0,WWF,0,1
VERT,25.8,102,0,WWF,90,1
**
*****WEB2 SECTION2 - MESH*****
**
*SHELL SECTION,ELSET=WEB2WWB2,MATERIAL=CON
167.32,5
*REBAR LAYER
HORIZ,25.8,102,0,WWF,0,1
VERT,25.8,102,0,WWF,90,1
*****
*SHELL SECTION,ELSET=WEB2WA2,MATERIAL=CON
170,5
*REBAR LAYER
HORIZ,25.8,102,0,WWF,0,1
VERT,25.8,102,0,WWF,90,1
*SHELL SECTION,ELSET=WEB2WB2,MATERIAL=CON
167.32,5
*REBAR LAYER
HORIZ,25.8,102,0,WWF,0,1
VERT,25.8,102,0,WWF,90,1
*SHELL SECTION,ELSET=WEB2WC2,MATERIAL=CON
161.95,5
*REBAR LAYER
HORIZ,25.8,102,0,WWF,0,1
VERT,25.8,102,0,WWF,90,1
*SHELL SECTION,ELSET=WEB2WD2,MATERIAL=CON
156.56,5
*REBAR LAYER
HORIZ,25.8,102,0,WWF,0,1
VERT,25.8,102,0,WWF,90,1
*SHELL SECTION,ELSET=WEB2WE2,MATERIAL=CON
151.18,5
*REBAR LAYER
HORIZ,25.8,102,0,WWF,0,1
VERT,25.8,102,0,WWF,90,1
*SHELL SECTION,ELSET=WEB2WF2,MATERIAL=CON
145.79,5
*REBAR LAYER
HORIZ,25.8,102,0,WWF,0,1
VERT,25.8,102,0,WWF,90,1
*SHELL SECTION,ELSET=WEB2WG2,MATERIAL=CON
140.41,5
*REBAR LAYER
HORIZ,25.8,102,0,WWF,0,1
VERT,25.8,102,0,WWF,90,1
*SHELL SECTION,ELSET=WEB2WH2,MATERIAL=CON
135.02,5
*REBAR LAYER
HORIZ,25.8,102,0,WWF,0,1
VERT,25.8,102,0,WWF,90,1
*SHELL SECTION,ELSET=WEB2WI2,MATERIAL=CON
129.64,5
*REBAR LAYER
HORIZ,25.8,102,0,WWF,0,1
VERT,25.8,102,0,WWF,90,1
*SHELL SECTION,ELSET=WEB2WJ2,MATERIAL=CON
124.26,5
*REBAR LAYER
HORIZ,25.8,102,0,WWF,0,1
VERT,25.8,102,0,WWF,90,1
*SHELL SECTION,ELSET=WEB2WK2,MATERIAL=CON
118.87,5
*REBAR LAYER
HORIZ,25.8,102,0,WWF,0,1
VERT,25.8,102,0,WWF,90,1
*SHELL SECTION,ELSET=WEB2WL2,MATERIAL=CON
113.49,5
*REBAR LAYER
HORIZ,25.8,102,0,WWF,0,1
VERT,25.8,102,0,WWF,90,1
*SHELL SECTION,ELSET=WEB2WM2,MATERIAL=CON
108.1,5
*REBAR LAYER
HORIZ,25.8,102,0,WWF,0,1
VERT,25.8,102,0,WWF,90,1

```

```

*SHELL SECTION,ELSET=WEB2RWN2,MATERIAL=CON
102.7,5
*REBAR LAYER
LONG4,600,50,0,REINF,0,1
HORIZ,25.8,102,0,WWF,0,1
VERT,25.8,102,0,WWF,90,1
*SHELL SECTION,ELSET=WEB2WN2,MATERIAL=CON
102.7,5
*REBAR LAYER
HORIZ,25.8,102,0,WWF,0,1
VERT,25.8,102,0,WWF,90,1
**
*****WEB2 SECTION3 - NO MESH*****
**
*SHELL SECTION,ELSET=WEB2A3,MATERIAL=CON
170,5
*SHELL SECTION,ELSET=WEB2B3,MATERIAL=CON
167.32,5
*SHELL SECTION,ELSET=WEB2C3,MATERIAL=CON
161.95,5
*SHELL SECTION,ELSET=WEB2D3,MATERIAL=CON
156.56,5
*SHELL SECTION,ELSET=WEB2E3,MATERIAL=CON
151.18,5
*SHELL SECTION,ELSET=WEB2F3,MATERIAL=CON
145.79,5
*SHELL SECTION,ELSET=WEB2G3,MATERIAL=CON
140.41,5
*SHELL SECTION,ELSET=WEB2H3,MATERIAL=CON
135.02,5
*SHELL SECTION,ELSET=WEB2I3,MATERIAL=CON
129.64,5
*SHELL SECTION,ELSET=WEB2J3,MATERIAL=CON
124.26,5
*SHELL SECTION,ELSET=WEB2K3,MATERIAL=CON
118.87,5
*SHELL SECTION,ELSET=WEB2L3,MATERIAL=CON
113.49,5
*SHELL SECTION,ELSET=WEB2M3,MATERIAL=CON
108.1,5
*SHELL SECTION,ELSET=WEB2N3,MATERIAL=CON
102.7,5
**
*****PRESTRESSING STEEL*****
**
*SOLID SECTION,ELSET=LPRE1,MATERIAL=PRESTEEL
148
*SOLID SECTION,ELSET=LPRE2,MATERIAL=PRESTEEL
148
*SOLID SECTION,ELSET=LPRE3,MATERIAL=PRESTEEL
148
*SOLID SECTION,ELSET=LPRE4,MATERIAL=PRESTEEL
148
*SOLID SECTION,ELSET=LPRE5,MATERIAL=PRESTEEL
148
*SOLID SECTION,ELSET=RPRE1,MATERIAL=PRESTEEL
148
*SOLID SECTION,ELSET=RPRE2,MATERIAL=PRESTEEL
148
*SOLID SECTION,ELSET=RPRE3,MATERIAL=PRESTEEL
148
*SOLID SECTION,ELSET=RPRE4,MATERIAL=PRESTEEL
148
*SOLID SECTION,ELSET=RPRE5,MATERIAL=PRESTEEL
148
*MATERIAL,NAME=PRESTEEL
*DENSITY
7850E-9
*ELASTIC
200000,0.3
*PLASTIC
1580
**
*****CARBON FRP*****
**
*MEMBRANE SECTION,ELSET=FRP1WEB1,MATERIAL=FRP
2
*MEMBRANE SECTION,ELSET=FRP2WEB1,MATERIAL=FRP
2
*MEMBRANE SECTION,ELSET=FRP3WEB1,MATERIAL=FRP
2

```



```

*MEMBRANE SECTION,ELSET=FRP1WEB2,MATERIAL=FRP
2
*MEMBRANE SECTION,ELSET=FRP2WEB2,MATERIAL=FRP
2
*MEMBRANE SECTION,ELSET=FRP3WEB2,MATERIAL=FRP
2
*MATERIAL,NAME=FRP
*ELASTIC,TYPE=LAMINA
72400,40.6,0.0001,0.0001,0.0001,0.0001,0,0
*PLASTIC
876,0
***44,0
***44,0.012
***44,0.024
**
*****PRESTRESSING OF TENDONS*****
**
*INITIAL CONDITIONS,TYPE=STRESS
LPRE1,1267
LPRE2,1267
LPRE3,1267
LPRE4,1267
LPRE5,1267
RPRE1,1267
RPRE2,1267
RPRE3,1267
RPRE4,1267
RPRE5,1267
**
*****BOUNDARY CONDITIONS (1/2 OF DT MODELED)*****
**
*NGEN,NSET=SLABSUPP
4802,4852,2
*NGEN,NSET=WEB1SUPP
9712,72125,4801
*NGEN,NSET=WEB2SUPP
9742,72155,4801
*NSET,NSET=WEB1BOTSUPP
43370
*NSET,NSET=WEB2BOTSUPP
43400
*BOUNDARY
SLABSUPP,1
SLABSUPP,4
***SLABSUPP,5
WEB1SUPP,1
WEB1SUPP,4
***WEB1SUPP,5
WEB2SUPP,1
WEB2SUPP,4
***WEB2SUPP,5
WEB1BOTSUPP,2,3
WEB2BOTSUPP,3
**
*****DEAD LOAD*****
**
*ELSET,ELSET=ENTIREDT,GENERATE
1201,2552,1
**
*NSET,NSET=RE1
43400,43370
*NSET,NSET=RE2
72155,72125
**
*STEP,NLGEOM
*STATIC
*DLOAD
SLAB,GRAV,9.81,0,0,-1
ENTIREDT,GRAV,9.81,0,0,-1
***ELPRINT,POSITION=AVERAGED AT NODES,ELSET=ENTIREDT
***S11
*ENDSTEP
**
*****BARRIER LOADING*****
**
*NGEN,NSET=LOADNODES
912,4712,100
942,4742,100
**
*NSET,NSET=NOUTPUT
72155,72055,72125,72025,4812,4842

```

```
LOADNODES
**
*ELSET,ELSET=EOUTPUT,GENERATE
1126,1200,1
**
*STEP,INC=5000
*STATIC,RIKS
0.0001,1.0,1E-40,0.5
*CLOAD
LOADNODES,3,-6000
**
*OUTPUT,HISTORY,OP=ADD
*NODE OUTPUT,NSET=NOUTPUT
U3,CF3
*ELEMENT OUTPUT,ELSET=EOUTPUT
SE1
*ENDSTEP
**
```

APPENDIX B

MANUAL CALCULATIONS

AASHTO TYPE III GIRDER FLEXURE CALCULATIONS

AASHTO Type III Girder Nominal Moment Capacity

For comparison purposes, the flexural strength for the AASHTO Type III prestressed girder was calculated by conventional methods. The design process listed below, is as described in *Prestressed Concrete Structures* (1997), by M.P. Collins.

The ACI Code exploits the use of the partial safety factor approach, where factors are applied to all loads and resistances. It states that the flexural requirement of a prestressed member section be as follows: the design strength, ϕM_n , must be equal to or greater than the required moment strength, M_u , as is expected. In the equation, M_n is the nominal flexural strength, M_u is the factored moment due to external loading, and load factor $\phi = 0.90$.

The nominal strength of any section is calculated with regard to the fact that all dimensions, material properties and other decisive factors, are as indicated on structural drawings, for instance. The AASHTO Type III prestressed girder has two main cross sections: at midspan, where tendons are straight and at support locations where the tendons are inclined, the former of which will be discussed. The nominal flexural strength calculation, for the Type III in this study, is shown below.

$$\text{Nominal flexural strength, } M_n = (A_p f_p) \left(d_p - \frac{a}{2} \right)$$

$$A_p = 26 \times 12.7 \text{ mm nominal strands} = 26 \times 99 \text{ mm}^2 = 2574 \text{ mm}^2$$

For members with bonded tendons, the prestressing steel stress at maximum moment is,

$$f_p = f_{pu} \left(1 - \frac{\gamma_p}{\beta_1} \left[\rho_p \frac{f_{pu}}{f'_c} + \frac{d}{d_p} (w - w') \right] \right)$$

The ultimate tensile strength, f_{pu} , for the 12.7 mm nominal strands is 1860 MPa.

To account for the shape of the stress-strain curve for the prestressing steel, the following factor is used and chosen appropriately,

$$\gamma_p = 0.28 \quad (\text{for low-relaxation strands, where } f_{py}/f_{pu} \geq 0.90)$$

Instead of determining the complete moment-curvature response, it is assumed that the maximum moment resistance for the girder occurs when the extreme top fibre reaches a compressive strain of 0.003. The corresponding stress block factors are,

$$\alpha_1 = 0.85$$

and

$$\begin{aligned} \beta_1 &= 0.85 - (f'_c - 4000)(0.00005) \geq 0.65 \quad \text{for } f'_c > 4000 \text{ psi} \\ &= 0.85 - (5000 - 4000)(0.00005) \\ &= 0.8 \end{aligned}$$

Since the top slab and I-girder have dissimilar concrete compressive strengths, 27.5 MPa and 34.5 MPa respectively, a transformed concrete section is calculated.

$$E = 3300 \sqrt{f'_c} + 6900$$

$$E_{girder} = 3300 \sqrt{34.5} + 6900 = 26,283 \text{ MPa}$$

$$E_{slab} = 3300\sqrt{27.5} + 6900 = 24,205 \text{ MPa}$$

$$n = \frac{E_{girder}}{E_{slab}} = 1.086$$

The ratio of prestressed reinforcement is calculated to be,

$$\rho_p = \frac{A_p}{bd_p} = \frac{2574}{(1600/n)(1216)} = 0.00144$$

Distances from the extreme compression fibre to the centroid of non-prestressed and prestressed reinforcement are computed:

$$d = (1143 + 190) - 46 = 1287 \text{ mm}$$

$$d_p = (1143 + 190) - 117.3 = 1216 \text{ mm}$$

Determination of the ratio of non-prestressed reinforcement is as below,

$$\rho = \frac{A_s}{bd} = \frac{(4 \times 200 \text{ mm}^2)}{(1600/n)(1287)} = 0.000422$$

$$w = \frac{\rho f_y}{f'_c} = \frac{(0.000422)(400)}{34.5} = 0.00489$$

Finally, the prestressing steel stress is found,

$$f_p = 1860 \left(1 - \frac{0.28}{0.80} \left[0.00144 \frac{(1860)}{(34.5)} + \frac{1287}{1216} (0.00489 - 0) \right] \right) = 1806 \text{ MPa}$$

The depth of the compression stress block is then found to be,

$$a = \frac{A_p f_p}{0.85 f'_c b} = \frac{(2574)(1806)}{0.85(34.5)(1600/n)} = 107.6 \text{ mm}$$

This, ascertains that the neutral axis lies in the top slab.

With the above established values, we have

$$M_n = (2574)(1806) \left(1216 - \frac{107.6}{2} \right) = 5403 \text{ kN}\cdot\text{m}$$

AASHTO Type III Girder Moment Capacity with CFRP Strengthening

The only known code, or set of regulations, to analyse FRP strengthened structures are the ISIS Canada Design Manuals. Their purpose is to provide the user with guidelines and is not considered a design code, but rather information based on experimental results and various research.

First off, an assumption was made to further the analysis. Four typical failure modes exist for reinforced concrete, being:

- (i) concrete crushing,
- (ii) steel yielding followed by concrete crushing,
- (iii) steel yielding followed by FRP rupture, and
- (iv) debonding of FRP.

We will consider our failure mode to consist of yielding of the tensile and prestressing reinforcement, with rupture of the CFRP placed on the bottom chamfer only, followed ultimately by crushing of the concrete. We also assume that all initial strains in the concrete, the tensile steel and the prestressing steel are negligible ($\epsilon_{ci} = \epsilon_{pi} = \epsilon_{si} = 0$). All assumptions are to be checked, and corrected if in disagreement.

For bridges, the equivalent stress block factors are:

$$\begin{aligned}\alpha_l &= 0.85 \quad \text{and} \quad 0.85 \geq \beta_l = 1.09 - 0.008 f'_c \geq 0.65 \\ &= 1.09 - (0.008)(34.5) \\ &= 0.814\end{aligned}$$

Next we compute the position of the neutral axis, assumed to lie in the concrete slab.

$$C = T$$

$$C_c = T_s + T_{frp} + T_p$$

$$\alpha_1 f'_c \beta_1 b c = f_y A_s + E_{frp} \epsilon_{cu} A_{frp,top} \left(\frac{d_{frp,top} - c}{c} \right) + E_{frp} \epsilon_{frpu} A_{frp,bot} + E_p \epsilon_{pu} A_p$$

$$0.85(27.5)(0.814)(1600) c^2 = (400)(4 \times 200) c + (86,900 \times 0.0035)(161.6)(424.95) -$$

$$(86,900 \times 0.0035)(161.6) c + (86,900 \times 0.0105)(269.4) c + (1860)(2574) c$$

$$c = 178.1 \text{ mm}$$

$$\alpha = \beta_1 c = 145 \text{ mm} < 190 \text{ mm slab thickness}$$

It is seen above that our assumption is true, and thus will carry on.

Above, A_{frp} for moment was decided by taking into account only the cross sectional area of the longitudinal CFRP strips, running along the chamfers, with a 0.25 mm thickness per layer.

$$A_{frp,top} = 0.25 \times 2 [2(161.6)] = 161.6 \text{ mm}^2$$

$$A_{frp,bot} = 0.25 \times 2 [2(269.4)] = 269.4 \text{ mm}^2$$

The centroids of CFRP moment reinforcement, at both the top and bottom chamfers:

$$y_{b,frp,top} = 908.05 \text{ mm} \quad d_{frp,top} = (1143 + 190) - 908.05 = 424.95 \text{ mm}$$

$$y_{b,frp,bot} = 273.05 \text{ mm} \quad d_{frp,bot} = (1143 + 190) - 273.05 = 1059.95 \text{ mm}$$

Next, a check of material strains to verify whether the assumed failure mode is prevalent.

$$\varepsilon_s = \varepsilon_{cu} \left(\frac{d - c}{c} \right) = 0.0035 \left(\frac{1287 - 178.1}{178.1} \right) = 0.022 > 0.002 \quad \text{tension steel yields}$$

$$\varepsilon_{frp,top} = \varepsilon_{cu} \left(\frac{d_{frp,top} - c}{c} \right) = 0.0035 \left(\frac{424.95 - 178.1}{178.1} \right) = 0.0048 < 0.0105$$

$$\varepsilon_{frp,bot} = \varepsilon_{cu} \left(\frac{d_{frp,bot} - c}{c} \right) = 0.0035 \left(\frac{1059.95 - 178.1}{178.1} \right) = 0.017 > 0.0105 \quad \text{CFRP ruptures}$$

$$\varepsilon_{ps} = \varepsilon_{cu} \left(\frac{d_p - c}{c} \right) = 0.0035 \left(\frac{1216 - 178.1}{178.1} \right) = 0.020 > 0.01 \quad \text{prestressing steel yields}$$

Since the tensile and prestressing steel have yielded, and the bottom chamfer FRP ruptured, our assumption is correct. The strengthened girder moment capacity, M_n , can now be found.

$$M_n = T_s \left(d - \frac{a}{2} \right) + T_{frp,top} \left(d_{frp,top} - \frac{a}{2} \right) + T_{frp,bot} \left(d_{frp,bot} - \frac{a}{2} \right) + T_p \left(d_p - \frac{a}{2} \right)$$

$$M_n = (400)(4 \times 200) \left(1287 - \frac{145}{2} \right) + (86,900 \times 0.0048)(161.6) \left(424.95 - \frac{145}{2} \right) +$$

$$(86,900 \times 0.0105)(269.4) \left(1059.95 - \frac{145}{2} \right) + (1860)(2574) \left(1216 - \frac{145}{2} \right)$$

$$M_n = 6130 \text{ kN}\cdot\text{m}$$

Strength gain, under nominal conditions, for flexure is therefore:

$$\text{Flexure strength gain} = \left(\frac{6130}{5403} - 1 \right) \times 100\% = 13.5\%$$

AASHTO TYPE III GIRDER SHEAR CALCULATIONS

AASHTO Type III Girder Nominal Shear Capacity

The shear capacity of the AASHTO Type III girder is calculated using the Modified Compression Field Theory, for support and midspan locations, as explained in *Prestressed Concrete Structures* (1997), by M.P. Collins. Below, only the support location computations are carried out in detail.

The nominal shear resistance of a prestressed concrete section is given by,

$$V_n = V_c + V_s + V_p$$

We begin by evaluating the first term on the right side of the equation, V_c , the nominal shear strength provided by tensile stresses in the concrete, which equals,

$$V_c = 0.17\sqrt{f'_c}b_wd + 0.05\sqrt{f'_c}b_wd$$

The linear lever arm values, in this case d , need not be taken less than $0.8h$, and jd not less than $0.9d$. Thus,

$$d = 0.8h = 0.8 (1143 + 190) = 1066.4 \text{ mm}$$

$$jd = 0.9d = 0.9 (1066.4) = 959.8 \text{ mm}$$

which is followed by,

$$\begin{aligned} V_c &= 0.17\sqrt{f'_c}b_wd + 0.05\sqrt{f'_c}b_wd \\ &= 0.22\sqrt{34.5}(177.8)(1066.4) \\ &= 245 \text{ kN} \end{aligned}$$

The second unknown is V_s , being the nominal shear strength provided by tensile stresses in the web reinforcement. Considering 15M, two leg stirrups at a 76.2 mm spacing near supports,

$$V_s = \frac{A_v f_y d}{s} = \frac{(2 \times 200)(400)(1066.4)}{76.2} = 2239 \text{ kN}$$

Lastly, V_p , the nominal shear strength, provided by the component in the direction of the applied shear, of the force in the longitudinal prestressing tendons is found as,

$$V_p = (26 \text{ strands})(99 \text{ mm}^2)(1058 \text{ MPa}) \frac{(397.56 - 37.86)}{(21895/2)} = 89.5 \text{ kN}$$

Above,

$f_{pe} = 1058 \text{ MPa}$, is the effective stress in the prestressing strands after all losses, eccentricity at midspan,

$$e_c = 397.56 \text{ mm}$$

$$= (y_b \text{ of girder} = 514.86 \text{ mm}) - (y_b \text{ of prestressing steel} = 117.3 \text{ mm})$$

and eccentricity at supports,

$$e_e = 37.86 \text{ mm}$$

$$= (y_b \text{ of girder} = 514.86 \text{ mm}) - (y_b \text{ of prestressing steel at supports} = 477 \text{ mm})$$

Therefore, the nominal shear strength at supports is concluded as being,

$$\begin{aligned} V_n &= 245 + 2239 + 89.5 \\ &= 2574 \text{ kN} \end{aligned}$$

Furthermore, nominal shear strengths at additional locations are listed below (calculations not shown):

$$V_n = 245 + 280 + 89.5 = 615 \text{ kN (at midspan)}$$

$$V_n = 245 + 960 + 89.5 = 1295 \text{ kN (at a distance } d \text{ from support)}$$

AASHTO Type III Girder Shear Capacity with CFRP Strengthening

Design, once again, is in accordance with the ISIS Canada Design Manuals.

The concrete and steel contributions to the shear capacity are as follows:

$$V_c = 0.2\sqrt{f'_c}b_wd = 0.2\sqrt{34.5}(177.8)(1287) = 269 \text{ kN}$$

$$V_s = \frac{A_v f_y d}{s} = \frac{(2 \times 200)(400)(1287)}{76.2} = 2702 \text{ kN}$$

$$V_p = 89.5 \text{ kN (previously calculated)}$$

The FRP contribution is found by first determining the FRP shear reinforcement ratio and then the FRP effective strain.

$$\rho_{frp} = \left(\frac{2t_{frp}}{b_w} \right) \left(\frac{w_{frp}}{s_{frp}} \right) = \left(\frac{2 \times 0.50}{177.8} \right) \left(\frac{600}{1200} \right) = 0.00281$$

$$A_{frp} = 2 w_{frp} t_{frp} = 2(600)(0.25 \times 2) = 600 \text{ mm}^2$$

$$\text{Effective anchorage length, } L_e = \frac{25350}{(t_{frp} \times E_{frp})^{0.58}} = \frac{25350}{(2 \times 0.25 \times 86,900)^{0.58}} = 51.75 \text{ mm}$$

The following parameters, k_1 and k_2 , account for the shear strength for the concrete and FRP configuration:

$$k_1 = \left[\frac{f'_c}{27.65} \right]^{2/3} = \left[\frac{34.5}{27.65} \right]^{2/3} = 1.16$$

d_{frp} = measured from free end, under the slab, to bottom of internal steel stirrups

$$= 1143 - (25.4 + 12.7)$$

$$= 1105 \text{ mm}$$

n_e = number of free ends of the FRP stirrups on one side of the girder = 1

$$k_2 = \frac{d_{frp} - n_e L_e}{d_{frp}} = \frac{1105 - (1)(51.75)}{1105} = 0.953$$

$$\text{Effective strain, } \epsilon_{frpe} = \frac{\alpha k_1 k_2 L_e}{9525} = \frac{0.8(1.16)(0.953)(51.75)}{9525} = 0.00480$$

The effective strain is also found using the ratio of effective strain to ultimate strain, R :

$$R = \alpha \lambda_1 \left[\frac{(f'_c)^{2/3}}{\rho_{frp} E_{frp}} \right]^{\lambda_2} = 0.8(1.35) \left[\frac{(34.5)^{2/3}}{(0.00281)(86,900)} \right]^{0.30} = 0.421$$

For CFRP rupture: $\lambda_1 = 1.35$

$$\lambda_2 = 0.30$$

$\alpha = 0.8$ (reduction coefficient for effective strain)

$$\epsilon_{frpe} = R \epsilon_{frpu} = (0.421)(0.012) = 0.00505$$

The effective strain is the lesser of 0.004, 0.00480 and 0.00505. Thus, $\epsilon_{frpe} = 0.004$.

The FRP contribution to shear capacity is,

$$\begin{aligned} V_{frp} &= E_{frp} \epsilon_{frpe} A_{frp} d_{frp} (\sin \beta + \cos \beta) / s_{frp} \\ &= (86,900)(0.004)(600)(1105)(\sin 90^\circ + \cos 90^\circ) / 1200 \\ &= 192 \text{ kN} \end{aligned}$$

where $\beta = 90^\circ$, signifies the angle of the FRP orientation with respect to the longitudinal axis of the girder.

The shear capacity of the girder after CFRP strengthening is,

$$\begin{aligned} V_n &= V_c + V_s + V_{ps} + V_{frp} \\ &= 269 + 2702 + 89.5 + 192 \\ &= 3253 \text{ kN} \end{aligned}$$

Strength gain, under nominal conditions, for shear is therefore:

$$\text{Shear strength gain} = \left(\frac{3253}{2574} - 1 \right) \times 100\% = 26.4\%$$

LIVE LOAD CAPACITY FACTOR CALCULATIONS

The Canadian Highway Bridge Design Code (CHBDC, 2000) provides a measure of evaluating the capacity of a given bridge using the load and resistance factor method. Calculations regarding the live load capacity factor, both theoretically, as would be the case as a part of the original bridge structure, and experimentally are presented below.

Theoretical Live Load Capacity Factor for Actual Type III Girder Bridge

From the CHBDC, clause 14.14, the live load capacity factor is given as:

$$F = \frac{U\phi R - \sum \alpha_D D - \sum \alpha_A A}{\alpha_L L(1+I)}$$

Where,

$U = 1.01$ (resistance adjustment factor)

$R = 6285 \text{ kN}\cdot\text{m}$ (nominal resistance, similar to previous calculations; page B.7)

$\phi = 0.95$ (resistance factor)

The target reliability index, β , is based on several evaluating factors:

Structural behaviour = S2; element failure does not lead to collapse

Element behaviour = E3; element fails gradually

Inspection = INSP2; regular inspection

From the above factors, $\beta = 3.00$.

The dead and live load resistance factors are categorized by the value of the target reliability index. Based on this, they are deciphered as follows:

$$\alpha_{D1} = 1.07 \quad \alpha_{D2} = 1.14 \quad \alpha_{D3} = 1.35 \quad \alpha_L = 1.49$$

The nominal unfactored dead loads, D , are classified as:

$$\begin{aligned} D1 &= \text{factory produced components, and cast-in-place concrete, excluding decks} \\ &= \text{dead load of the Type III girder} \\ &= (8.52 \text{ kN/m})(21.895 \text{ m})^2 \div 8 \\ &= 510.5 \text{ kN}\cdot\text{m} \end{aligned}$$

$$\begin{aligned} D2 &= \text{cast-in-place concrete decks, wood, and non-structural components} \\ &= \text{dead load of the Type III girder's top slab, barrier and sidewalk} \\ &= [(1.9805 \text{ m} \times 0.190 \text{ m}) + (0.254 \text{ m} \times 0.6096 \text{ m}) + (0.863 \text{ m} \times 0.3048 \text{ m})] \times \\ &\quad (24 \text{ kN/m}^3)(21.895 \text{ m})^2 \div 8 \\ &= 1142 \text{ kN}\cdot\text{m} \end{aligned}$$

$$\begin{aligned} D3 &= \text{bituminous concrete surfacings} \\ &= \text{dead load of the Type III girder's overlying asphalt wearing surface} \\ &= (1.5235 \text{ m} \times 0.090 \text{ m})(23.5 \text{ kN/m}^3)(21.895 \text{ m})^2 \div 8 \\ &= 193 \text{ kN}\cdot\text{m} \end{aligned}$$

The nominal static live load, L (considered as M_g in the CHBDC), is given by placing the CL-625-ONT truck on the girder, and obtaining the maximum possible moment. To achieve this, the resultant force of the truck is placed 1.4775 m from the midspan center

line. After calculating the reaction forces at the supports as 354.7 kN and 270.3 kN, the maximum moment may be found. Via simple beam analysis, this moment is calculated as,

$$M_{beam} = (270.3 \text{ kN} \times 8.695 \text{ m}) - (50 \text{ kN} \times 4.8 \text{ m}) - (140 \text{ kN} \times 1.2 \text{ m}) = 1942.2 \text{ kN}\cdot\text{m}$$

Afterwards, in accordance with the CHBDC, clause 5.7.1.2, the maximum longitudinal moment for a one lane width of truck, M_T , including the dynamic load allowance factor ($I = 0.25$ from clause 3.8.4.5) is:

$$M_T = 1942.2 (1 + 0.25) = 2428 \text{ kN}\cdot\text{m}$$

The maximum longitudinal moment due to live load, M_g , is calculated by first establishing the following parameters:

$$F = 6.80 - (3/L) = 6.80 - (3 / 21.895) = 6.66$$

$$C_f = 5 - (15/L) = 5 - (15 / 21.895) = 4.31$$

$$\mu = \frac{W_e - 3.3}{0.6} = \frac{4.267 - 3.3}{0.6} = 1.62 > 1.00, \text{ thus } \mu = 1.00$$

$$F_m = \frac{SN}{F \left(1 + \frac{\mu C_f}{100} \right)} = \frac{(2.743 \times 4)}{6.66 \left(1 + \frac{(1.0 \times 4.31)}{100} \right)} = 1.579$$

Thus we obtain,

$$L = M_g = F_m M_{g \text{ avg}} = F_m \frac{n M_T R_L}{N} = (1.579) \frac{(2)(2428)(0.9)}{4} = 1725 \text{ kN}\cdot\text{m}$$

Where n is the number of lanes, R_L is the modification factor for multi-lane loading, and N is the number of girders in the bridge system.

Now, the theoretical live load capacity factor may be determined:

$$F = \frac{(1.01)(0.95)(6285) - [(1.07 \times 510.5) + (1.14 \times 1142) + (1.35 \times 193)]}{(1.49)(1725)} = 1.53$$

Experimental Live Load Capacity Factor for the Type III Girder as Tested

The live load capacity factor attained experimentally is assessed as:

$$F = \frac{M_{exp}}{\alpha_L L(1+I)}$$

The load achieved experimentally was equal to 1368 kN, corresponding to a maximum midspan moment of 3744 kN·m. To achieve the correct value of L , it is multiplied by the ratio of experimental to actual moment resistance, being $(6130 \div 6285) = 0.975$.

Thus,

$$F = \frac{(3744)}{(1.49)(1725)(0.975)} = 1.49$$

It is to be noted that in both calculations for the live load capacity factor, the $(1 + I)$ value was omitted. This is because the dynamic load allowance factor, I , had already been introduced when calculating M_T . Also of importance to state is the fact that the girder was loaded experimentally with 1368 kN. This equates to approximately twice the design ultimate load which is given by,

$$(625 \text{ kN})(1.75)(2 \text{ lanes})(1 + 0.25) \div (4 \text{ girders}) = 683 \text{ kN}$$

$$\frac{\text{Experiment Load}}{\text{Design Load}} = \frac{1368}{683} = 2.00$$

MOMENT OF INERTIA CALCULATIONS

The moment of inertia was determined for the AASHTO Type III girder with and without the contribution of the CFRP. For each calculation, the top slab width is taken into account as: (1) $b = 1600$ mm; as tested experimentally, and (2) $b = 1980.5$ mm; as was the case when the girder was part of its original integral four girder bridge system.

For the AASHTO Type III girder:

$$I_x = 5.22 \times 10^{10} \text{ mm}^4$$

$$y_b = 514.86 \text{ mm}$$

$$A = 361,290 \text{ mm}^2$$

$$n_{slab} = E_{slab} \div E_{girder} = (24,200 \div 26,200) = 0.924$$

$$n_{girder} = E_{frp} \div E_{girder} = (86,900 \div 26,200) = 3.32$$

Moment of Inertia for the AASHTO Type III Girder without CFRP

With $b = 1600$ mm:

$$y_b = \frac{\sum A y_i}{\sum A} = \frac{(0.924)(1600 \times 190)(1238) + (361,290)(514.86)}{(0.924)(1600 \times 190) + (361,290)} = 831 \text{ mm}$$

$$I_x = \sum I_i + \sum A_i (y_b - y_i)^2$$

$$= 5.22 \times 10^{10} + (361,290)(316.14)^2 + \frac{(1600)(190)^3}{1.082(12)} + \frac{(1600)(190)(407)^2}{1.082}$$

$$= 1.357 \times 10^{11} \text{ mm}^4$$

With $b = 1980.5 \text{ mm}$:

$$y_b = \frac{\sum Ay_i}{\sum A} = \frac{(0.924)(1980.5 \times 190)(1238) + (361,290)(514.86)}{(0.924)(1980.5 \times 190) + (361,290)} = 869.5 \text{ mm}$$

$$\begin{aligned} I_x &= \sum I_i + \sum A_i (y_b - y_i)^2 \\ &= 5.22 \times 10^{10} + (361,290)(354.64)^2 + \frac{(1980.5)(190)^3}{1.082(12)} + \frac{(1980.5)(190)(368.5)^2}{1.082} \\ &= 1.459 \times 10^{11} \text{ mm}^4 \end{aligned}$$

Moment of Inertia for the AASHTO Type III Girder with CFRP

With $b = 1600 \text{ mm}$:

$$\begin{aligned} y_b &= [(0.924)(1600 \times 190)(1238) + (361,290)(514.86) + (3.32)(161.6)(908.05) + \\ &\quad (3.32)(269.4)(273.05)] \div [(0.924)(1600 \times 190) + 361,290 + (3.32)(161.6 + 269.4)] \\ &= 830.5 \text{ mm} \end{aligned}$$

$$\begin{aligned} I_x &= [5.22 \times 10^{10} + (361,290)(315.64)^2] + \left[\frac{(1600)(190)^3}{1.082(12)} + \frac{(1600)(190)(407.5)^2}{1.082} \right] + \\ &\quad \left[(3.32) \frac{(161.6)(114.3)^2}{12} + (3.32)(161.6)(77.55)^2 \right] + \\ &\quad \left[(3.32) \frac{(269.4)(190.5)^2}{12} + (3.32)(269.4)(557.45)^2 \right] \\ &= 1.360 \times 10^{11} \text{ mm}^4 \end{aligned}$$

With $b = 1980.5 \text{ mm}$:

$$\begin{aligned} y_b &= [(0.924)(1980.5 \times 190)(1238) + (361,290)(514.86) + (3.32)(161.6)(908.05) + \\ &\quad (3.32)(269.4)(273.05)] \div [(0.924)(1980.5 \times 190) + 361,290 + (3.32)(161.6 + 269.4)] \\ &= 868.8 \text{ mm} \end{aligned}$$

$$\begin{aligned} I_x &= 1.459 \times 10^{11} + \left[(3.32) \frac{(161.6)(114.3)^2}{12} + (3.32)(161.6)(38.55)^2 \right] + \\ &\quad \left[(3.32) \frac{(269.4)(190.5)^2}{12} + (3.32)(269.4)(596.45)^2 \right] \\ &= 1.462 \times 10^{11} \text{ mm}^4 \end{aligned}$$

DT-41 GIRDER FLEXURE CALCULATIONS

DT-41 Girder Nominal Moment Capacity

Calculations presented are similar to those for the AASHTO Type III girder.

The nominal flexural strength calculation, for the DT-41 girder, is shown below.

$$\text{Nominal flexural strength, } M_n = (A_p f_p) \left(d_p - \frac{a}{2} \right)$$

$$A_p = 14 \times 12.7 \text{ mm nominal strands} = 14 \times 99 \text{ mm}^2 = 1386 \text{ mm}^2$$

For members with bonded tendons, the prestressing steel stress at maximum moment is,

$$f_p = f_{pu} \left(1 - \frac{\gamma_p}{\beta_1} \left[\rho_p \frac{f_{pu}}{f'_c} + \frac{d}{d_p} (w - w') \right] \right)$$

The ultimate tensile strength, f_{pu} , for the 12.7 mm nominal strands is 1860 MPa.

$$\gamma_p = 0.28 \quad (\text{for low-relaxation strands, where } f_{py}/f_{pu} \geq 0.90)$$

The corresponding stress block factors are,

$$\alpha_1 = 0.85$$

and

$$\begin{aligned} \beta_1 &= 0.85 - (f'_c - 4000)(0.00005) \geq 0.65 \quad \text{for } f'_c > 4000 \text{ psi} \\ &= 0.85 - (5100 - 4000)(0.00005) \\ &= 0.795 \end{aligned}$$

It shall be noted that, at the midspan section of the girder, only prestressing reinforcement is prevalent.

The ratio of prestressed reinforcement is calculated to be,

$$\rho_p = \frac{A_p}{bd_p} = \frac{1386}{(3190)(581.4)} = 0.000747$$

Distance from the extreme compression fibre to the centroid of the prestressed reinforcement is computed:

$$d_p = (710 + 100) - 228.6 = 581.4 \text{ mm}$$

Finally, the prestressing steel stress is found,

$$f_p = 1860 \left(1 - \frac{0.28}{0.795} \left[0.000747 \frac{(1860)}{(35)} \right] \right) = 1834 \text{ MPa}$$

The depth of the compression stress block is then found to be,

$$a = \frac{A_p f_p}{0.85 f'_c b} = \frac{(1386)(1834)}{0.85(35)(3190)} = 26.78 \text{ mm}$$

This, ascertains that the neutral axis lies in the top slab.

With the above established values, we have

$$M_n = (1386)(1834) \left(581.4 - \frac{26.78}{2} \right) = 1444 \text{ kN}\cdot\text{m}$$

DT-41 Girder Moment Capacity with CFRP Strengthening

The ISIS Canada Design Manual is used for the following calculations, as was with the AASHTO Type III girder.

We will consider our failure mode to consist of yielding of the prestressing reinforcement, with rupture of the CFRP, followed ultimately by crushing of the concrete. We also assume that all initial strains in the concrete, and the prestressing steel are negligible ($\epsilon_{ci} = \epsilon_{pi} = 0$). All assumptions are to be checked, and corrected if in disagreement.

The equivalent stress block factors are:

$$\begin{aligned}\alpha_1 &= 0.85 - 0.0015 f'_c \geq 0.67 & \text{and} & \quad \beta_1 = 0.97 - 0.0025 f'_c \geq 0.67 \\ &= 0.85 - 0.0015(35) & & \quad = 0.97 - 0.0025(35) \\ &= 0.798 & & \quad = 0.883\end{aligned}$$

Next we compute the position of the neutral axis, assumed to lie in the concrete slab.

$$C = T$$

$$C_c = T_{frp} + T_p$$

$$\alpha_1 f'_c \beta_1 b c = E_{frp} \epsilon_{frpu} A_{frp} + E_p \epsilon_{pu} A_p$$

$$0.798(35)(0.883)(3190) c = (61,500 \times 0.01)(1800) + (1860)(1386)$$

$$c = 46.8 \text{ mm}$$

$$a = \beta_1 c = 41.3 \text{ mm} < 100 \text{ mm slab thickness}$$

It is seen above that our assumption is true, and thus will carry on.

Above, A_{frp} for moment was decided by taking into account only the cross sectional area of the CFRP U-wraps, at midspan, with a 1.0 mm thickness per layer.

$$A_{frp} = 1.0 \times 2 [2(400) + 100] = 1800 \text{ mm}^2$$

The centroid of CFRP moment reinforcement:

$$y_{bfrp} = \frac{2[(100 \times 1.0)(0.5) + 2(400 \times 1.0)(201)]}{2(900)} = 178.7 \text{ mm}$$

$$d_{frp} = (710 + 100) - 178.7 = 631.3 \text{ mm}$$

Next, a check of material strains to verify whether the assumed failure mode is prevalent.

$$\varepsilon_{frp} = \varepsilon_{cu} \left(\frac{d_{frp} - c}{c} \right) = 0.0035 \left(\frac{631.3 - 46.8}{46.8} \right) = 0.044 > 0.01 \quad \text{CFRP ruptures}$$

$$\varepsilon_{ps} = \varepsilon_{cu} \left(\frac{d_p - c}{c} \right) = 0.0035 \left(\frac{581.4 - 46.8}{46.8} \right) = 0.040 > 0.01 \quad \text{prestressing steel yields}$$

Since the prestressing steel has yielded, and the FRP ruptured, our assumption is correct. The strengthened girder moment capacity, M_n , can now be found.

$$M_n = T_{frp} \left(d_{frp} - \frac{a}{2} \right) + T_p \left(d_p - \frac{a}{2} \right)$$

$$M_n = (61,500 \times 0.01)(1800) \left(631.3 - \frac{41.3}{2} \right) + (1860)(1386) \left(581.4 - \frac{41.3}{2} \right)$$

$$M_n = 2122 \text{ kN}\cdot\text{m}$$

Strength gain, under nominal conditions, for flexure is therefore:

$$\text{Flexure strength gain} = \left(\frac{2122}{1444} - 1 \right) \times 100\% = 47\%$$

DT-102A GIRDER FLEXURE CALCULATIONS

DT-102A Girder Nominal Moment Capacity

Calculations presented are similar to those for the AASHTO Type III girder.

The nominal flexural strength calculation, for the DT-41 girder, is shown below.

$$\text{Nominal flexural strength, } M_n = (A_p f_p) \left(d_p - \frac{a}{2} \right)$$

$$A_p = 10 \times 15.8 \text{ mm nominal strands} = 10 \times 148 \text{ mm}^2 = 1480 \text{ mm}^2$$

For members with bonded tendons, the prestressing steel stress at maximum moment is,

$$f_p = f_{pu} \left(1 - \frac{\gamma_p}{\beta_1} \left[\rho_p \frac{f_{pu}}{f'_c} + \frac{d}{d_p} (w - w') \right] \right)$$

The ultimate tensile strength, f_{pu} , for the 15.8 mm nominal strands is 1760 MPa.

$$\gamma_p = 0.28 \quad (\text{for low-relaxation strands, where } f_{py}/f_{pu} \geq 0.90)$$

The corresponding stress block factors are,

$$\alpha_1 = 0.85$$

and

$$\begin{aligned} \beta_1 &= 0.85 - (f'_c - 4000)(0.00005) \geq 0.65 \quad \text{for } f'_c > 4000 \text{ psi} \\ &= 0.85 - (6500 - 4000)(0.00005) \\ &= 0.725 \end{aligned}$$

It shall be noted that, at the midspan section of the girder, only prestressing reinforcement is prevalent.

The ratio of prestressed reinforcement is calculated to be,

$$\rho_p = \frac{A_p}{bd_p} = \frac{1480}{(3400)(540)} = 0.000806$$

Distance from the extreme compression fibre to the centroid of the prestressed reinforcement is computed:

$$d_p = (660 + 100) - 220 = 540 \text{ mm}$$

Finally, the prestressing steel stress is found,

$$f_p = 1760 \left(1 - \frac{0.28}{0.725} \left[0.000806 \frac{(1760)}{(45)} \right] \right) = 1739 \text{ MPa}$$

The depth of the compression stress block is then found to be,

$$a = \frac{A_p f_p}{0.85 f'_c b} = \frac{(1480)(1739)}{0.85(45)(3400)} = 19.79 \text{ mm}$$

This, ascertains that the neutral axis lies in the top slab.

With the above established values, we have

$$M_n = (1480)(1739) \left(540 - \frac{19.79}{2} \right) = 1364 \text{ kN}\cdot\text{m}$$

DT-102A Girder Moment Capacity with CFRP Strengthening

The ISIS Canada Design Manual is used for the following calculations, as was with the AASHTO Type III girder.

We will consider our failure mode to consist of yielding of the prestressing reinforcement, with rupture of the CFRP, followed ultimately by crushing of the concrete. We also assume that all initial strains in the concrete, and the prestressing steel are negligible ($\epsilon_{ci} = \epsilon_{pi} = 0$). All assumptions are to be checked, and corrected if in disagreement.

The equivalent stress block factors are:

$$\begin{aligned}\alpha_1 &= 0.85 - 0.0015 f'_c \geq 0.67 & \text{and} & \quad \beta_1 = 0.97 - 0.0025 f'_c \geq 0.67 \\ &= 0.85 - 0.0015(45) & & \quad = 0.97 - 0.0025(45) \\ &= 0.783 & & \quad = 0.858\end{aligned}$$

Next we compute the position of the neutral axis, assumed to lie in the concrete slab.

$$C = T$$

$$C_c = T_{frp} + T_p$$

$$\alpha_1 f'_c \beta_1 b c = E_{frp} \epsilon_{frpu} A_{frp} + E_p \epsilon_{pu} A_p$$

$$0.783(45)(0.858)(3400) c = (61,500 \times 0.01)(1800) + (1760)(1480)$$

$$c = 36.1 \text{ mm}$$

$$a = \beta_1 c = 31 \text{ mm} < 100 \text{ mm slab thickness}$$

It is seen above that our assumption is true, and thus will carry on.

Above, A_{frp} for moment was decided by taking into account only the cross sectional area of the CFRP U-wraps, at midspan, with a 1.0 mm thickness per layer.

$$A_{frp} = 1.0 \times 2 [2(400) + 100] = 1800 \text{ mm}^2$$

The centroid of CFRP moment reinforcement:

$$y_{b,frp} = \frac{2[(100 \times 1.0)(0.5) + 2(400 \times 1.0)(201)]}{2(900)} = 178.7 \text{ mm}$$

$$d_{frp} = (660 + 100) - 178.7 = 581.3 \text{ mm}$$

Next, a check of material strains to verify whether the assumed failure mode is prevalent.

$$\epsilon_{frp} = \epsilon_{cu} \left(\frac{d_{frp} - c}{c} \right) = 0.0035 \left(\frac{581.3 - 36.1}{36.1} \right) = 0.053 > 0.01 \quad \text{CFRP ruptures}$$

$$\epsilon_{ps} = \epsilon_{cu} \left(\frac{d_p - c}{c} \right) = 0.0035 \left(\frac{540 - 36.1}{36.1} \right) = 0.049 > 0.01 \quad \text{prestressing steel yields}$$

Since the prestressing steel has yielded, and the FRP ruptured, our assumption is correct. The strengthened girder moment capacity, M_n , can now be found.

$$M_n = T_{frp} \left(d_{frp} - \frac{a}{2} \right) + T_p \left(d_p - \frac{a}{2} \right)$$

$$M_n = (61,500 \times 0.01)(1800) \left(581.3 - \frac{31}{2} \right) + (1760)(1480) \left(540 - \frac{31}{2} \right)$$

$$M_n = 1992 \text{ kN}\cdot\text{m}$$

Strength gain, under nominal conditions, for flexure is therefore:

$$\text{Flexure strength gain} = \left(\frac{1992}{1364} - 1 \right) \times 100\% = 46\%$$